UNIVERSITA' DEGLI STUDI DI PAVIA
Dipartimento di Biologia e Biotecnologie "L. Spallanzani"

Brain Development in Prolidase Deficient Mice

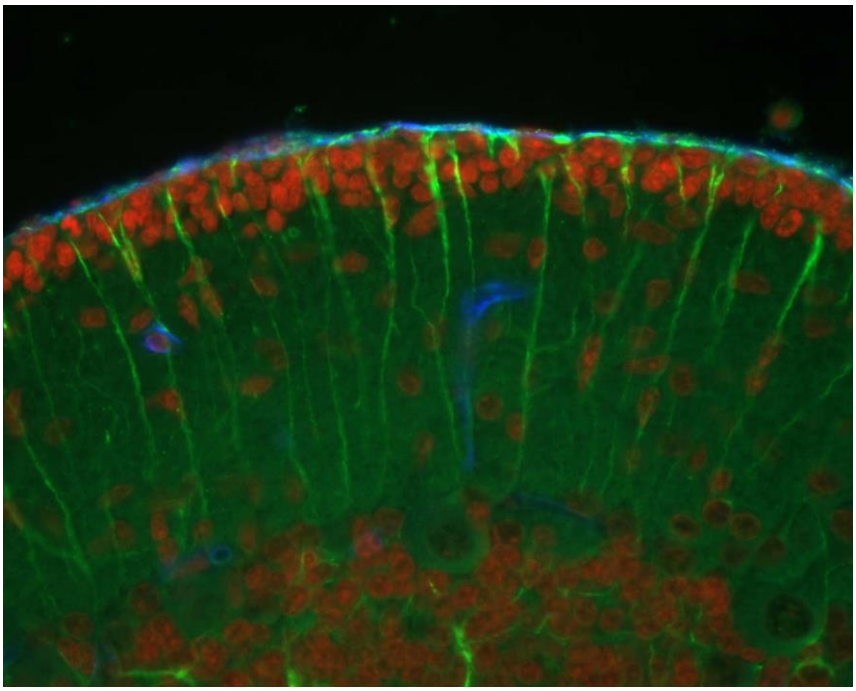

Violetta Insolia

PhD Program in Genetics, Molecular and Cellular Biology
XXIX Cycle – 2013-2016

UNIVERSITA' DEGLI STUDI DI PAVIA

Dipartimento di Biologia e Biotecnologie "L. Spallanzani"

Ph.D Program in Genetics, Molecular and Cellular Biology

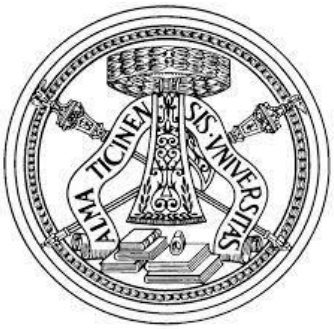

Brain Development in Prolidase Deficient Mice

Advisors:
Prof. Graziella Bernocchi
Dr. Maria Grazia Bottone

Ph.D student

Violetta Insolia

XXIX Cycle – 2013-2016

INDEX

ABSTRACT

Prolidase deficiency (PD) is a rare autosomal recessive disorder caused by mutations in the prolidase gene, the PEPD, causing the reduction or the loss of the prolidase enzyme activity. PD patients present a variable onset, and severe skin ulcers mainly characterize the pathology. However, PD has a broad spectrum of phenotypes including mental impairment and developmental delay of variable degrees.

Prolidase is a member of the matrix metalloproteinase (MMP) family. MMPs together with their inhibitors (tissue inhibitor of metalloproteinases, TIMPs) regulate the extracellular matrix maturation and remodelling life-long. Among them, prolidase is able to cleave dipeptides when prolin or hydroxyprolin residues are located at the C-terminal end. According to prolidase activity, its function has an impact on the metabolism of many biologically important molecules, particularly during the biosynthesis and degradation of collagen and procollagen. Therefore, prolidase indirectly has a role in the ECM remodelling. In particular, the ECM adjustments are essential in the brain, especially during the critical period of development: from passive structural property, to a direct influence on cell proliferation, migration, axonal guidance, synaptogenesis, homeostatic plasticity, learning and memory processes, and angiogenesis. In particular, the basement membrane beside the pial meninx (pBM) is a specialized structure of ECM whose integrity and proper assembly is essential for a correct cortical development and the collagen IV plays an essential role in pBM stability. Ruptures, even localized, in the pBM are accompanied by changes in the morphology of radial glia cells, subsequent cortical dysplasia, overmigration of neurons, decrease in the proliferation and migration of granule cell precursors, and reduction in Purkinje neuron dendrites.

Recently, a mutant mouse with reduced prolidase activity has been identified with a spontaneous 4 bp deletion in the exon 14 of Pepd gene. The mutant mouse was named dark-like (*dal*) because of its darkened-coat color in homozygosis. The *dal/dal* phenotype includes small body size, reproductive degeneration, vacuolated cells at the cortical medullary junction of the adrenal

gland, mild hydrocephalus, dark urine and altered bone phenotype. The prolidase activity was strongly reduced in cerebrum and cerebellum in *dal* mice. Moreover, they develop hypertrophic cardiomyopathy, but neither skin lesions nor recurrent infections were reported (in contrast to the reported human cases).

The aim of this thesis was the study the brain development of *dal*/+ and *dal*/*dal* mice. Since no information were available, the analysis started with a morphological evaluation of the cerebellum, neocortex and hippocampus, through histological stainings. Then, immunohistochemistry reactions and western blotting analysis helped the anomalies characterizations. In particular, the attention has been mainly focused on the cerebellum, since it is the structure in which the ontogenetic events occurred also postnatally. The neocortex and hippocampal results were not described in details.

Our results suggested that the absence of a full functional prolidase enzyme in the *dal/dal* mice results in a damage of the integrity of the pBM with an altered collagen, laminin and reelin profile. Such damage, could affect as a cascade of developmental events the proper lamination process of the cerebellum, leading to a cortical dysplasia together with the presence of degenerating and ectopic cells, defects in cerebellar lobulation and in the excitation/inhibition pattern of the cerebellar circuit.

Furthermore, since PD is still a critical and less known disease and prolidase is a dysregulated enzyme in many other neurological disorders, other studies will be directed in understanding its peculiar role, as part of important pathways beside the ECM maturation and remodeling, in the CNS, and the relation between the brain anomalies in *dal* mice and the human phenotype.

This latter goal is ambitious since this study was only the first step that is contributing for the first time with a neurobiological approach.

ACKNOWLEDGEMENTS

I would like to express my gratitude to my advisors Prof. Garziella Bernocchi and Dr. Maria Grazia Bottone for the continuous support of my study and research and for believing in me from beginning.
In particular, Prof. Graziella Bernocchi for her scientific advice and knowledge, constructive criticism and extensive discussions about my work.

I am also very grateful to all my students Caterina, Federica, Giacomo, Ilenia, Erica, Marco, Erika and my colleagues Valeria and Irene. A special thanks to Dr. Ilaria Dutto for her time spent helping me in some experiments and graph design, and Prof. Marco Biggiogera.

Prof. Antonella Forlino for the mouse model and for the opportunity of this collaboration.

I would like to extend my thanks to all the people I met during my experience in Ireland, expecially Prof. Siobhain O'Mahony and Dr. Valeria Felice.

ABBREVIATIONS

ADAM with thrombospondin motifs (ADAMTS)

Basement Membrane (BM)

Calbindin (CB)

Carleretinin (CR)

Central Nervous System (CNS)

Chondroitin Sulfate Proteoglycan (CSPG)

Climbing Fibres (CF)

Cornus Ammonis (CA)

dark-like (dal)

Dentate Gyrus (DG)

Doublecortin (DCX)

External Granular Layer (EGL)

Extracellular Matrix (ECM)

Glial Fibrillary Acidic Protein (GFAP)

Glutamate Decarboxylase (GAD)

Glutamate Receptor (GluR)

Haematoxylin and Eosin (H&E)

Hyaluronan (HA)

Hyaluronan And Proteoglycan Link Protein (HAPLN)

Hyaluronan Synthases (HASs)

Immunoglobulin Superfamily (IgSF)

Internal Granular Layer (IGL)

Magnetic Resonance Imaging (MRI)

Matrix Metalloproteinases (MMPs)

Microtubule-Associated Proteins (MAPs)

Molecular Layer (ML)

Molecular Layer Interneurons (MLI)

Neurofilament-Heavy (NF-H)

N-methyl-D-aspartate (NMDA)

Optical Density (OD)

Parvalbumin (PV)

Perineuronal Nets (PNNs)

Peptidase D (PEPD)

pial Basement Membrane (pBM)

Plasma Membrane Calcium ATPase (PMCA)

Post-natal day 15 (P15)

Prolidase Deficiency (PD)

Proliferating Cell Nuclear Antigen (PCNA)

Proteoglycans (PG)

Purkinje Layer (PL)

Room Temperature (RT)

Sirius Red (SR)

Sodium Dodecyl Sulfate PolyAcrylamide Gel Electrophoresis

ABBREVIATIONS

(SDS-PAGE)

Sonic Hedgehog (SHH)

Tenascin-R (TN-R)

Tissue Inhibitors of MMPs (TIMPS)

Vascular Endothelial Growth Factor (VEGF)

Vesicular Glutamate Receptor Transporter (VGLUT)

Western Blotting (WB)

α Disintegrin And Metalloproteinase (ADAM)

γ-AminoButyric Acid (GABA)

Wild Type (wt)

Standard Deviation (SD)

1. INTRODUCTION

1.1. Prolidase Deficiency

1.1.1 The prolidase enzyme

Among the 20 amino acids coded in protein synthesis, proline (Figure 1) has a unique structure in which the a-nitrogen atom is part of the rigid pyrrolidine ring and, at the same time, is covalently bound by means of a secondary amide bond to the preceding amino acid. Because of proline structure imposes strong conformational restraints in a peptide chain and peculiar enzymes to hydrolyze the peptide bonds in which it is involved. Indeed prolidase (peptidase D, EC. 3.4.13.9) and prolinase (EC 3.4.13.8) respectively are able to hydrolyze the peptide bond of dipeptides containing respectively a C- or N-terminal proline or hydroxyproline residue (Royce & Steinmann 2002; Lupi et al. 2008).

Prolidase is encoded by the peptidase D (PEPD) gene (Gene ID: 5184), located in humans on chromosome 19 in position 19q13.11. The gene size is around 130 kb and consists of 15 exons and 14 long introns, representing about 98% of the gene.

The human prolidase enzyme works as a homodimer of 123 kDa (493 amino acids) in the cytosol (Besio et al. 2013). Two isoforms have been demonstrated (PD I and PD II) which differ for the substrate specificity: PD I showed higher activity against seryl-proline and glycyl-proline, while PD II was particularly active against methionyl-proline. Prolidase activity in the whole brain and in the different brain regions showed higher activity against methionyl-proline and seryl-proline. PD II activity was highest in the hippocampus, followed by the cerebellum, cerebral cortex, caudate nucleus, and the midbrain. The most rapid changes in the activities of PD I and PD II occurred perinatally, with a peak at three days before birth and a nadir at two days after birth, which then gradually increased until 21 days (Cosson et al. 1992; Chi et al. 2009). The crystal structure of human prolidase was deposited in 2007 and was obtained by X-ray diffraction (Mueller et al. 2007) (Figure 1).

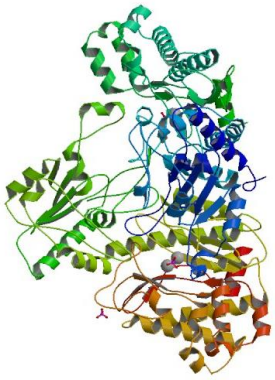

Figure 1. Crystal Structure of human prolidase.
Retrieved from Protein Data Bank.
http://www.rcsb.org/pdb/explore.do?structureId=2OKN

Since prolidase is involved in the last step of intracellular protein degradation, its function can be linked to the metabolism of many biologically important molecules that contain a large amount of proline in their primary structure and has a key role in the recycling of proline. This latter case may be rate limiting for the synthesis of proline-rich proteins. There is a high degree of conservation found in many proteins and peptides containing proline, especially cytokines, growth factors, neuro- and vasoactive peptides (Wess et al. 1993; Vanhoof et al. 1995). In particular, prolidase has a central role in the extracellular matrix (ECM) remodeling, since collagen (a proline-rich protein) is one of its major target (Surazynski et al. 2008). Furthermore, it was demonstrated that type I and IV collagen are responsible for the activation of prolidase activity (Palka & Phang 1997).

The alterations in prolidase activity, detected as either decrease or increase, characterize many disease states as well as the progression of many disorders, also related to Central Nervous System (CNS). A list of medical conditions associated to prolidase activity changes was published by Kitchener & Grunden (2012); an updated version is presented in table 1.

Table 1. Prolidase activity in different medical conditions

Medical condition	Prolidase activity	References
Alzheimer disease	Increase	(Arikanoglu et al. 2013)
Behçet's disease	Increase	(Bozkurt et al. 2014)
Bipolar disorder	Increase	(Andreazza et al. 2008; Selek et al. 2011)
Bladder cancer	Increase	(Geçit et al. 2012)
Breast cancer	Increase	(Cechowska-Pasko et al. 2006)
Cerebral ischemia/reperfusion	Increase	(Caliskan et al. 2014; Uzar et al. 2012)
Diabetic foot ulcers	Increase	(Eren et al. 2013)
Dysplasia of the hip	Increase	(Soran et al. 2013)
Early progeny failure-placenta	Increase	(Namiduru et al. 2001; Toy et al. 2010; Vural et al. 2011)
Endometrial cancer	Increase	(Arioz et al. 2009)
Epithelial ovarian cancer	Increase	(Camuzcuoglu et al. 2009)
Erectile dysfunction	Increase	(Savas et al. 2010)
Fibromyalgia	Increase	(Bozkurt et al. 2014)
Intestinal bacterial infection	Increase	(Aslan et al. 2007)
Hemorrhagic stroke	Increase	(Gonullu et al. 2014)
Hypertension	Increase	(Demirbag et al. 2007)
Ischemic cardiomyopathy	Increase	(Toprak et al. 2013)
Keloid scar formation	Increase	(Duong et al. 2006)
Liver disease	Increase	(Myara et al. 1984; Abraham et al. 2000)
Lung cancer	Increase	(Karna et al. 2000)
Melanoma	Increase	(Mittal et al. 2005)
Nephropathy	Increase	(Verma et al. 2014)
Placental abruption	Increase	(Incebiyik et al. 2015)
Polycystic ovary syndrome	Increase	(Hilali et al. 2013)
Pulmonary tuberculosis	Increase	(Gumus et al. 2011)

Renal tumors	Increase	(Pirinççi et al. 2016)
Rheumatoid arthritis	Increase	(Sezer et al. 2013)
Stomach cancer	Increase	(Guszczyn et al. 2004)
Thalassemia major	Increase	(Cakmak et al. 2010)
Lupus erythematosus	Decrease	(Kurien et al. 2013)
Rarely epileptic seizure	Decrease	(Royce & Steinmann 2002)
Asthma	Decrease	(Cakmak et al. 2009)
Chronic obstructive pulmonary disease	Decrease	(Gencer et al. 2011)
Chronic pancreatitis	Decrease	(Palka et al. 2002)
Diabetic neuropathy	Decrease	(Sayın et al. 2014)
Dilated cardiomyopathy	Decrease	(Sezen et al. 2010)
Early progeny-mother	Decrease	(Namiduru et al. 2001; Toy et al. 2010; Vural et al. 2011)
Myeloproliferative neoplasms	Decrease	(Nowicka et al. 2012)
Osteoarthritis	Decrease	(Altindag et al. 2007)
Pancreatic cancer	Decrease	(Palka et al. 2002)

1.1.2 Prolidase Deficiency (PD)

Prolidase deficiency (PD) (OMIM 170100) is a rare autosomal recessive disorder (incidence of 1-2:1,000,000, probably underestimated) caused by mutations in the PEPD gene with a variable clinical phenotype including skin ulcers, facial dysmorphism, splenomegaly, susceptibility to recurrent respiratory infections, hypotonia, skeletal and vascular anomalies. PD patients show reduced or absent prolidase activity in erythrocytes, leukocytes or cultured fibroblasts and a consequent massive urinary excretion of X-proline and X-hydroxyproline dipeptides (imidodipeptiduria) (Bissonnette et al. 1993; Royce & Steinmann 2002; Lupi et al. 2008). The clinical manifestations are usually detectable after birth or in early childhood, but late-onset cases were also reported (Dyne et al., 2001). Moreover, intellectual disability of variable degree has been described with different percentage of incidence in individuals with PD. Hechtman reported approximately the 75% of cases (2014), while according to Lupi et al. (2008) twelve of thirty individuals with molecularly confirmed prolidase deficiency had intellectual disability. In a case series of twelve individuals with PD, one had speech delay, two had mild developmental delay, and six had intellectual disability, while three had no delays (Besio et al. 2015). In a case series of twenty, all had some degree of developmental delay, mainly moderate cognitive or speech delay (Falik-Zaccai et al. 2010). More specifically, two had speech delay, eight had mild developmental delay, five had moderate delay, and three had severe delay. Moreover, rare epileptic seizures have been described (De Rijcke et al. 1989, Wang et al. 2006, Butbul Aviel et al. 2012). Furthermore, brain magnetic resonance imaging (MRI) findings include: multiple microthromboses bilaterally in the cerebral white matter (Arata et al. 1991), multiple bilateral subcortical white matter lesions, accompanied by leptomeningeal enhancement (one affected individual) (Butbul Aviel et al. 2012), and findings compatible with vasculitis (Falik-Zaccai et al. 2010). On nerve conduction studies, one affected individual had decreased amplitude of motor action potentials and sensory action potentials (Cantatore et al. 1993).

There is no definitive cure for PD although several treatments have been evaluated with varying degrees of success at alleviating the clinical symptoms of PD and improving patient quality of life. The majority of them were related to the most critical one, the skin ulcers on legs and feet such as occlusive dressings, topical antiseptics and antibiotics, topical glycine and proline, topical growth hormone, oral supplements of manganese and ascorbic acid, oral corticosteroids, blood transfusions as enzyme replacement therapy and skin grafts (Kokturk et al. 2002; Lupi et al. 2002, 2008; Viglio et al. 2006). All of these treatments have shown limited success, with short-lived results. A promising avenue for treatment of PD using enzyme replacement therapy involves employing micro- and nanoparticles to deliver prolidase directly to the cells, since prolidase cannot be administered freely (Colonna et al. 2008). Therefore, several targeted prolidase delivery systems have been tested with some success including: enzyme microencapsulation in biodegradable microspheres, enzyme-loaded liposomes intended for injection, and enzyme-loaded chitosan glutamate nanoparticles intended for topical application (Genta et al. 2001; Lupi et al. 2004; Perugini et al. 2005; Colonna et al. 2007; Ferreira & Wang 2015).

Different mutations in the PEPD gene have been identified spanning from deletions, insertions and splicing errors. As described above, the severity of the disease varies widely but no relationship between the type of mutation and the phenotype has yet been established due mainly to the limited number of described mutations on the PEPD gene (Royce & Steinmann 2002; Lupi et al. 2008).

The diagnosis is established in a proband (who has the characteristic clinical findings and imidodipeptiduria) by detection of either biallelic PEPD pathogenic variants or reduced prolidase enzyme activity (Ferreira & Wang 2015).

1.1.3 The PD mouse model

In 2008 a mutant mouse line was identified (figure 2) exhibiting a darkened coat color in homozygosity, so that was named '*dal*' (dark-like). The phenotype in homozygosis includes: smaller size (growth rate is reduced in ~36% of young dal/dal mice), gonad abnormalities, vacuolated cells at the cortical medullary junction of the adrenal gland, loss of lipid raft domains, mild hydrocephalus, compromised skeletogenesis and dark staining urine (Cota et al. 2008). Only in 2011, it was demonstrated that the mutant mice had a spontaneous 4bp deletion in the 14th exon of the PEPD gene on the mouse chromosome 7 and it was observed that they developed congenital cardiomyocyte hypertrophy due to the disruption of collagen-mediated integrin signaling, enhancing so the angiogenesis. From that discovery, *dal* mice were identified as PD mouse model (Cota et al. 2008; Jung et al. 2011; Besio et al. 2015) even if no skin ulcers had been detected in these mice (in contrast to the reported human cases). The prolidase activity was evaluated in the cerebrum and cerebellar cortex using the method described in Myara et al. (1983). The prolidase activity in *dal/dal* mice was strongly reduced with respect to wt animals both in cerebrum (4.3±3.7%) and in cerebellum (3.7±1.4%). Interestingly prolidase activity in both tissues was less than 50% in *dal*/+ mice with respect to wt, 36.7±21% in cerebrum and 30.0±8.8% in cerebellum (confidential results, from Prof. Forlino's laboratory).

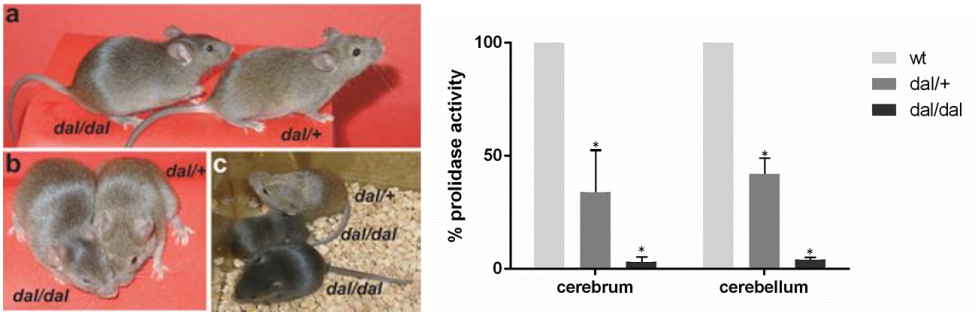

Figure 2. Prolidase deficiency mouse model: dal mutant mice. A. Mice homozygous for the dal mutation have dark dorsal hairs but retain agouti banded hairs on their flank and ventrum (a,b) (Cota et al. 2008). B. Prolidase activity in cerebrum (a) and cerebellum (b) in dal mice and wt controls. P-value < 0,05.

1.2. The extracellular matrix of the Central Nervous System

1.2.1 Extracellular Matrix in the CNS

The ECM of the CNS forms a large component of brain, consisting of a dense substratum, which surround neurons and glial cells. ECM components comprise ~10–20% of the total brain volume (Nicholson & Syková 1998). The ECM is synthesized and secreted by embryonic cells beginning at the earliest stages of development. The understanding of the composition, structure and function of the ECM is continuously evolving. It started associating to the ECM the role of a passive structure that supports CNS cells. Nowadays it is becoming more clear that the roles of ECM are multiple and variable. This is aided by the discovery of novel ECM molecules, ECM-interaction mediated signaling, and the characterization of the proteases and the protease inhibitors that are responsible for ECM degradation and turnover (Rozario & DeSimone 2010; Mouw et al. 2014). In the CNS, the ECM is arranged in: diffuse interstitial matrix; condensed structures around nodes of Ranvier and in the form of perineuronal nets (PNNs) which surround the cell soma, proximal dendrites and axon initial segments of some neurons; and basement membranes surrounding blood vessels and beside the pial meninx (figure 3) (Burnside & Bradbury 2014). The ECM components in the CNS are very specialized and undergo dynamic changes in the composition and distribution providing so external cues for neurons and glial cells. In fact, CNS ECM actively influences cell migration, axonal guidance, myelination and synaptogenesis during development and in adulthood plays an important role in maintaining synaptic stability and restricting aberrant remodeling (Barros et al. 2011).

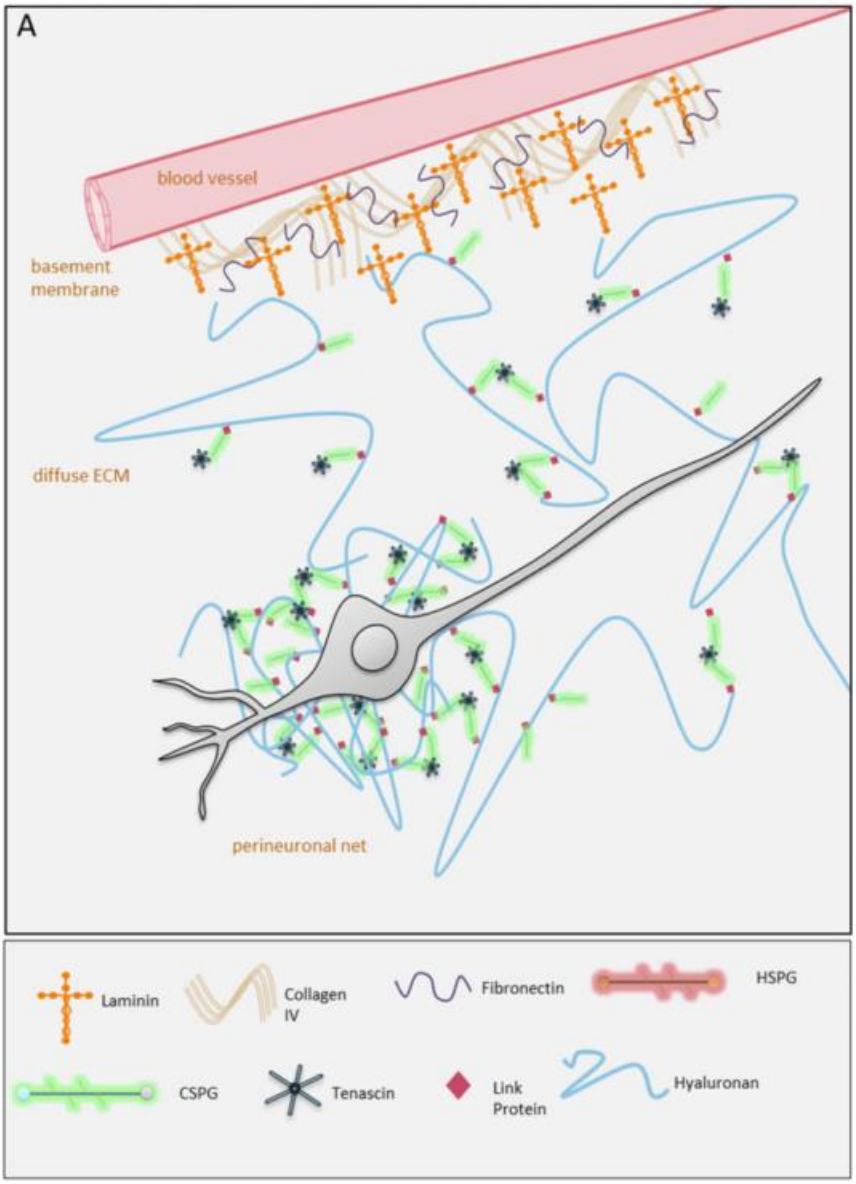

Figure 3. Structure and components of the extracellular matrix
In the CNS, the ECM is arranged in a diffuse interstitial matrix, condensed structures in the form of perineuronal nets, and in the basement membranes (Burnside & Bradbury 2014).

The diffuse and condensed ECM structures

The core component of the diffuse interstitial ECM is the hyaluronan (HA; also known as hyaluronic acid or hyaluronate) that is a linear polysaccharide. It is ubiquitously expressed in the ECM of mammals (McDonald & Camenisch 2003) and besides the contribution to the tissue hydration, mechanical properties and correct architecture, hyaluronan plays important biological functions interacting with different molecules and cell-surface receptors (Vigetti et al. 2014). Cell receptor activation has wide-ranging downstream consequences, including proliferation, cytoskeletal reorganization and regulating inflammation and its organization of other matrix components enables a complex network of protein–protein interactions. In fact, HA together with other molecules that are anchored to it organizes the extracellular space and forms the scaffold for neurons and glial cells. Glycoproteins and proteoglycans (PG), i.e. tenascins and sulfate proteoglycans, are capable of binding HA. Moreover, there are different link proteins known as hyaluronan and proteoglycan link protein (HAPLN) that have very specific function in the brain, for instance HAPLN1 stabilizes chondroitin sulfate proteoglycan (CSPG) and HA complexes and HPLN4 localizes with CSPG brevican and stabilizes PNN (reviewed in Burnside & Bradbury 2014; Evanko et al. 2007).

During brain development, HA interacts with cell surface receptors and influences cell proliferation, survival and differentiation. Additionally, high hydration of a HA-rich matrix is suggested to optimize biophysical properties of migrating neural precursor cells (Sherman et al. 1994; Toole 2001; Evanko et al. 2007). These components may be arranged diffusely in the interstitial space or in more condensed structures which comprise small ‘axonal coats’ encapsulating presynaptic terminal fibers and synaptic buttons, clustered matrix assemblies around nodes of Ranvier and PNN (Burnside & Bradbury 2014; Oohashi et al. 2015).

The PNN is a unique ECM structure that is thought to play a major role in restricting synaptic plasticity during postnatal development, and is altered in several models of neurodevelopmental disorders. PNN is most prominently displayed around GABAergic interneurons, with parvalbumin (PV) expressing cells having the highest level of colocalization (Celio et al. 1998; McRae et al.

2007). However, it was recently described a dense expression of PNNs around excitatory pyramidal neurons in hippocampal area CA2 (*cornus ammonis*), proving insight into a previously unrecognized role for PNNs in restricting plasticity also at excitatory synapses (Carstens et al. 2016). Although the exact function of the PNN is unknown, it is likely involved in the stabilization of existing synapses, the prevention of new synapses on mature neurons, the linkage of the ECM with the cytoskeleton, and may facilitate neuron-astrocyte interactions (Carulli et al. 2016). Some PNN components are hyaluronan, hyaluronan synthases (HASs), CSPGs – primarily lecticans, HAPLNs, and tenascin-R (TN-R) (Carulli et al. 2006; McRae et al. 2007; McRae & Porter 2012; Kwok et al. 2014).

An example of how ECM molecules located around synapses modulate the activities of pre- and postsynaptic receptors and ion channels is represented by the structure of the so called "synaptic quadriga or the tetrapartite synapse". These terms refer to the presence of four components in a synapse: presynapse, postsynapse, glial cells, ECM components (figure 4). The ECM can respond to network activity either by incorporating secreted molecules and shed extracellular domains of transmembrane molecules, or by freeing products of its activity-dependent proteolytic cleavage as signaling messengers (Dityatev & Schachner 2003; Dityatev et al. 2006; 2010).

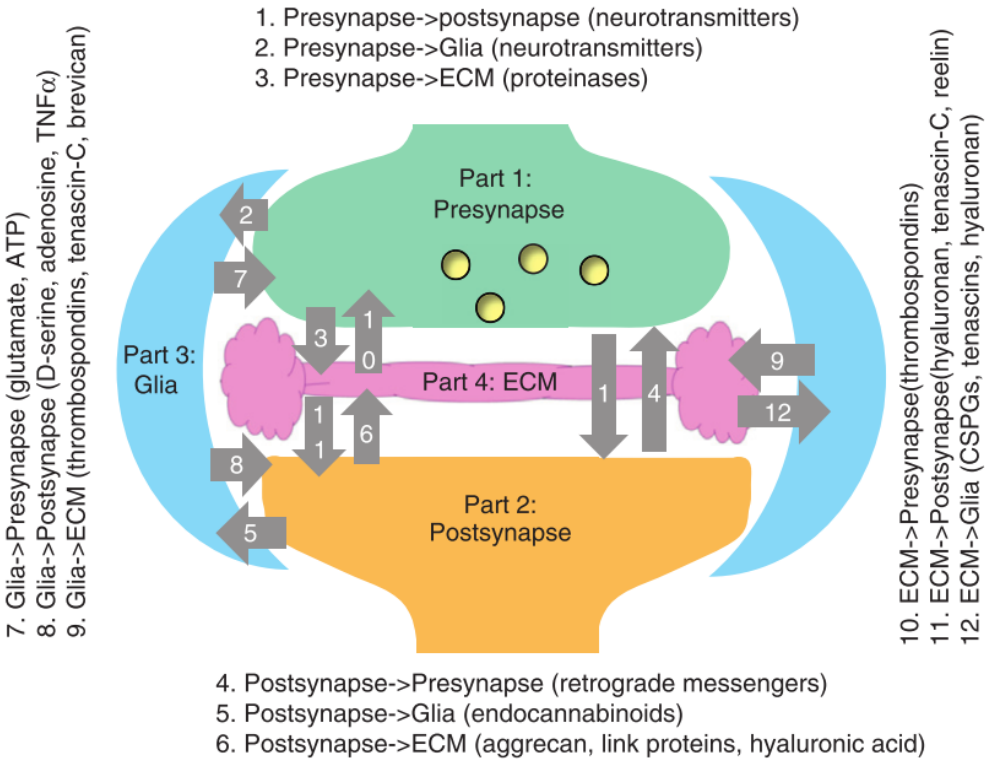

Figure 4. The tetrapartite synapse components (Dityatev et al. 2010).

The pial-meningeal basement membrane

Meninges originates from mesenchymal cells that give rise to the three-layers connective tissue structure: dura, arachnoid and pia mater (Richtsmeier & Flaherty 2013). Meningeal cells actively participate in the formation of the ECM. Collagens are the most abundant ECM structures in meninges and the most represented types are I, III, and IV. In addition to collagen, meningeal cells synthesize non-collagen proteins including fibronectin, laminin and tenascin (Siegenthaler & Pleasure 2011). Cells of the meninges have been shown to be highly responsive to numerous growth factors, trophic factors, retinoic acid, cytokines, and important mitogen including those promoting stem cell proliferation and differentiation. In fact the role of meninges is being reevaluated and updated as stem cell niche population with neural differentiation potential (Decimo et al. 2012).

Meningeal-derived factors are involved in several, critical developmental events in the brain. This raises the possibility that defects in meningeal development or function, either through genetic mutation or through damage to the meninges in utero, may underlie certain neurodevelopmental disorders in humans. It was demonstrated, for instance, that primary meningeal defects cause neocortical dysplasia and dyslamination (Hecht et al. 2010).

Immediately below the pial meningeal layer is the pial basement membrane (pBM). It is made up of a variety of ECM proteins like laminin, fibronectin, collagen IV, nidogen and proteoglycans (Timpl 1989) (figure 4).

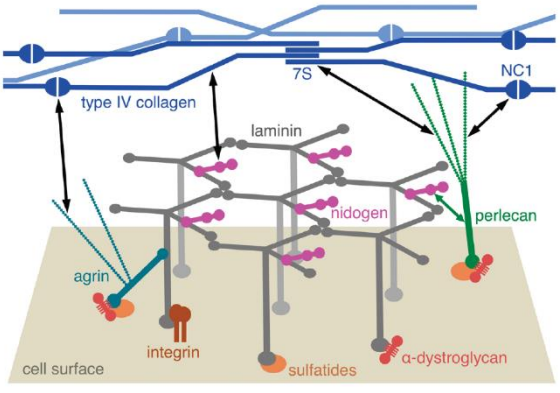

Figure 4. Laminin network is anchored to the cell surface by interactions of the long arms with cellular receptors. Collateral interactions are made with the heparan sulfate proteoglycans agrin and perlecan. The laminin and collagen networks are linked by nidogen and heparan sulfates (black double-headed arrows) (Hohenester & Yurchenco 2013).

The meninges are not required for pBM establishment but are needed for its remodeling, organization and maintenance (Sievers et al. 1994). The primary functions of pBM during brain development concern the proper cortical histogenesis and lamination (of both cerebellum and cerebral cortex). In particular its roles are to give a critical attachment point for the endfeet of radial processes (glial limitans, see later) and to provide a physical barrier for migrating neurons (Hecht et al. 2010; Choe et al. 2012). Abnormal brain development has been observed after chemical ablation of the meningeal cells (Sievers et al., 1994) and after the targeted deletions of basement membrane constituents, such as deletion of the nidogen-binding site of laminin-γ1 (Smyth et al. 1999; Halfter et al. 2002), laminin-α1 chain (Ichikawa-Tomikawa et al. 2012), and dystroglycan (Moore et al. 2002).
Moreover, many human pathologies can be grouped as "disorders of cortical development" in which defects of the basement membrane (BM) were recorded at the pial surface such as microcephaly, microlissencephaly, pachygyria and Zellweger syndrome (Francis et al. 2006).

Collagen type IV

Kefalides (1971), for the first time recognizes that BMs contain a unique collagen, different from collagens I, II and III, which he named type IV. More detailed analysis of proteolytic collagen IV fragments revealed 400 nm long flexible molecules. Collagen IV plays an important role in the BM interaction with cells (Kühn 1995) and it forms a more flexible triple helix which self-polymerizes into a network, acting as a scaffold to integrate laminin and fibronectins into sheet-like basement membrane; a matrix meshwork additionally interconnected via other glycoproteins and sulfate proteoglycans (Yurchenco 2011). This is possible thanks to an amino acid residue long triple helical segment, ~100 nm away from the NH_2-terminal end of the molecule, which appears to possess the major cell binding sites of type IV collagen. In this region, the triple helix is stabilized by intramolecular disulfide bonds and contains the recognition site for the integrin type α1β1 and α2β1 receptors (Vandenberg et al. 1991).

Laminin

Laminin consists of three polypeptide chains, A, B1 and B2, linked via disulfide bonds to form the typical laminin asymmetric cross-structure (Mecham 1991). Chains are arranged in a cruciform or T-shaped structure and contain globular (G) and rod-like domains required for self-assembly, polymerization with adjacent laminins and interaction with other molecules, such as the collagen IV scaffold and receptors. Laminin polymerization occurs via interactions between the N-terminal G domains of the short-arms and cell surface interactions are thought to occur predominantly through the longest arm via a tandem of five laminin G-like domains of the α-chain C-terminus (Yurchenco & Cheng 1993; Hohenester & Yurchenco. 2013). Considering the data from BM protein knockouts, it was suggested that laminin is sufficient for basement membrane-like matrices during early development, but at later stages of development, the specific composition of components including collagen IV in the BM defines the integrity, stability and functionality of the BM itself (Pöschl et al. 2004). Laminin is a protein with adhesive properties therefore it is essential for BM assembly (Timpl 1989; Smyth et al. 1999; McKee et al. 2007). It is the major player for the attachment of the radial glial endfeet to the pBM and it has been suggested that in the cerebellum could be used by granule cells to initiate their migration (Selak et al. 1985; Sasaki et al. 2004; Berrier & Yamada 2007;).

Reelin

Another ECM molecule is reelin, whose extracellularly presence is important for neighboring cells and it confers to pBM important functions. It is actively involved in signaling to orient neurons for reaching their correct positions. Reelin is an extracellular glycoprotein with a crucial role during neurodevelopment and in postnatal period participating in regulation of dendritic and axonal growth, synaptogenesis, neurotransmission and contributing to synaptic plasticity necessary for learning and memory functions (Lakatosova & Ostatnikova 2012). The discovery of the gene was possible thanks to a spontaneous mutant mouse named reeler, firstly described in 1951 (Falconer 1951). Further studies allowed the identification of the extracellular

protein reelin (D'Arcangelo et al. 1995). The reeler mice present severe motor defects (Falconer 1951) and impaired migration of cortical neurons, leading to an inversion of the cerebral cortex organization (inverted cortex) (reviewed in Rakic & Caviness 1995 and Ross & Walsh 2001) and in the cerebellum development (Mariani et al. 1977; Mikoshiba et al. 1980). Reelin starts to be expressed and secreted during embryonic development, then in postnatal cerebellum the stainining does not present regional differences but is restricted along the pial surface: reelin is expressed by the internal granule cell layer and by cells present in the inner part of the external granule cell layer (Hirotsune et al. 1995), after P10 to P20 there is no more extracellular and intracellular reelin with the exception of the pial basement membrane (Miyata et al. 1996; D'Arcangelo 2014).
Recent evidence has shown that the reelin signaling system contributes to synapse formation and density and acts as a modulator of synaptic transmission and synaptic plasticity by regulating Ca^{2+} entry through N-methyl-D-aspartate (NMDA) receptors (Senkov et al. 2014; Beffert et al. 2005; Chen et al. 2005; Groc et al. 2007; Ventruti et al. 2011).

1.2.2 ECM-remodeling enzymes

The ECM components and their respectively functions change during the different developmental stages and from the adulthood to aging, as well as from healthy to diseased CNS. Therefore, there should be many levels of regulation of individual ECM components either by controlling their expression or by post-translational modifications. Important posttranslational ECM modifiers include extracellular proteases, such as the matrix metalloproteinases (MMPs), in which family is also comprised the prolidase enzyme, and their physiological antagonist, the tissue inhibitors of MMPs (TIMPS). Even the expression pattern of MMPs and TIMPs change over time, during physiological and pathological states and after chemotherapeutic treatments. It is important to highlight that the balance between MMPs and TIMPs in the extracellular environment is important since it determines the tissue remodeling and pathological status beat this balance and affects the ECM component and integrity (Yong et al. 1998;

Agrawal et al. 2008; Iyer et al. 2012). Then, since the tissue-remodeling enzymes are important also during the brain development, their perturbation during this critical period could alter the morphology and histology of the tissue. Regional and cell-specific expression of MMPs and TIMPs in the brain closely reflects the successive stages of neuronal development, thereby suggesting a pivotal role for ECM proteolysis in brain development and plasticity (Vaillant et al. 1999; Ulrich et al. 2006; V. M. Piccolini et al. 2012b).

MMP

The first MMP (MMP-1) was identified by Jerome Gross and Charles Lapiere in 1962 in tadpole (Gross & Lapiere 1962). Since then, a large family of MMPs has been described in various species. In 1971, MMPs were shown to be biosynthesized as inactive precursors (zymogens) that require activation (Harper et al. 1971). Currently, 24 human MMP homologues have been described and are usually categorized counting six sub-families: collagenases (MMPs-1, -8, and -13), gelatinases (MMPs-2 and -9), stromelysins (MMPs-3, -10, and -11), matrilysins (MMPs-7 and -26), membrane-type metalloproteinases (MT1-6-MMPs, also referred to as MMPs-14, -15, -16, -17, -24, and -25), and other MMPs (MMPs-12, -18, -19, -20, -21, -22, -23, -27, and -28) (Rempe et al. 2016). Despite this classification, the profile of almost all of the MMPs has been investigated and emerged that MMP substrates are extremely wide-ranging and many are highly nonspecific. As an example, while MMP-3 degrades candidate CSPGs upregulated after CNS injury, it also degrades collagen types II, III, IV, IX and X, fibronectin, laminin and elastin and activates other MMPs including MMP-1, MMP-7 and the pro-inflammatory MMP-9; aggrecan, as an example, is cleaved by MMP-1, -2, -3, -7, -8, -9, -11, -13, -14, -15, -19, -20. Therefore, there is redundancy and for that is very difficult to make a precise connection between MMPs and targets. In general, MMPs participate in many physiological and pathological processes in the brain, in both development and adulthood (Overall 2002; Malemud 2006; Agrawal et al. 2008; Candelario-Jalil et al. 2009; Iyer et al. 2012; Burnside & Bradbury 2014; Rempe et al. 2016) as it is shown in figure 5.

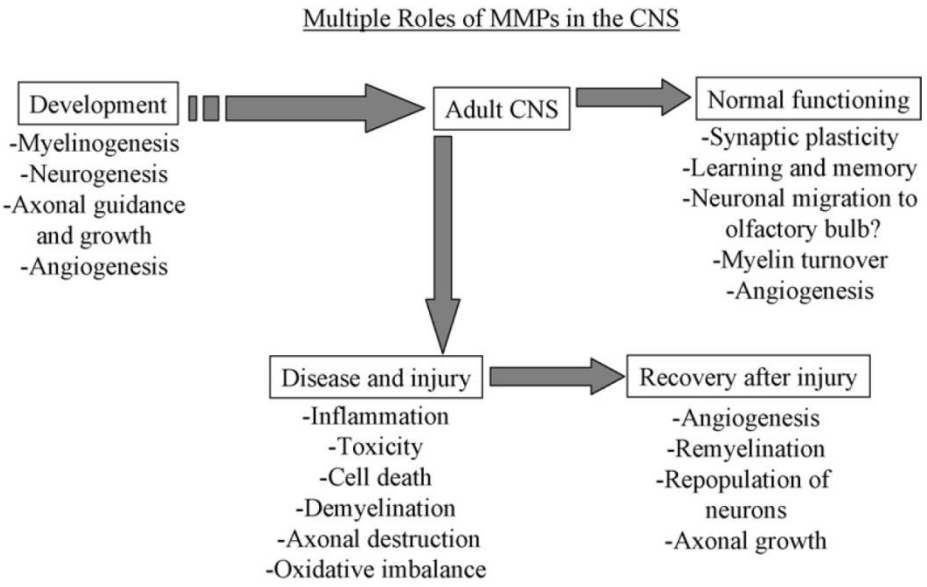

Figure 5. Multiple roles of matrix metalloproteinases in Central Nervous System (CNS) development, normal adult physiology, and in response to injury (Agrawal et al. 2008).

The expression of MMPs in the nervous tissues, considering both constitutive and induced expression, vary enormously between regions, cell types and species. For instances, in the cerebellum MMP-2 and MMP-9 have been the most frequently investigated. They are involved in different neuronal functions including migration, process extension and synaptic plasticity especially during cerebellar morphogenesis. They share many targets as: collagens (type IV, V, and XI), gelatin, elastin, fibronectin, vitronectin, laminin, entactin, tenascin, SPARC, aggrecan, link protein, galectin-36, versican, decorin, myelin basic protein. In addition MMP-2 acts also on fibronectin and other collagen types (Ayoub et al. 2005; Nagase et al. 2006; Milward et al. 2007; Verslegers et al. 2015). MMP-3 is linked to neuronal migration and neurite outgrowth and guidance in the developing CNS and contributes to synaptic plasticity and learning in the adult CNS. Moreover, a strict spatiotemporal MMP-3 up-regulation in the injured or diseased CNS might support remyelination and

neuroprotection, as well as genesis and migration of stem cells in the damaged brain (Van Hove et al. 2012). According to the cell specificity and timing, an example in represented by the pattern of MMPs expressed in the cerebellum. In rats high levels of MMP-2 and low levels of MMP-9 are found in the mature Purkinje and granule cells, while high levels of MMP-3 and MMP-9 have been detected at post-natal day 15 (P15) when a high rate of synaptogenesis occurs (Vaillant et al. 1999). In the mouse cerebellum, MMP-24 appears in post-natal neurons and associates with the dendritic tree formation of Purkinje cells in the cerebellum and it localized in neurons of the growth cone. Therefore, it was proposed that MMP-24 functions to promote neuronal and axonal growth (Hayashita-Kinoh et al. 2001).

TIMP

The tissue inhibitor of metalloproteinases (TIMPs 1-4) inhibit the MMPs activation, forming a complex with the pro-MMPs, therefore they are able to modulate and regulate the MMPs action. In addition to their anti-MMP activity, TIMP-1, -2 and -3 also have other biological functions, such as regulation of cell proliferation, survival and angiogenesis (Jiang et al. 2002; Luo 2005). TIMP-1, TIMP-2 and TIMP-4 are present in soluble forms while TIMP-3 is tightly bound to the matrix. TIMPs inhibit all MMPs tested so far, but seems that there are some preferences in the targets. For instances, TIMP-1 and TIMP-2 preferentially associate with MMP-9 and MMP-2, respectively, while TIMP-3 with both. TIMP-2 and TIMP-3, unlike TIMP-1, are also effective inhibitors of the membrane-type MMPs (MT-MMPs) that contain a transmembrane C-terminal domain anchoring the enzymes to the cell surface, which are MMP-14, MMP-15, MMP-16, MMP-17, MMP-24 and MMP-25. TIMP-4 can also binds to the C-terminal domain of proMMP-2. In the meantime, TIMP-3 has been shown to inhibit also the family of α disintegrin and metalloproteinase (ADAM) and the ADAMTS (ADAM with thrombospondin motifs) (Lambert et al. 2004; Nagase et al. 2006; Iyer et al. 2012).

Even for TIMPs there is a cell specific expression: cerebellar TIMP-1, TIMP-2 and TIMP-3 appear to be expressed by Purkinje cells, and TIMP-2 and TIMP-3 by granule (Vaillant et al. 1999).

1.3. The post-natal development

The development of the CNS begins in the early prenatal life. Most of the neurons of the adult CNS born during the prenatal and early postnatal periods. However, the development and maturation of the CNS are continuous processes extended to the post-natal life, although in less extent and in restricted regions (Altman 1969a,b; Paxinos et al. 2007; Bandeira et al. 2009; Fu 2013). The main histogenetic processes of neural development include the proliferation of stem cell precursors, differentiation of cells in neurons or glial cells and the migration of immature cells from their birthplaces in the embryo to their final positions. Then, there is outgrowth of axons and dendrites from neurons, guidance of the motile growth cone through the embryo towards postsynaptic partners, synaptogenesis and finally the lifelong changes in synapses in the form of synaptic plasticity (Altman 1982; Rice & Barone 2000; Martinez-Ferre & Martinez 2012). Moreover, the proper development cannot disregard from apoptosis, a form of programmed cell death that systematically removes large number of neurons in some structures produced during ontogeny. Apoptosis occurs during both pre- and postnatal development of the CNS in two waves. The earlier wave occurs in proliferative zones; the second occurs in post-mitotic cells that are both neuronal and glial cells (Rothenberg et al. 1994; Blaschke et al. 1996; Lossi and Merighi 2003). All these processes lead to the establishment of functioning and correct neuronal connections making finally anatomical regions with specific programs of structural and functional maturation (Rice & Barone 2000; Martinez-Ferre & Martinez 2012). The development of brain is a critical issue and it is subjected to environmental cues like substrates, chemoattractive/chemorepulsive factors, and detachment/stop signals. In this view a particular role is played by the extracellular matrix as discussed later and cytoskeleton (Cayre et al 2009; Sanchez-Arrones et al. 2012; Jiang & Nardelli 2016).

1.3.1 Role of cytoskeleton in CNS development

The shape, polarization, migration, and cell-connectivity of all cell types are dictated by intracellular filamentous network of proteins that constitute the cytoskeleton. The dynamics of the cytoskeleton in terms of polymerization and depolymerization, the organization of cytoskeletal proteins in higher-order structure or architecture, and the orchestrated interplay between cytoskeletons are essential events beside the nervous system development. It is possible to recognize different proteins such as the microfilaments of actin, intermediate filaments that in neurons are neurofilaments, and microtubules. Moreover, there are many cytoskeleton-associated proteins that regulate their dynamics and organization within the cells and during the different developmental stages of the brain (Yamada et al. 1970; Matus 1988; Lian & Sheen 2015; Menon & Gupton 2016). For instance, it was demonstrated that microtubule dynamics is essential for neuron-specific migration (Kawauchi 2015). Several cytoskeleton proteins change in their rate of expression, degree of phosphorylation, subcellular distribution, or biochemical properties during the different developmental stages. For instance, phosphorylation is an essential mechanism to regulate the plasticity of the early juvenile-type cytoskeleton. Among such proteins, several are microtubule-associated proteins (MAPs) or tau proteins (belonging to the MAPs/tau family). Phosphorylation may also act on neurofilaments, postulated to be involved in the adult-type stabilization of axons (Riederer 1992).

Microtubule-associated proteins/tau family

Three MAP (1-3) species have been shown to be differentially distributed in the brain, differing in both cell type and intracellular localization. Whereas MAP4 is present in many other tissues but is generally absent from neurons. MAP1 is associated with neurons in the adult brain and is more abundant in dendrites than in axons. MAP2 is also neuron specific and is predominantly located in dendrites. MAP3 occurs in both neurons and glia, but in neurons it is restricted to neurofilament-rich axons (Riederer & Matus 1985; Menon & Gupton 2016). As known, microtubules exhibit dynamic instability, the MAP2 is able to bind

and stabilize microtubules, increases microtubule rigidity, and induces microtubule bundles formation. Moreover, MAP2 can bind both microtubules and F-actin. There are three main forms of MAP2: a, b and c. MAP2c, which is relatively short, represents the juvenile isoform and is downregulated after the early stages of neuronal development. MAP2a and MAP2b have longer projection domains; in particular, MAP2b is expressed during both development and adulthood, while MAP2a becomes expressed when MAP2c levels are falling and is not detected uniformly in all mature neurons. These suggest that the presence of MAP2 is important for the different stages of neuronal development as well as cortical histological development (Yamada et al. 1970; Matus 1988; Komuro et al. 2001; Dehmelt & Halpain 2004; Francis et al. 2006).

In the brain, smaller splice forms of tau (of 50-65 kDa) are differentially expressed during early development as well as in pathological conditions. Tau is a major microtubule-associated protein, which was discovered, purified and characterized as a microtubule assembly- promoting factor by groups of Kirschner and Nunez (Weingarten et al. 1975; Cleveland et al. 1977; Fellous et al. 1977). Specifically, tau isoforms with three microtubule-binding repeats are predominantly expressed during early development, whereas isoforms with four repeats are expressed during adulthood. In addition, high-molecular-weight variants of tau (110-120 kDa) are expressed in peripheral neurons and also at a much lower level in the brain.

During normal development, tau protein undergoes various posttranslational modifications, including phosphorylation, glycosylation, glycation, ubiquitination, truncation, nitration, etc. As an increased amount of the modified tau has been found in a large number of neurodegenerative disorders, the study of tau in pathological conditions was intensified. In particular, considering the phosphorylation, it is possible nowadays to have a huge amount of information on the relation between the phosphorylation sites of tau amino acid residue and biological functions. The binding of MAP2/tau family proteins stabilize microtubules as it was already described. This binding can be regulated by the phosphorylation of the KXGS motif within each microtubule-binding repeat, leading to a decreased affinity for microtubules.

The expression and phosphorylation of tau seem developmentally regulated. The hyperphosphorylation of tau residues is found during embryonic development and in early postnatal period while a much lower level of tau phosphorylation has been detected in adulthood (Goedert et al., 1993; Johnson & Stoothoff 2004). However, tau becomes hyperphosphorylated during neurodegeneration, suggesting an immanent relationship between neuronal development and degeneration. What is surprisingly is that the specific amino acid residues that characterize the hyperphosphorylation in embryo and post-natal brain are in common with those found in degenerating neurons, including Thr181, Ser198, Ser199, Ser202, Thr217, Thr231, Ser235, Ser396, Ser400, Thr403, Ser404 and Tyr394 (Goedert et al. 1993; Illenberger et al. 1998; Delobel et al. 2002; Avila et al. 2004).
Aberrant phosphorylation patterns appear associated with different neurological diseases, collectively named tauopathies, such as: Alzheimer's disease, Amyotrophic lateral sclerosis/parkinsonism-dementia complex, argyrophilic grain disease, chronic traumatic encephalopathy, corticobasal degeneration, down's syndrome, mytotonic dystrophy, Niemann–Pick disease type C, Pick's disease, prion protein cerebral amyloid angiopathy and progressive subcortical gliosis (Hernández & Avila 2007; Medina et al. 2016).

1.3.2 Cerebellum and postnatal development

In mammals, the cerebellum ("little brain") is a structure located at the back of the brain, underlying the occipital and temporal lobes of the cerebral cortex. Although the cerebellum accounts for approximately 10% of the brain's volume, it contains over 50% of the total number of brain neurons (Constantin et al. 2006). The cerebellum is most understood in terms of its contributions to motor control; however it is also involved in certain cognitive functions, such as emotion and language processing (Schmahmann 2004; Tavano et al. 2007) and spatial navigation that is an active process requiring accurate and dynamic representation of location, determined by the combination of both external and self-motion cues (Rochefort et al. 2013).

The cerebellar cortex differs from the cerebral one for its uniform structure, divided in ten lobules (I-X) in which cells are organized in three layers (from the outer to the inner: molecular layer, Purkinje cell layer, internal granule layer) at the mature stage. The development of the cerebellum goes from the 4th week of gestational stage to the 20th month after birth in humans, and to 21-22 days after birth in rodents (Millen et al. 1994). The development of the lobules occurs according to a specific temporal pattern: the I and X lobules are formed firstly and the last are VIb, VII and VIII. Even the formation of each single lobule follows a well defined order: the basal zone develops at the beginning and then the apical one (figure 6) (Altman 1982).

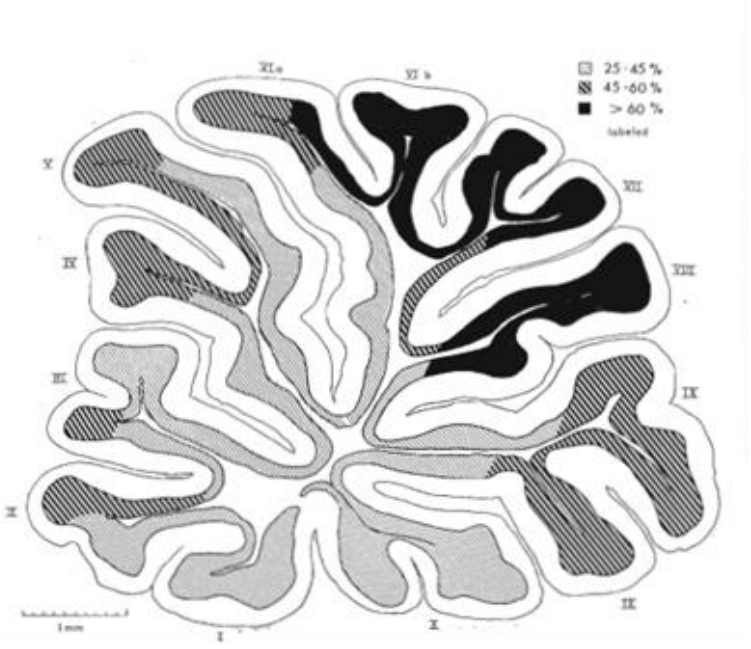

Figure 6. Schematic representation of the progressive development of the lobules in a sagittal section of the cerebellar vermis. Regions where less than 45% of the cells could be tagged are considered early forming (light grey); those where more than 60% of the cells were labelled are late forming (black) (Altman 1982).

From the prenatal toward the post-natal stage, the layering of the cerebellar cortex undergoes changes in structure and cell-composition (figure 7).

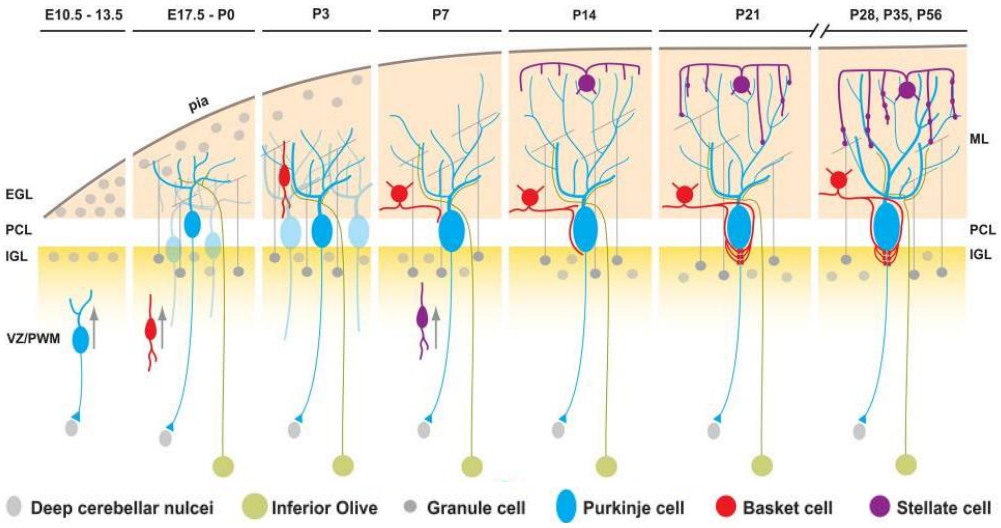

Figure 7. Schematic representation of the anatomical changes during cerebellar development with emphasis on the postnatal stages (Paul et al. 2012).
E: Embryonic; P: Postnatal; ML: Molecular Layer; PCL: Purkinje Cell Layer; IGL: Internal Granular Layer; EGL: External Granular Layer; VZ/PWM: Ventricular Zone/Prospective White Matter.

During the embryonic development, the ventricular zone (VZ) is responsible for the generation of inhibitory neurons, whereas the rhombic lip for the glutamatergic neurons. In particular, Purkinje cells are produced at the onset of cerebellar neurogenesis in VZ microdomains and acquire mature phenotypes largely according to cell-autonomous programs. On the other hand, the different classes of inhibitory interneurons, including basket and stellate cells, derive from a single population of precursors that delaminate into the prospective white matter, where they continue to divide until the end of the first postnatal week (Altman & Bayer 1997; Leto et al. 2012). During early postnatal life, at least in rats and mice, the Purkinje cell undergoes numerous changes. Initially Purkinje neurons are organized in a multilayer structure and then their soma

spread into a monolayer, orientating the dendrites toward the pial surface with the subsequent outgrowth of its dendritic branches. The settling of Purkinje cells into a monolayer has been hypothesized to be a mechanical process due to the migration of granule cells below and growth of parallel fibres above the Purkinje cells. In pathological cases where the granule-cell population is disrupted, the Purkinje cells are poorly aligned in a rather ragged layer, and the Purkinje cell dendrites exhibit altered morphologies ranging from stunted to misoriented dendritic trees (Altman & Bayer 1997; Goldowitz & Hamre 1998). Moreover, the correct positioning and development of Purkinje neurons is strongly correlated to some ECM cues. For instances, lack of reelin leads to defects in the *reeler* mice cerebellum showing defects in the layering with errors in cell positioning, and with Purkinje cells that were decreased in size, distributed in a multilayer and with abnormal dendrites (Mariani et al. 1977; Mikoshiba et al. 1980; Rice & Curran 2001; Castagna et al. 2014). Indeed, as it was already mentioned, this molecule provide positional information to migrating neurons that instructs them to stop and detach from their guides. Therefore, the close proximity of reelin-producing cells to granule and Purkinje cells is critical for the subsequent organization of the cerebellar cortex (Frotscher 1997; Lakatosova & Ostatnikova 2012). In particular, during embryonic development, reelin is expressed by Cajal-Retzius cells that are located at the pial surface. Whereas, during postnatal cerebellar development, reelin is expressed by the internal granule cell layer and by cells present in the inner part of the external granule cell layer (Hirotsune et al. 1995).

Another important process in the postnatal development of the cerebellum is the rearrangement of granule cells within the layers. Around the 7^{th} day of embryonic life, close to the pial surface the granule cells are organized in the so called external granular layer (EGL) that initially covers the majority of the cerebellar surface and with time decreases in thickness. In the very first stages of the postnatal development a clonal expansion of the half surface of the EGL occurs, followed by the production of post mitotic granule cells. These post mitotic cells are able to migrate from the EGL toward their final collocation, named internal granular layer (IGL). This process ends around the 3^{rd} postnatal week in rodents leading to the complete disappearance of EGL and the

establishment of IGL (Miale & Sidman 1961; Altman 1972; Xu et al. 2013). There are two different modes of granule neuron migration, the radial and tangential that are classified according to the relative direction taken by the migrating neuronal precursor cells. Both of these migratory patterns are involved in determining the final position of granule neurons in the cerebellum during development. In the early postnatal cerebellum, the cerebellar granule cells in the EGL migrate tangentially. At the interface of the EGL and ML of the mouse cerebellum, pairs of granule cells begin to migrate in a radial pattern across the ML along the Bergmann glial processes (the astrocytes of the cerebellum) (figure 8) (Komuro et al. 2001; Komuro & Yacubova 2003; Xu et al. 2013).

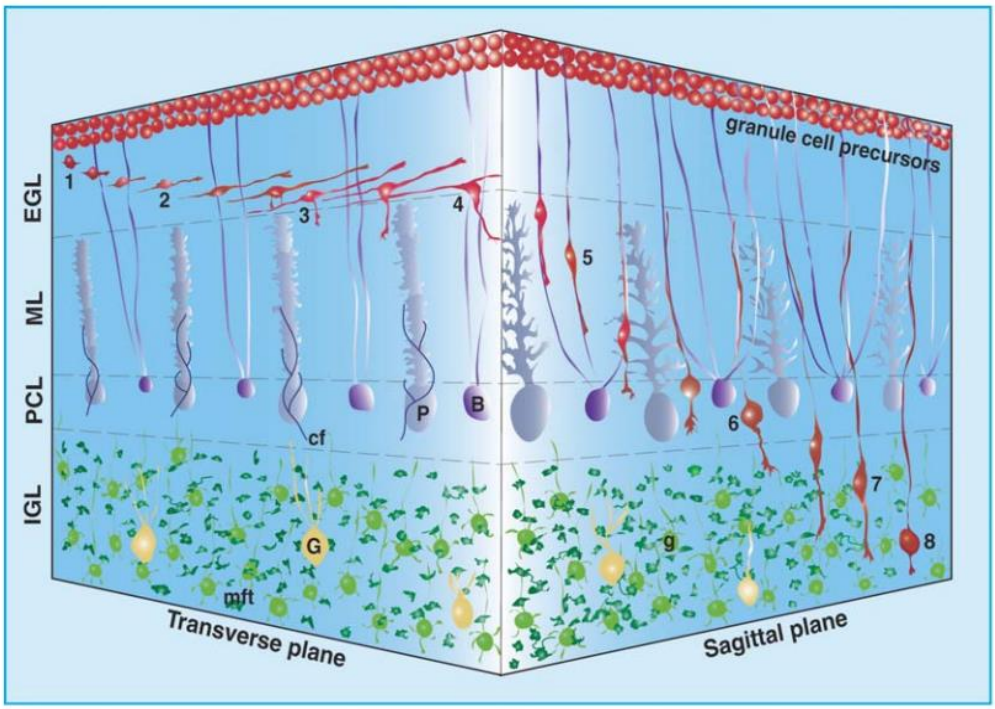

Figure 8. Granule cells migration in tangential and radial directions during cerebellar development through the Bergmann glia fibers. P, Purkinje cell; B, Bergmann glia; G, Golgi cell; g, postmigratory granule cell; cf, climbing fiber; mft, mossy fiber terminal (Komuro & Yacubova 2003).

Even in this case, the ECM molecules give a fundamental contribution to the correct cerebellar development. In fact the pBM, and in particular laminin, is used by Bergmann glial fibres as an anchor point. From the attachment of the endfeet of radial glial fibres to the pBM depends the correct migration of granule cells (figure 9) (Selak et al. 1985; Siegenthaler & Pleasure 2011; Morrens et al. 2012; Xu et al. 2013).

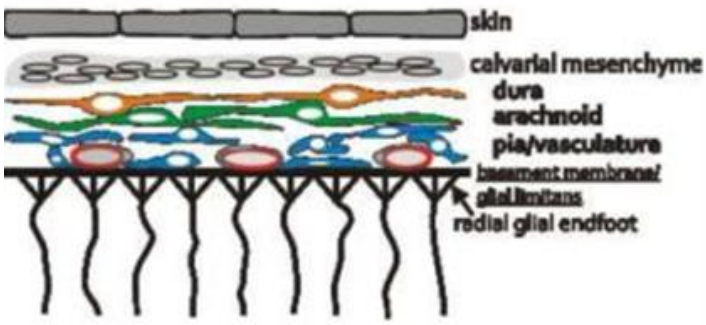

Figure 9. Relation between meninges, pBM and radial glial endfeet. (Siegenthaler & Pleasure 2011)

In fact, laminin deficient mice showed defects in the conformation of pBM, with a decrease in the proliferation and migration of cerebellar granule cell precursors, and disorganization of the Bergmann glial fibers and endfeet. A marked reduction in numbers of dendritic processes in Purkinje cells was also observed, since, as it was already mentioned, the migration of granule cells is important for the Purkinje cell development (Ichikawa-Tomikawa et al. 2012).
Moreover, a huge number of different molecules and signaling pathways are involved in radial migration of granule cells along Bergmann glia during cerebellum development; here follows some examples. The intracellular signaling pathways such as Sonic Hedgehog (SHH), Notch, TGF-β, and Wnt/β-catenin have been indicated to play key roles in proliferation, fate determination, growth and maturation of Bergmann cells; thyroid hormones are also important in the cerebellum development (Martinez et al. 2011); immunoglobulin superfamily (IgSF) molecules are actively involved in cell-cell adhesion, neuronal migration, axonal guidance and synapse formation in the nervous system; G-actin-binding proteins essential for cytoskeletal dynamics are involved in neuronal migration, cell-cell adhesion and synaptic physiology

(Rust et al. 2012); a novel role for vascular endothelial growth factor (VEGF) in the control of cerebellar granule cell migration from EGL toward the Purkinje cell layer (Ruiz de Almodovar et al. 2010).

It is important to highlight that the cerebellar development is a critical ensemble of events that should be perfect orchestrated. Defects during development can also arouse spontaneously in the form of heterotopic neurons and glia in the molecular layer of the vermis. Usually these malformations are almost exclusively found along the primary fissure and suggest defects in neuronal migration during cerebellar development. These alterations are often associated to anomalies in the integrity of pBM (Griffin et al. 1980; Necchi et al. 2000; Necchi & Scherini 2002; Cerri et al. 2010; Ramos et al. 2013; Van Dine et al. 2013; Ramos et al. 2015).

The emergence of the mature brain requires that appropriate synaptic connections are formed (synaptogenesis) and refined, which in the rodent cerebellum occurs primarily during the first three postnatal weeks (in other species the process is similar but with different timing). Developing circuits typically differ substantially from their mature counterparts, which suggests that development may not simply involve synaptic refinement, but rather involves restructuring of key synaptic components and network connections (figure 10) (van Welie et al. 2011).

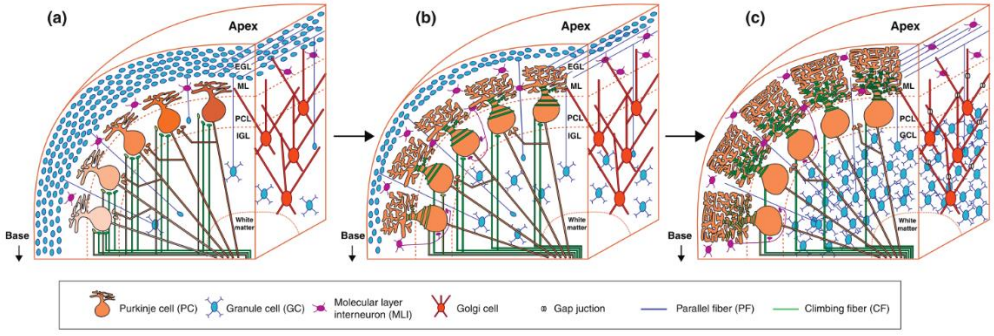

Figure 10. Synaptogenesis and synaptic remodeling during the cerebellar development in rodents (van Welie et al. 2011).

Considering the Figure 10, it is possible to compare the different developmental stages that correspond to postnatal week 1 (a), postnatal week 2 (b), and adult (c) in rodent. Purkinje neurons exhibit the phenomenon called "traveling waves" that consist in the connection of one to one Purkinje neuron and the transmission of the activity (depolarization or hyperpolarization) from one Purkinje neuron to the closest. This transmission of activity is travelling from one Purkinje to the other one in a process whose progress can be considered a wave-like. The travelling wave described in Purkinje cells was restricted to the developing cerebellum and is absent in the mature/old cerebellum. This could be due to reduction in the connectivity rate, with the majority of Purkinje–Purkinje synapses being pruned by the third postnatal week. This means that this process is critical in establishing the accurate synaptic connectivity of a future mature circuits (Watt et al. 2009). These traveling waves are showed in the first postnatal week (illustrated by orange colour gradient in a), reduced in number by postnatal week 2 (b), and absent in adult (c). Purkinje neurons receive multiple somatic climbing fibres (CF) inputs (green) in the 1st postnatal week, with one winner CF innervating the dendrites by the 2nd postnatal week, with at least 1 weaker somatic inputs remaining (b). Mono-innervation of Purkinje neurons by CFs is seen later in adulthood (c). Granule cells (blue) migrate from the EGL to the IGL during the 1st (a) and 2nd (b) postnatal week. Molecular layer (ML) interneurons (MLI) (purple) innervate Purkinje neurons and each other in the 2nd postnatal week (b), and in the adult (c). Golgi cells (red) exhibit gap-junction coupling in the adult (c), although possibly earlier as well (not shown).

The synaptogenesis as well as the synaptic stability depend also on the integrity of ECM in the form of PNN, as already mentioned. In fact, it was demonstrated that enzymatic degradation of the PNN, using chondroitinase or hyaluronidase leads to increased number of synaptic puncta on the neurons (McRae & Porter 2012; Pyka et al. 2011). Moreover, the presence of ECM-adhesion molecules at the level of synapses ensures the synaptic structure and the compartmentalization of receptors and other proteins within the synaptic cleft (Levy et al. 2014).

At the end of all histological processes and synapses metamorphosis in the mature cerebellum cortex it is possible to recognize three layer-structure. The outer **molecular layer** that contains granule neuron axons (parallel fibres), climbing fibres, Purkinje and Golgi cell dendrites, Bergmann glial fibres, basket and stellate cells. The middle **Purkinje cell layer** that contains the Purkinje cells and Bergmann glial bodies, forming the border between the granule and molecular layer. The **inner granule cell laye**r that contains the granule, Lugaro, brush and Golgi cells. In Figure 11 are illustrated the interactions of Purkinje neurons with the some of the other cells within the mature cerebellar circuit (Altman 1982; Komuro et al. 2001; Ito 2006; Nieuwenhuys et al. 2010).

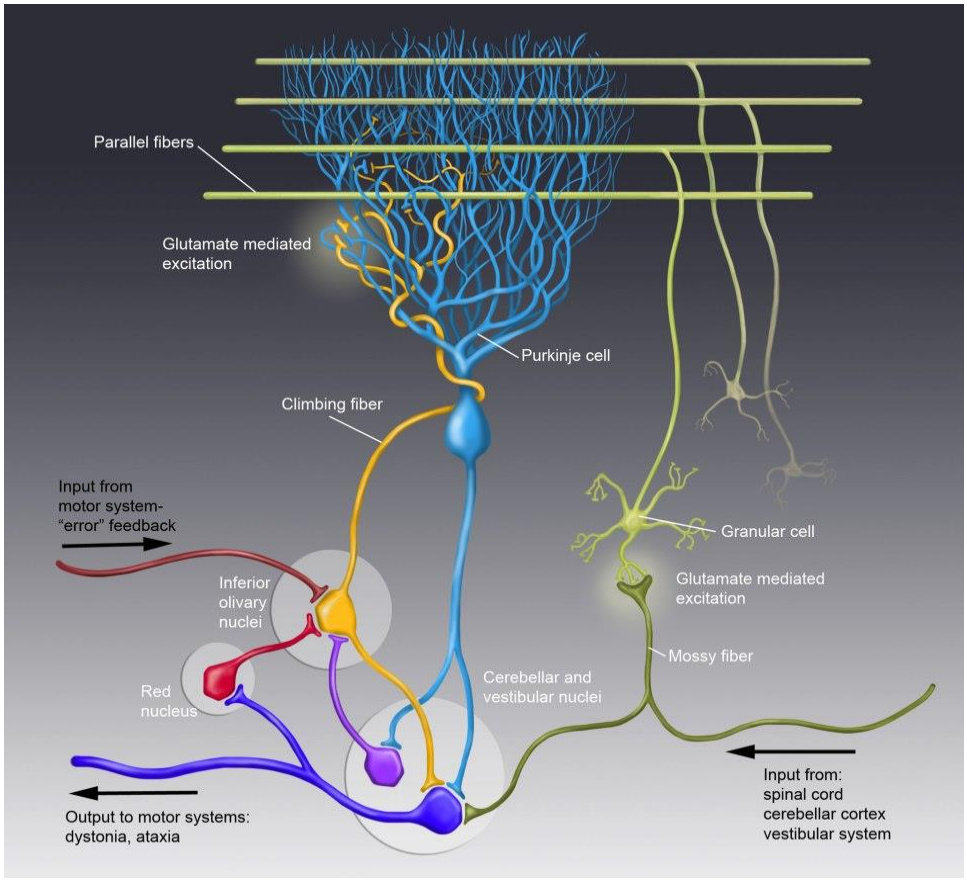

Figure 11. Mature cerebellar circuit (Bell's Palsy; Neuroanatomy 2013).

2. AIM OF THE RESEARCH

This research started in 2012 from the collaboration between Prof. A Forlino of the Molecular Medicine Department (Biochemistry Unit) and Prof. G Bernocchi and Dr. MG Bottone of the Biology and Biotechnology Department (Cell Biology and Neurobiology laboratory) at the University of Pavia.

Prof Forlino's laboratory is the international centre for the biochemical and molecular study of PD. She proposed the collaboration with our laboratory to verify the presence of possible brain anomalies in the PD mouse model (dark-like mutant mice), in the reason of human mental retardation phenotype of this pathology.

Since the onset of the pathology is variable (from early childhood until adulthood), we decided to study the postnatal brain development as well as the adult brain of *dal* mice. Moreover, the postnatal development is a critical period in which many of the ontogenetic processes are still occurring. Therefore, this gave us the possibility to investigate not only anatomical and morphological aspects but also dynamic events whose timing, regulation and march are fundamental for a correct brain maturation.

During the work of my Ph.D thesis I evaluated whether and when the prolidase activity induces damages in the developing and adult brain and I started the characterization of morphological alterations in the cerebellum, neocortex (Insolia & Piccolini, 2014) and hippocampal formation in *dal/dal*, *dal*/+ and wt mice.

The study of cerebellum proceeded during the years and was the main project of this Ph.D thesis while the anomalies found in the neocortex and hippocampus were not presented here in details, however, results were discussed together with the one of the cerebellum since they share same points.

After confirming the presence of brain anomalies in *dal* mice, the aim of the research was a more thorough the investigation on the postnatal cerebellar development.

2. AIM OF THE RESEARCH

The research plan considered different topics:

1. The analysis of **ECM components and ECM remodeling enzymes** since prolidase is involved in ECM remodeling. In particular the attention has been focused on **pial basement membrane** due to its critical involvement in regulation of cortical lamination and histogenesis.

2. The study of key events in **postnatal development of cerebellum**: granule cells proliferation and migration; morphological Purkinje neurons differentiation; cerebellar circuit synaptogenesis and maturation.

3. The investigation of **calcium homeostasis** considering CBPs and plasma membrane Ca^{2+} ATPase for the internalization and buffering of Ca^{2+}.

4. The evaluation of **cytoskeleton stability** and dynamics; the further analysis of hyperphosphorylation tau presence in Purkinje neurons in relation to other neuronal types that synapse with them.

3. MATERIALS and METHODS

3.1. Mouse Model

The prolidase deficiency dark-like mice (dal/+), on a mixed CBA × C3H background, were provided by Dr. Gunn TM (Great Falls, MT) and C3H wild-type (wt) mice were purchased from Charles River. The animals were maintained under standard experimental animal care protocol following the Italian Laws (Protocol N 1/2010) in the animal facility at the Department of Molecular Medicine of the University of Pavia (Italy). The animals were sacrificed at different postnatal ages: 10 postnatal day (P10), P21, P30 and P60 to study the postnatal development in *dal* mice. Five mice for each genotype (wt, *dal/+* and *dal/dal*), per each postnatal day were considered. In addition, other three mice per genotype were analyzed at P10 and P60.

3.1.1. Genotyping

To detect the presence of the mutant allele lacking 4bp in exon 14, genomic DNA was extracted from tail clip biopsies (at P21 or in case at P10). Biopsies were digested in lysis buffer (100 mM Tris-HCl pH 8.5, 5 mM EDTA, 0.2 % SDS, 200 mM NaCl, 1 mg/ml K proteinase; Sigma, USA) overnight at 55°C. The lysate was centrifuged for 5 minutes at the highest speed, supernatant was transferred into new eppendorf and the DNA was precipitated with the same volume of isopropanol. The sample was centrifuged for 15 minutes at the highest speed and the supernatant was removed; a final wash with ethanol 70% was performed to eliminate salt traces. The DNA pellet was re-suspended in TE (10 mM Tris-HCl, 1 mM EDTA, pH 8.0) at 55°C overnight and the final concentration of DNA was determined through the spectrophotometer at 260 nm. The DNA was kept at -20°C. Then, the mutant allele was PCR amplified using the following primers: 5'-AGCGCATCGATGAACCTG-3', sense and 5'-TCCAAGAGGTGGTCAATGAA-3', reverse. The amplification reaction was conducted using 100-300 ng of genomic DNA, 1.5 mM MgCl2, 0.2 mM dNTPs, 0.3 mM of primers and 2 U of Taq polimerase (Euroclone, Italy). The PCR conditions included a pre-denaturation step at 94°C for 3 min followed by

35 cycles characterized by denaturation at 94°C for 2 min, annealing at 55°C for 1 min, and extension at 72°C for 10 min was performed. The products of the wt and mutant alleles were 190 and 186 bp long, respectively, and were visualized through electrophoresis analysis on 3% low melting agarose gel (Biorad, Italy) in TBE (0.89 M Tris-HCl, 0.88 M acido borico, 0.03 M EDTA disodium) (not shown in the "Results" section).

Moreover, to identify the sex of P10 mice a multiplex PCR was carried out with the following primers:

- Sry gene (forword 5'-TCATGATACTGCCAACCACAG-3', reverse 5'-CATGACCACCACCACCACCAA-3');
- Myog gene (forword 5'-TTACGTCCATCGGACAGC-3', reverse 5'-TGGGCTGGGTGTTAGTCTTA-3').

The amplification reaction was conducted using 100-300ng of genomic DNA, 1.2mM MgCl2, 0.2mM dNTPs, 0.4mM for each primer and 2U of Taq polimerase (Euroclone). The PCR conditions included a pre-denaturation step at 94°C for 5min followed by 35 cycles characterized by denaturation at 94°C for 30seconds, annealing at 58°C for 30 seconds, and extension at 72°C for 30seconds. A final extension step at 72°C for 5min was performed. The amplification products were visualized through electrophoresis analysis on 0.8 % agarose gel (Biorad) in TBE. The product of the Sry gene was 441bp for male, while the internal control band for the Myog was 245bp long.

3.1.2. Tissues collection

Heterozygous and homozygous *dal* mice and wt littermate were sacrificed by decapitation after an intraperitoneal injection of 35% chloral hydrate (100 µl/100 g b.w.; Sigma) at P10, P21, P30 and P60 (n=5 per genotype and stage). The brains were quickly isolated and separated in two halves, one for morphological studies and the other for biochemical evaluations as prolidase activity (reported as confidential result in "Introduction" section). In addition, at P10 and P60, halves of other cerebella were kept at -20°C for western blotting analysis.
The flow diagram below (Figure 1) explain how we proceed for histological evaluations followed by quantitative analysis and statistics.

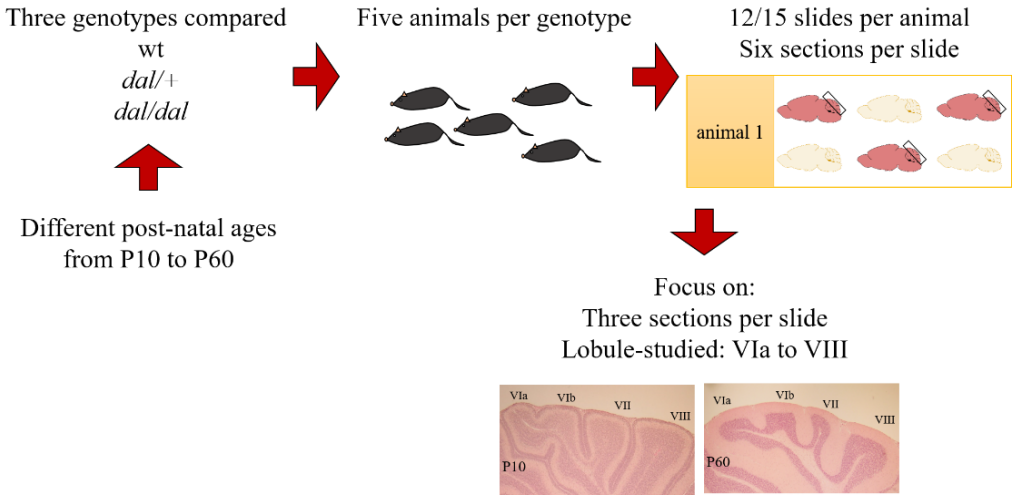

Figure 1. Flow diagram of the experimental plan

3.2 Histological analysis

One half of the brains were fixed in Carnoy's solution (absolute ethanol, chloroform, acetic acid; 6:3:1) for 48 h, then placed in absolute ethanol and in acetone, and embedded in Paraplast X-tra (Sigma). For each sample 12/15 slides were prepared. Six sections (8 μm thick) were cut serially in sagittal plane and were collected on each silan-coated slides.
For the immunohystochemical reactions and histological stainings, the paraplast embedded sections were deparaffinized in xylene and rehydrated in a decreasing ethanol series (absolute, 95%, 80% and 70%, Carlo Erba, Italy) and rinsed in Phosphate-Buffered Saline (PBS; Sigma).

3.2.1. Histological stainings

Haematoxylin and Eosin (H&E) staining

The sections were immersed for 10 min in Carazzi's haematoxylin (Sigma) at room temperature, washed in running tap water and immersed in eosin (Sigma) for 5 sec. Sections were washed in distilled water, dehydrated in absolute ethanol, cleared in xylene (Carlo Erba), and mounted in Eukitt (Kindler, Freiburg, Germany).

Picrosirius red staining

Brain sections were dipped for 1 h in a picrosirius red solution, made by 0.5 g of Sirius red powder (Direct Red 80, Sigma) melted in 500 ml of saturated aqueous solution of picric acid (Picric acid solution, 1.3% in H_2O, Sigma). Then, the samples were washed in 5% acidified water, dehydrated in absolute ethanol, cleared in xylene and finally mounted in Eukitt.

3.2.2. Immunohistochemistry reactions

Light microscopy immunoreactions (Immunoperoxidase staining)

The slides were incubated, at room temperature (RT), for 7 min in a blocking buffer for the suppression of the endogenous peroxidases (3% H_2O_2 in 10% methanol in PBS), then for 20 min in fetal calf serum in order to block non-specific antigen binding sites. The incubation with the primary antibody was carried out at RT for 1h in PBS overnight in a dark moist chamber.

- mouse polyclonal anti-calbindin (CB) 28kDa (1:5000; Sigma);
- mouse monoclonal anti-PV 11kDa (1:5000; Swant, Switzerland);
- rabbit polyclonal anti-MAP2 280kDa (1:250 Santa Cruz Biotechnology, Santa Cruz, CA);
- rabbit polyclonal anti-doublecortin (DCX) 45kDa (1:6000; Abcam, UK)
- rabbit polyclonal anti-phospho-Tau$^{(pSer519/202)}$ (1:100; Sigma);
- mouse monoclonal anti-Neurofilament Heavy (NF-H) 200KDa (1:100; Abcam).
- goat polyclonal anti-GluR2 99kDa (1:500; Sigma);
- rabbit polyclonal anti-GluRδ2 113kDa (1:75; Chemicon, CA, USA):
- mouse monoclonal anti-GAD67 67kDa (1:1000; Abcam);
- rabbit polyclonal anti-GABAα6 51kDa (1:250; Merck Millipore, MA);

Thereafter, the sections were sequentially incubated with biotinylated secondary anti-rabbit, anti-mouse or anti-goat antibodies (1:200; Vector Laboratories, CA, USA) for 30min and horseradish peroxidase conjugated avidin-biotin complex (Vector Laboratories) for 30min at RT. Then, 0.05% 3,3'- diaminobenzidine tetrahydrochloride (DAB; Sigma) with 0.01% H2O2 in Tris-HCl buffer (0.05M, pH 7.6) was used as a chromogen. After each reaction step, sections were washed thoroughly in PBS (two changes of 5 minutes each). Sections were dehydrated in ethanol, cleared in xylene, and mounted in Eukitt. For control staining, some sections were incubated with PBS instead of the primary antibody. No immunoreactivity was present in this condition.

The slides after histological and immunoperoxidase stainings were observed with an Olympus BX51microscope, and the images were recorded with an Optronics MagnaFire Camera through the Cell^F program (Olympus Software Inc). Corrections to brightness and contrast were made with the same software.

Immunofluorescence reactions

After the deparaffinization procedure, some antigens were detected through immunofluorescence reactions. To avoid the nonspecific antigen binding sites the brain sections were treated for 30min at RT with a PBS-blocking solution (100mg BSA, 10µl Tween 20, 3.3ml glycine 0.3M in 7ml PBS). Then, the slices were incubated 1h in a dark moist chamber with the primary antibodies diluted in a solution containing PBS.

- rabbit polyclonal anti-laminin (1:100; Sigma);
- mouse monoclonal anti-reelin (1:1000; Santa Cruz Biotechnology);
- rabbit polyclonal anti-MMP2 (1:250; Chemicon);
- rabbit polyclonal anti-MMP3(1:250; Chemicon);
- mouse monoclonal anti-TIMP 2 (1:100, Chemicon);
- mouse polyclonal anti-proliferation cell nuclear antigen (PCNA) (1:600; Oncogene Science Inc, NY);
- goat polyclonal anti-glial fibrillary acidic protein (GFAP) (1:100; Santa Cruz Biotechnology);
- rabbit polyclonal anti-CB (1:2000; Sigma);
- rabbit polyclonal anti-PMCA 1 (1:500: Abcam):
- rabbit polyclonal anti-MAP2 280kDa (1:250; Santa Cruz Biotechnology);
- rabbit polyclonal anti-phospho-Tau$^{(pSer519/202)}$ (1:100; Sigma);
- mouse monoclonal anti-NF-H 200KDa (1:100; Abcam).
- guinea pig polyclonal anti-vesicular glutamate transporter 1 (VGLUT1) (1:2000; Merck Millipore)
- guinea pig polyclonal anti-VGLUT2 (1:1500; Merck Millipore):

Sections were washed in PBS and incubated with the appropriate secondary antibodies in PBS for 1h: Alexa-Fluor 594 anti-goat, anti-rabbit and anti-mouse; Alexa-Fluor 488 anti-rabbit and anti-guinea pig (1:200, Molecular Probes, Milan, Italy). If a second antigen should be detected on the same section, the slides were twice washed in PBS for 5 min and then, re-incubated with the primary antibody following the same protocol as explained before. Only rarely, it was carried out again the blocking buffer step between the two antibody incubations.

After washing in PBS, the nuclei were counterstained with 0.1 μg/mL Hoechst 33258 for 6min, and coverslips were lastly mounted in a drop of Mowiol (Calbiochem, CA, USA).

The slides were viewed by fluorescence microscopy with an Olympus BX51 equipped with a 100W mercury lamp used under the following conditions: 330–385nm excitation filter (excf), 400 nm dichroic mirror (dm), and 420 nm barrier filter (bf) for Hoechst 33258, 450-480 nm excf, 500 nm dm, and 515 nm bf for Alexa 488, and 540 nm excf, 480 nm dm, and 620 nm bf for Alexa 594. Images were recorded with an Optronics MagnaFire camera through Cell^F software. Images were optimized for color, brightness and contrast by using the same software. For control staining, some sections were incubated with PBS instead of the primary antibodies. No immunoreactivity was present in these sections.

3.3 Western blotting

Cerebellum lysates were obtained from wt, dal/+ and dal/dal mice at P10 and P60, by homogenization in lysis buffer (5mM HePES pH7.4, 320mM sucrose, EDTA 2mM pH8, phosphatases and proteases inhibitors (Sigma)), the protein concentration was determined performing the Bradford Assay (Sigma, St. Louis, MO). Proteins (40µg) were separated using 7.5%, 10% or 12% polyacrilammide (35%) gel (according to the molecular weight of the antigens needed), Dodecyl Sulfate PolyAcrylamide Gel Electrophoresis (SDS-PAGE) under reducing conditions. Then, the proteins were electro-transferred to a nitrocellulose membrane (Hybond-P, GE Healthcare Life Sciences, Euroclone Spa, Milan, Italy), at 100 V and 38 mA for 2 h. The membrane was than washed with PBS-Tween 0.02% (PBS-T; Tween 20, Sigma) and then blocked using 5% milk, incubated for 1h at RT with the following primary antibodies, diluted in PBS-Tween 0.02%:

- rabbit polyclonal anti-collagen IV 200KDa (1:500; Abcam);
- mouse polyclonal anti-PCNA 29kDa (1:600; Oncogene Science Inc);
- rabbit polyclonal anti-CB 28kDa (1:1000; Sigma);

Furthermore, for normalization, the mouse monoclonal anti-actin 42kDa (1:2000; Sigma), diluted in PBS-T was used. Goat polyclonal antibody anti-mouse and anti-rabbit (1:2000; DAKO, Denmark) were used as secondary antibody. LuminataTM crescendo western HRP substrate and LuminataTM normal western HRP substrate (Merck Millipore, Billerica, MA) were used as substrates. The chemoluminescent bands were impressed on Amersham Hyperfilm ECL (GE healthcare).

Each experiment was carried out three times and the band quantification was performed with the software Image J. The statistical analysis were performed using GraphPad (2016, GraphPad Software, Inc.).

3.4. Quali-quantitative analysis and statistical evaluations

In this study, particular attention has been paid to the cerebellum (see the flow diagram above).
Three brain sections per slide, per animal were used for the observations that allowed quantitative analysis and statistical observations among the three genotypes, each of which was made of five animals. All the measurements concerned the vermis cerebellar lobules VIa, VIb, VII and VIII. The results of wt, *dal/+* and *dal/dal* were compared as follows: wt versus *dal/+*, wt versus *dal/dal*, and *dal/+* versus *dal/dal*.
The results of statistical evaluations (e.g. mean, SD, and P value) were reported in the text within the results chapter or in small tables close to each reference figures. The mean values were compared by t-test (2016 GraphPad software, Inc).

Laminin-reelin overlapping

These two markers highlighted the pBM. To evaluate how long they were overlapping each other, the "polyline" function was used (Cell^F Software, Olympus). This function allowed to follow with a line the positive pBM with high precision. In three sections of each slide for each animal, the length of the positive pBM was measured. In particular, the measurements concerned the tracts in which the two markers were present together (overlapping) and the one in which it was detectable only the reelin and not the laminin (no laminin). The total length of the pBM was the sum of both measurements. The average value and the standard deviation (SD) of the length of "overlapping" and "no laminin" tracts were calculated for each genotype (wt, *dal/+* and *dal/dal*). The means were compared by t-test (2016 GraphPad software, Inc). Then a graph was built expressing the length of "overlapping" and "no laminin" as percentage to be reported on the results section.

Thickness of collagen pBM

The color of collagen fibers stained with picrosirius red and viewed with polarized light depends upon fiber thickness; as fiber thickness increases, the color changes from green to red. To determine the proportion of different colored collagen fibers, we used an automated function provided by the image-analysis software ("green average" and "red average" measured the average value of all intensity (density of pixels) of green and red respectively within the selection: Cell^F, Olympus). The background was subtracted. Then, the green and red averages were expressed as a percentage of the total number of collagen pixels detected in the image.

EGL thickness and ratio

The thickness of the total EGL and of the two subgroups of cells within this layer, the proliferative and pre-migrating granule cells, were evaluated. To this purpose the function "arbitrary line" provided by the image-analysis software (Cell^F, Olympus) allowed to measure the layers thickness using a line spanning all the layer, whose length was recorded, and it was perpendicular to the pial surface, as it is shown in Figure 2. The thickness measurements was carried out using 25 lines per picture.

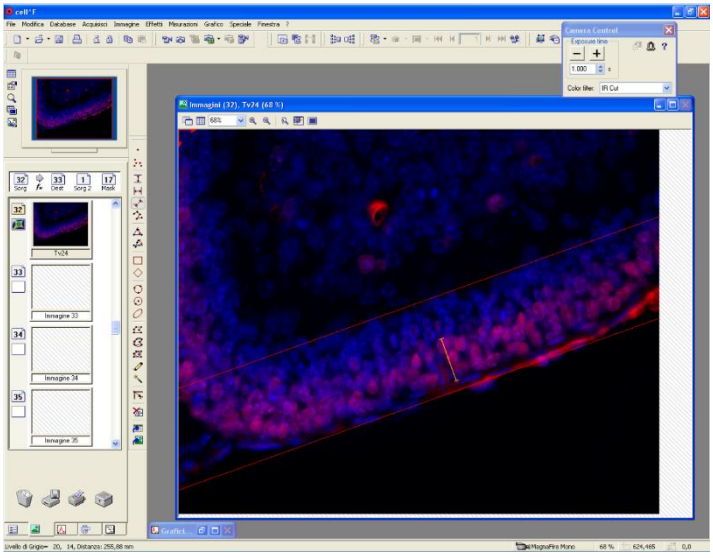

Figure 2.

Screenshot of cell^F software showing the measurements of PCNA positive EGL and total EGL, perpendicular to the lobule surface.

The average values and the standard deviations (SD) of the length of "total EGL" and "proliferative EGL" layers were calculated for each genotype (wt, *dal/+* and *dal/dal*). The means were compared by t-test (2016 GraphPad software, Inc). Then, the thickness of the pre-migrating EGL layer was calculated by subtracting the mean value of the proliferative EGL thickness from the one of the total EGL for each animal. Furthermore, the mean values of the two subgroup of layers were expressed as a percentage, in which the 100% was the total EGL thickness, calculating then a ratio of proliferative/pre-migrating layer that was reported in a graph.

Cell count

For several markers it was useful to count the number of "normal" positive cells/structures and the altered positive ones. The software used was cell^F with the function of "multi-point counting". The results were then analyzed according to the pourpose of the counting:

- Parvalbumin: the number of sharp and flat pinceau at the Purkinje axon hillock was counted. From this counting were excluded those Purkinje neurons in which it was not possible to define the shape of the pinceau. Then, the count of each brain section was used to make an average per slide and at the end per genotype. These mean values were shown in a graph.
- phospho-tau$^{(pSer202-509)}$: at P60 Purkinje soma, and some other neurons within the ML, IGL and white matter were labeled at P60 and easily counted. The number of these cells were reported to compare the results among the genotypes.
- GAD67: it marks not only the soma of Purkinje neurons but in some cases the main dendrite branches. Therefore, the number of positive-Purkinje dendrite was counted out of the total number of positive Purkinje neurons.
- VGLUT2 and tau: VGLUT2^{+} and VGLUT2^{-} Purkinje cell soma were counted. Then, among the VGLUT2^{+}, Purkinje tau^{+} cells were counted (Purkinje soma VGLUT^{+} and tau^{+}).

Optical density (OD)

For several markers it was useful to measure the optical density (OD; as the density of the pixel) of the areas labeled after immunohistochemical reactions. In the case of immunofluorescence reactions it was necessary to acquire the picture in gray scale, while in the case of light microscopy immunoreactions, after the acquisition in gray scale, the color were inverted to have the positivity lighter and the background darker (the contrary of what is visible after the immunoperoxidase staining). The background was always subtracted. Then a fixed area (mask) was used to evaluate the optical density of the labeling for each marker through an automatic function of Cell^F. To apply a statistical analysis, the OD average was calculated per animal and then per genotype. The mean values were compared by t-test (2016 GraphPad software, Inc). The OD was measured using masks with different sizes according to the layer or the cell bodies. For the OD measurements of layers (i.e. EGL, ML, IGL) rectangular masks were created. The size established ensured to measure only the positivity within the specific layer. Many measurements were done within the same figure according to the size of the mask. The mask dimensions, the number of measurements and the magnification of the figure were kept constant according to the layer and the postnatal age of the animal analyzed. The single cell body-OD measurements were carried out using the same method as layer-OD but the mask was circular. The size of this mask changed according to the postnatal age of the animals. Layer- and single cell body-OD were used, according to the marker positivity, for:

- PMCA1, VGLUT1 and 2: EGL, ML and IGL at P10, and ML and IGL P60; Purkinje neurons at P10 and P60;
- GLUR2: Purkinje neurons at P10 and P60; ML and IGL at P60;
- GluRδ2: ML and IGL at P10 and P60; Purkinje neurons at P10 and P60;
- GAD67: ML at P10 and P60; Purkinje neurons at P10 and P60;
- GABAα6: (IGL) at P10 and P60;
- MAP 2: ML and IGL at P10 and P60;
- DCX: proliferative EGL, pre-migratory EGL, ML and IGL at P10.

Phospho-tau$^{(pSer202-509)}$ positive Purkinje neurons

At P60, phospho-tau$^{(pSer202-509)}$ labeled some dendrites in the ML. To obtain a quantitative data two Cell^F functions were used. The perimeter of the ML was traced using the function “closed polygon”; the area (number of pixel within the selection multiplied by the calibration factor in x-y directions) and the OD inside the perimeter were measured. Then, the perimeter of each positive dendrite was traced using the function “magic wand” and again the area and OD were calculated within the perimeter of each positive dendrite, as it is was in figure 3.

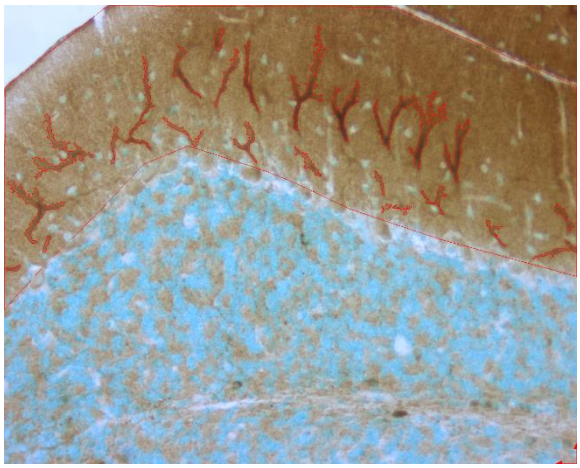

Figure 3.

Phospho-tau$^{(pSer202-509)}$ positive Purkinje dendrites marked through the “magic wand” function; ML perimeter marked through the “closed polygon” function (Cell^F software, Olympus).

To get information on the percentage of the area occupied by positive dendrites within the ML of each figure, we proceeded as follows: all the area of dendrites were summed together, divided for the area of the ML and multiplied by 100. Then the average values were obtained per genotype. To compare the OD ratio of the ML among the genotypes, we subtracted the average value of the dendrites OD from the ML OD. In graphs, we compared for the different genotypes:

- the ML OD without positive dendrites;
- the OD of positive dendrites;
- the percentage of dendrite area within the ML.

4. RESULTS

In the study of the postnatal brain development, we have chosen animals at different postnatal day paying particular attention to two important and critical steps of mouse postnatal life: P10 and P60. This comparison is the most meaningful considering the mouse post-natal cerebellar development. In fact, at P10 there are the majority of the histogenesis and morphogenesis processes ongoing as the proliferation, migration and differentiation of neurons as well as the formation of fundamental synaptic contacts. Instead, P60 represents the stage of mature cerebellum in which the processes above mentioned ended. However, when we considered relevant to better understand some results, we also reported data on other stages in-between (P21 and P30) as in the case of the phospho-tau$^{ser202\text{-}509}$marker (see "the cytoskeleton" paragraph below). Moreover, all the figures regarded the apex of the lobules VIa VIb VII and VIII in the *vermis* since these lobules share the same developmental timing and pattern; when other lobules were considered it is always specified in the figure captions.

The following points should be highlighted:

- the type of alterations we found did not differ comparing *dal/dal* and *dal/+* animals (see below);
- the same anomaly has not covered all the specimens and all cerebellar sections of the same animal. This variability has led to quantification and statistical analysis of the anomalies per animal, in order to obtain a more objective evaluation of the alterations in prolidase deficient mice. Moreover, to preserve the physiological heterogeneity found even in the wt animals, the results of *dal* animals were not normalized to wt animals.

With regard to the documentation:

- the figures show the most representative anomalies of *dal/dal* or *dal/+* in comparison with wt animals; to this purpose, we unified the two genotypes *dal/dal* and *dal/+* indicating them as "*dal*" mice. This means that the figures are made of wt compared to *dal* mice (*dal/dal* or *dal/+)* cerebellum. Then, in each panel, only heterozygous or homozygous is shown to display the types of anomalies;
- instead, the graphs of the measurements and statistics compared results obtained separately on wt versus *dal/dal,* wt versus *dal/+*, and *dal/+* versus *dal/dal* to highlight possible differences in the alterations among the animals of the three genotypes. The results of statistical evaluations (e.g. mean, SD, p-value) can be found in tables in the appendix section.

4.1 The brain extracellular matrix

4.1.1. ECM components of pial basement membrane

We studied different components of the basement membrane (BM) located close to the pial surface (pBM), which is known to be a key regulator of the cortical development. In particular, we evaluated by immunohistochemistry laminin and reelin markers and collagens; the nuclei were counterstained in blue (Hoechst 33258) fluorescence. Moreover, through picrosirius red staining we analyzed the thickness of collagen structure of pBM; this analysis was carried out only at P60 since the thickness of pBM under the polarized light was not perceptible in the other stages. However, this staining allow to evaluate collagens in general, while the most abundant collagen in the brain is the type IV; then, trough WB we measured the amount of this collagen in cerebellar lysates at P10 and P60.

Postnatal day 10

At P10 it was possible to highlight differences between wt and *dal* mice pBM considering the pattern of labelling of laminin and reelin. The alterations were scattered and not homogenously present all over the cerebellar cortex. In fact, it was possible to find normal and altered portions of the cerebellum within the same animal. In the figure 1, the markers labelled the pBM; in wt animals the EGL beside the pBM had a homogeneous thickness all over the cerebellar cortex analyzed (fig. 1a; white interrupted line) and the pBM marked by laminin and reelin was a continuous layer (fig. 1b,c; green and red arrowhead indicating the laminin and reelin respectively) and the two markers overlapped each other (fig. 1d). Whereas *dal* mice showed changes in EGL thickness (for EGL thickness measurements see "The granule cells proliferation and migration" paragraph). In fig. 1e, observing the right and left side of the figure it was possible to notice an abrupt reduction in the EGL thickness (fig. 1e-h; white dotted line). In correspondence of this anomaly even the organization of the pBM was altered. In fig. 1f, the laminin layer was interrupted, highlighting portions of pBM not marked for laminin (green arrowheads). In fig. 1g, reelin was detected in the pBM (red arrowheads), but in the right side of the figure, it was also found in the EGL and in part in the ML (asterisk) as well as in the

soma of two Purkinje neurons (white arrows). In addition, reelin positivity was concentrated in the pBM in all animals studied, but there was a diffuse and weak labelling for this marker in other cerebellar layers in three *dal/dal* and two *dal/+* always in correspondence of layering alterations. In fact, the merge (fig. 1h) clearly showed that the alterations related to the pBM marker profile occurred in correspondence of EGL thickening.

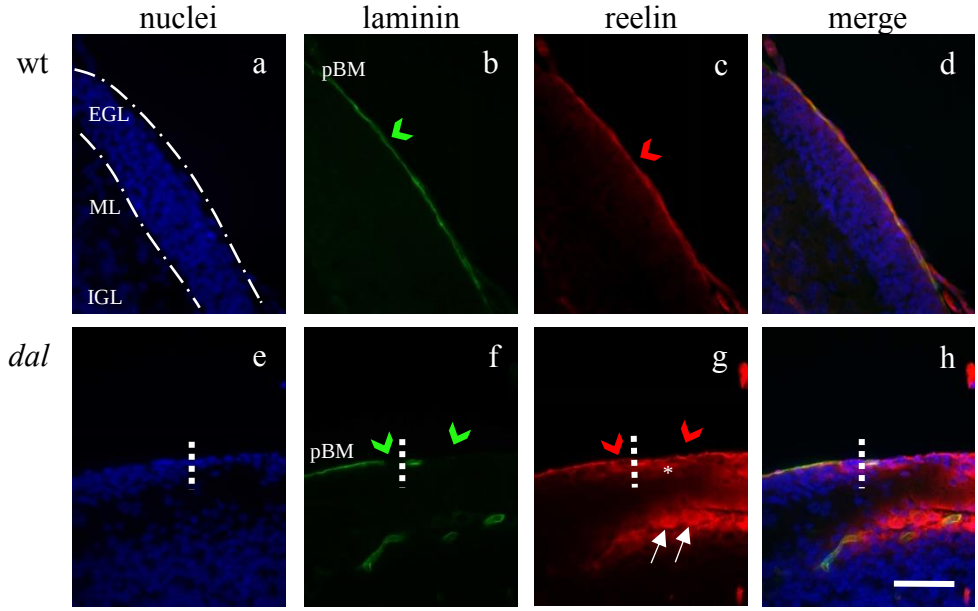

Figure 1. Immunofluorescence reaction at P10 for laminin (green fluorescence) and reelin (red fluorescence); nuclei (blue fluorescence). *dal* figure retrieved from *dal/dal* mouse. Abbreviations: wt: wild type; *dal*: prolidase deficient mice; EGL: External Granular Layer; ML: Molecular Layer; IGL: Internal Granular Layer; pBM: pial Basement Membrane. Magnification: scale bar of 100 µm a-h.

Since in *dal/dal* and *dal/+* the pBM of lobules VIa, VIb, VII and VIII had an interrupted laminin layer and a continuous reelin one, the absence of laminin and the overlap of the two markers were measured; results were reported in terms of percentage. In particular, laminin and reelin overlapped for 99% (±0.003%) in wt, 87% (±4.5%) in *dal/+* and 77% (±10%) in *dal/dal*, the remaining percentage represents portion of pBM positive only for reelin (Figure 2). The differences were not significant among *dal* mice ($p>0.5$), and very statistically significant comparing wt vs *dal/+* and *dal/dal* ($p<0.001$).

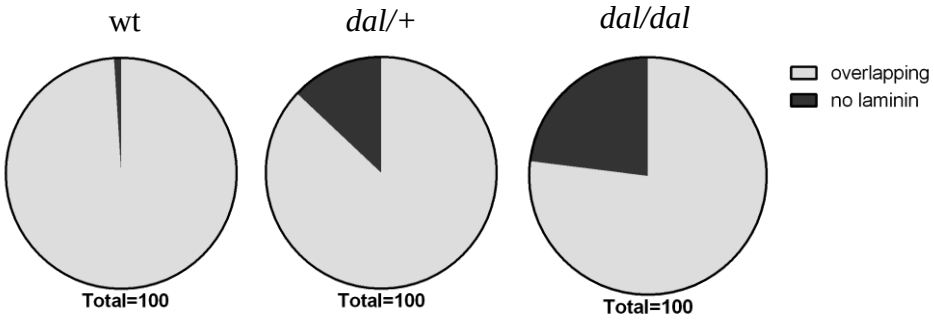

Figure 2. Measurements of length expressed as percentage of cerebellar pial surface covered by laminin and reelin overlapping each other (light grey) and only reelin with the absence of laminin (dark grey). Lobules VIa, VIb, VII and VIII were included in the measurements. Abbreviations: wt: wild type;

Postnatal day 60

At P60 in wt animals (fig. 3 a-d), the laminin (green fluorescence) and reelin (red fluorescence) highlighted always a continuous layer of immunopositive pBM, even if the reelin positivity was lower in comparison with P10 animals. In *dal* mice (fig. 3e-h) the alterations were weaker comparing those found at P10. In fact only in one *dal/dal* and one *dal/+* there were restricted portions of pBM marked only with laminin (not shown), other tracts with reelin (fig. 3h; red arrowhead), and other ones in which the two markers overlapped each other (fig. 3h; white arrowheads). This is the reason why the laminin/reelin overlapping measurements were not shown. In these animals, it was also possible to detect an increased positivity for reelin at the level of pBM, as well as in the ML and IGL as previously described at P10.

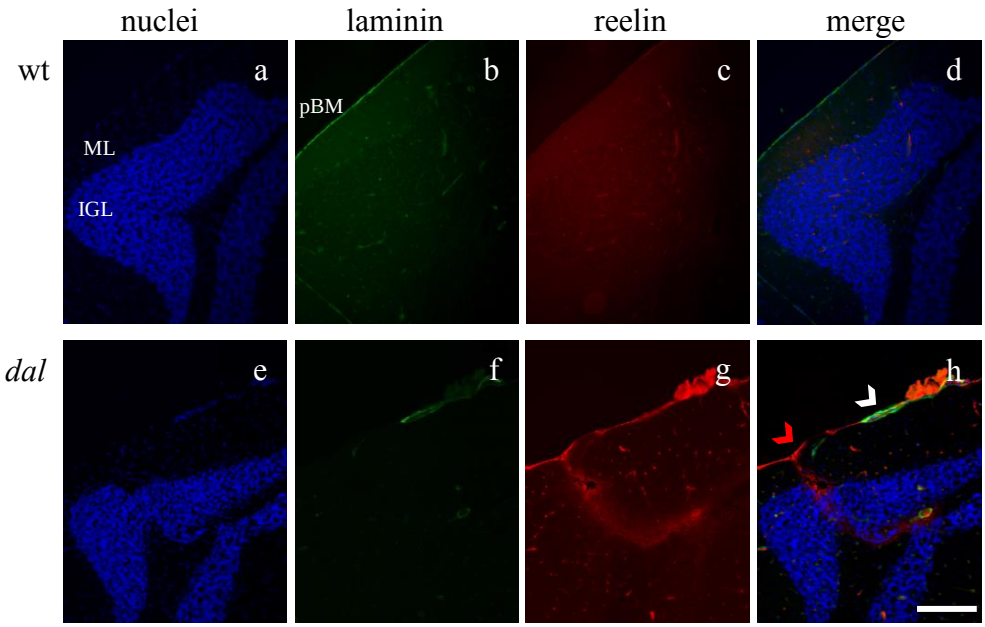

Figure 3. Immunofluorescence reaction at P60 for laminin (green fluorescence) and reelin (red fluorescence); nuclei (blue fluorescence). *dal* figure retrieved from *dal/dal* mouse. Abbreviations: wt: wild type; *dal*: prolidase deficient mice; ML: Molecular Layer; IGL: Internal Granular Layer; pBM: pial Basement Membrane. Magnification: scale bar of 150µm (a-h).

The ECM profile included the analysis of collagens. The collagens component of the pBM was evaluated using picrosirius red staining, which highlighted the differences between wt and *dal* mice regarding the thickness of collagen structure within the pBM. In particular, the color of collagen fibers stained with picrosirius red and observed with polarized light depends upon fiber thickness; as fiber thickness increases, the color changes from green to yellow to orange to red. In particular in Figure 4 there are the bright field images of cerebellar lobules of a wt (fig. 4a) and *dal*/+ (fig. 4b) mice, while fig. 4a' and 4b' are insets viewed under a polarized light. The graph (fig. 4c) shows the measurements concerning the amount of green (wt 5.5±0.6; *dal*/+ 7.9±0.9; *dal/dal* 8.04±1.2) and red (wt 9.26±2.7; *dal*/+ 11.6±2.7; *dal/dal* 10.36±3.4) components (as mean density of each color). Then, the statistical analysis relieved a significant increase ($p<0.01$) in the green component in *dal*/+ and *dal/dal* mice compared with the results of the wt animals. This means that in *dal* mice the pBM presented more portions with a thin collagen structure than the wt; regarding the amount of red component there were not statistically significant differences, indicating that no relevant differences in the amount of the thicker collagen structures within the pBM among the different animals analyzed can be pointed out. Moreover, we performed a western blotting to evaluate if differences were present considering the collagen type IV (fig. 4d), since it is the most abundant type of collagen present in the brain, but no statistically significant differences emerged comparing wt, *dal*/+ and *dal/dal* animals since a great variability within the same genotype group was detected.

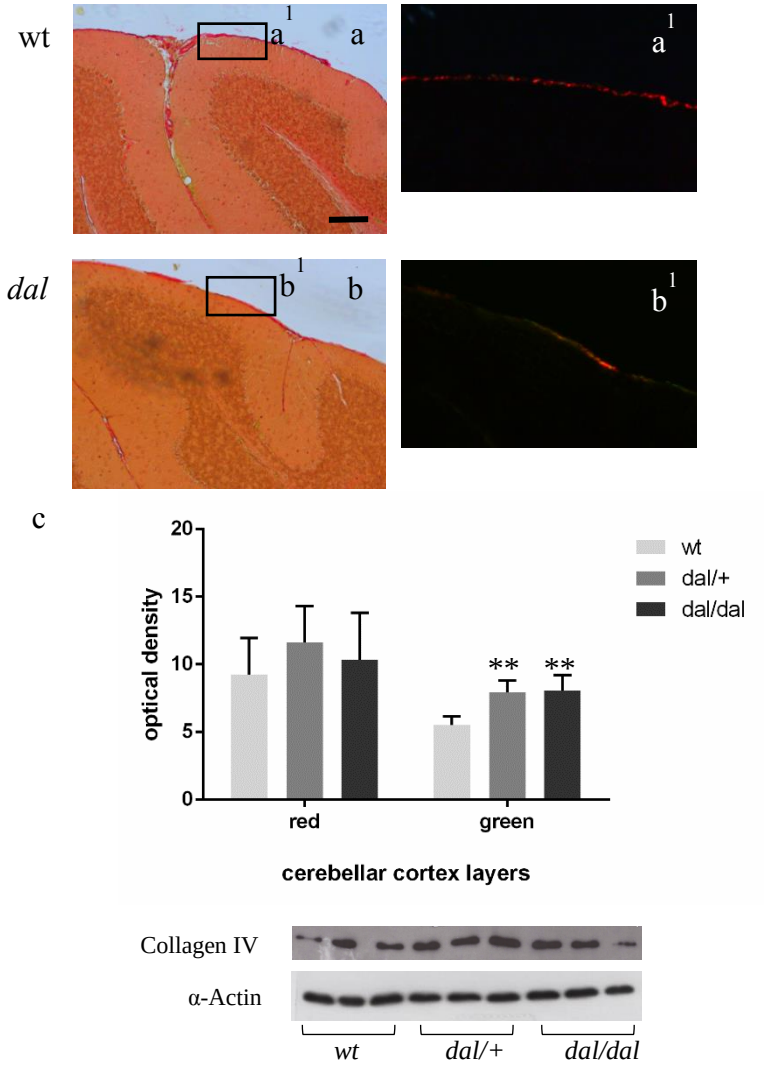

Figure 4. Picrosirius red staining of pBM collagen component. Bright field pictures (a,b); Inset: the same field, observed with polarized light (a' and b'). "Green" stands for thinner collagens structure and "red" for thicker collagens structure (c). wb analysis to quantify the amount of collagen IV (d). *dal* figure retrieved from dal/+ mouse. Abbreviations: wt: wild type; *dal*: prolidase deficient mice; ML: Molecular Layer; IGL: Internal Granular Layer; pBM: Magnification: scale bars of 200µm a, b; 40µm(a', b').

4.1.2. ECM remodeling enzymes

Since prolidase is indirectly involved in the ECM remodeling and we observed alterations in the organization of some components of the ECM, we decided to monitor other ECM remodeling enzymes as the MMPs (MMP-2 and MMP-3) and TIMP2, one of the inhibitor of MMP-2. The two MMPs chosen, together with MMP-9, are the most studied in the cerebellum and share many targets as collagen type IV and laminin. MMP-2, -3 and TIMP 2 are involved in different neuronal functions especially during cerebellar morphogenesis.

At all post-natal day we analyzed the results did not come out with marked differences detectable between wt and *dal* mice, the only few exceptions in which in *dal* mice there was a difference compared to the wt were here reported. Figure 5 and 6 shown the positivity for the three markers above mentioned at P10 and P60 respectively.

At P10 there were no relevant differences between wt (fig. 5a-c) and *dal* (fig. 5d-f) mice for MMP-2 labelling. Regarding the MMP-3 there were no divergences in term of positivity between the wt (fig. 5g-i) and *dal* mice, even in the case shown of one *dal/dal* (fig. 5j-l) in which there was a inhomogeneous thickness of the EGL (white arrowhead). Concerning the TIMP immunolabelling, no distinctions can be done between the wt (fig. 5m-o) and *dal* mice (fig. 5p-r).

Considering the post-natal day 60, no evident differences emerged in the comparison between wt and *dal* mice for MMP-2 (wt, fig. 6a-c; *dal*, fig. 6d-f), MMP-3 (wt, fig. 6g-i; *dal*, fig. 6j-l) and TIMP 2 (wt, fig. 6m-o; *dal*, fig. 6p-r). There were no changes in the positivity also in the context of serious morphological alterations as the detachment of a ML portion (fig. 6d-f. These anomalies are fully explained in the following paragraph). To better observe the anomaly, the inset within the fig. 6d was added. It represents the same section at a lower magnification; the perimeter drown in yellow delimits the IGL, while the white one the ML that is detached from the ML in continuum with the remaining tissue (fig. 6d inset, Fig. 6e).

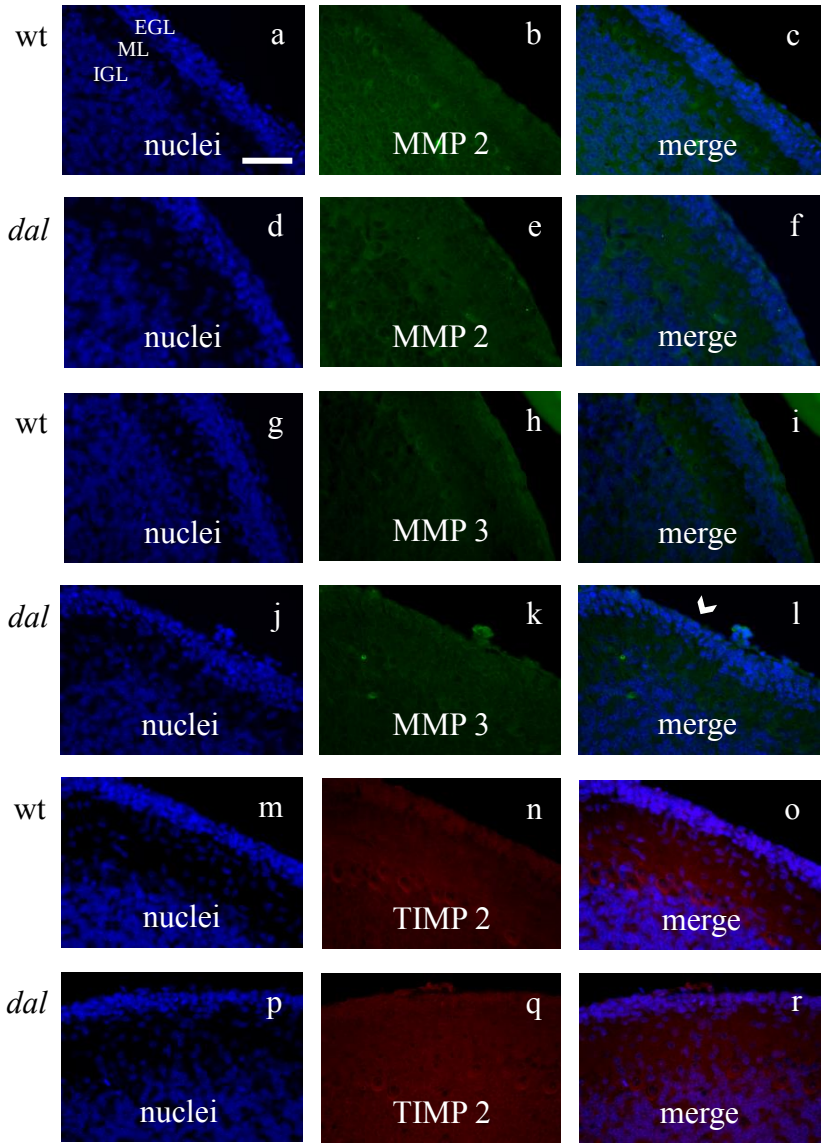

Figure 5. Immunofluorescence reaction at P10 for MMP-2 (green fluorescence; b,c,e,f) MMP-3 (green fluorescence; h,i,k,l) and TIMP 2 (red fluorescence; n,o,q,r); nuclei (blue fluorescence; a,d,g,j,m,p). *dal* figure retrieved from *dal/dal* mouse, with the exception of 5d-f from *dal*/+. Abbreviations: wt: wild type; *dal*: prolidase deficient mice; EGL, External Granular Layer; ML: Molecular Layer; IGL: Internal Granular Layer. Magnification: scale bar of 100μm (a-r).

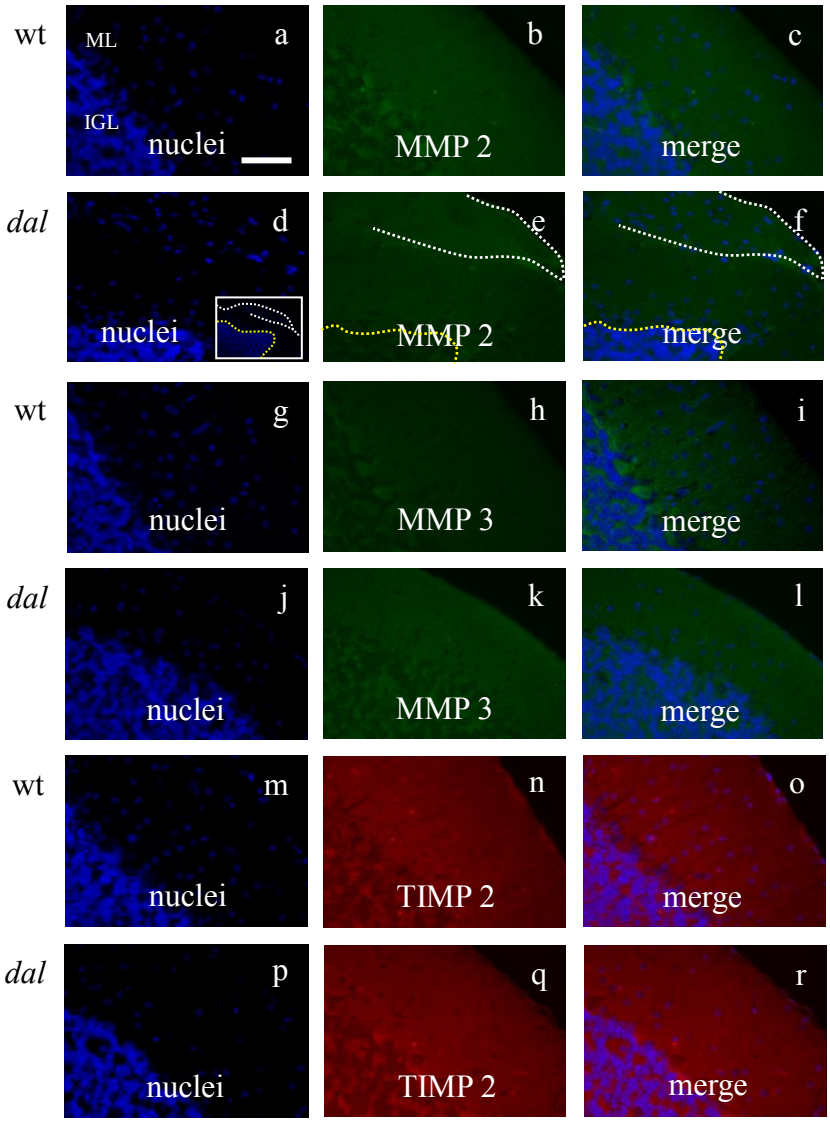

Figure 6. Immunofluorescence reaction at P60 for MMP-2 (green fluorescence; b,c,e,f) MMP-3 (green fluorescence; h,i,k,l) and TIMP 2 (red fluorescence; n,o,q,r); nuclei (blue fluorescence; a,d,g,j,m,p). *dal* figure retrieved from *dal/dal* mouse. Abbreviations: wt: wild type; *dal*: prolidase deficient mice; ML: Molecular Layer; IGL: Internal Granular Layer. Magnification: scale bar of 50μm (a-r), 200μm (d-inset).

4.2. The cerebellar cortex morphology

Defects in the cerebellar cortex regarded not only the layering, but also the morphology of the lobules in both *dal/dal* and *dal/+* animals at different post-natal days. Haematoxylin and eosin staining highlighted these anomalies.
In particular, at P10 (Figure 7) the morphology of the apical portion of the lobules IV-V in one *dal/dal* and one *dal/+*was altered, creating undulations on the surface (fig. 7b, d; black arrows). In *dal* mice, in some lobules, usually VIa-VIb, there was a reduction in the EGL thickness (fig. 7f; black arrowhead), as it was also demonstrated with more specific markers as PCNA and labelling as Hoechst (for EGL thickness measurements see "The granule cells proliferation and migration" paragraph). Moreover, huge blood vessels (BV) penetrating the tissue and within the lobules were detected (fig. 7h; perimeter of the BV is delineated with a white line) of different sizes in all *dal* mice.
At P21 (one *dal/+*) and P60 (one *dal/+* and one *dal/dal*) (Figure 8) were detected pial surface anomalies as undulations (fig. 8b) similar to those found at P10 (fig. 7b,d), and ML portions partially detached from the tissue below (fig. 8c,d). In this cases between the two ML portions (red asterisks), blood cells were detectable. Moreover, huge blood vessels penetrated the cerebellar cortex and destroyed the tissue detaching ML portions forming a sort of "ML island" (fig. 8f,g; black asterisks; perimeter of the BV delineated with black dotted line). In the case of fig. 8h, the BV penetrated the cortex and interrupted the IGL (red arrows). Furthermore, several granule cells had nuclei intensely stained by eosin (fig. 8j-k; black arrowheads) in some lobules (IV-V; VIII-IX) spread throughout their length, from the apex (fig. 8j) to the bottom (fig. 8k) of the fissure. In addition, at P60 ectopic granule and Purkinje cells were also visible detached from the lobule IGL and immersed within the ML (fig. 8l; black arrowhead) or in the "ML island" (fig. 8g; black boxes).

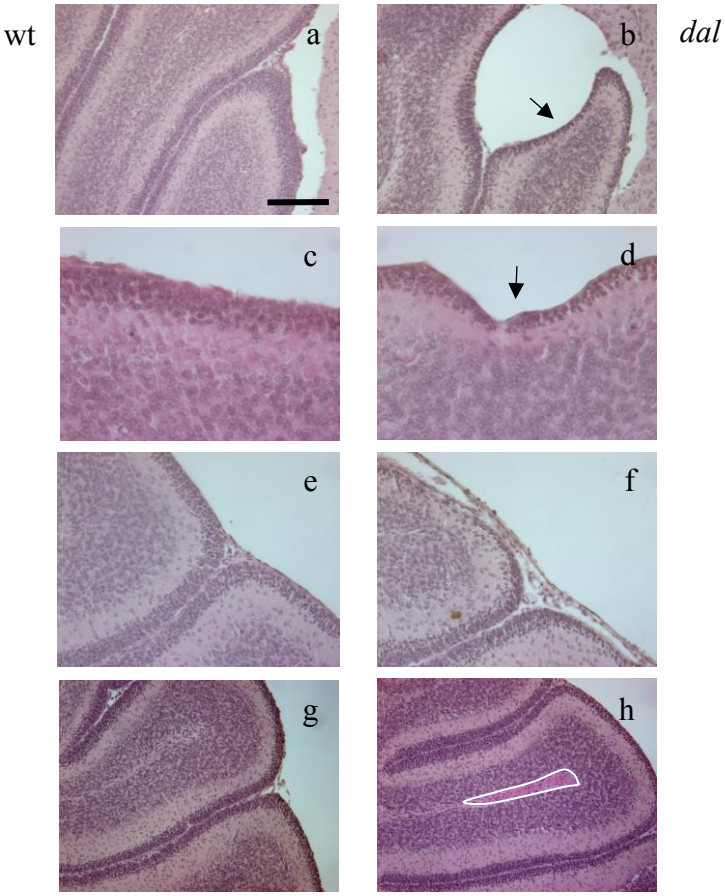

Figure 7. Haematoxylin and eosin staining at P10. *dal* figures retrieved from wt (a,c,e,g) *dal/dal* (b,f) and *dal*/+ (d,h) mice. Abbreviations: wt: wild type; *dal*: prolidase deficient mice; EGL, External Granular Layer; ML: Molecular Layer; IGL: Internal Granular Layer. Magnification: scale bar of 200µm (a,b,g,h); 50 µm (c,d); 100µm (e,f).

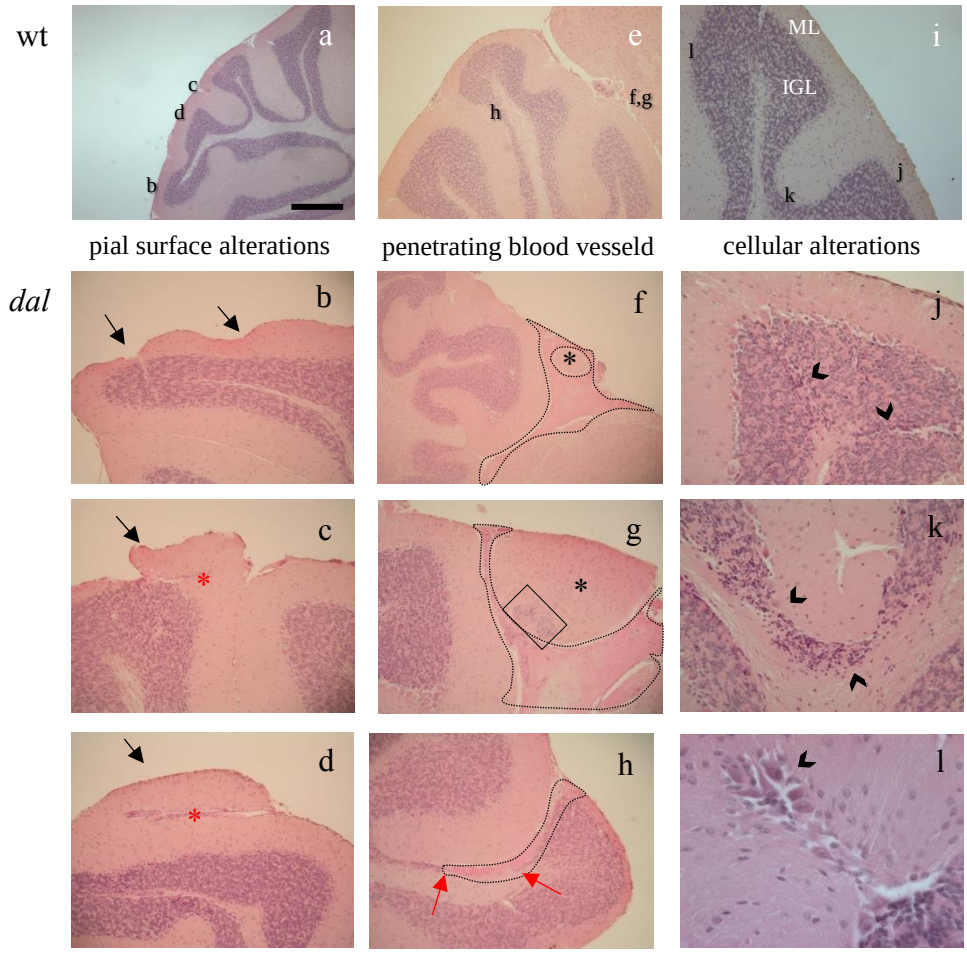

Figure 8. Haematoxylin and eosin staining at P21 and P60. *dal* figures retrieved from P60 wt (a,e,i) *dal/dal* (b,c,g,h,l) and *dal/+* (f,j,k) and P21 *dal/+* (d) mice. Abbreviations: wt: wild type; *dal*: prolidase deficient mice; ML: Molecular Layer; IGL: Internal Granular Layer. Magnification: scale bar of 400 µm (a,f), 150 µm (b-e,g-i), 80 µm (j-k), 40 µm (l).

4.3. The granule cells proliferation and migration

Granule Cells Proliferations

During the cerebellar postnatal development, immature granule cells, located in the EGL, proliferate adjacent to the pBM and then migrate through the ML toward the IGL. In particular, in the EGL it is possible to distinguish a proliferative layer and a pre-migratory layer. The first one is formed by proliferating cells that can be labelled using the Proliferating Cell Nuclear Antigen (PCNA) antibody by immunofluorescence reactions (red fluorescence); nuclei are counterstained in Hoechst 33538 (blue fluorescence) (Figure 9). Comparing the wt with *dal* mice was evident a reduction in the thickness of the PCNA-positive proliferative layer (fig. 9a-c, wt; 9d-f, *dal*) and of the total EGL. Fig. 9g represents a graph of the thickness measurements of total EGL, and of the proliferative and pre-migratory layers. As the immunofluorescence reactions highlighted, a general reduction in the thickness of the total EGL in *dal* mice compared to wt mice emerged, even if this differences was not significant (wt 0.23±0.04; *dal/+* 0.173±0.05; *dal/dal* 0.193±0.05). Despite that, the measurements of the thickness of proliferative EGL layer revealed a reduction in *dal/+* (0,093±0,04; $p<0.05$) and *dal/dal* (0,0773±0,03; $p<0.01$) animals compared to the wt (0,163±0,04) and no significant differences among *dal* mice ($p>0.05$) (fig. 9g). Moreover, the ratio of proliferative EGL/pre-migratory EGL was evaluated in *dal* and wt mice: 70:30 in wt, 53:47 in *dal/+* and 40:60 in *dal/dal*. The reduction of the PCNA was also confirmed by a decreased amount of the protein detected through western blotting analysis in *dal* (*dal/+* 64%±12; *dal/dal* 63%±9) animals compared to wt (100%) (fig. 9h)

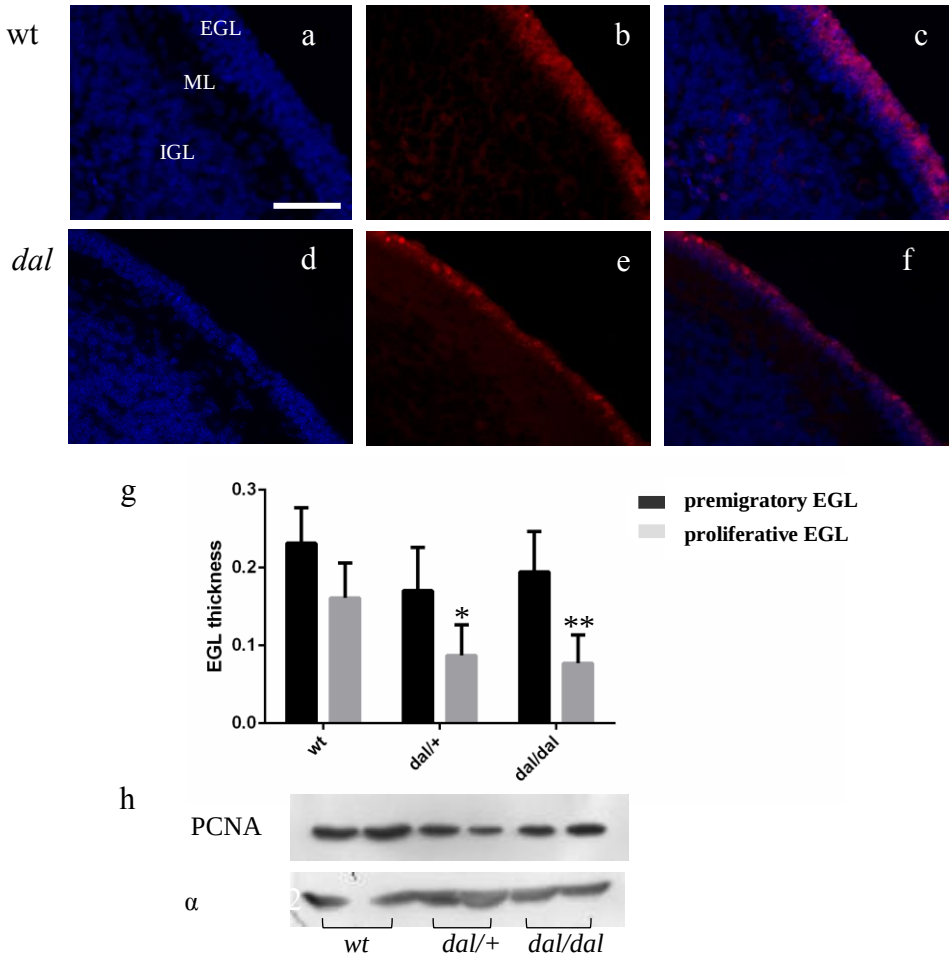

Figure 9. Immunofluorescence reaction at P10 for PCNA (red fluorescence); nuclei (blue fluorescence). *dal* figure retrieved from *dal/dal* mouse. Abbreviations: wt: wild type; *dal*: prolidase deficient mice; EGL, External Granular Layer; ML: Molecular Layer; IGL: Internal Granular Layer. Magnification: scale bar of 100 μm (a-f)

GFAP & Laminin immunofluorescence reactions

The laminin detection was useful not only to study the integrity of pBM, but also to evaluate the involvement of the pBM in the migration process of granule cells and its interaction with the radial glial fibers. The radial glial fibers are anchored to the laminin layer of pBM being so able to act as scaffold for the migrating neurons from EGL toward IGL. Laminin in green fluorescence; radial glia cells were detected by GFAP antibody in red fluorescence; and nuclei were counterstained in blue fluorescence.

In the cerebellar cortex at P10 (Figure 11), wt mice (fig. 11a-c) had a continuous layer of laminin positive pBM and the glial endfeet were perpendicularly attached to the laminin layer. In *dal* mice the laminin sheet was interrupted in correspondence of which the glial fibers were not detectable or weakly stained (fig. 11d-f; white arrows). Fig. 11g-i shown that even if the laminin layer seemed to be whole, in correspondence of apical malformations, the glial fibers were bend and no more perpendicular to the pial surface (white arrowhead), following the windy of the surface; or the glial endfeet were lost (red arrows).

At P60, the positivity for GFAP was the same of P10 mice; therefore, in wt mice the GFAP fibers were organized in the ML perfectly perpendicular to the continuous laminin pBM and anchored to it. In *dal* mice, GFAP fibers were interrupted in correspondence of apical anomalies. The inner portion of the detached-ML was emitting in green fluorescence. This can be due to the presence of blood cells (red blood cells lightly fluoresce in green) detected (also by haematoxylin and eosin staining) between the two ML portions, and on the other hand to the presence of laminin positive BM. In turn, it can be the pBM and/or BV BM. Since there were GFAP fibers that seemed to be anchored to the laminin positive BM, it was possible to assume that the BM observed was the one of pial meninx. Moreover, the GFAP fibers were present even in the outer-ML and attached to the laminin layer below.

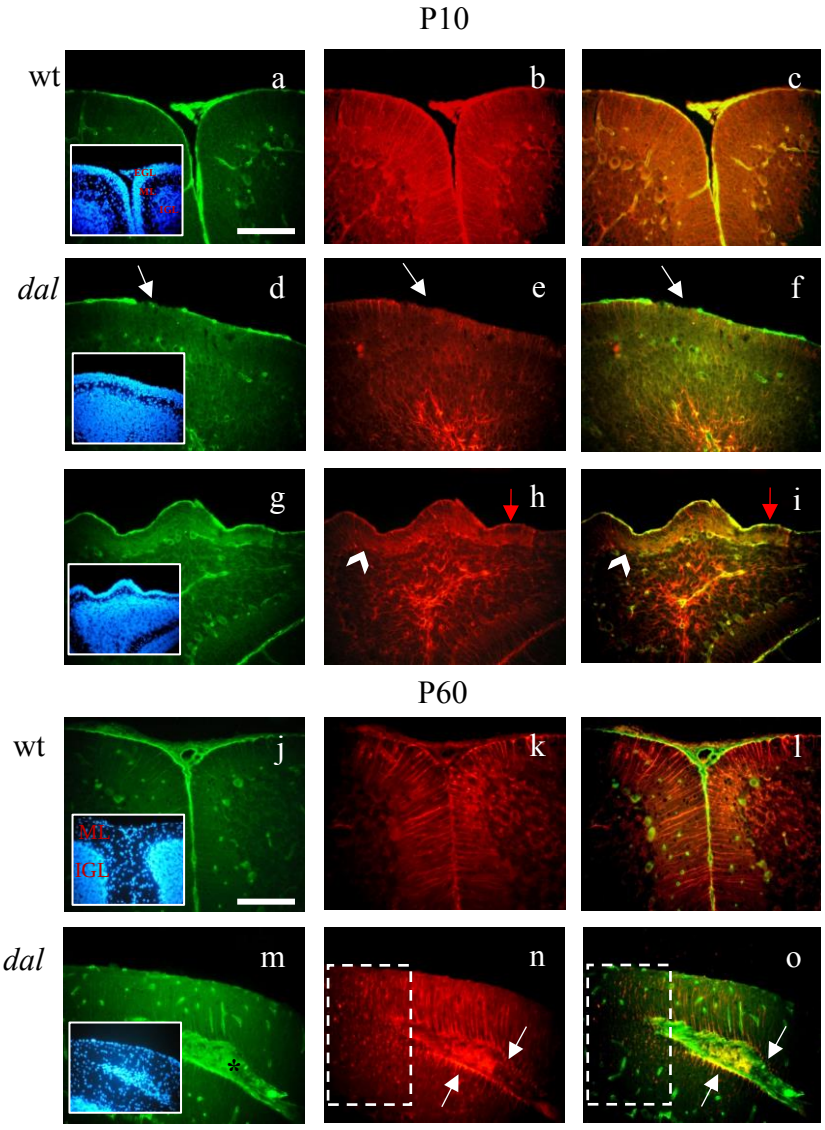

Figure 11. Immunofluorescence reaction at P10 (a-i) and P60 (j-o) for laminin (green fluorescence) and GFAP (red fluorescence); nuclei (blue fluorescence). *dal* figures retrieved from *dal/dal* (d-f) and *dal/+* (g-i,m,o) mice. Abbreviations: wt: wild type; *dal*: prolidase deficient mice; pBM: pial Basement Membrane; EGL, External Granular Layer; ML: Molecular Layer; IGL: Internal Granular Layer. Magnification: scale bars of 100 μm (a-i); 50 μm (j-o; insets a,d,g) 25 μm (insets j,m).

4.4. The Calcium Homeostasis

Calcium plays a fundamental role in the cells as second messenger and its concentration as free ion in the cytoplasm is principally regulated by Calcium-Binding Proteins (CBPs) and pumps anchored to the cell membrane for the extrusion and the internalization of the ion itself. CBPs present different cell specificity and developmental timing expression. Calbindin (CB) and parvalbumin (PV) are respectively fast and slow calciμm buffer proteins: both mark Purkinje neurons, in particular CB the entire soma, dendrite and axon, while PV only the Purkinje cell soma and the pinceau at the axon-hillock. CB appears early, after mitosis while neurons are migrating and differentiating, PV is expressed later with an increase in neuronal activity. Moreover, PV also labels basket, Golgi and stellate cells. The Plasma Membrane Calciμm ATPase 1 (PMCA1) is involved in the extrusion of calciμm from the cell, it marks at P10 Purkinje soma and dendrites, while at P60 is mainly localized in the ML, and at both ages the granule cells of IGL.

Calbindin

CB immunostainings pointed out Purkinje neurons whose morphology could be appreciated in its entirety. In wt mice, at both ages P10 and P60, the Purkinje neurons are intensely marked and with a perfect dendritic arborisation (fig. 12a-c, P10; 12g-h, P60). At P10, Purkinje alterations came out in *dal* mice with cerebellar apical anomalies and layering defects ,as loss of Purkinje cells or differently oriented Purkinje dendrites (fig. 12d-f; white arrow).

At P60, the dendrites of Purkinje neurons of *dal* mice appeared less branched (fig. 12i) and ectopic Purkinje neurons within the IGL, lacking dendrite branches were also detected (fig. 12j). To exclude that this observations were due to a wrong cerebellar inclusion and cut, only cerebella in which it was possible to detect a correct general organization of the lobules were taken in consideration.

The findings related to the Purkinje morphology and the intensity of the labelling were similar at P10 and P60 mice. However, by western blotting analysis no relevant differences in CB content among wt and *dal* mice at P10 were detected. The mean values of wt after actin normalizations were considered 100% and the *dal/+* and *dal/dal*, normalized to wt, showed a mean of 100%±0.3% and 100%±0.2% respectively. At P60, there was a statistical significant decrease in CB content at P60 in *dal* mice (*dal/+* 83%±0.01%; *dal/dal* 58%±0.07%; p-value<0.001) compared to wt cerebellμm tissue lysates. Even the differences between *dal/+* and *dal/dal* was statistically significant (p<0.005).

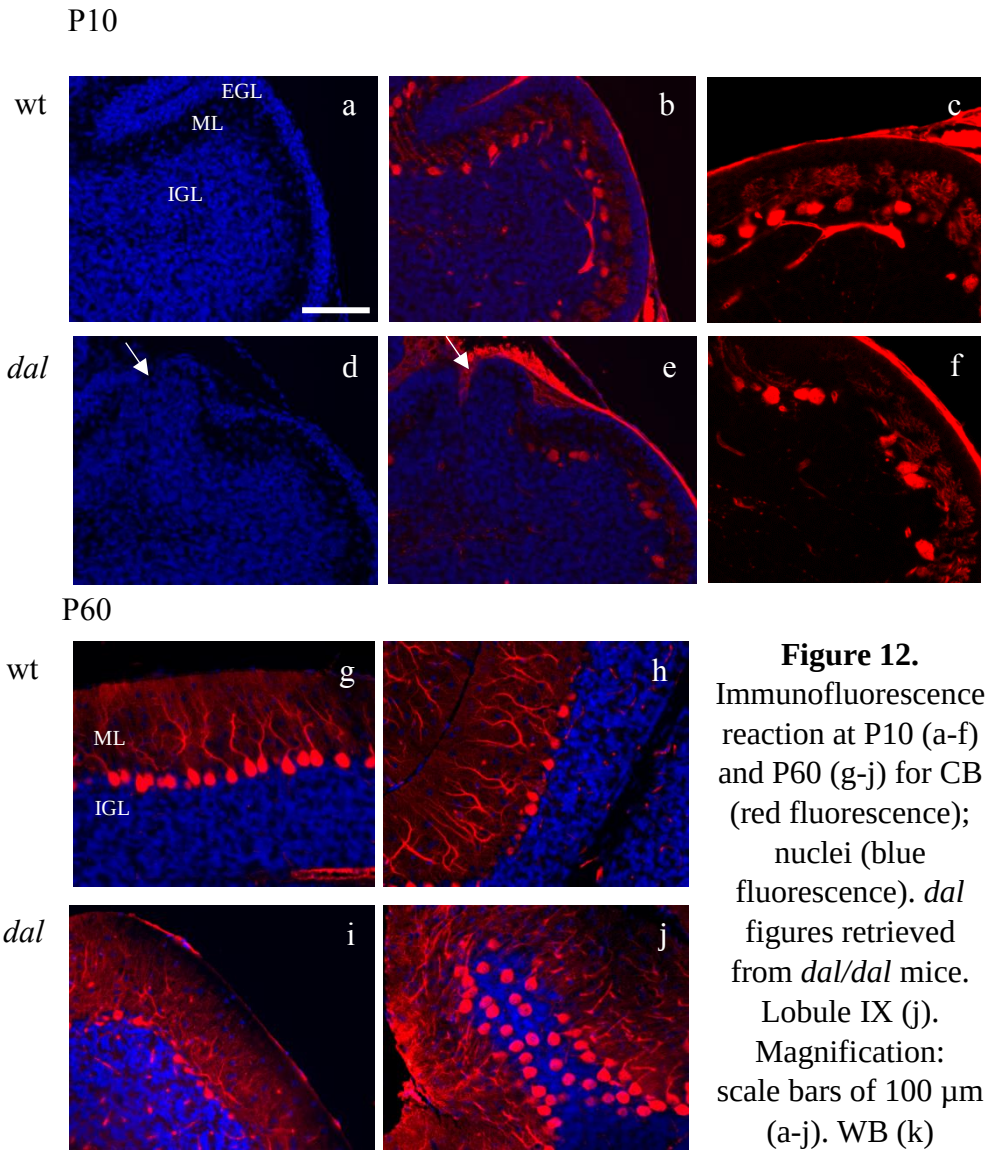

Figure 12. Immunofluorescence reaction at P10 (a-f) and P60 (g-j) for CB (red fluorescence); nuclei (blue fluorescence). *dal* figures retrieved from *dal/dal* mice. Lobule IX (j). Magnification: scale bars of 100 µm (a-j). WB (k)

Parvalbumin

The PV immunolabeling pointed out the morphology of the Purkinje pinceaux at the axon hillock (Figure 13). Generally, the pinceaux should be cone-shaped. To verify the aspect of the pinceau the number of visible, well defined cone-shaped pinceaux (fig. 13a) and of altered with a flattened shape (fig. 13b) were counted. For some Purkinje cells the pinceau was not detectable or ascribable to any of the above-mentioned groups, therefore these pinceaux were excluded from the count. Comparing the mean values of the count of cone-shaped and flattened pinceau for each genotype, the results that came out were interesting. There was no significant difference between the number of cone-shaped pinceaux among the three genotypes, since the high variability within each animal (wt 76%±15%; *dal/+* 37%±19%; *dal/dal* 45±15%). A significant increase in the number of flattened one in *dal/+* and *dal/dal* (p-value<0.01) compared to wt mice, and in *dal/dal* compared to *dal/+* (p-value<0.05) animals (wt 24%±15%; *dal/+* 63%±19%; *dal/dal* 55%±15%). In fig. 9c the mean value percentages of cone-shaped and flattened pinceaux was illustrated for the three genotypes.

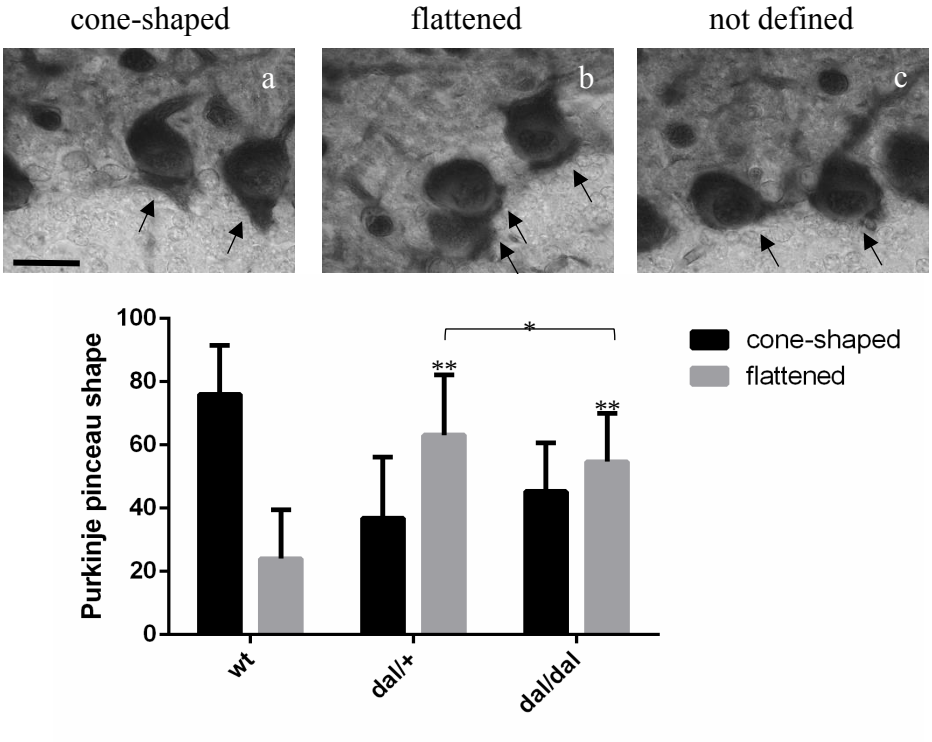

Figure 13. Immunohistochemical reaction at P60 for parvalbumin (a-c). Figures retrieved from *dal/+* mice. Magnification: scale bar of 20µm (a-c). Graph (d) represented the percentage of cone-shaped and flattened pinceaux divided per genotype.

PMCA1

At P10 PMCA1 should mark the Purkinje dendrites in the ML and the cell membrane of Purkinje soma. There were no evident differences in the labeling comparing the cerebellar layers among wt (fig. 14a-c) and *dal* (fig. 14d-f) animals. This was also confirmed by OD measurements in which the p-value was $p>0.05$ for each group comparison (data not shown).

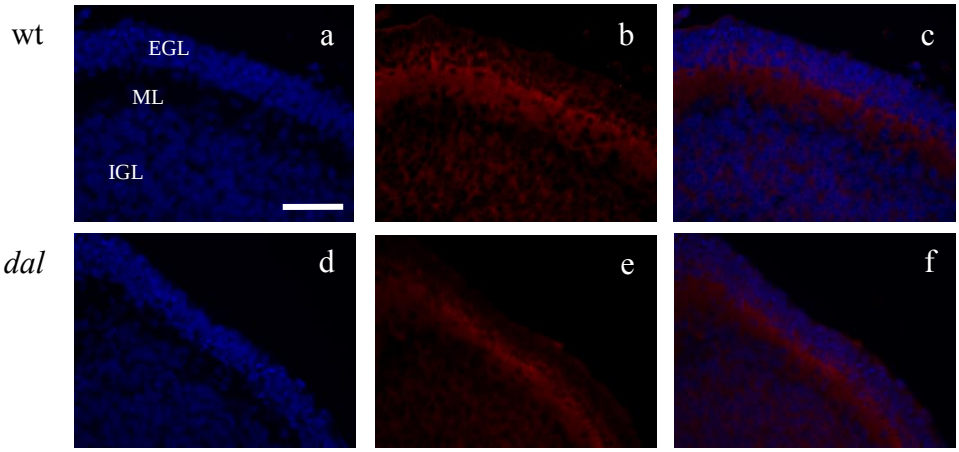

Figure 14. Immunofluorescence reaction at P10 for PMCA1 (red fluorescence); nuclei (blue fluorescence). *dal* figure retrieved from *dal/dal* mouse. Abbreviations: wt: wild type; *dal*: prolidase deficient mice; EGL, External Granular Layer; ML: Molecular Layer; IGL: Internal Granular Layer. Magnification: scale bar of 100µma-r.

At P60 (fig. 15) there was a general decrease in the detection of PMCA1 in all layers, but the differences among the ML, PL and IGL in the three genotypes were not statistical significant ($p<0.05$; data not shown).

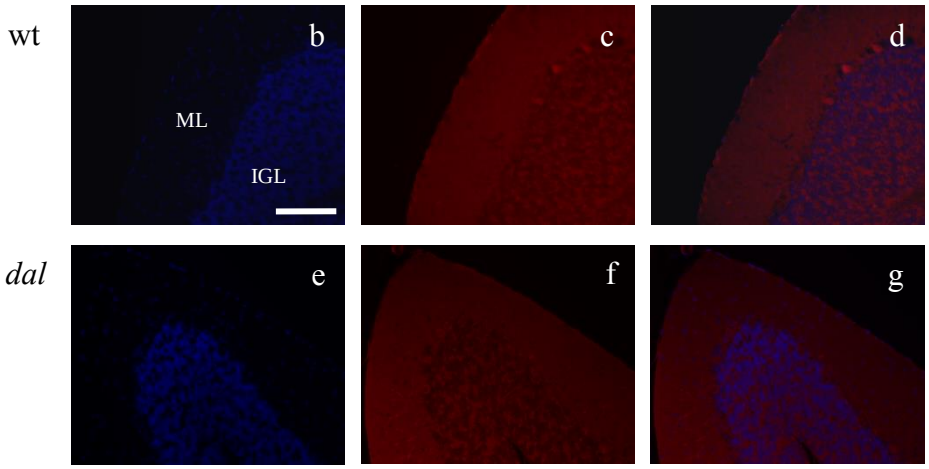

Figure 15. OD measurement graph (a) and immunofluorescence reactions (b-g) at P60 for PMCA1 (red fluorescence); nuclei (blue fluorescence). *dal* figure retrieved from *dal/dal* mouse. Abbreviations: wt: wild type; *dal*: prolidase deficient mice; ML: Molecular Layer; IGL: Internal Granular Layer. Magnification: scale bar of 200µma-r.

4.5. The Cytoskeleton

To study the role of cytoskeleton, particularly in relation to the Purkinje cells, different markers with different cell localization and expression timing were considered; these markers were related to microtubules and intermediate filaments. The stability/dynamics of microtubules was evaluated through microtubule associated proteins as MAP 2, DCX and phospho-tau$^{(pSer202/509)}$. In particular MAP 2 is essential for the stability of microtubules and it is expressed by Purkinje and mature granule cells at P10 and P60; DCX is highly expressed by migrating granule cells at P10 and it is no more express at P60; and phospho-tau$^{(pSer202/509)}$ represents one of the hyperphosphorylated form of the tau protein which is physiologically present at P10 during the development and decrease as the brain is maturing, then its presence is associated no more with the instability of microtubules for the cellular maturation, but becomes a neurodegeneration sign.

MAP2, DCX and phospho-Tau$^{(pSer202/509)}$

At P10, within the cerebellar layers different markers were considered: MAP2, DCX and phospho-Tau$^{(pSer202/509)}$. Concerning the MAP2 and phospho-Tau$^{(pSer202/509)}$ immunelabeling no relevant differences were found comparing wt and *dal* mice. The positivity was detected in the pre-migratory-EGL, ML and IGL for MAP2 (fig.16a-b) and in the ML and IGL for phospho-Tau$^{(pSer202/509)}$ (fig.16c-d). DCX marked stronger the pre-migratory-EGL, and weaker the ML and IGL, while the proliferative-EGL was almost unlabeled (fig. 16e-f); at P60 there was a strong decrease for DCX (immunohistochemical reactions not showed) as the neuronal migration ended.

The OD measurements did not highlighted significant differences among the cerebellar layers, comparing wt, *dal/+* and *dal/dal* for the three markers above mentioned at P10 (data not shown).

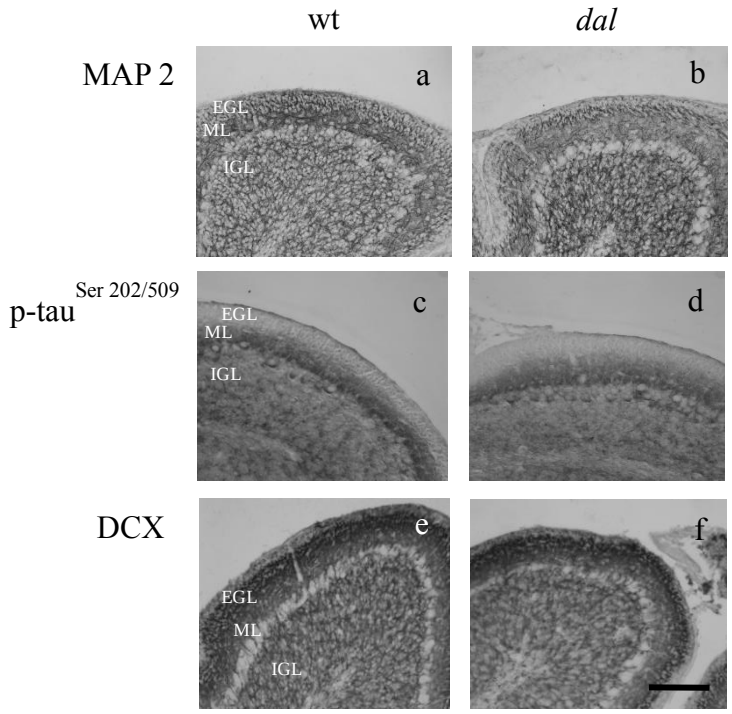

Figure 16. Immunohistochemical reactions at P10 for MAP 2 (a,b), phospho-tau$^{(pSer202/509)}$ (c,d) and DCX (e,f). *dal* figure retrieved from *dal/dal* mice. Abbreviations: wt: wild type; *dal*: prolidase deficient mice; EGL: External Granular Layer; ML: Molecular Layer; PL:Purkinje Layer; IGL: Internal Granular Layer. Magnification: scale bar of 200µma-h.

phospho-Tau $^{(Ser202/509)}$

At P60, the phospho-Tau $^{(Ser202/509)}$ labeling was drastically decreased in wt mice in the ML and IGL (fig. 17a) in comparison to P10 mice. However, rarely phospho-tau$^{(pSer202/509)}$ positive Purkinje cells in the apical part of some lobules were visible (fig. 17b, lobule V). The results in terms of positivity for Purkinje neurons were very different comparing wt and *dal* mice for this marker, since the amount of positive Purkinje cells in the ML was higher in *dal/+* and *dal/dal* animals in apex (fig. 17c) as well as in fissures (fig. 17d) of lobules, compared to wt mice.

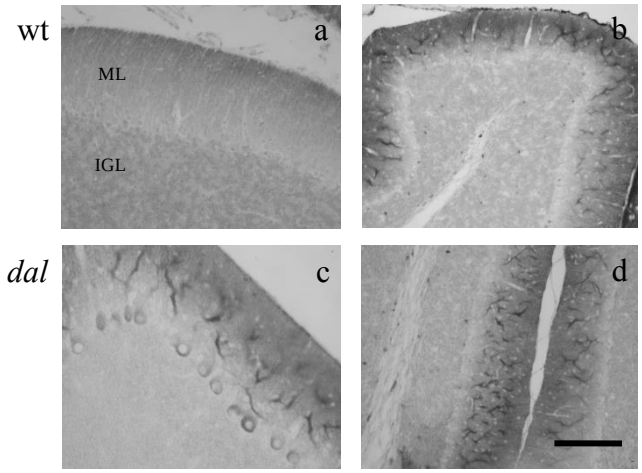

Figure 17. Immunohistochemical reaction at P60 for phospho-tau$^{(pSer202/509)}$. *dal* figure retrieved from *dal/dal* mice. Abbreviations: wt: wild type; *dal*: prolidase deficient mice; ML: Molecular Layer; PL: Purkinje Layer; IGL: Internal Granular Layer. Magnification: scale bar of 100 μm (a-h).

After the immunohistochemistry reactions for phospho-tau$^{(pSer202/509)}$ marker, several measurements were carried out:

- Tau-positive Purkinje soma and other positive cells in the IGL and white matter were counted, but the results did not shown statistical significant differences among the three genotypes;
- the area occupied by positive Purkinje dendrites along lobules from VIa to VIII was measured, normalized for the area of total ML and expressed as percentage. The average of the area calculated for each animal was then used to compare the mean values with a t test. The results relevead that in wt only the 0.4%±0.1 of ML area was occupied by positive Purkinje dendrites, 2%±0.6 in *dal/+* and 2.1%±0.9 in *dal/dal.* The differences compared *dal* to wt animals were statistically significant (p-value<0.001), while no evident differences were present among *dal* animals;

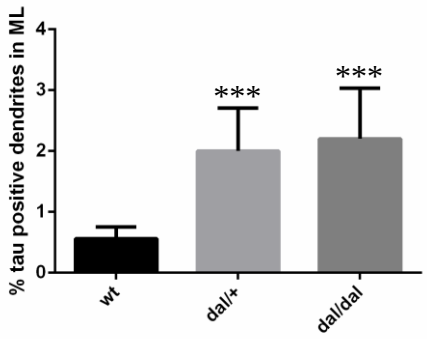

- the OD was evaluated for the ML. The results confirmed an increase in the OD of ML in both *dal/+* (p-value<0.001) and in *dal/dal* (p-value<0.001) compared to the wt animals (wt 102±7.3; *dal/+*134±6; *dal/dal* 130±7.2).

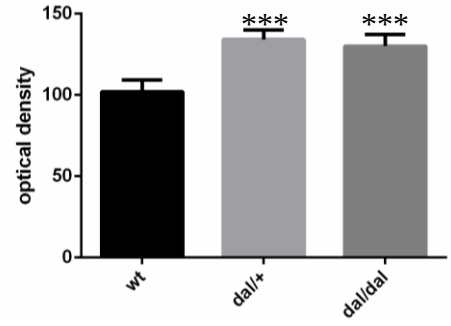

Since there were strong differences between the labeling for this marker at P10 and P60 and at P60 between wt and *dal* mice, we also checked the positivity for phospho-Tau$^{(pSer202/509)}$ at other postnatal ages in-between as P21 and P30. The labeling at P21 was very similar to the P10 one concerning the wt with labelled ML and IGL (fig. 18a); while the positivity of wt at P30 (fig. 18b) was similar to that at P60, with a strong reduction in the ML labeling. Even in these postnatal ages rare Purkinje neurons were immunopositive in wt mice (not shown). In *dal* mice, at both P21 (fig. 18c) and P30 (fig. 18d), the Purkinje were labelled as in the *dal* animals at P60.

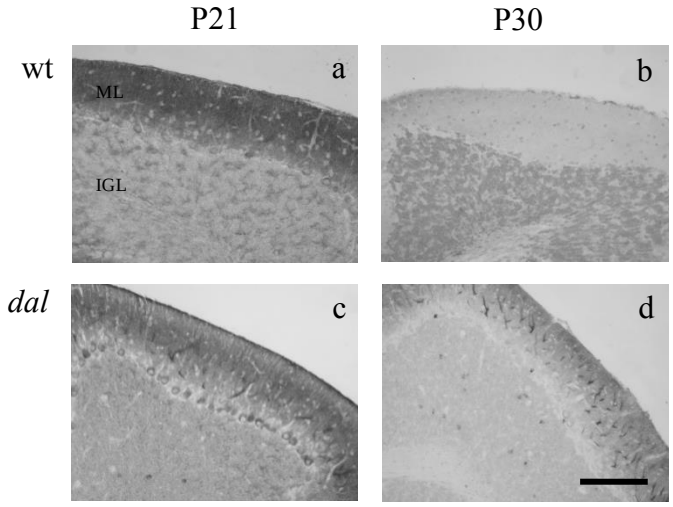

Figure 18. Immunohistochemical reaction at P21 (a,c) and P30 (b,d) for phospho-tau$^{(pSer202/509)}$. *dal* figure retrieved from *dal/dal* mice. Abbreviations: wt: wild type; *dal*: prolidase deficient mice; ML: Molecular Layer; PL: Purkinje Layer; IGL: Internal Granular Layer. Magnification: scale bar of 100 μm (a-h).

phospho-Tau $^{(Ser202/509)}$ and MAP2

The presence of phospho-tau$^{(pSer202/509)}$ at P60 in *dal* mice indicated an increase in the instability of microtubules, therefore the concomitant presence of MAP2 (a microtubule stabilizer protein) was evaluated. Double immunofluorescence reactions (red fluorescence MAP2; green fluorescence phospho-tau$^{(pSer202/509)}$; nuclei counterstained in blue fluorescence) shown that in the wt the positivity for MAP2 was always homogeneous (fig. 19a,b) and mainly in the thinner Purkinje dendrite branches. In *dal* mice there were different circumstances: *i.* the Purkinje dendrites were labelled by phospho-tau$^{(pSer202/509)}$ and the positivity for MAP2 did not change (fig. 19c,d); *ii.* some Purkinje neurons were immunopositive to phospho-tau$^{(pSer202/509)}$ with a decrease in the labeling for MAP2 (fig. 19e,f). There was no lobule specificity for these observations and it was not correlated to the number of neurons immunopositive for phospho-tau$^{(pSer202/509)}$. Anyway, in *dal* mice the MAP2 immunostaining evidenced thicker Purkinje dendrite branches. It is not possible to exclude that these branches acquired an enlarged caliber branches or they represented the main dendrite branches of Purkinje cells.

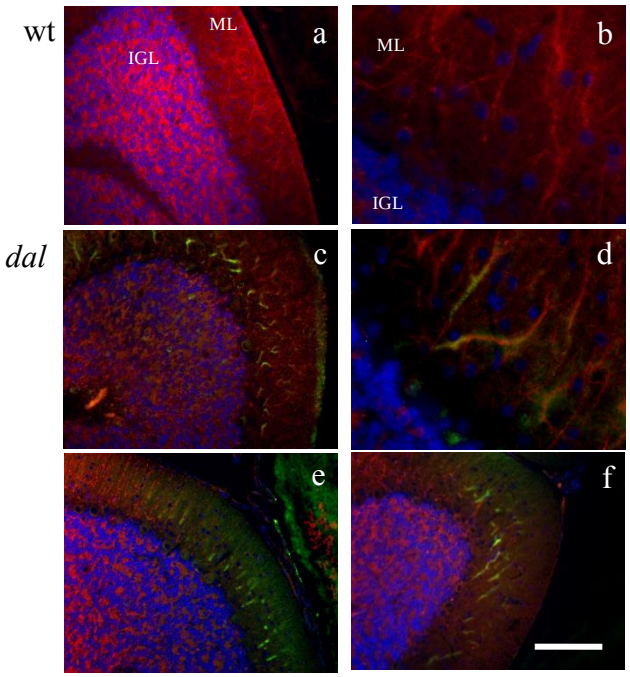

Figure 19. Immunofluorescence reactions at P60 for MAP2 (red fluorescence), phospho-tau$^{(pSer202/509)}$ (green fluorescence); nuclei (blue fluorescence). *dal* figure retrieved from *dal/dal* mice. Abbreviations: wt: wild type; *dal*: prolidase deficient mice; ML: Molecular Layer; PL: Purkinje Layer; IGL: Internal Granular Layer. Magnification: scale bar of 100 µm (a,c,e-f) and 20 µm (b,d).

phospho-Tau $^{(Ser202/509)}$ and CB

To better investigate the localization of phospho-tau$^{(pSer519/202)}$, the marker was co-localized with the labelling for CB (Figure 20) (red fluorescence CB; green fluorescence phospho-tau$^{(pSer202/509)}$; nuclei blue fluorescence). Therefore, the positivity of phospho-tau$^{(pSer519/202)}$ in *dal* mice was in Purkinje neurons and in particular in thicker dendrite branches (fig. 20b,c) and in some cell body (fig.20 d, white arrows), in lobules apex and fissures, without lobules specificity. Moreover, it was highlighted that Purkinje neurons in wt were perfectly shaped and labelled by CB (fig. 20a), while in *dal*, Purkinje neurons positive for the phospho-tau$^{(pSer519/202)}$ were less labelled by CB. On the other hand, the reduction in the amount of this protein at P60 was already shown in "the calcium homeostasis" paragraph through the western blotting analysis.

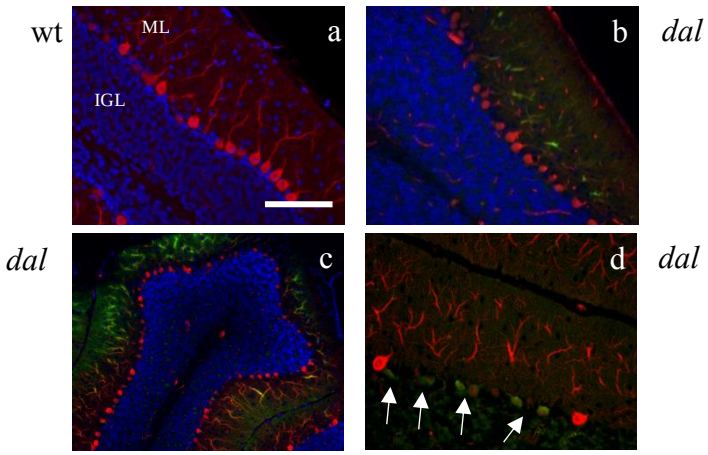

Figure 20. Immunofluorescence reaction at P60 for calbindin (red fluorescence), phospho-tau$^{(pSer202/509)}$ (green fluorescence); nuclei (blue fluorescence). *dal* figure retrieved from *dal/dal* mice; lobule V in c. Abbreviations: wt: wild type; *dal*: prolidase deficient mice; ML: Molecular Layer; PL: Purkinje Layer; IGL: Internal Granular Layer. Magnification: scale bar of 100 µm (a,b,d) 150 µm (c).

phospho-Tau $^{(Ser202/509)}$ and NF-H

The marker chosen for the intermediate filament is the NF-H; it is present in the mature brain and labels axons of basket cells, which form synaptic contacts with Purkinje dendrite branches in the ML, and the basket pinceau around the Purkinje axon hillock. The heavy neurofilaments were quantified at P60, since its expression at P10 is very low.

In particular, at P60 in wt mice the basket-like structure around the Purkinje soma was strongly labelled as well as the axons which run perpendicular to the Purkinje dendrite tree (fig. 21a). In *dal* mice was evident a strong decrease in the positivity for this marker highlighting thinner basket-like structures and less or weaker stained axons in the ML (fig. 21 b).

In particular, through double immunofluorescence reactions (fig. 21c,d; red fluorescence NF-H; green fluorescence phospho-tau$^{(pSer202/509)}$; nuclei blue fluorescence), a noticeable decrease in the NF-H positivity was detected close to Purkinje neurons expressing the phospho-tau$^{(pSer519/202)}$. Moreover, abnormal or less developed pinceaux were observed.

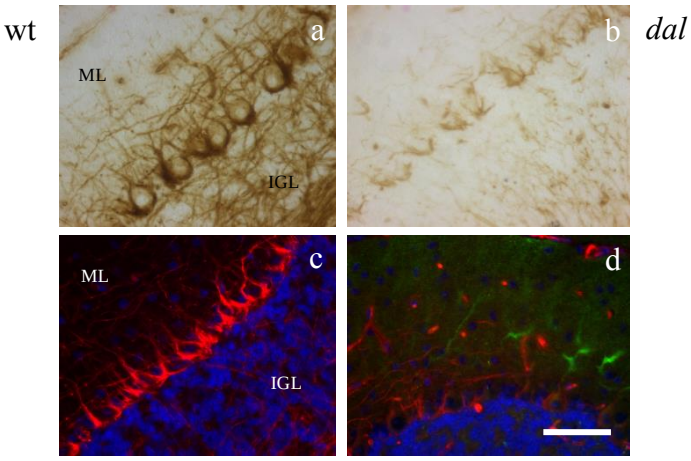

Figure 21. Immunohistochemical reaction for NF-H and immufluorescence reaction at P60 for NF-H (red fluorescence), phospho-tau$^{(pSer202/509)}$ (green fluorescence); nuclei (blue fluorescence). *dal* figure retrieved from *dal/dal* mice. Abbreviations: wt: wild type; *dal*: prolidase deficient mice; ML: Molecular Layer; PL: Purkinje Layer; IGL: Internal Granular Layer. Magnification: scale bar of 100 µma-h.

4.6. The glutamatergic and GABAergic systems

The major excitatory and inhibitory neurotransmission systems were taken in consideration, i.e. the glutamatergic and GABAergic systems, respectively. In particular the markers used were: glutamate receptors (gluR2 and gluRδ2) and vesicular glutamate transporters (VGLUT1 and 2); GABA synthesis enzyme (GAD67) and GABAα6 receptor.

Glutamate Receptors

The immunohistochemical reaction for GluR2 and the OD measurements did not highlight significant differences between the genotypes at P10 (fig. 22a,b; OD results not shown, p-value>0.05). However, at P60 even if the differences were not statistical significant, after the OD measurements between wt (fig. 22c) and *dal* mice (data not shown), it was important to highlight the heterogeneity in the Purkinje labeling. In the *dal* animals there were Purkinje cells with intensely labelled and shrunken soma (fig. 22d), others with a very weak positivity in the soma (fig. 22f), and even others with dendrite branches also immunopositive (fig. 22e). However, there was no lobule specificity in these observations.

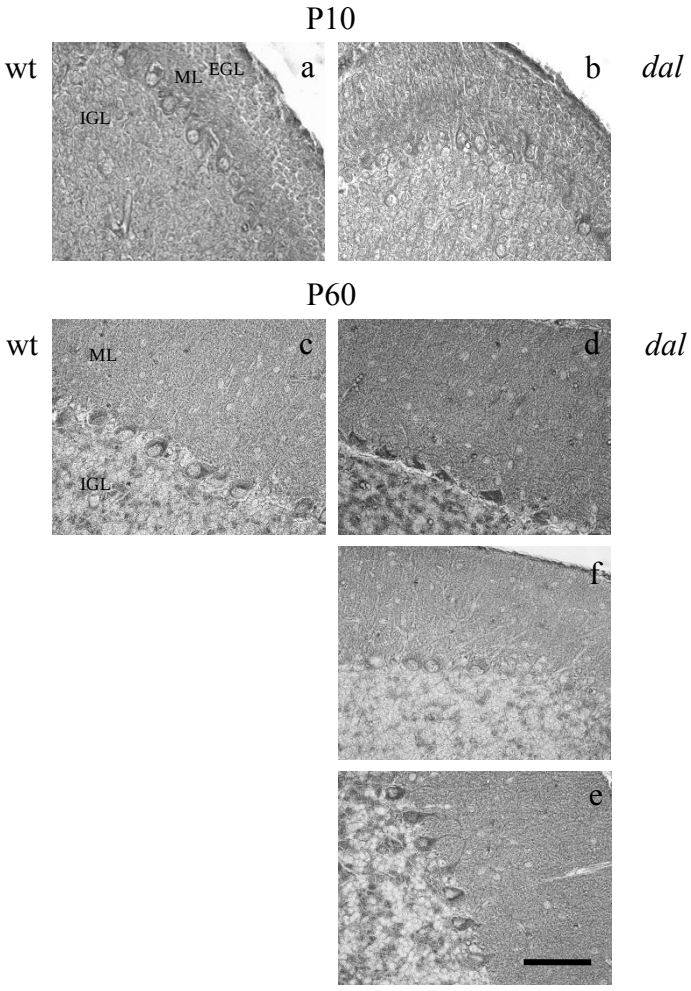

Figure 22. Immunohistochemical reaction for GluR2 at P10 (a,b) and P60 (c-e). *dal* figure retrieved from *dal/dal* mice. Abbreviations: wt: wild type; *dal*: prolidase deficient mice; ML: Molecular Layer; PL: Purkinje Layer; IGL: Internal Granular Layer. Magnification: scale bar of 200 μm (a,b) 100 μm (c-e).

The immunohistochemical reaction and OD measurements for GluRδ2 did not highlight significant differences between the genotypes (fig. 23a,b; OD results not shown, p-value>0.05) at P10. At P60, there were different intensity of labelling between wt (fig. 23c) and *dal* mice (23d,e), but the differences were not statistically significant after the OD measurements . This may be due to the heterogeneity in the Purkinje cell labeling, particularly of *dal* mice. In fact, there were Purkinje cells with an intensely immunopositive soma (fig. 23d) as in the wt mice, and other cells with a very weak positivity (fig. 23e). Even in this case there was no lobule specificity.

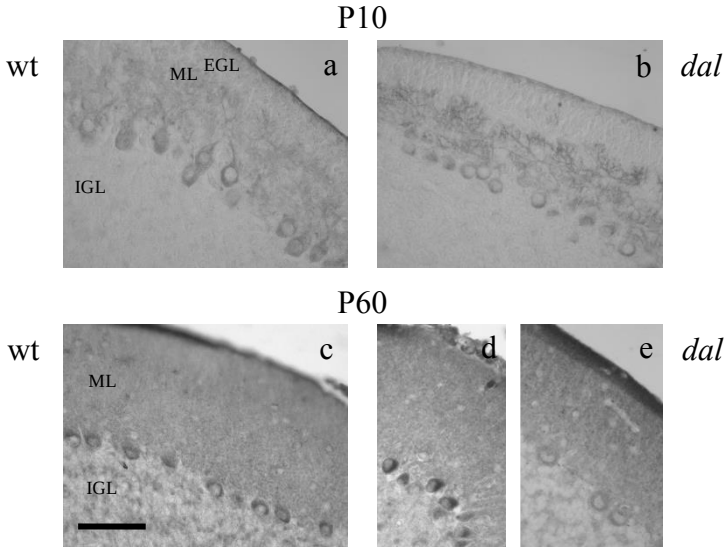

Figure 23. Immunohistochemical reactions for GluRδ2 at P10 (a,b) and P60 (c-e). *dal* figure retrieved from *dal/dal* mice. Abbreviations: wt: wild type; *dal*: prolidase deficient mice; EGL: External Granular Layer; ML: Molecular Layer; PL: Purkinje Layer; IGL: Internal Granular Layer. Magnification: scale bar of 100μm (a-e).

Vesicular Glutamate Transporters

In the cerebellum VGLUT1 is mainly located in parallel and mossy fiber terminals. Immunofluorescence reactions allowed to label these fibers with VGLUT1 in green fluorescence; nuclei counterstained in blue fluorescence. According to VGLUT1 labeling at P10 (fig. 24a,b) and P60 (fig. 24c,d) there were no evident differences among the animals, as it was also pointed out by OD measurements and statistical evaluations (OD results not shown, p-value>0.05). The positivity for VGLUT1 did not change also in cerebellar lobules with layering defects as in fig. 24b and 24d. Moreover, the double immunofluorescence reactions (fig. 24e,f), demonstrated that the labelling for VGLUT1 (green fluorescence) of ML in which Purkinje dendrites were immunopositive for phospho-tau$^{(pSer202/509)}$ (red fluorescence) did not change.

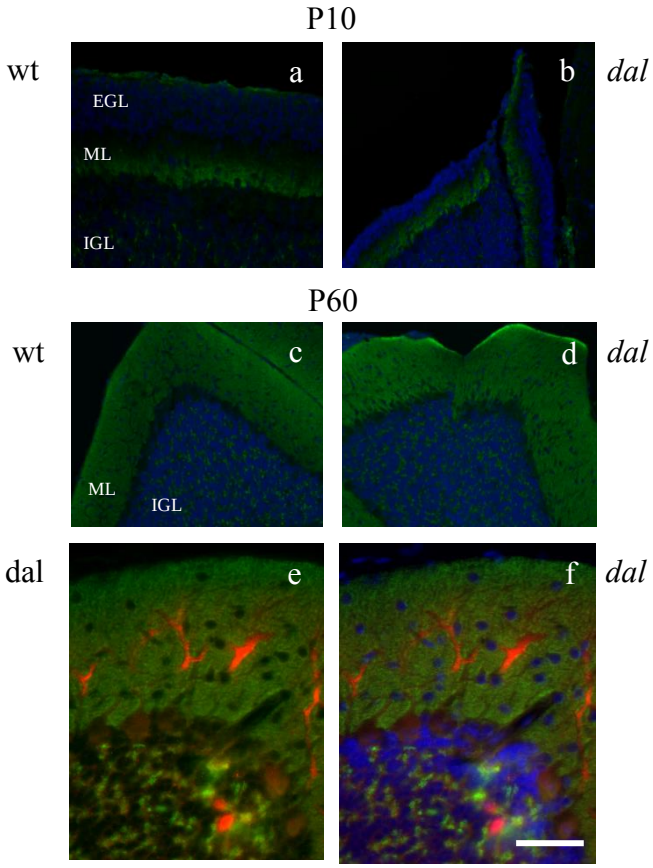

Figure 24. Single and double immunofluorescence reactions for VGLUT1 at P10 and P60, and VGLUT1 (green fluorescence) with phospho-tau$^{(pSer202/509)}$ (red fluorescence) at P60; nuclei (blue fluorescence). *dal* figure retrieved from *dal/dal* mice. Abbreviations: wt: wild type; *dal*: prolidase deficient mice; EGL: External Granular Layer; ML: Molecular Layer; PL: Purkinje Layer; IGL: Internal Granular Layer. Magnification: scale bar of 200 µm (a,d) 100 µm (e,f).

In the cerebellum, VGLUT2 (green fluorescence) is mainly located in climbing fiber terminals in ML and mossy fibers in IGL; CB allowed to mark Purkinje neurons in red fluorescence and nuclei were counterstained in blue fluorescence. At P10 a trend of increased positivity for VGLUT2 in all layers in *dal* mice compared to wt was detected, however, t test analysis relevead no statistically significant difference. The intensity of labeling in wt was homogeneous (fig. 25 a,b) and there were no particular changes in the *dal* mice, even in correspondence of apical anomalies (fig. 25d,e).
As the post-natal development is proceeding, the positivity of VGLUT2 in the ML should be concentrated mainly on the proximal portion of Purkinje dendrite branches. It was observed, especially in fissures, that there was already at P10 this stratification of positivity for VGLUT 2 (fig. 25c) in wt, while in *dal* mice the majority of lobules showed the positivity over the entire ML (fig. 25f).

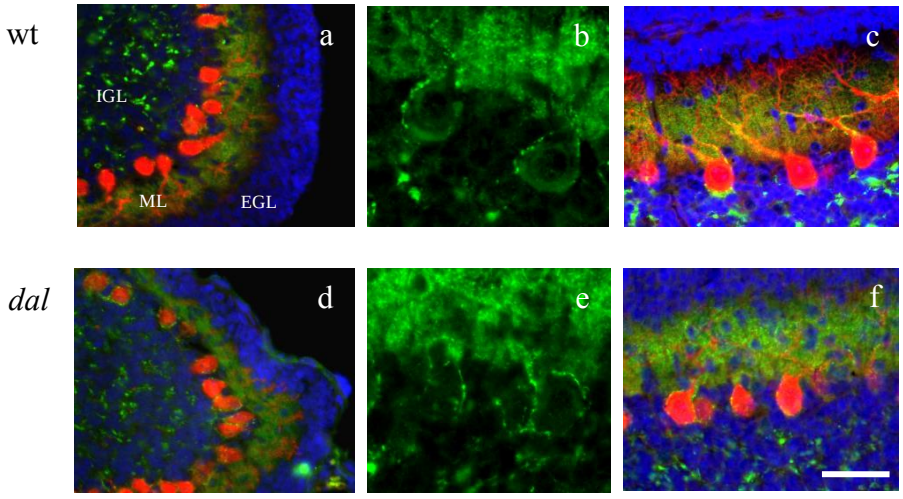

Figure 25. Immunofluorescence reactions for VGLUT2 (green fluorescence) with CB (red fluorescence) at P10; nuclei (blue fluorescence). *dal* figure retrieved from *dal/dal* mice. Abbreviations: wt: wild type; *dal*: prolidase deficient mice; EGL: External Granular Layer; ML: Molecular Layer; PL: Purkinje Layer; IGL: Internal Granular Layer. Magnification: scale bar of 100 µm (a,d), 50 µm (b,e) 75 µm (c,f).

In P60 mice (figure 26), VGLUT2 (green fluorescence) immunoreactive terminals were mainly identifiable on the main branches of Purkinje cell dendrite (labelled by CB, red fluorescence), in both wt (fig. 26a-c) and *dal* (fig. 26d-f) mice. Rarely, in mature brain the positivity was found around the soma: in wt mice this condition was observed in the 27% of Purkinje neurons while it was more frequent in *dal* mice (43% in *dal/+* and 42.5% in *dal/dal*). Significant increases of VGLUT2-positive nerve puncta on the dendrite branches were detected in ML in both *dal/+* ($p<0.01$) and *dal/dal* ($p<0.001$) animals; in the IGL glomeruli there was an increase labeling in both *dal/+* and *dal/dal* ($p<0.05$) animals.

Moreover, through double immunofluorescence reactions, it was observed the labeling of VGLUT2 (green fluorescence) together with phospho-tau$^{(pSer202/509)}$ (red fluorescence) (fig. 26g-i). From the Hoechst counterstaining it was possible to recognize the Purkinje nucleus that in this case was shrunken, then in green emerged on the plasma membrane of Purkinje soma the positivity for VGLUT2 and in red fluorescence the presence of VGLUT2 in the soma and the phospho-tau$^{(pSer202/509)}$ labeling, Purkinje cells with the two labeling were counted. From the counting emerged that none of the 27% of VGLUT^{+} Purkinje soma in wt was labeled by tau, while in *dal/+* mice among the 43% of VGLUT2^{+} Purkinje soma, the 4.3% was VGLUT2^{+} tau^{+} and in *dal/dal* mice among the 43% of VGLUT2^{+} Purkinje soma, the 26% was VGLUT2^{+} tau^{+}.

Moreover, considering the positivity for VGLUT2 on Purkinje dendrite branches, there were no differences comparing tau^{+} and tau^{-} dendrites.

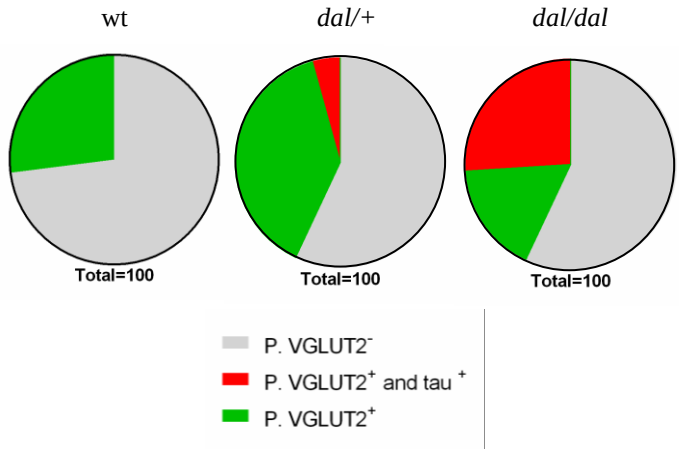

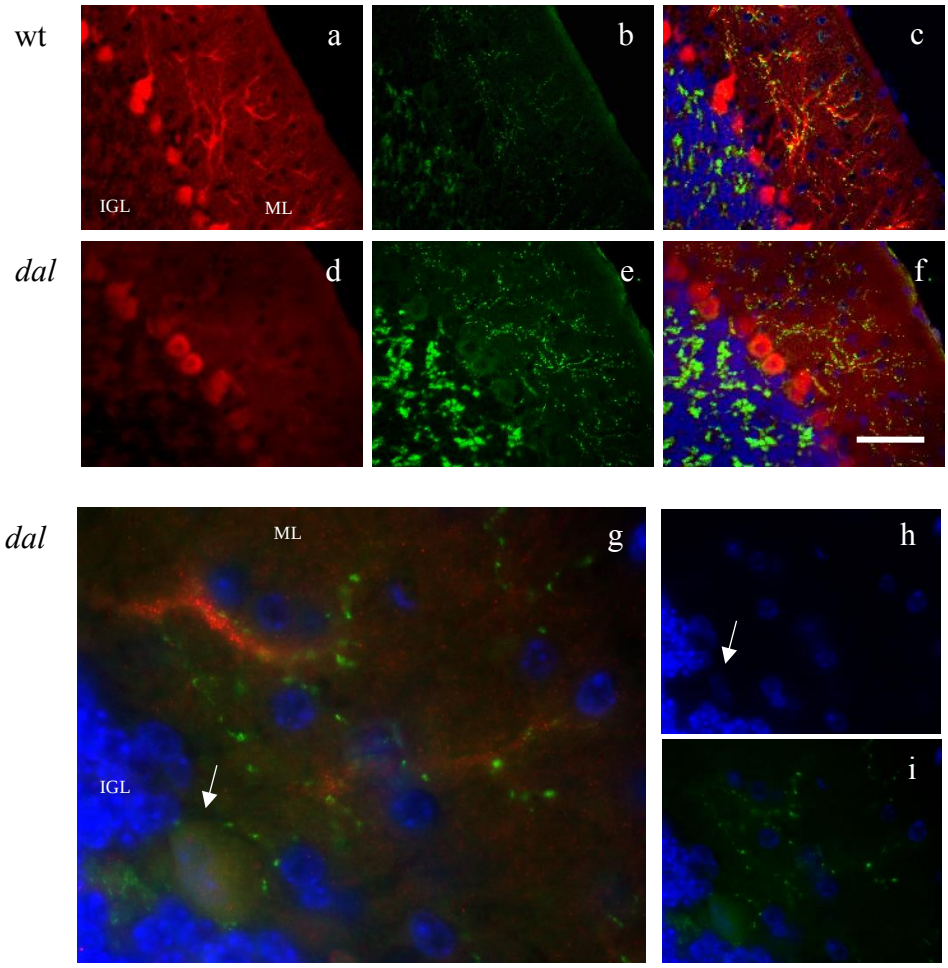

Figure 26. Double immunofluorescence reactions for VGLUT2 (green fluorescence) with CB (red fluorescence) (a-f), and VGLUT2 (green fluorescence) with phospho-tau$^{(pSer202/509)}$ (red fluorescence) (g-i) at P60; nuclei (blue fluorescence). *dal* figure retrieved from *dal/dal* mice. Abbreviations: wt: wild type; *dal*: prolidase deficient mice; ML: Molecular Layer; PL: Purkinje Layer; IGL: Internal Granular Layer. Magnification: scale bar of 100μm (a-f) 20 μm (g), 30 μm (h,i).

The enzyme of GABA synthesis

GAD67 is the synthesis enzyme of GABA; it gradually, during the postnatal development, becomes localized in the mature inhibitory synaptic terminals in association with synaptic vesicle, mitochondrial and presynaptic junctional membranes at the axon hillock of Purkinje neurons, which dendrite tree make also synaptic contacts with the ML basket cells. At P10 the staining showed differences between the wt (fig. 27a) and *dal* (fig. 27b) mice in terms of signal localization. In wt mice the formation of a cone-shaped pinceaux at the Purkinje cell axon hillock was started already, even if it was not clearly visible in all cells; instead, in *dal* mice, especially in correspondence of the apical surface of cerebellar anomalies, Purkinje cells were weakly labelled by GAD67 and cone-shaped pinceaux at the axon hillock were detected yet. Moreover, in all genotypes there were few cells with the labelled cytoplasm. The 29%±5 of Purkinje neurons in *dal* mice showed the positivity in the main dendrite branches, while only the 17%±3 was detectable in wt mice (fig. 27a,b; black arrows).

At P60 (fig. 27c,d), the presence of GAD67 highlighted, as parvalbumin staining, the basket pinceaux at the Purkinje cell axon hillock. Even with this marker differences in the shape of pinceau considering the wt, *dal/+* and *dal/dal* animals were detected: cone-shaped (fig. 27c, black V) and flattened (fig. 27d, black asterisks). Moreover, in *dal* mice, often Purkinje neurons with a flattened pinceau were found very close each other so that it was difficult to distinguish the pinceau of each Purkinje cell. Even at P60, almost exclusively in *dal* mice, the Purkinje main dendrite branches were found labelled. This finding mainly regarded the Purkinje with flattened pinceaux (fig.27c,d; black arrows).

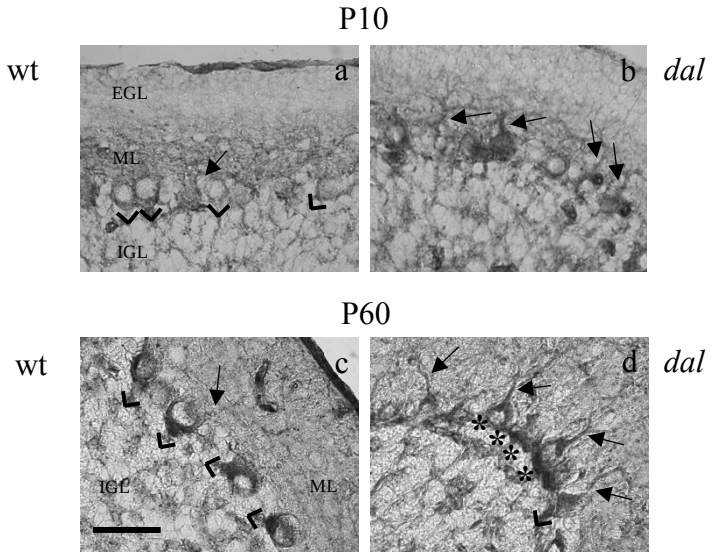

Figure 27. Immunohistochemical reaction for GAD67 at P10 (a,b) and P60 (c,d). *dal* figure retrieved from *dal/dal* mice. Abbreviations: wt: wild type; *dal*: prolidase deficient mice; EGL: External Granular Layer; ML: Molecular Layer; PL: Purkinje Layer; IGL: Internal Granular Layer. Magnification: scale bar of 200 µm (a,b) 100 µm (c-d).

GABAergic receptors

GABAα6 is a marker of mature granule cells of IGL; the scattering of immunopositive granule cells is different within the IGL comparing the different lobules and according to the histological maturation. The lobules that develop last (VIa, VIb and VII) showed a weaker staining for GABAα6; this was visible in the wt, *dal/+* and *dal/dal* mice. However, at P10 (fig. 28a,b) in *dal* mice the immunohistochemical reaction highlighted clusters of migrating immature granule cells in the ML that were positive for GABAα6 (fig. 28b; black arrowheads), while in wt, the migrating cells were visible always as scattered within the ML. At P60 (fig. 28c,d) in *dal* mice, the presence of mature and strongly immunopositive granule cells within the IGL was not homogeneous as in the wt; there were weakly immunopositive cells also in the ML. These findings were not lobule specific.

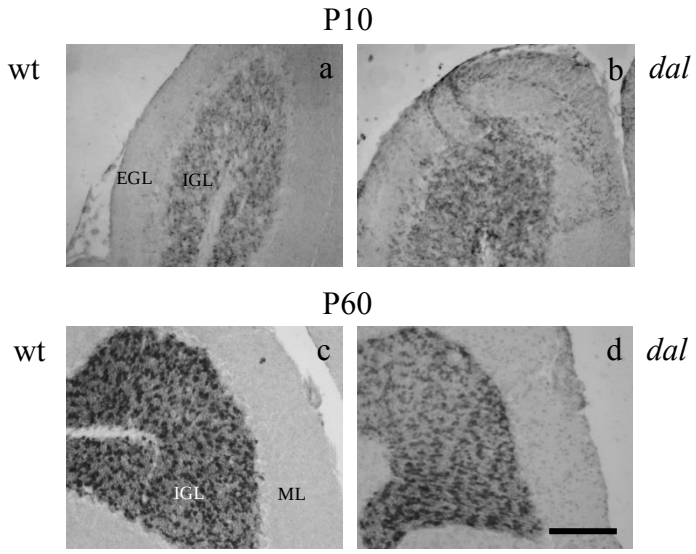

Figure 28. Immunohistochemical reaction for GABAα6 at P10 (a,b) and P60 (c,d). *dal* figure retrieved from *dal/dal* mice. Abbreviations: wt: wild type; *dal*: prolidase deficient mice; EGL: External Granular Layer; ML: Molecular Layer; PL: Purkinje Layer; IGL: Internal Granular Layer. Magnification: scale bar of 200 μm (a-d).

5. DISCUSSION

In the present research we studied the postnatal cerebellar development in dark-like (*dal*) mice, heterozygous and homozygous for a loss-of-function mutation in the gene encoding prolidase. In humans, this condition causes the prolidase deficiency, a rare autosomal recessive disorder. Patients show a variable clinical manifestation onset and a wide range of clinical phenotype including different degrees of mental retardation (Lupi et al. 2008).

Nowadays the *dal* mice are only used as a model of *dal* to study the bone phenotype, very similar to the humans one (Besio et al. 2015). While no studies were available on the brain of *dal* mice. This research was based on the evaluation of several markers to assess the cerebellar integrity related to postnatal developmental processes and structures beside the reduction in *dal* mice of prolidase enzyme activity (not published data). Regarding the bone phenotype the heterozygous animals were comparable to the wt, while in our studies we detected the same anomalies in both mutant genotypes. Either the 50% of the enzyme is not sufficient to guarantee the proper brain development or the presence of the mutant allele generates a dominant negative effect in this tissue. The analysis were performed at different days of postnatal brain development: from P10 when the brain is still developing to the maturation, P60, in order to monitor the possible alterations during this period between development and maturity and the consequences at the adult stage of prolidase activity deficiency. Moreover the study was performed considering the vermis lobules since they share the same developmental timing and are particularly vulnerable to neurodevelopmental malformations (Altman 1982; Cerri et al. 2010; Ramos et al. 2015).

Since prolidase exerts an indirect impact on ECM remodeling, being involved in the collagen and procollagen metabolism (Kitchener & Grunden, 2012), some ECM components were analyzed. In particular, the attention has been focused on those of pBM as it is a specialized structure of ECM and a fundamental regulator of cortical development (Halfter et al., 2002). Pial BM was present in both wt and *dal* mice cerebellar cortex. However, in wt was uniform and continuous, whereas in *dal* was discontinuous and irregular. In

fact, the pBM collagen components in *dal* mice was represented by a majority of thicker structure than in the pBM of wt animals. Moreover, the collagen IV was not expressed differently comparing the three genotypes even if there was a high inter-genotype variability. The type IV collagen is the most abundant in the CNS and acts as a scaffold to integrate laminin and other ECM components into sheet-like BM, which in turn, are thought to be essential for pBM assembly (Burnside & Bradbury 2014). Since the collagen turnover is partially regulated by the prolidase enzyme (Surazynski et al. 2008), the collagen structural alterations and then the wrong positioning of the other pBM components in *dal* mice might be related to the absence or reduced activity of this enzyme. Laminin and reelin did not overlap each other all over the pBM. Moreover the reelin was also found extracellularly in correspondence of apical anomalies suggesting defects in neurotransmission patterns (Senkov et al. 2014). It was previously demonstrated that changes in the quantity, structure and distribution of collagens in tissues might affect cell signaling, metabolism and function (Karna et al. 2000; Guszczyn & Sobolewski 2004). Moreover, it is well documented that the impairment of pial ECM components leads to syndromes accompanied by cortical dysplasia (Halfter et al. 2002; Francis et al. 2006; Barkovich et al. 2012), molecular layer heterotopia (Ramos et al. 2013; Ramos et al. 2014) and morphological anomalies of the cerebellum (Cerri et al. 2010; Qiu et al. 2010; Siegenthaler & Pleasure, 2011; Ichikawa-Tomikawa et al. 2012;). In this light, it was possible to speculate that the apical anomalies (as the surface abnormalities, layering defects and heterotopias) are linked to the pBM impairment. These could also explain why the anomalies were not diffused along the cerebellar cortex, but were scattered only in regions without lobule specificity, as the pBM defects herein recorded. Other ECM remodeling enzymes were considered as MMPs (2 and 3) and TIMP 2, having as target components of the pBM, but no differences were highlighted comparing the three genotypes at both P10 and 60. This suggests that even if there was absence or decrease in prolidase enzyme activity, the other MMPs did not change their expression levels to balance the prolidase activity.

The pBM organization and integrity is essential for the proliferation and then migration of neuronal precursors during prenatal and post-natal cerebellar

development (Porcionatto 2006; Barros et al. 2011; Lakatosova & Ostatnikova, 2012; Folsom & Fatemi 2013). The proliferating granule cells are located in the more apical surface of the EGL during the first postnatal stages (Altman 1972); a layer thickening in *dal* mice was accompanied by a decrease in the PCNA protein amount in the developing brain of *dal* mice compared to wt. Once the granule cells proliferate in the EGL, they should migrate, toward the IGL, following the scaffold provided by the radial glial cells that are able to anchor their end-feet to the laminin protein sheet of pBM (Ichikawa-Tomikawa et al. 2012). In *dal* mice there were gaps in the laminin sheet that caused either the retraction of GFAP immunostained radial glia fibers: they appeared interrupted without reaching the pial surface, or devoid of radial orientation or absent in correspondence of the apical surface anomalies. These physical changes in the radial glia may interfere with the ability of granule neurons to find a suitable fiber near the EGL/ML interface. Furthermore, it was demonstrated that even after a granule neuron has found a suitable glial fiber, the traveling along these fibers may be less efficient (Komuro & Yacubova 2003; Qu & Smith 2005; Xu et al. 2013). It is also possible that some granule neurons migrate normally along adequate fibers and that only a subpopulation of neurons are dramatically detained in their migration. In fact, after DCX immunoreaction, a marker of migrating neurons (Takacs et al. 2008), no statistical significant differences in OD were detected at P10 among the three genotypes. This could be explained by the fact that the SD was high in *dal* mice considering the surface of all apical lobules from VIa to VIII. In addition, it was possible to follow the migration/maturation of granule cells by their GABAα6 immunopositivity. GABAα6 is a marker of mature granule neurons and should be present only after the migration, when granules are in the IGL (Laurie et al. 1992; Thompson & Stephenson 1994; Cerri et al. 2010). In *dal* mice, a wrong pattern of migration/maturation was highlighted at P10. In fact, clusters of migrating granule cells were found scattered in the ML and labeled by GABAα6. Then at P60, the granule cells were still labeled in the IGL, but this positivity was not homogeneous in intensity, suggesting defects in the inhibitory synaptic system in the cerebellar glomeruli (Takayama & Inoue 2004).

5. DISCUSSION

It has been well established that an altered migration and maturation of granule cells affects the cerebellum lamination, the distribution of Purkinje neurons in a monolayer and the growth of Purkinje cell dendrites, since the granule cells represent trophic factors for Purkinje cell differentiation (Altman 1982; Altman & Bayer 1997; Goldowitz & Hamre 1998; Hatten 1999; Cerri et al. 2010; Xu et al. 2013;). Indeed, in *dal* mice Purkinje cell morphology was altered, with dendrite trees poor of branches. Moreover, there were Purkinje neurons in ectopic positions within the internal granule cell layer, or distributed in a multilayer, confirming a wrong cortical lamination: this finding was highlighted with calbindin immunohistochemistry, but was also clearly detected with haematoxylin and eosin as well.

Purkinje neurons are key cells in the cerebellar circuit since represent the sole output of the cerebellum (Ito 2006). Therefore, to get information concerning not only the morphology but also the functionality of these neurons, the calcium homeostasis markers of Purkinje cells were considered together with other of excitatory and inhibitory neurotransmission markers. It was investigated the positivity of Purkinje neurons for CB and PV, a fast and low Ca^{2+} binding protein respectively. Both of them releveled anomalies in the Purkinje neurons. However, the impairment of Ca^{2+} homeostasis detected by the CBPs could be associated with the changes in the positivity for the PMCA1 in *dal* mice.

The CB, as marker of Purkinje neurons highlighted alterations of dendrite tree branches and their organization within the ML. Moreover, there was a decrease in the amount of CB detected through western blotting in *dal* mice compared to wt at P60, although has been reported that morphological impairment of Purkinje neurons cannot be necessarily attributed to a reduction in CB content (Schwaller et al. 2002). The PV marker led to the detection of alterations of the basket pinceau at the Purkinje axon hillock. In fact, it was observed an increase of aberrant flat pinceau instead of physiological cone-shaped one in *dal* mice. This evidence together with the labeling of GAD67, that showed the same anomalies at the Purkinje axon hillocks, could suggest deficits in the inhibitory transmission pattern (Scherini et al. 1992; Lazarus et al. 2013). The pinceau disorganization can result in a significant reduction of basket neuron inhibitory

input to Purkinje neurons (Buttermore et al. 2012). In fact, these alterations were also accompanied by a decrease in GAD67 immunolabelling in the Purkinje cells of *dal* mice, especially in correspondence of tissue morphological alterations and aberrant Purkinje neurons. Moreover, GAD67 level is profoundly altered in multiple brain regions in a variety of neuropsychiatric disorders (Torrey et al. 2005; Lazarus et al. 2013), even associated with alteration of reelin protein level (Fatemi et al. 2005), as in *dal* mice.
The role of CBPs was not only associated to the Ca^{2+} buffering, but at many other cellular events, as the maturation of cerebellar circuitry, synaptogenesis, axonal elongations, dendritic remodeling, spine morphology, neuronal migrations, and stabilization and maintenance of cytoskeletal elements (reviewed in Hof et al. 1999; Vecellio et al. 2000; Schwaller et al. 2002).

Then, it must be taken into great consideration that the morphology, polarization, migration, and cell-connectivity of cells are dictated by cytoskeleton filamentous network of proteins whose regulation is essential during the different developmental stages of the brain (Matus 1988; Menon & Gupton 2016). In *dal* mice cytoskeleton components were studied as MAP2, a microtubule stabilizer protein, tau protein that in the phosphorylated form at Ser519/202 residues destabilizes the microtubules and the NF-H. At P10, as expected, there were high levels of MAP2 and phospho-tau$^{(pSer202/509),}$ since this developmental stage is characterized by microtubule rearrangements (Riederer & Matus 1985; Avila et al. 2004); in *dal* mice did not emerge relevant differences in comparison with the wt animals. At P60 in wt mice the positivity was maintained in the cerebellar cortex for MAP2 while there was a strong decrease for phospho-tau$^{(pSer202/509)}$. The presence in mature neurons of this latter marker, is no more considered physiological. In this context, in *dal* mice and significantly less in wt mice, different cell populations were found immunopositive to phospho-tau$^{(pSer202/509)}$ in the ML, IGL and in the white matter. It was important to highlight that spread in the cerebellar lobules there were also Purkinje neurons labeled by phospho-tau$^{(pSer202/509)}$; the positivity was in the soma and/or in the dendrites, was co-localized with CB, and was associated to a different degrees of MAP2 immunopositivity reduction. The positive dendrites were always of big caliber. These findings could be

interpreted as follow: the phospho-tau$^{(pSer202/509)}$ positivity was either localized in the main Purkinje dendrite or the dendrites positive for this marker were enlarged.

To understand whether the presence of tau is indicative of further functional damages of Purkinje cells, the attention has been focused on the evaluations of synaptic contacts of phospho-tau$^{(pSer202/509)}$ positive-Purkinje neurons. Therefore, it was evaluated the NF-H as a marker of inhibitory basket cell axons (White & Sillitoe 2013); VGLUT1 and VGLUT2 as markers of parallel and climbing fibers respectively.

NF-H was not present at P10 yet, while in wt mice at P60 highlighted the axons of basket cells which form synaptic contacts with Purkinje dendrite branches in the ML, and the basket pinceau at the Purkinje axon hillock. In *dal* mice, a strong decrease in NF-H labelling was evident since there were a loss of positive axons in the ML and flattened basket at Purkinje axon hillock, in particular in those Purkinje neurons positive for the phospho-tau$^{(pSer202/509)}$ either in cell soma or in dendrites. These results are in agreement with the findings of GAD67 and PV concerning defects of pinceaux at the Purkinje axon hillock, and confirm anomalies in the inhibitory pattern system.

Neverthless, Purkinje neuron dendrites were also contacted by excitatory fibers as the parallel and climbing ones. In *dal* mice there were no significant changes in VGLUT1 (parallel fibers) positivity at P10 and P60 in correspondence of both apical anomalies and at P60 of phospho-tau$^{(pSer202/509)}$ positivity of dendrite branches. Instead, there were some anomalies concerning the climbing fibers (VGLUT2 immunopositive), especially in the mature cerebellum. The mature stage (as P60) is characterized by a mono-innervation of climbing fiber for each Purkinje neuron on the proximal portion of dendrite arborization (Watanabe & Kano 2011). In *dal* mice, there were still Purkinje soma positive to VGLUT2 and the positivity in the ML was significantly higher in *dal* mice compared to wt. These results suggested that the critical pruning process of climbing fibers was not concluded yet or it was delayed. Interestingly, a percentage of Purkinje neurons labeled by phospho-tau$^{(pSer202/509)}$ presented the retention of climbing fibers in the soma, whith the exception of wt animals. Different hypothesis could be formulated (not

necessarly mutually exclusive): Purkinje dendrites maturation, altered in *dal* mice, strongly influences the development of synaptic contacts (Qiao et al. 2013); the presence of phospho-tau$^{(pSer202/509)}$ could be either a first sign of neurodegeneration that is described as associated to synaptic alterations or a sign of developmental delay in the maturation of microtubules cytoskeleton and Purkinje cell synapses contacts (Goedert et al. 1993; Wang & Liu 2008); imbalance in Ca^{2+} homeostasis (Hof et al. 1999; Vecellio et al. 2000; Schwaller et al. 2002); presence of extracellular reelin within the cerebellar layers in adul mice leading to the potentiation of glutamatergic neurotransmission together with the increase in spine density (Senkov et al. 2014).

For a more in-deep analysis of glutamatergic neurotransmission, GluR2 and GluRδ2 were considered. The changes in these markers positivity are integrated with those already described. For both markers at P10 there were no important differences to be pointed out, while at P60 the alterations found were heterogeneous. GluR2 revealed changes in the labelling of Purkinje neurons that could be associated to an impairment of calcium homeostasis (Piccolini et al. 2012a). There were clusters of more intensely labelled Purkinje cells in *dal* mice.; these changes in GluR2 positivity, together with a decrease of presynaptic inhibition, pointed out by GAD67 and PV and the NF-H positive axons of basket cells, could increase glutamatergic neurotransmission, and result in an increase in the reactivity of glutamate receptors and/or up-regulation of glutamate receptor production, as previously demonstrated (Lynd-Balta et al. 1996). An other hypothesis could be again inked to the extracellular reelin in adult mice, since it was demonstrated that reelin in this context can uncreae the expression of AMPA receptors subunits (Senkov et al. 2014). However, there were other Purkinje neurons with a weak labeled soma or with dendrite immunopositivities. These findings reflect the heterogeneity of Purkinje cells proper of many animal species (Bernocchi et al. 1986). It is important to underline that the AMPA receptors, like GluR2, become rapidly desentisized to glutamate and the increased expression of AMPA receptors may be a compensatory mechanism to protect against further excitotoxic damage linked to excessive accumulation of calcium in the cell (Piccolini et al. 2012a), hypothesized in *dal* mice through the decrease in calcium buffering.

Furthermore, even GluRδ2, gave rise the coexistence of different Purkinje labeling even in the same lobule. As previously described, the changes in *dal* mice could be linked to the impaired maturation of Purkinje neurons (Takayama et al. 1996; Yuzaki 2004). In particular, GluRδ2 is required for consolidating parallel fiber synapses and restricting climbing fiber synapses to the proximal dendrites, which occur during postnatal cerebellar development (Hashimoto et al. 2001; Hashimoto & Kano 2013). In fact, in GluRδ2 mutant rats it was demonstrated an increased in climbing fiber synapses in the distal portion of Purkinje neuron dendrites, due to a lack in the physiological reduction during the development (Hashimoto et al. 2009). These evidences can suggest that the VGLUT2 increases and GluRδ2 changes could be related one to each other.

The morphological alterations of *dal* mice were not only related to these molecular and cellular pathways, but also to the physical damages of cortical portions caused by injuring blood vessels. In *dal* mice there was an overgrowth of blood vessels both in term of number and size. The causes could be several: *dal* mice embryonically develop the cardiomyocyte hypetrophy (Jung et al. 2011), that physiologically results in a net induction of angiogenesis (Laughlin et al. 2012); prolidase indirectly is involved in the angiogenesis signaling pathways (Rhodes & Simons 2007). These big blood vessels were observed not only in correspondence of cerebellum but also close to the hippocampal formation (Insolia & Piccolini 2014).

Additionally the pBM defect, as well as the layering alterations and apical anomalies (as cortical undulations) were also present in the neocortex at both P10 and P60 mice (Insolia & Piccolini 2014).

6. CONCLUSION and FUTURE PERSPECTIVES

To explain the ontogeny of the multiple anomalies in *dal* mice cerebellum, we propose a cascade of molecular/morphological events that begins with the absence of a full functional prolidase enzyme. The deficiency in prolidase results in the alteration in collagen metabolism, and the increase in the thinner collagen structures as well as disorganized pBM. Such demage, leads to the localized aberrant cortical granule cell proliferation and migration with consequent defects in brain lamination, cortical dysplasia, and maturation of Purkinje neuron; calcium homeostasis imbalance; phosphorylation of tau proteins which is considered a pathological marker associated to alterations in the inhibitory and excitatory synaptic neurotransmission systems.

Further studies will be indispensable to be directed toward the ultrastructure analysis of basement membrane integrity, and, on the other hand, toward the electrophysiological characterizations. Moreover, it will be necessary to investigate the behaviors of *dal* mice since did not shown any particular defects either in motor coordination or in cage daily life.Additionally, the cerebrum cortical anomalies and heterotopias will be evaluated in more details.

Since *dal* is still a critical and less known disease and prolidase is an essential enzyme misregulated in many other neurological disorders, other studies will be directed in understanding its peculiar role, as part of intracellular pathways beside the ECM maturation and remodelling, in the CNS.

7. BIBLIOGRAPHY

Abraham P, Wilfred G, Ramakrishna B. Plasma prolidase may be an index of liver fibrosis in the rat. Clin Chim Acta. 2000;295:199–202.

Agrawal SM, Lau L, Yong VW. MMPs in the central nervous system: Where the good guys go bad. Semin Cell Dev. Biol. 2008;19:42-51.

Altindag O, Erel O, Aksoy N, Selek S, Celik H, Karaoglanoglu M. Increased oxidative stress and its relation with collagen metabolism in knee osteoarthritis. Rheumatol Int. 2007;27:339-344.

Altman J, Bayer SA. Development of the Cerebellar System: In Relation to its Evolution, Structure, and Functions. CRC Press, New York; 1997.

Altman J. Autoradiographic and histological studies of postnatal neurogenesis. IV. Cell proliferation and migration in the anterior forebrain, with special reference to persisting neurogenesis in the olfactory bulb. J Comp Neurol. 1969a;137:433-457.

Altman J. Autoradiographic and histological studies of postnatal neurogenesis. 3. Dating the time of production and onset of differentiation of cerebellar microneurons in rats.J Comp Neurol. 1969b;136:269-293.

Altman J. Morphological Development of the Rat Cerebellum and Some of Its Mechanisms 1. Heidelberg: Springer-Verlag; 1982.

Altman J. Postnatal development of the cerebellar cortex in the rat. II. Phases in the maturation of Purkinje cells and of the molecular layer. J Comp Neurol. 1972;145:399-463.

Andreazza AC, Kauer-Sant'anna M, Frey BN, Bond DJ, Kapczinski F, Young LT, Yatham LN. Oxidative stress markers in bipolar disorder: a meta-analysis. J Affect Disord. 2008;111:135-144.

Arata J, Tada J, Yamada T, Oono T, Yasutomi H, Oka E. Angiopathic pathogenesis of clinical manifestations in prolidase deficiency. Arch Dermatol. 1991;127:124-125.

Arikanoglu A, Akil E, Varol S, Yucel Y, Yuksel H, Cevik MU, Palanci Y, Unan F. Relationship of cognitive performance with prolidase and oxidative stress in Alzheimer disease. Neurol Sci. 2013;34:2117-2121.

Arioz DT, Camuzcuoglu H, Toy H, Kurt S, Celik H, Aksoy N. Serum prolidase activity and oxidative status in patients with stage I endometrial cancer. Int J Gynecol Cancer. 2009;19:1244-1247.

7. BIBLIOGRAPHY

Aslan M, Nazligul Y, Horoz M, Bolukbas C, Bolukbas FF, Aksoy N, Celik H, Erel O. Serum prolidase activity and oxidative status in Helicobacter pylori infection. Clin Biochem. 2007;40: 37-40.

Avila J, Lucas JJ, Perez M, Hernandez F. Role of tau protein in both physiological and pathological conditions. Physiol. Rev. 2004;84:361-384.

Ayoub AE, Cai TQ, Kaplan RA, Luo J. Developmental expression of matrix metalloproteinases 2 and 9 and their potential role in the histogenesis of the cerebellar cortex. J Comp Neurol. 2005;481:403-415.

Bandeira F, Lent R, Herculano-Houzel S. Changing numbers of neuronal and non-neuronal cells underlie postnatal brain growth in the rat. Proc Natl Acad Sci USA. 2009;106:14108-14113.

Barkovich AJ, Guerrini R, Kuzniecky RI, Jackson GD, Dobyns WB. A developmental and genetic classification for malformations of cortical development: update 2012. Brain. 2012;135:1348-1369.

Barros CS, Franco SJ, Müller U. Extracellular matrix: functions in the nervous system. 2011;3:a005108.

Beffert U, Weeber EJ, Durudas A, Qiu S, Masiulis I, Sweatt JD, Li WP, Adelmann G et al. Modulation of synaptic plasticity and memory by Reelin involves differential splicing of the lipoprotein receptor Apoer2. Neuron. 2005;47:567–579.

Bernocchi G, Barni S, Scherini E. The annual cycle of Erinaceus europaeus L. as a model for a further study of cytochemical heterogeneity in Purkinje neuron nuclei. Neuroscience. 1986;17:427-437.

Berrier AL, Yamada KM. Cell-matrix adhesion. J Cell Physiol. 2007;213:565-573.

Besio R, Baratto MC, Gioia R, Monzani E, Nicolis S, Cucca L, Profumo A, Casella L, Basosi R, Tenni R, Rossi A, Forlino A. A Mn(II)-Mn(II) center in human prolidase. Biochim. Biophys. Acta 2013;1834:197-204.

Besio R, Maruelli S, Gioia R, Villa I, Grabowski P, Gallagher O, Bishop NJ, et al. Lack of Prolidase Causes a Bone Phenotype Both in Human and in Mouse. Bone. 2015;72:53-64.

Bissonnette R, Friedmann D, Giroux J, Dolenga M, Hechtman P, Der Kaloustian V, Dubuc R. Prolidase deficiency: a multisystemic hereditary disorder. J Am Acad Dermatol. 1993;29:818–821.

7. BIBLIOGRAPHY

Blaschke AJ, Staley K, Chun J. Widespread programmed cell death in proliferative and postmitotic regions of the fetal cere- bral cortex. Development. 1996;122:1165-1174.

Bonfanti L, Peretto P. Adult neurogenesis in mammals - a theme with many variations. Eur J Neurosci. 2011;34:930-950.

Bozkurt M, Caglayan M, Oktayoglu P, Em S, Batmaz I, Sariyildiz MA, Nas K, Ucar D, Yüksel H, Sarac AJ. Serum Prolidase Enzyme Activity and Oxidative Status in Patients with Fibromyalgia. Redox Rep. 2014;19:148-153.

Burnside ER, Bradbury EJ. Manipulating the extracellular matrix and its role in brain and spinal cord plasticity and repair. Neuropathol. Appl. Neurobiol. 2014;40:26-59.

Butbul Aviel Y, Mandel H, Avitan Hersh E, Bergman R, Adiv OE, Luder A, Brik R. Prolidase deficiency associated with systemic lupus erythematosus (SLE): single site experience and literature review. Pediatr Rheumatol Online J. 2012;10:18.

Buttermore ED, Piochon C, Wallace ML, Philpot BD, Hansel C, Bhat MA. Pinceau organization in the cerebellum requires distinct functions of neurofascin in Purkinje and basket neurons during postnatal development. J Neurosci. 20124;32:4724-4742.

Cakmak A, Soker M, Koc A, Aksoy N. Prolidase activity and oxidative status in patients with thalasse- mia major. J Clin Lab Anal. 2010;24:6-11.

Cakmak A, Zeyrek D, Atas A, Celik H, Aksoy N, Erel O. Serum prolidase activity and oxidative sta- tus in patients with bronchial asthma. J Clin Lab Anal. 2009;23:132-138.

Caliskan A, Yavuz C, Karahan O, Yazici S, Guclu O, Demirtas S, Mavitas B. Factor-Xa inhibitors protect against systemic oxidant damage induced by peripheral-ischemia reperfusion. J Thromb Thrombolysis. 2014;37:464-468.

Camuzcuoglu H, Arioz DT, Toy H, Kurt S, Celik H, Aksoy N. Assessment of preoperative serum prolidase activity in epithelial ovarian cancer. Eur J Obstet Gynecol Reprod Biol. 2009;147:97-100.

Candelario-Jalil E, Yang Y, Rosenberg GAA. Diverse roles of matrix metalloproteinases and tissue inhibitors of metalloproteinases in neuroinflammation and cerebral ischemia. Neuroscience 2009;158:983-994.

Cantatore FP, Papadia F, Giannico G, Simonetti S, Carrozzo M. Chronic leg ulcerations resembling vasculitis in two siblings with prolidase deficiency. Clin Rheumatol. 1993;12:410-414.

7. BIBLIOGRAPHY

Carstens KE, Phillips ML, Pozzo-Miller L, Weinberg RJ, Dudek SM. Perineuronal Nets Suppress Plasticity of Excitatory Synapses on CA2 Pyramidal Neurons. J. Neurosci. 2016;36:6312-6320.

Carulli D, Kwok JCF, Pizzorusso T. Perineuronal Nets and CNS Plasticity and Repair. Neural Plast. 2016;2016:4327082.

Carulli D, Rhodes KE, Brown DJ, et al. Composition of perineuronal nets in the adult rat cerebellum and the cellular origin of their components. J. Comp. Neurol. 2006;494:559-577.

Castagna C, Aimar P, Alasia S, Lossi L. Post-natal development of the Reeler mouse cerebellum: An ultrastructural study. Ann Anat. 2014;196:224-235.

Cayre M, Canoll P, Goldman JE. Cell migration in the normal and pathological postnatal mammalian brain. Prog Neurobiol. 2009;88:41-63.

Cechowska-Pasko M, Palka J, Wojtukiewiez MZ. Enhanced prolidase activity and decreased collagen content in breast cancer tissue. Int J Exp Path 2006;87:289–296.

Celio MR, Spreafico R, De Biasi S, Vitellaro-Zuccarello L. Perineuronal nets: past and present. Trends Neurosci. 1998;21:510-515.

Cerri S, Piccolini VM, Bernocchi G. Postnatal development of the central nervous system: anomalies in the formation of cerebellum fissures. Anat. Rec. 2010;293:492-501.

Chen Y, Beffert U, Ertunc M, Tang TS, Kavalali ET, Bezprozvanny I, Herz J. Reelin modulates NMDA receptor activity in cortical neurons. J Neurosci; 2005;25:8209-8216.

Chi H, Lu J, Liu G, Tong J, Nakayama K, Yamashita K, Kitaoka N, Kodama H. Activity of prolidase isoenzymes in the rat brain: subcellular and regional distribution during development. Brain Res. 2009;1303:8-14.

Choe Y, Siegenthaler JA, Pleasure SJ. A cascade of morphogenic signaling initiated by the meninges controls corpus callosum formation. Neuron 2012;73:698-712.

Cleveland DW, Hwo SY, Kirschner MW. Physical and chemical properties of purified tau factor and the role of tau in microtubule assembly. J Mol. Biol. 1977;116:227-247.

Colonna C, Conti B, Perugini P, Pavanetto F, Modena T, Dorati R, Genta I. Chitosan glutamate nano- particles for protein delivery: development and effect on prolidase stability. J Microencapsul. 2007;24:553-564.

Colonna C, Conti B, Perugini P, Pavanetto F, Modena T, Dorati R, Iadarola P, Genta I. Ex vivo eval- uation of prolidase loaded chitosan nanoparticles for the enzyme replacement therapy. Eur J Pharm Biopharm. 2008;70:58-65.

7. BIBLIOGRAPHY

Constantin R, Colbourne H, Dobell D. Inquiry Into Biology. 1st ed. (McGraw-Hill Ryerson, ed.); 2006.

Cosson C, Myara I, Miech G, Moatti N, Lemonnier A. Only prolidase I activity is present in human plasma. 1992;24:427-432.

Cota CD, Liu RR, Sumberac TM, Jung S, Vencato D, Millet YH, Gunn TM. Genetic and phenotypic studies of the dark-like mutant mouse. Genesis 2008;46:562-573.

D'Arcangelo G. Reelin in the Years: Controlling Neuronal Migration and Maturation in the Mammalian Brain. Adv. Neurosci. 2014;2014:1-19.

De Rijcke S, De Maubeuge J, Laporte M, Bron D, Hariga C, Ledoux M. Prolidase deficiency. Apropos of a peculiar case. Ann Dermatol Venereol. 1989;116:309-312.

Decimo I, Fumagalli G, Berton V, Krampera M, Bifari F. Meninges: from protective membrane to stem cell niche. Am. J. Stem Cells 2012;1:92-105.

Dehmelt L, Halpain S. Protein family review The MAP2 / Tau family of microtubule-associated proteins. 2. Genome Biol. 2005;6:204.

Delobel P, Flament S, Hamdane M, Mailliot C, Sambo AV, Begard S, Sergeant N, Delacourte A, Vilain JP, Buee L. Abnormal Tau phosphorylation of the Alzheimer-type also occurs during mitosis. J Neurochem. 2002;83:412- 420.

Demirbag R, Yildiz A, Gur M, Yilmaz R, Elci K, Aksoy N. Serum prolidase activity in patients with hypertension and its relation with left ventricular hypertro- phy. Clin Biochem. 2007;40:1020-1025.

Dityatev A, Frischknecht R, Seidenbecher CI. Extracellular matrix and synaptic functions. Results Probl. Cell Differ. 2006;43:69-97.

Dityatev A, Schachner M, Sonderegger P. The dual role of the extracellular matrix in synaptic plasticity and homeostasis. Nat. Rev. Neurosci. 2010;11:735-746.

Dityatev A, Schachner M. Extracellular matrix molecules and synaptic plasticity. Nat. Rev. Neurosci. 2003;4:456-468.

Duong HS, Zhang QZ, Le AD, Kelly AP, Kamdar R, Messadi DV. Elevated prolidase activity in keloids: correlation with type I collagen turnover. Br J Dermatol. 2006;154:820-828.

Dyne, K., Zanaboni, G., Bertazzoni, M., Cetta, G., Viglio, S., Lupi, A. and Iadarola, P. Mild, late-onset prolidase deficiency: another Italian case. Br J Dermatol. 2001;144:635-636.

7. BIBLIOGRAPHY

Eren MA, Torun AN, Tabur S, Ulas T, Demir M, Sabuncu T, Aksoy N. Serum prolidase activity in diabetic foot ulcers. Acta Diabetol. 2013;50:423-427.

Evanko SP, Tammi MI, Tammi RH, Wight TN. Hyaluronan-dependent pericellular matrix. Adv. Drug Deliv. Rev. 2007;59:1351-1365.

Falconer DS. Two new mutants, trembler and 'reeler', with neurological actions in the house mouse. J Genet. 1951;1:82e201.

Falik-Zaccai TC, Khayat M, Luder A, Frenkel P, Magen D, Brik R, Gershoni-Baruch R, Mandel H. A broad spectrum of developmental delay in a large cohort of prolidase deficiency patients demonstrates marked interfamilial and intrafamilial phenotypic variability. Am J Med Genet B Neuropsychiatr Genet. 2010;153B:46-56.

Fatemi SH, Stary JM, Earle JA, Araghi-Niknam M, Eagan E. GABAergic dysfunction in schizophrenia and mood disorders as reflected by decreased levels of glutamic acid decarboxylase 65 and 67 kDa and Reelin proteins in cerebellum. Schizophr Res. 2005;1;72:109-22

Fellous A, Francon J, Lennon AM, Nunez J. Microtubule assembly in vitro. Purification of assembly-promoting factors. Eur J Biochem. 1977;8:167–174.

Ferreira C, Wang H. Prolidase Deficiency. Edited by Pagon RA, Adam MP, Ardinger HH, et al. NCBI Bookshelf. Pagon. 1993rd–2015th ed. Vol. 72. Seattle (WA): University of Washington, Seattle: GeneReviews®, 2015.

Folsom TD, Fatemi SH. The involvement of Reelin in neurodevelopmental disorders. Neuropharmacology. 2013;68:122-135.

Francis F, Meyer G, Fallet-Bianco C, Moreno S, Kappeler C, Socorro AC, Tuy FP, Beldjord C, Chelly J. Human disorders of cortical development: From past to present. Eur J Neurosci. 2006;23:877-893.

Frotscher M. Dual role of Cajal-Retzius cells and reelin in cortical development. Cell Tissue Res. 1997;290:315-322.

Fu Y, Rusznák Z, Herculano-Houzel S, Watson C, Paxinos G. Cellular composition characterizing postnatal development and maturation of the mouse brain and spinal cord. Brain Struct Funct. 2013;218:1337-1354.

Gecit I, Aslan M, Gunes M, Pirincci N, Esen R, Demir H, Ceylan K. Serum prolidase activity, oxidative stress, and nitric oxide levels in patients with bladder cancer. J Cancer Res Clin Oncol. 2012;138:739-743.

7. BIBLIOGRAPHY

Gencer M, Aksoy N, Dagli EC, Uzer E, Aksoy S, Selek S, Celik H, Cakir H. Prolidase activity dysre- gulation and its correlation with oxidative-antioxidative status in chronic obstructive pulmonary disease. J Clin Lab Anal. 2011;25:8-13.

Genta I, Perugini P, Pavanetto F, Maculotti K, Modena T, Casado B, Lupi A, Iadarola P Conti B. Enzyme loaded biodegradable microspheres in vitro ex vivo evalua- tion. J Control Release. 2001;77:287-295.

Goedert M, Jakes R, Crowther RA, Six J, Lübke U, Vandermeeren M, Cras P, Trojanowski JQ, Lee VM. The abnormal phosphorylation of tau protein at Ser-202 in Alzheimer disease recapitulates phosphorylation during development. Proc Natl Acad Sci USA. 1993;90:5066-5070.

Goldowitz D, Hamre K. The cells and molecules that make a cerebellum. Trends Neurosci. 1998;21:375-382.

Gonullu H, Aslan M, Karadas S, Kati C, Duran L, Milanlioglu A, Aydin MN, Demir H. Serum prolidase enzyme activity and oxidative stress levels in patients with acute hemorrhagic stroke. Scand J Clin Lab Invest. 2014;74:199-205.

Griffin WS, Eriksson MA, del Cerro M, Woodward DJ, Stampfer N. Naturally occurring alterations of cortical layers surrounding the fissura prima of rat cerebellum. J Comp Neurol. 1980;192:109-118.

Groc L, Choquet D, Stephenson FA, Verrier D, Manzoni OJ, Chavis P. NMDA receptor surface trafficking and synaptic sub- unit composition are developmentally regulated by the extracellular matrix protein Reelin. J Neurosci. 2007;27:10165-10175.

Gross J, Lapiere CM. Collagenolytic activity in amphibian tissues: a tissue culture assay. Proc Natl Acad Sci USA. 1962;48:1014-1022.

Gumus S, Yaman H, Ozcan O, Deniz O, Karaman B, Cakir E, Tozkoparan E, Ozkan M, Bilgic H. Serum prolidase activity in patients with pulmonary tuberculosis. Scand J Clin Lab Invest. 2011;71:467-472.

Guszczyn T, Sobolewski K. Deregulation of collagen metabolism in human stomach cancer. Pathobiology. 2004;71:308-313.

Halfter W, Dong S, Yip Y-P, Willem M, Mayer U. A critical function of the pial basement membrane in cortical histogenesis. J Neurosci. 2002;22:6029-6040.

Harper E, Bloch KJ, Gross J. Zymogen of tadpole collagenase. Biochemistry. 1971;10:3035-3041.

Hashimoto K, Ichikawa R, Takechi H, Inoue Y, Aiba A, Sakimura K, Mishina M, Hashikawa T, et al. Roles of glutamate receptor delta 2 subunit (GluRdelta 2) and metabotropic glutamate receptor subtype 1 (mGluR1) in climbing fiber synapse elimination during postnatal cerebellar development. J Neurosci. 2001;21:9701-9712.

Hashimoto K, Kano M. Synapse elimination in the developing cerebellum. Cell Mol Life Sci. 2013;70:4667-4680.

Hashimoto K, Yoshida T, Sakimura K, Mishina M, Watanabe M, Kano M. Influence of parallel fiber-Purkinje cell synapse formation on postnatal development of climbing fiber-Purkinje cell synapses in the cerebellum. Neuroscience. 2009;162:601-611.

Hatten ME. Central Nervous System. Annu. Rev. Neurosci. 1999;22:511-539.

Hayashita-Kinoh H, Kinoh H, Okada A, Komori K, Itoh Y, Chiba T, Kajita M, Yana I, Seiki M. Membrane-type 5 matrix metalloproteinase is expressed in differentiated neurons and regulates axonal growth. Cell Growth Differ. 2001;12:573-580.

Hecht JH, Siegenthaler JA, Patterson KP, Pleasure SJ. Primary cellular meningeal defects cause neocortical dysplasia and dyslamination. Ann. Neurol. 2010;68:454-464.

Hechtman P. Prolidase deficiency. In: Valle D, Beaudet AL, Vogelstein B, Kinzler KW, Antonarakis SE, Ballabio A, Gibson K, Mitchell G, eds. The Online Metabolic and Molecular Bases of Inherited Disease (OMMBID). Chap 82. New York, NY: McGraw-Hill. 2014.

Hernández F, Avila J. Tauopathies. Cell Mol Life Sci. 2007;64:2219-2233.

Hilali N, Vural M, Camuzcuoglu H, Camuzcuoglu A, Aksoy N. Increased prolidase activity and oxidative stress in PCOS. Clin Endocrinol 2013;79:105-110.

Hirotsune S, Takahara T, Sasaki N Hirose K, Yoshiki A, Ohashi T, Kusakabe M, Murakami Y, Muramatsu M, Watanabe S, et al. The reeler gene encodes a protein with an EGF-like motif expressed by pioneer neurons. Nat Genet. 1995;10:77-83.

Hof PR, Glezer II, Condé F, et al. Cellular distribution of the calcium-binding proteins parvalbumin, calbindin, and calretinin in the neocortex of mammals: Phylogenetic and developmental patterns. J. Chem. Neuroanat. 1999;16:77-116.

Hohenester E, Yurchenco PD. Laminins in basement membrane assembly. Cell Adh Migr. 2013;7:56-63.

Ichikawa-Tomikawa N, Ogawa J, Douet V, Xu Z, Kamikubo Y, Sakurai T, Kohsaka S, Chiba H, Hattori N, Yamada Y, Arikawa-Hirasawa E. Laminin α1 is essential for mouse cerebellar development. Matrix Biol. 2012;31:17-28.

7. BIBLIOGRAPHY

Illenberger S, Zheng-Fischhofer Q, Preuss U, Stamer K, Baumann K, Trinczek B, Biernat J, Godemann R, Mandelkow EM, Mandelkow E. The endogenous and cell cycle-dependent phosphorylation of tau protein in living cells: implications for Alzheimer's disease. Mol Biol Cell 1998;9:1495–1512.

Incebiyik A, Vural M, Camuzcuoglu A, Camuzcuoglu H, Hilali NG, Taskin A, Aydin H, Aksoy N. Comparison of tissue prolidase enzyme activity and serum oxidative stress level between pregnant women with placental abruption and those with a healthy pregnancy. Arch Gynecol Obstet. 2015;291:805-809.

Ito M. Cerebellar circuitry as a neuronal machine. Prog. Neurobiol. 2006;78:272-303.

Iyer RP, Patterson NL, Fields GB, Lindsey ML. The history of matrix metalloproteinases: milestones, myths, and misperceptions. Am JPhysiol Circ Physiol. 2012;303:H919-H930.

Jiang X, Nardelli J. Cellular and molecular introduction to brain development. Neurobiol Dis. 2016;92:3-17.

Jiang Y, Goldberg ID, Shi YE. Complex roles of tissue inhibitors of metalloproteinases in cancer. Oncogene 2002;21:2245-2252.

Johnson GVW, Stoothoff WH. Tau phosphorylation in neuronal cell function and dysfunction. J Cell Sci. 2004;117:5721-5729.

Jung S, Silvius D, Nolan KA, Borchert GL, Millet YH, Phang JM, Gunn TM. Developmental cardiac hypertrophy in a mouse model of prolidase deficiency. Birth Defects Res A Clin Mol Teratol. 2011;91:204-217.

Karna E, Surazynski A, Palka J. Collagen metabolism disturbances are accompanied by an increase in prolidase activity in lung carcinoma planoepitheliale. Int J Exp Pathol. 2000;81:341-347.

Kawauchi T. Cellullar insights into cerebral cortical development: focusing on the locomotion mode of neuronal migration. Front Cell Neurosci. 2015 7;9:394.

Kefalides NA. Isolation of a collagen from basement membrane Collagen IV containing three identical ct chains. Biochem Biophys Res Commun. 1971;45:226-234.

Kitchener RL, Grunden AM. Prolidase function in proline metabolism and its medical and biotechnological applications. J Appl Microbiol. 2012;113:233-247.

Kokturk A, Kaya TI, Ikizoglu G, Koca, A. Prolidase deficiency. Int J Dermatol. 2002;41:45-48.

Komuro H, Yacubova E, Rakic P. Mode and tempo of tangential cell migration in the cerebellar external granular layer. J Neurosci. 2001;21:527-540.

Komuro H, Yacubova E. Review Recent advances in cerebellar granule cell migration. C. Cell. Mol. Life Sci. 2003;60:1084-1098.

Kriegstein A, Alvarez-Buylla A. The glial nature of embryonic and adult neural stem cells. Annu Rev Neurosci. 2009;32:149-184.

Kühn K. Basement membrane (type IV) collagen. Matrix Biol. 1995;14:439-445.

Kurien BT, D'Sousa A, Bruner BF, Gross T, James JA, Targoff IN, Maier-Moore JS, Harley IT, Wang H, Scofield RH. Prolidase deficiency breaks tolerance to lupus-associated antigens. Int J Rheum Dis. 2013;16:674-680.

Kwok JCF, Yang S, Fawcett JW. Brain Extracellular Matrix in Health and Disease. Elsevier Science; 2014.

Lakatosova S, Ostatnikova D. Reelin and its complex involvement in brain development and function. Int. J Biochem. Cell Biol. 2012;44:1501-1504.

Lambert E, Dassé E, Haye B, Petitfrère E. TIMPs as multifacial proteins. Crit Rev Oncol Hematol. 2004;49:187-198.

Laughlin MH, Bowles DK, Duncker DJ. The coronary circulation in exercise training. Am J Physiol Heart Circ Physiol. 2012;302:10-23.

Laurie DJ, Seeburg PH, Wisden W. The distribution of 13 GABAA receptor subunit mRNAs in the rat brain. II. Olfactory bulb and cerebellum. J. Neurosci. 1992;12:1063-1076.

Lazarus MS, Krishnan K, Huang ZJ. GAD67 Deficiency in Parvalbumin Interneurons Produces Deficits in Inhibitory Transmission and Network Disinhibition in Mouse Prefrontal Cortex. Cereb. Cortex 2013:1-7.

Leto K, Rolando C, Rossi F. The genesis of cere- bellar GABAergic neurons: fate potential and specification mech- anisms. Front. Neuroanat. 2012;6:6.

Levy AD, Omar MH, Koleske AJ. Extracellular matrix control of dendritic spine and synapse structure and plasticity in adulthood. Front Neuroanat. 2014;8:116.

Lian G, Sheen VL. Cytoskeletal proteins in cortical development and disease: actin associated proteins in periventricular heterotopia. Front. Cell. Neurosci. 2015;9:99.

Lossi L, Merighi A. In vivo cellular and molecular mechanisms of neuronal apoptosis in the mammalian CNS. Prog Neurobiol. 2003;69:287-312.

Luo J. The role of matrix metalloproteinases in the morphogenesis of the cerebellar cortex. Cerebellum. 2005;4:239-245.

Lupi A, Casado B, Soli M, Bertazzoni M, Annovazzi L, Viglio S, Cetta G, Iadarola P. Therapeutic apheresis exchange in two patients with prolidase defi- ciency. Br J Dermatol. 2002;147:1237-1240.

Lupi A, Perugini P, Genta I, Modena T, Conti B, Casado B, Cetta G, Pavanetto F, Iadarola P. Biodegradable microspheres for prolidase delivery to human cultured fibroblasts. J Pharm Pharmacol. 2004;56:597-603.

Lupi A, Tenni R, Rossi A, Cetta G, Forlino A. Human prolidase and prolidase deficiency: an overview on the characterization of the enzyme involved in proline recycling and on the effects of its mutations. Amino Acids 2008;35(4):739-752.

Lynd-Balta E, Pilcher WH, Joseph SA. Distribution of AMPA receptor subunits in the hippocampal formation of temporal lobe epilepsy patients. Neuroscience. 1996;72:15-29.

Malemud CJ. Matrix metalloproteinases (MMPs) in health and disease: an overview. Front Biosci. 2006;11:1696-1701.

Mariani J, Crepel F, Mikoshiba K, Changeux JP, Sotelo C. Anatomical, physi- ological, and biochemical studies of the cerebellum from reeler mutant mouse. Philos Trans R Soc Lond B Biol Sci. 1977;281:1-28.

Martinez R, Eller C, Viana NB, Gomes FC. Thyroid hormone induces cerebellar neuronal migration and Bergmann glia differentiation through epidermal growth factor/mitogen-activated protein kinase pathway. Eur J Neurosci. 2011;33:26-35.

Martinez-Ferre A, Martinez S. Molecular regionalization of the diencephalon. Front. Neurosci. 2012;6:73.

Matus A. Microtubule-Associated Proteins: Their Potential Role in Determining Neuronal Morphology. Annu Rev Neurosci. 1988;11:29-44.

McDonald JA, Camenisch TD. Hyaluronan: Genetic insights into the complex biology of a simple polysaccharide. Glycoconj. J.2003;19:331-339.

McKee KK, Harrison D, Capizzi S, Yurchenco PD. Role of laminin terminal globular domains in basement membrane assembly. J Biol Chem. 2007;282:21437-21447.

McRae PA, Porter BE. The perineuronal net component of the extracellular matrix in plasticity and epilepsy. Neurochem. Int. 2012;61:963-972.

McRae PA, Rocco MM, Kelly G, Brumberg JC, Matthews RT. Sensory deprivation alters aggrecan and perineuronal net expression in the mouse barrel cortex. J. Neurosci. 2007;27:5405-5413.

Mecham RP. Laminin receptors. Annu Rev Cell Biol. 1991;7:71-91.

Medina M, Hernández F, Avila J. New Features about Tau Function and Dysfunction. Biomolecules 2016;6:21.

Menon S, Gupton SL. Building Blocks of Functioning Brain: Cytoskeletal Dynamics in Neuronal Development. Int. Rev. Cell Mol. Biol. 2016;322:183-245.

Miale IL, Sidman RL. An autoradiographic analysis of histogenesis in the mouse cerebellum. Expl Neurol. 1961;4:277–296.

Mikoshiba K, Nagaike K, Kosaka S, Takamatsu K, Aoki E, Tsukada Y. Developmental studies on the cerebellum from reeler mutant mice in vivo and in vitro. Dev Biol. 1980;79:64-80.

Millen KJ, Wurst W, Herrup K, Joyner AL. Abnormal embryonic cerebellar development and patterning of postnatal foliation in two mouse Engrailed-2 mutants. Development. 1994;120:695-706.

Milward EA, Fitzsimmons C, Szklarczyk A, Conant K. The matrix metalloproteinases and CNS plasticity: An overview. J Neuroimmunol. 2007;187:9-19.

Mittal S, Song X, Vig BS, Landowski CP, Kim I, Hilfinger JM, Amidon GL. Prolidase, a potential enzyme target for melanoma: design of proline- containing dipeptide-like prodrugs. Mol Pharm. 2005;2:37-46.

Miyata T, Nakajima K, Aruga J, Takahashi S, Ikenaka K, Mikoshiba K, Ogawa M. Distribution of a reeler gene-related antigen in the developing cerebellum: an immunohistochemical study with an allogeneic antibody CR-50 on normal and reeler mice. J Comp Neurol. 1996;372:215-228.

Moore S a, Saito F, Chen J, Michele DE, Henry MD, Messing A, Cohn RD, Ross-Barta SE, Westra S, Williamson RA, Hoshi T, Campbell KP. Deletion of brain dystroglycan recapitulates aspects of congenital muscular dystrophy. Nature. 2002;418:422-425.

Morrens J, Van Den Broeck W, Kempermann G. Glial cells in adult neurogenesis. Glia 2012;60:159-174.

Mouw JK, Ou G, Weaver VM. Extracellular matrix assembly: a multiscale deconstruction. Nat. Rev. Mol. Cell Biol. 2014;15:771-785.

Mueller U, Niesen F., Roske Y, Goetz F, Behlke J, Buessow K, Heinemann U. Crystal Structure of Human Prolidase: The Molecular Basis of PD Disease. Protein Data Bank 2007. (Retrieved from: http://www.rcsb.org/pdb/explore.do?structureId=2OKN)

7. BIBLIOGRAPHY

Myara I, Charpentier C, Lemonnier A. Minireview: Prolidase and prolidase deficiency. Life Sci. 1984;34:1985-1998.

Nagase H, Visse R, Murphy G. Structure and function of matrix metalloproteinases and TIMPs. Cardiovasc. Res. 2006;69:562-573.

Namiduru ES, Ozdemir Y, Kutlar I, Ersoy U. A study of prolidase in mothers, their newborn babies and in non-pregnant controls. Arch Gynecol Obstet. 2001;265:73-75.

Necchi D, Scherini E. The malformation of the cerebellar fissura prima : a tool for studying histogenetic processes. The Cerebellum 2002;1:137-142.

Necchi D, Soldani C, Bernocchi G, Scherini E. Development of the anatomical alteration of the cerebellar fissura prima. Anat Rec. 2000;259:150-156.

Nicholson C, Syková E. Extracellular space structure revealed by diffusion analysis. Trends Neurosci. 1998;21:207-215.

Nowicka J, Nahaczewska W, Owczarek H, Woźniak M. The decrease in prolidase activity in myeloproliferative neoplasms. Adv Clin Exp Med. 2012;21:767-771.

Oohashi T, Edamatsu M, Bekku Y, Carulli D. The hyaluronan and proteoglycan link proteins: Organizers of the brain extracellular matrix and key molecules for neuronal function and plasticity. Exp Neurol. 2015;274:134-144.

Overall CM. Molecular Determinants of Metalloproteinase Substrate Specificity: Matrix Metalloproteinase Substrate Binding Domains, Modules, and Exosites. Mol Biotechnol. 2002;22:051-086.

Palka J, Phang JM. Prolidase activity in fibroblasts is regulated by interaction of extracellular matrix with cell surface integrin receptors. J. Cell. Biochem. 1997;67:166-175.

Palka J, Surazynski A, Karna E, Orlowski K, Puchalski Z, Pruszynski K, Laszkiewicz J, Dzienis H. Prolidase activity disregulation in chronic pancreatitis and pancreatic cancer. Hepatogastroenterol. 2002;49:1699-1703.

Paul A, Cai Y, Atwal GS, Huang ZJ. Developmental Coordination of Gene Expression between Synaptic Partners During GABAergic Circuit Assembly in Cerebellar Cortex. Front Neural Circuits. 2012;6:37.

Paxinos G, Halliday G, Watson C, Koutcherov Y, Wang HQ. Atlas of the developing mouse brain at E17.5, P0, and P6. Elsevier Academic Press, San Diego; 2007.

Perugini P, Hassan K, Genta I, Modena T, Pavanetto F, Cetta G, Zanone C, Iadarola P, Asti A, Conti B. Intracellular delivery of liposome-encapsulated prolidase in cultured fibroblasts from prolidase-deficient patients. J Control Release. 2005;102:181-190.

Piccolini V, Cerri S, Romanelli E, Bernocchi G. Interactions of neurotransmitter systems during postnatal development of the rat hippocampal formation: Effects of cisplatin. Exp Neurol. 2012a;234:239-252.

Piccolini VM, Avella D, Bottone MG, Bottiroli G, Bernocchi G. Cisplatin induces changes in the matrix metalloproteinases and their inhibitors in the developing rat cerebellum. Brain Res. 2012b;1484:15-28.

Pirinççi N, Kaba M, Geçit İ, Güneş M, Yüksel MB, Tanık S, Arslan A, Demir H. Serum prolidase activity, oxidative stress, and antioxidant enzyme levels in patients with renal cell carcinoma. Toxicol Ind Health. 2016;32:193-199.

Porcionatto MA. The extracellular matrix provides directional cues for neuronal migration during cerebellar development. Braz J Med Biol Res. 2006;39:313-320.

Pöschl E, Schlötzer-Schrehardt U, Brachvogel B, Saito K, Ninomiya Y, Mayer U. Collagen IV is essential for basement membrane stability but dispensable for initiation of its assembly during early development. Development 2004;131:1619-1628.

Pyka M, Wetzel C, Aguado A, Geissler M, Hatt H, Faissner A. Chondroitin sulfate proteoglycans regulate astrocyte-dependent synaptogenesis and modulate synaptic activity in primary embryonic hippocampal neurons. Eur J Neurosci. 2011;33:2187-2202.

Qiao S, Kim SH, Heck D, Goldowitz D, LeDoux MS, Homayouni R. Dab2IP GTPase activating protein regulates dendrite development and synapse number in cerebellum. PLoS One. 2013;8(1):e53635.

Qiu Z, Cang Y, Goff SP. Abl family tyrosine kinases are essential for basement membrane integrity and cortical lamination in the cerebellum. J Neurosci. 2010;30:14430-14439.

Qu Q, Smith F. Neuronal migration defects in cerebellum of the Large myd mouse are associated with disruptions in Bergmann glia organization and delayed migration of granule neurons. The Cerebellum 2005;4:261-270.

Rakic P, Caviness VSJ. Cortical development: view from neuro- logical mutants two decades later. Neuron. 1995;14:1101-1104.

Ramos RL, Siu NY, Brunken WJ, et al. Cellular and Axonal Constituents of Neocortical Molecular Layer Heterotopia. Dev Neurosci 2014;36:477-489.

Ramos RL, Van Dine SE, George E, et al. Molecular layer heterotopia of the cerebellar vermis in mutant and transgenic mouse models on a C57BL/6 background. Brain Res. Bull. 2013;97:63-68.

Ramos RL, Van Dine SE, Gilbert ME, Leheste JR, Torres G. Neurodevelopmental Malformations of the Cerebellar Vermis in Genetically Engineered Rats. Cerebellum 2015;14:624-631.

Rempe RG, Hartz AM, Bauer B. Matrix metalloproteinases in the brain and blood–brain barrier: versatile breakers and makers. J Cereb Blood Flow Metab. 2016:0271678X16655551.

Rhodes JM, Simons M. The extracellular matrix blood vessel formation: not just a scaffold. J Cell Mol Med. 2007; 11:176-205.

Rice D, Barone SJ. Critical Periods of Vulnerability for the Developing Nervous System : Evidence from Humans and Animal Models. Birth Environ Health Perspect. 2000;108 Suppl 3:511-533.

Rice D, Curran T. Role of the reelin signaling pathway in Central Nervous System development. Annu Rev Neurosci. 2001;24:1005-1039.

Richtsmeier JT, Flaherty K. Hand in glove: brain and skull in development and dysmorphogenesis. Acta Neuropathol. 2013;125:469-489.

Riederer B, Matus A. Differential expression of distinct microtubule-associated proteins during brain development. Proc Natl Acad Sci USA. 1985;82:6006-6009.

Riederer BM. Differential phosphorylation of some proteins of the neuronal cytoskeleton during brain development. Histochem. J. 1992;24:783-790.

Rochefort C, Lefort JM, Rondi-Reig L. The cerebellum: a new key structure in the navigation system. Front Neural Circuits. 2013;13;7:35.

Ross ME, Walsh CA. Human brain malformations and their lessons for neuronal migration. Annu Rev Neurosci. 2001;24:1041-1070.

Rothenberg SJ, Poblano A, Garza-Morales S. Prenatal and peri- natal low level lead exposure alters brainstem auditory evoked responses in infants. Neurotoxicol. 1994;15:695-699.

Royce PM, Steinmann B. Prolidase Deficiency. In: Connective Tissue and Its Heritable Disorders. Hoboken, NJ, USA: John Wiley & Sons, Inc.; 2002:727-743.

Rozario T, DeSimone DW. The extracellular matrix in development and morphogenesis: A dynamic view. Dev. Biol. 2010;341:126-140.

Ruiz de Almodovar C, Coulon C, Salin PA, Knevels E, Chounlamountri N, Poesen K, Hermans K, Lambrechts D et al. Matrix-binding vascular endothelial growth factor (VEGF) isoforms guide granule cell migration in the cerebellum via VEGF receptor Flk1. J Neurosci. 2010;30:15052-15066.

Rust MB, Kullmann JA, Witke W. Role of the actin-binding protein profilin1 in radial migration and glial cell adhesion of granule neurons in the cerebellum. Cell Adh Migr. 2012;6:13-17.

Sanchez-Arrones L, Stern CD, Bovolenta P, Puelles L. Sharpening of the anterior neural border in the chick by rostral endoderm signaling. Development. 2012;139:1034-1044.

Sasaki T, Fässler R, Hohenester E. Laminin: The crux of basement membrane assembly. J Cell Biol. 2004;164:959-963.

Savas M, Yeni E, Celik H, Ciftci H, Utangac M, Oncel H, Altunkol A, Verit A. The association of serum prolidase activity and erectile dysfunction. J Androl. 2010; 31:146-154.

Sayın R, Aslan M, Kucukoglu ME, Luleci A, Atmaca M, Esen R, Demir H. Serum prolidase enzyme activity and oxidative stress levels in patients with diabetic neuropathy. Endocrine. 2014;47:146-151.

Scherini E, Necchi D, Vignola C, Bernocchi G. cis-Dichlorodiammineplatinum alters GABAergic structures in the immature rat cerebellum. Neuroscience 1992;50:987-997.

Schmahmann JD. Disorders of the cerebellum: ataxia, dysmetria of thought, and the cerebellar cognitive affective syndrome. J Neuropsychiatry Clin Neurosci. 2004;16:367-378.

Schwaller B, Meyer M, Schiffmann S. "New" functions for "old" proteins: the role of the calcium-binding proteins calbindin D-28k, calretinin and parvalbumin, in cerebellar physiology. Studies with knockout mice. Cerebellum 2002;1:241-258.

Selak I, Foidart JM, Moonen G. Laminin promotes cerebellar granule cells migration in vitro and is synthesized by cultured astrocytes. Dev Neurosci. 1985;7:278-285.

Selek S, Altindag A, Saracoglu G, Celik H, Aksoy N. Prolidase activity and its diagnostic performance in bipolar disorder. J Affect Disord. 2011;129:84-86.

Senkov O, Andjus P, Radenovic L, Soriano E, Dityatev A. Neural ECM molecules in synaptic plasticity, learning, and memory. Prog Brain Res. 2014;214:53-80.

Sezen Y, Bas M, Altiparmak H, Yildiz A, Buyukhatipoglu H, Faruk Dag O, Kaya Z, Aksoy N. Serum prolidase activity in idiopathic and ischemic cardiomyopa- thy patients. J Clin Lab Anal. 2010;24:213-218.

Sezer U, Erciyas K, Ustün K, Pehlivan Y, Şenyurt SZ, Aksoy N, Tarakçıoğlu M, Taysı S, Onat AM. Effect of chronic periodontitis on oxidative status in patients with rheumatoid arthritis. J Periodontol. 2013;84:785-792.

Sherman L, Sleeman J, Herrlich P, Ponta H. Hyaluronate receptors: key players in growth, differentiation, migration and tumor progression. Curr. Opin. Cell Biol. 1994;6:726-733.

Siegenthaler JA, Pleasure SJ. We have got you "covered": how the meninges control brain development. Curr Opin Genet Dev. 2011;21:249-255.

Sievers J, Pehlemann FW, Gude S, Berry M. Meningeal cells organize the superficial glia limitans of the cerebellum and produce components of both the interstitial matrix and the basement membrane. J Neurocytol. 1994;23:135-149.

Smyth N, Vatansever HS, Murray P, Meyer M, Frie C, Paulsson M, Edgar D. Absence of basement membranes after targeting the LAMC1 gene results in embryonic lethality due to failure of endoderm differentiation. J Cell Biol. 1999;144:151-160.

Soran N, Altindag O, Aksoy N, Cakır H, Taşkın A, Soran M, Işıkan E. The association of serum prolidase activity with developmental dysplasia of the hip. Rheumatol Int. 2013;33:1939-1942.

Surazynski A, Miltyk W, Palka J, Phang JM. Prolidase-dependent regulation of collagen biosynthesis. Amino Acids 2008;35:731-738.

Takacs J, Zaninetti R, Vig J, Vastagh C, Hamori J. Postnatal expression of Doublecortin (Dcx) in the developing cerebellar cortex of mouse. Acta Biol. Hung. 2008;59:147-161.

Takayama C, Inoue Y. Morphological development and maturation of the GABAergic synapses in the mouse cerebellar granular layer. Dev. Brain Res. 2004;150:177-190.

Takayama C, Nakagawa S, Watanabe M, Mishina M, Inoue Y. Developmental changes in expression and distribution of the glutamate receptor channel delta 2 subunit according to the Purkinje cell maturation. Brain Res Dev Brain Res. 1996;92:147-155.

Tavano A, Grasso R, Gagliardi C, Triulzi F, Bresolin N, Fabbro F, Borgatti R. Disorders of cognitive and affective development in cerebellar malformations. Brain. 2007;130:2646-2660.

Thompson CL, Stephenson FA. GABAA Receptor Subtypes Expressed in Cerebellar Granule Cells: A Developmental Study. J Neurochem. 1994;62:2037-2044.

Timpl R. Structure and biological activity of basement membrane proteins. Eur. J. Biochem. 1989;180:487-502.

Toole BP. Hyaluronan in morphogenesis. Semin. Cell Dev. Biol. 2001;12:79-87.

Toprak G, Yüksel H, Demirpençe Ö, Islamoglu Y, Evliyaoglu O, Mete N. Fibrosis in heart failure subtypes. Eur Rev Med Pharmacol Sci. 2013;17:2302-2309.

Torrey EF, Barci BM, Webster MJ, Bartko JJ, Meador-Woodruff JH, Knable MB. Neurochemical markers for schizophrenia, bipolar disorder, and major depression in postmortem brains. Biol Psychiatry. 2005;57:252-260.

Toy H, Camuzcuoglu H, Camuzcuoglu A, Celik H, Aksoy N. Decreased serum prolidase activity and increased oxidative stress in early pregnancy loss. Gynecol Obstet Invest. 2010;69:122-127.

Ulrich R, Baumgärtner W, Gerhauser I, Seeliger F, Haist V, Deschl U, Alldinger S. MMP-12, MMP-3, and TIMP-1 Are Markedly Upregulated in Chronic Demyelinating Theiler Murine Encephalomyelitis. J Neuropathol Exp Neurol. 2006;65:783-793.

Uzar E, Tamam Y, Evliyaoglu O, Tuzcu A, Beyaz C, Acar A, Aydın B, Tasdemir N Serum prolidase activity and oxi- dative status in patients with diabetic neuropathy. Neurol Sci. 2012;33:875-880.

Vaillant C, Didier-Bazès M, Hutter A, Belin MF, Thomasset N. Spatiotemporal expression patterns of metalloproteinases and their inhibitors in the postnatal developing rat cerebellum. J Neurosci. 1999;19:4994-5004.

Van Dine SE, Salem E, Patel DB, George E, Ramos RL. Axonal anatomy of molecular layer heterotopia of the cerebellar vermis. J Chem Neuroanat. 2013;47:90-95.

Van Hove I, Lemmens K, Van De Velde S, Verslegers M, Moons L. Matrix metalloproteinase-3 in the central nervous system: A look on the bright side. J Neurochem. 2012;123:203-216.

van Welie I, Smith IT, Watt AJ. The metamorphosis of the developing cerebellar microcircuit. Curr Opin Neurobiol. 2011;21:245-253.

Vandenberg P, Kern A, Ries A, Luckenbill-Edds L, Mann K, Kiihn K. Characterization of a type IV collagen major cell binding site with affinity to the α1β and the α2β1 integrins. J Cell Biol. 1991;113:1475-1483

Vanhoof G, Goossens F, De Meester I, Hendriks D, Scharpe S. Proline motifs in peptides and proteins. FASEB J. 1995;9:736-744.

Vecellio M, Schwaller B, Meyer M, Hunziker W, Celio MR. Alterations in Purkinje cell spines of calbindin D-28 k and parvalbumin knock-out mice. Eur J Neurosci. 2000;12:945-954.

Ventruti A, Kazdoba TM, Niu S, D'Arcangelo G. Reelin deficiency causes specific defects in the molecular composition of the synapses in the adult brain. Neuroscience. 2011;189:32-42.

Verma AK, Chandra S, Singh RG, Singh TB, Srivastava S, Srivastava R. Serum prolidase activity and oxidative stress in diabetic nephropathy and end stage renal disease: a correlative study with glucose and creatinine. Biochem Res Int. 2014;2014:291458.

Verslegers M, Van Hove I, Dekeyster E, Gantois I, Hu TT, D'Hooge R, Arckens L, Moons L. MMP-2 mediates Purkinje cell morphogenesis and spine development in the mouse cerebellum. Brain Struct Funct. 2015;220:1601-1617.

Vigetti D, Karousou E, Viola M, Deleonibus S, De Luca G, Passi A. Hyaluronan: biosynthesis and signaling. Biochim Biophys Acta. 2014;1840:2452-2459.

Viglio S, Annovazzi L, Conti B, Genta I, Perugini P, Zanone C, Casado B, Cetta G, Iadarola P. The role of emerging techniques in the investigation of prolidase deficiency: from diagnosis to the development of a possible therapeutical approach. J Chromatogr B Analyt Technol Biomed Life Sci. 2006;832:1-8.

Vural M, Toy H, Camuzcuoglu H, Aksoy N. Comparison of prolidase enzyme activities of maternal serum and placental tissue in patients with early pregnancy failure. Arch Gynecol Obstet. 2011;283:953-958.

Wang H, Kurien BT, Lundgren D, Patel NC, Kaufman KM, Miller DL, Porter AC, D'Souza A, Nye L, Tumbush J, Hupertz V, Kerr DS, Kurono S, Matsumoto H, Scofield RH. A nonsense mutation of PEPD in four Amish children with prolidase deficiency. Am J Med Genet A. 2006;140:580-585.

Wang JZ, Liu F. Microtubule-associated protein tau in development, degeneration and protection of neurons. Prog. Neurobiol. 2008;85(2):148-175.

Watanabe M, Kano M. Climbing fiber synapse elimination in cerebellar Purkinje cells. Eur. J. Neurosci. 2011;34:1697-1710.

Watt AJ, Cuntz H, Mori M, Nusser Z, Sjöström PJ, Häusser M. Traveling waves in developing cerebellar cortex mediated by asymmetrical Purkinje cell connectivity. Nat Neurosci. 2009;12:463-473.

Weingarten MD, Lockwood AH, Hwo SY, Kirschner MW. A protein factor essential for microtubule assembly. Proc Natl Acad Sci USA. 1975;72:1858-1862.

Wess J, Nanavati S, Vogel Z, Maggio R. Functional role of proline and tryptophan residues highly conserved among G protein-coupled receptors studied by mutational analysis of the m3 muscarinic receptor. EMBO J. 1993;12:331-338.

White JJ, Sillitoe R V. Postnatal development of cerebellar zones revealed by neurofilament heavy chain protein expression. Front. Neuroanat. 2013;7:9.

7. BIBLIOGRAPHY

Xu H, Yang Y, Tang X, et al. Bergmann glia function in granule cell migration during cerebellum development. Mol Neurobiol. 2013;47:833-844.

Yamada KM, Spooner BS, Wessellst NK. Axon Growth: Roles of Microfilaments and Microtubules. Proc Natl Acad Sci U S A. 1970;66:1206-1212.

Yong VW, Krekoski CA, Forsyth PA, Bell R, Edwards DR. Matrix metalloproteinases and diseases of the CNS. Trends Neurosci. 1998;21:75-80.

Yurchenco PD, Cheng YS. Self-assembly and calcium-binding sites in laminin. A three-arm interaction model. J Biol Chem. 1993;268:17286-17299.

Yurchenco PD. Basement membranes: cell scaffoldings and signaling platforms. Cold Spring Harb Perspect Biol. 2011;3: a004911.

Yuzaki M. The delta2 glutamate receptor: a key molecule controlling synaptic plasticity and structure in Purkinje cells. Cerebellum. 2004;3:89-93.

List of Original Manuscripts

Brain morphological defects in prolidase deficient mice: first report

V. Insolia,[1] V.M. Piccolini[1,2]

[1]Department of Biology and Biotechnology "Lazzaro Spallanzani", University of Pavia
[2]Histochemistry and Cytometry Section, Institute of Molecular Genetics of CNR, Pavia, Italy

Abstract

Prolidase gene (*PEPD*) encodes prolidase enzyme, which is responsible for hydrolysis of dipeptides containing proline or hydroxyproline at their C-terminal end. Mutations in *PEPD* gene cause, in human, prolidase deficiency (PD), a rare autosomal recessive disorder. PD patients show reduced or absent prolidase activity and a broad spectrum of phenotypic traits including various degrees of mental retardation. This is the first report correlating PD and brain damages using as a model system prolidase deficient mice, the so called dark-like (*dal*) mutant mice. We focused our attention on *dal* postnatal brain development, revealing a panel of different morphological defects in the cerebral and cerebellar cortices, such as undulations of the cerebral cortex, cell rarefaction, defects in cerebellar cortex lobulation, and blood vessels overgrowth. These anomalies might be ascribed to altered angiogenic process and loss of pial basement membrane integrity. Further studies will be directed to find a correlation between neuroarchitecture alterations and functional consequences.

Introduction

Prolidase deficiency (PD) (OMIM 170100) is a rare autosomal recessive disorder whose incidence of 1-2:1,000,000 people is probably underestimated. PD patients have a broad and variable phenotypic spectrum, as well as a diverse clinical onset (as early as shortly after birth or as late as 22 years of age). The principal clinical feature is dermatological manifestation with chronic, recurrent, slowly healing ulcerations mainly located on the lower legs and feet.[1,2] Typically, the phenotype includes moderate to severe degree of mental retardation, rarely epileptic seizures, facial dysmorphism, splenomegaly, susceptibility to recurrent respiratory infections, hypotonia, skeletal and vascular anomalies. The severity of the disease varies widely, but no relationship between genotype and phenotype has been established yet, mainly due to the limited number of mutations described.[3]

Prolidase is linked to the metabolism of many biologically important molecules and it has a central role in extracellular matrix (ECM) remodelling, being essential for normal physiology including embryonic development, tissue resorption, wound healing, cell migration, and cell differentiation.[4-6] In particular, the ECM structure participating to the last two processes in the brain is the pial basement membrane (BM).[7] One of its major constituents is laminin,[8] which has adhesive properties anchoring the plasma membrane of cells adjacent to BM.[6,9] Meningeal cells actively participate in ECM formation[10] and BM remodelling,[11] in fact, impaired meningeal integrity could be the cause of migration defects.[10,12]

The dark-like mutant mouse (*dal*), obtained through random mutagenesis (Mouse Mutant Resource Web Site, The Jackson Laboratory, 2008), could be used as animal model for PD, because of a 4bp deletion in the 14th exon of the murine PEPD gene. Moreover, mice develop congenital cardiomyocyte hypertrophy due to a significant reduction in the levels of several integrin transducers and, being collagen the major ligand of integrins, it was suggested that prolidase, through its effects on the ECM, influences cardiomyocyte growth.[13] At present, no information are available on the functional correlation between PD and the mental retardation described in these patients. Therefore, this is the first neuromorphological study on postnatal brain development in *dal* mutant mice, representing a suitable model to study the morphological/molecular causes of brain defects. Mainly two brain regions were analyzed: cerebral and cerebellar cortices, with the challenging goal to find a parallelism between the human phenotype and brain defects we found in PD mouse model. To investigate the general neuroarchitecture organization haematoxylin and eosin staining and MAP2 immunoreaction[14] were used; to evaluate a possible involvement of meningeal BM, immunoreaction for laminin was carried out (this marker labels the ECM of BM and also wall blood vessels).[15] Simultaneously, GFAP antibody was used to understand the possible consequences of disorganized BM,[1] since it is an important anchor point for astrocyte endfeet, resulting fundamental during brain development, because GFAP-containing fibers provide a migratory scaffold for neurons.[10]

Materials and Methods

Dark-like mice and their wild-type (WT) littermates (C3H/J) used for this study were provided by Prof. T. Gunn (Great Falls, MT, USA). Five animals per genotype, per age were sacrificed at 10 postnatal day (P10), 21 postnatal day (P21), 30 postnatal day (P30), and 60 postnatal day (P60). Mice were deeply anesthetized with an intraperitoneal injection of 35% chloral hydrate (100 μL/100 g b.w.; Sigma, St. Louis, MO, USA); the brain was quickly removed and isolated. The use of mice was approved by the local Pavia City Hall authorities (reference no. 7287/00) and by the Italian Ministry of Health according to Art. 12, Leg. Decree 116/92. All efforts were made to minimize the number of animals and their suffering. The samples were fixed in Carnoy's solution (6 absolute ethanol/3 chloroform/1 glacial acetic acid) for 48 h with a change with fresh solution after 1 h, then placed in absolute ethanol, in acetone, and then embedded in Paraplast X-tra (Sigma-Aldrich, St. Louis, MO, USA). Brain sections (8 μm thick) were obtained serially in the sagittal plane and collected on silan-coated slides.

Haematoxylin and eosin staining

Paraplast embedded sections were deparaf-

Correspondence: Dr. Valeria Maria Piccolini, Department of Biology and Biotechnology "Lazzaro Spallanzani", University of Pavia, via Ferrata 9, 27100 Pavia, Italy.
Tel. +39.0382.986305 - Fax: +39.0382.986325.
E-mail: valeria.piccolini@unipv.it

Key words: Mental retardation, prolidase deficiency, postnatal development, CNS alteration, cardiac hypertrophy, extracellular matrix.

Contributions: VI, work plan projecting, operative research, results discussion and interpretation; VMP, supervision, work plan projecting, operative research, results discussion and interpretation.

Conflict of interests: the authors declare no conflict of interests.

Acknowledgments: the authors would like to thank Prof. Graziella Bernocchi and Dr. Maria Grazia Bottone for their extensive scientific mentoring and their constructive advices on the study of brain development.

Received for publication: 14 April 2014.
Accepted for publication: 8 July 2014.

European Journal of Histochemistry 2014; 58:2417
doi:10.4081/ejh.2014.2417

finized in xylene and rehydrated in a decreasing ethanol series and rinsed in distilled water. Then, sections were immersed for 10 min in Carazzi's haematoxylin at room temperature, washed in running tap water for 20 min and immersed in eosin for 2 s. Sections were washed in distilled water, dehydrated in ethanol, cleared in xylene, and mounted in Eukitt (Kindler, Freiburg, Germany). Slides were observed with an Olympus BX51 microscope, and images were recorded with an Olympus Camedia C-5050 digital camera and stored on a PC. Corrections to brightness and contrast were made with Paint Shop Pro 7 (Jasc Software Inc.).

Immunoperoxidase staining

Paraplast embedded sections were deparaffinized in xylene, rehydrated in a decreasing ethanol series and rinsed in phosphate-buffered saline (PBS; Sigma). The endogenous peroxidases were suppressed by incubation of sections with 3% H_2O_2 in 10% methanol in PBS for 7 min. Sections were incubated for 20 min in normal serum at room temperature. Localization of MAP2, was achieved by applying on brain sections a rabbit polyclonal anti-MAP2 (1:250 Santa Cruz Biotechnology, Santa Cruz, CA, USA) in PBS overnight in a dark moist chamber. Thereafter, the sections were sequentially incubated with biotinylated secondary antibodies (anti-rabbit, 1:200; Vector Laboratories, Burlingame, CA, USA) for 30 min and horseradish peroxidase conjugated avidin-biotin complex (Vector Laboratories) for 30 min at room temperature. Then, 0.05% 3,3'-diaminobenzidine tetrahydrochloride (DAB; Sigma) with 0.01% H_2O_2 in Tris-HCl buffer (0.05M, pH 7.6) was used as a chromogen. After each reaction step, sections were washed thoroughly in PBS, then dehydrated in ethanol, cleared in xylene, and mounted in Eukitt (Kindler). The slides were observed with an Olympus BX51 microscope, and the images were recorded with an Olympus Camedia C-5050 digital camera and stored on a PC. Corrections to brightness and contrast were made with Paint Shop Pro 7 (Jasc Software Inc). For control staining, some sections were incubated with PBS instead of the primary antibody. No immunoreactivity was present in this condition.

Immunofluorescence reactions

Localization of laminin and GFAP was achieved by applying on Paraplast-embedded sections a rabbit polyclonal anti-laminin (1:100; Sigma) and a goat polyclonal anti-GFAP (1:100; Santa Cruz Biotechnology) in PBS overnight in dark moist chamber. Sections were washed in PBS and incubated for 1 h with secondary antibodies Alexa Fluor 488-conjugated anti-rabbit (1:100; Molecular Probes,

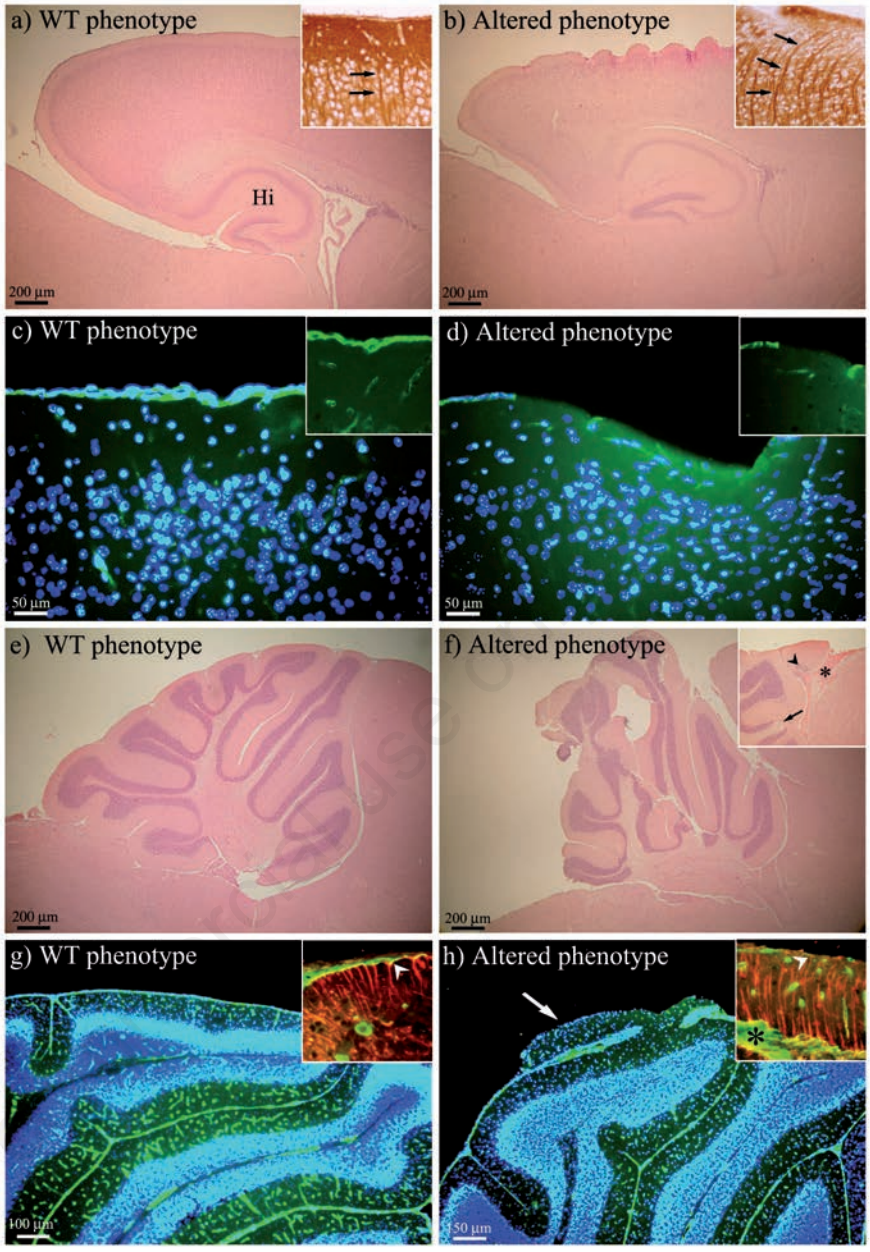

Figure 1. H&E staining, and MAP2, laminin (green fluorescence) and GFAP (red fluorescence) immunoreactions. In panel (a) H&E staining shows the WT lissencephaly, while the altered phenotype is shown in panel (b). In the cerebral cortex, MAP2 immunoreaction (insets of a and b, arrows) evidences the run of neuron dendrites and their positioning. Laminin immunopositivity highlights differences of cortical meningeal BM between WT (c and inset) and altered phenotype (d and inset). The WT cerebellum morphology is illustrated in panel (e), while the altered phenotype in panel (f), where the insertion points to the abnormal vascularization (asterisk), ectopic cells (arrowhead) and absence of granule cells (arrow). In the cerebellum, laminin immunopositivity brings out BM as a continuous layer in WT and small blood vessels within the molecular layer (g). The altered phenotype displays cortical abnormality with lack of BM and large blood vessels penetrating the molecular layer (h). GFAP immunopositive fibers and their endfeet are shown to reach the cerebellar surface only in WT (red fluorescence in the inset of panel g, arrowhead), while in altered phenotype (inset in h, arrowhead) they are disorganized and the endfeet are not detectable. In panels (c, d, g, h) nuclei are counterstained with Hoechst 33258 (blue fluorescence). Altered phenotype, *dal/+* and *dal/dal* mice; Hi, hippocampal formation.

Milan, Italy) and Alexa Fluor 594-conjugated anti-rabbit (1:100; Molecular Probes). After washing with PBS, nuclei were counterstained with 0.1 μg/mL Hoechst 33258 for 6 min and coverslips were lastly mounted in a drop of Mowiol (Calbiochem, San Diego, CA, USA). Slides were observed by fluorescence microscopy with an Olympus BX51 equipped with a 100W mercury lamp used under the following conditions: 450-480 nm excf, 500 nm dm, and 515 nm bf for Alexa 488 and 540 nm excf, 480 nm dm, and 620 nm bf for Alexa 594. Images were recorded with an Olympus Camedia C-5050 digital camera and stored on a PC. Images were optimized for colour, brightness and contrast by using Paint Shop Pro 7 software (Jasc Software Inc).

For control staining, some sections were incubated with PBS instead of the primary antibodies. No immunoreactivity was present in these sections.

Results

In Figure 1, a panel of the most relevant features are presented. Compared to WT, alterations here described were not strictly age-specific or genotype-specific (*dal*/+ and *dal*/*dal*). As it is shown, WT mice presented a smooth cerebral cortex (a,c), while the altered phenotype was characterized by undulations usually localized above the hippocampal formation, where the overall organization was compromised (b,d). In correspondence to these anomalies the normal layering seems to be damaged, as well as the dendrite organization and positioning marked by the MAP2 immunoreaction. In WT, neuron dendrites ran linear and parallel each other (insert in a), while in altered phenotype (insert in b) they followed cortex undulations. The immunopositivity for laminin remarked a completely different profile: BM was continuous in WT (c and insert), and interrupted and thinner in *dal*/+ and *dal*/*dal* (d and insert). Defects in cerebellar cortex were evident regarding lobulation in *dal*/+ and *dal*/*dal* mice (f,h) compared to WT (e,g); protruding cortical portions with a lack of laminin immunopositive BM were also found (h, arrow). These detachments of molecular layer were accompanied by penetration of large blood vessels (inserts in f and h, asterisk) and altered GFAP-positive fibers whose endfeet were not visible and did not reach the surface of the cerebellar cortex (insert in h, arrowhead). On the other hand, in WT the meningeal BM appears continuous shearing uniform thickness (insert in g) with well structured GFAP-positive fibers anchored, through their endfeet, to the laminin-positive BM layer (insert in g, arrowhead). The spectrum of alterations include also the absence of granule cells (insert in f, arrow) or their ectopic position surrounded by molecular layer (insert in f, arrowhead), fusion of cerebellar fissures, and presence of degenerating cells (*not shown*).

Discussion

PD is a rare autosomal recessive disorder caused by a mutation in the *PEPD* gene, which results in a broad spectrum of phenotype including mental retardation.[3] Therefore, we focused our attention on brain morphology and possible factors involved in these anomalies. The presence of vascularisation defects in the cerebral and cerebellar cortices probably is linked to two different causes: i) embryonic cardiomyocyte hypertrophy in *dal* mutant mice;[13] ii) prolidase role in angiogenic signalling processes.[17] The cardiomyocyte hypertrophy results, physiologically, in net induction of angiogenesis,[18] and as it is reported by previous studies,[19,20] this can obstruct the normal migration of cells in the central nervous system (CNS), as we also detected. Moreover, prolidase is involved in ECM remodelling,[5] which acts as scaffold for cellular support in all tissues and organs, and plays crucial roles during development of the CNS in the spatial organization of molecules and cells.[2] ECM, with its constituents, is also known to contribute to other neuronal functions such as cell proliferation, migration, morphological differentiation, synaptogenesis, synaptic stability, and cell signalling cascades.[4,6,22] The absence of a fully functional prolidase enzyme might result in an altered ECM remodelling leading to meningeal defects, one of the possible causes of the brain development impairments,[23] the loss of pial BM integrity and the consequent disorganized cytoarchitecture in *dal* mutant mice.

Further studies will be directed to understand the peculiar role of prolidase in brain development, and to investigate other meningeal BM components. We will focus also on the detection of important molecules and cells involved in the proliferation, migration and differentiation pathways during neurogenesis. Our experimental findings in *dal* mutant mice with inherited PD underline the importance of prolidase, being relevant also for understanding PD physiology in humans.

References

1. Lupi A, Tenni R, Rossi A, Cetta G, Forlino A. Human prolidase and prolidase deficiency: an overview on the characterization of the enzyme involved in proline recycling and on the effects of its mutations. Amino Acids 2008;35:739-52.
2. Kiratli H, Satilmiş M. Prolidase deficiency associated with pathologic myopia. Ophthalmic Genet 1998;19:49-53.
3. Royce PM, Steinmann B. Prolidase deficiency. New York, Wiley-Liss: 2002.
4. Berrier AL, Yamada KM. Cell–Matrix Adhesion. J Cell Physiol 2007;213:565-73.
5. Hu CA, Phang JM, Valle D. Proline metabolism in health and disease. Preface. Amino Acids 2008;35:651-52.
6. McRae PA, Porter BE. The perineuronal net component of the extracellular matrix in plasticity and epilepsy. Neurochem Int 2012;61:963-72.
7. Halfter W, Dong S, Yip YP, Willem M, Mayer U. A critical function of the pial basement membrane in cortical histogenesis. J Neurosci 2002;22:6029-40.
8. Timpl R. Structure and biological activity of basement membrane proteins. Eur J Biochem 1989;180:487-502.
9. Aumailley M. The laminin family. Cell Adh Migr 2013;7:48-55.
10. Decimo I, Fumagalli G, Berton V, Krampera M, Bifari F. Meninges: from protective membrane to stem cell niche. Am J Stem Cells 2012;1:92-105.
11. Hecht JH, Siegenthaler JA, Patterson KP, Pleasure SJ. Primary cellular meningeal defects cause neocortical dysplasia and dyslamination. Ann Neurol 2010;68:454-64.
12. Zarbalis K, Choe Y, Siegenthaler JA, Orosco LA, Pleasure SJ. Meningeal defects alter the tangential migration of cortical interneurons in Foxc1hith/hith mice. Neural Dev 2012;7:2.
13. Jung S, Silvius D, Nolan KA, Borchert GL, Millet YH, Phang JM, et al. Developmental cardiac hypertrophy in a mouse model of prolidase deficiency. Birth Defects Res A Clin Mol Teratol 2011;91:204-17.
14. Yamaguchi S, Fujii-Taira I, Murakami A, Hirose N, Aoki N, Izawa EI, et al. Up-regulation of microtubule-associated protein 2 accompanying the filial imprinting of domestic chicks (Gallus gallus domesticus). Brain Res Bull 2008;76:282-8.
15. Qiu Z, Cang Y, Goff SP. Abl family tyrosine kinases are essential for basement membrane integrity and cortical lamination in the cerebellum. J Neurosci 2010;27:14430-9.
16. Siegenthaler JA, Pleasure SJ. We have got you 'covered': how the meninges control brain development. Curr Opin Genet Dev 2011; 21:249-55.
17. Rhodes JM, Simons M. The extracellular matrix and blood vessel formation: not just a scaffold. J Cell Mol Med 2007;11:176-205.
18. Laughlin MH, Bowles DK, Duncker DJ. The coronary circulation in exercise training.

Am J Physiol Heart Circ Physiol 2012;302: 10-23.
19. Akbarian S, Kim JJ, Potkin SG, Hetrick WP, Bunney WE, Jones EG. Maldistribution of interstitial neurons in prefrontal white matter of the brains of schizophrenic patients. Arch Gen Psychiatry 1996;53: 425-36.
20. Chevassus-au-Louis N, Represa A. The right neuron at the wrong place: biology of heterotopic neurons in cortical neuronal migration disorders, with special reference to associated pathologies. Cell Mol Life Sci 1999;55:1206-15.
21. Pearlman AL, Sheppard AM. Extracellular matrix in early cortical development. Prog Brain Res 1996;108:117-34.
22. Hensch TK. Controlling the critical period. Neurosci Res 2003;47:17-22.
23. Cerri S, Piccolini VM, Bernocchi G. Postnatal development of the central nervous system: anomalies in the formation of cerebellum fissures. Anat Rec (Hoboken) 2010;293:492-501.

Toxics **2015**, *3*, 224-248; doi:10.3390/toxics3020224

OPEN ACCESS

toxics

ISSN 2305-6304

www.mdpi.com/journal/toxics

Article

Neurotoxic Effects of Platinum Compounds: Studies *in vivo* on Intracellular Calcium Homeostasis in the Immature Central Nervous System

Graziella Bernocchi [1,*], Francesco P. Fanizzi [2], Sandra A. De Pascali [2], Valeria M. Piccolini [1], Caterina Gasperini [1], Violetta Insolia [1] and Maria Grazia Bottone [1]

[1] Dipartimento di Biologia e Biotecnologie "L. Spallanzani" Università di Pavia, via Ferrata 9, 27100 Pavia, Italy; E-Mails: valeria.piccolini@unipv.it (V.M.P.); caterina.gasperini01@ateneopv.it (C.G.); violetta.insolia01@ateneopv.it (V.I.); bottone@unipv.it (M.G.B.)

[2] Dipartimento di Scienze e Tecnologie Biologiche e Ambientali (Di.S.Te.B.A.), Università del Salento, via provinciale Lecce-Monteroni centro Ecotekne, 73100 Lecce, Italy; E-Mails: fp.fanizzi@unisalento.it (F.P.F.); sandra.depascali@unisalento.it (S.A.P.)

* Author to whom correspondence should be addressed; E-Mail: graziella.bernocchi@unipv.it; Tel.: +39-0382-986-327.

Academic Editors: Guido Cavaletti and Valentina Carozzi

Received: 30 April 2015 / Accepted: 9 June 2015 / Published: 19 June 2015

Abstract: Platinum compounds cause significant clinical neurotoxicity. Several studies highlight neurological complications especially in paediatric oncology patients with Central Nervous System (CNS) and non-CNS malignancies. To understand the toxicity mechanisms of platinum drugs at cellular and molecular levels in the immature brain, which appears more vulnerable to injury than in the adult one, we compared the effects *in vivo* of the most used platinum compounds, *i.e.*, cisdichlorodiammineplatinum (cisplatin, cisPt), and the new [Pt(*O*,*O*′-acac)(γ-acac)(DMS)] (PtAcacDMS). As models of developing brain areas, we have chosen the cerebellum and hippocampus dentate gyrus. Both areas show the neurogenesis events, from proliferation to differentiation and synaptogenesis, and therefore allow comparing the action of platinum compounds with DNA and non-DNA targets. Here, we focused on the changes in the intracellular calcium homeostasis within CNS architecture, using two immunohistochemical markers, the calcium buffer protein Calbindin and Plasma Membrane Calcium ATPase. From the comparison of the cisPt and PtAcacDMS effects, it emerges how essential the equilibrium and synergy between CB and PMCA1 is or how

important the presence of at least one of them is to warrant the morphology and function of nervous tissue and limit neuroarchitecture damages, depending on the peculiar and intrinsic properties of the developing CNS areas.

Keywords: platinum compounds; neurotoxicity; CNS development; calcium homeostasis systems; purkinje neurons; dentate granule cells

1. Introduction

1.1. State of Art on Toxicity of Platinum Compounds and Aim

Platinating compounds have been recognized for over 30 years as anticancer agents used for the treatment of several types of tumors. Cisplatin (cis-dichlorodiammineplatinum II, cisPt) in particular, when introduced into clinical trials, has had a great impact in cancer medicine. Its clinical benefits were addressed to testicular, ovarian, cervical head and neck, non-small cell lung, and lymphoma cancers [1–3]. The discovery of cisPt was therefore a corner stone [4], which triggered great interest in platinum (II) derivatives. Besides cisPt, several platinum compounds were tested in clinical trials: The different platin compounds are used for different types of cancers because each varies in its efficiency for a specific tumor. For instance, it has been demonstrated in chemotherapies that cisplatin is superior to carboplatin in treatment of tumor testis, bladder, head and neck, small cell lung cancer and in paediatric malignancies whereas in other cancer types, carboplatin has tended to replace cisplatin. On the other hand, the use of platinum compounds is limited due to toxic side effects in normal tissues.

Toxicities associated with cisPt, that remains the most potent chemotherapeutic drug, range from mild to severe, being the most serious ototoxicity, nephrotoxicity, peripheral neurotoxicity and nausea and vomiting [3,5,6]. The benefit of cisPt is limited not only to neurotoxicity but also to resistance ascribable to the fact that cisPt is a multifactorial agent. In fact, its biochemical mechanism is based on the interaction of more intercellular changes [7], such as reduced drug intracellular transport, activation of oncogenes, inactivation of tumor suppressor genes, alterations in the cell cycle and checkpoints, and in apoptotic pathways, enhanced intracellular detoxification mediated by glutathione S-transferase (GST), and increased DNA repair or insensitivity to apoptotic cell death [8–10].

With regard to neurotoxicity, peripheral sensory neuropathy (PNS) is commonly observed in 50% of patients treated with cisPt [11,12], being the spinal dorsal root ganglia the primary location of cisPt damage [3]. Severely affected patients have sensory ataxia, but minimal or absent motor involvement [1]. In addition, cognitive deficits are a significant clinical problem after treatment with chemotherapeutic drugs that do not exclude persistent memory problems [13,14]. The deficits might be related to damages to central nervous system (CNS). A number of animal studies have shown that cisPt and its analogs affect several neurobiological processes [15], although the presence of mature brain blood barrier (BBB) would preserve from the cytotoxic effects since platinum-based agents do not have the propensity to enter the brain but only the dorsal root ganglia and peripheral nerves [16]. However, studies show that cisPt treatment is associated with increased BBB permeability, which further facilitates the passage of it across the barrier [17]. Neural and vascular lesions produced by cisPt are shown as hemorrhagic foci

accompanied by necrosis and edema [18]. Neurotoxic effects on mature neurons were described in the cerebellar cortex and ventral horn of adult rats [19]. In addition, cisPt comes in contact with normal neuronal cells, such as stem or immature cells in the hippocampus [20], where long exposures to cisPt injured dendritic branches and reduced dendritic complexity that might contribute to cognitive impairment [21].

Neurotoxicity in the CNS should be seen as among the most serious problems to be addressed for tumors chemotherapy in infancy. Platinum compounds are widely used for childhood malignancies since they are essential components of multidrug frontline therapy regimens [22] given to children with CNS solid tumors (e.g., neuroblastoma) and non-CNS malignancies (e.g., leukemia) [23]. It is important to note that there are several long-term behavioural effects (such as depression, anxiety or antisocial behavior) in pediatric patients with cancer [24]. On the other hand, the immature CNS is more vulnerable to damage from toxic agents than the adult one and prone to impairment [25–27]. In mammals, there are crucial phases of CNS maturation during which the brain regions may have differential effects induced by various chemicals [25,28–30].

Based on the last remarks, in our research, we followed two goals: First, the study of *in situ* damages induced by platinum compounds on normal and immature neuroarchitecture, by means of morphological and molecular markers; second, the *in vivo* analysis of neurotoxic effects on normal tissue of a new platinum compound [Pt(*O*,*O'*-acac)(γ-acac)(DMS)] (PtAcacDMS) that encompasses the chemoresistance in comparison with cisPt.

1.2. An Old Platinum Compound vs. a New Platinum Compound. CisPt vs. PtAcacDMS: Action Mechanisms and Cytotoxicity

The main cellular target of cisPt is genomic DNA [31], although the full understanding of the process that translate DNA damages into its drug-mediated cellular effects is very critical. CisPt is a square planar neutral inorganic complex that reacts with DNA; for this interaction, the neutral cisPt has to be activated through spontaneous aquation reactions that make it strongly reactive. The cytotoxicity is first ascribed to its interaction with endogenous nucleophiles of purine bases to form interstrand and intrastrand DNA–protein and DNA–DNA crosslinks. The intrastrand DNA adducts are the main factor responsible for the cytotoxic action [2,32], which results in several biological effects, not necessarily directly correlated with cell death. Pro-survival and pro-apoptotic signals such as Bcl2 and Bax proteins are activated after cisPt exposure [2]. Nevertheless, cisPt is considered a very potent apoptosis inducer [33,34]. However, in the cytoplasm many cellular components with soft nucleophilic sites, such as cytoskeleton microfilaments, thiol-containing peptides and protein and RNA, may react with cisPt, being the most important non-DNA target glutathione (GSH) and thiol-containing biomolecules [32].

On the other hand, resistances to cisPt have been observed especially when in therapy protocols the standard clinical dose is doubled or chronic drug exposure is made. A number of cytoplasmic constituents inactivate cisPt. The concentrations of thiol-containing molecules increase after chronic cisPt administration, and induce resistance by decreasing the availability of the antitumor agent to interact with the target DNA. Increase in GSH has been shown in a number of cisPt-resistant tumor models and in the clinical studies [2,3]. Finally, increased repair of platinum-DNA adducts by several

types of proteins, increased tolerance of cisPt adducts and failure of cell death are to be considered in the multifactorial resistance of cisPt [32].

Among the approaches to overcome toxicity and resistance linked to the clinical use of cisplatin, the synthesis of new platinum compounds having different target and a low toxicity profile should be highlighted. A class of new platinum complexes, specifically designed and synthesized by some of us, have shown some interesting biological properties; these complexes contain acetylacetonate (Acac) and sulfur ligands such as dimethylsulphoxide (DMSO) or dimethylsulphide (DMS) in the platinum coordination sphere [35,36]. The complex [Pt(*O*,*O*′-acac)(γ-acac)(DMS)] **(**PtAcacDMS) contains two Acac (one *O*,*O*-chelate, one sigma linked by methine in gamma position) and dimethylsulphide (DMS) in the metal coordination sphere. It was able to induce apoptosis in endometrial cancer cells (HeLa). In particular, its activity was about 100 times higher compared to the one of cisPt; moreover, PtAcacDMS showed an increased cytotoxicity in MCF-7 breast cancer cells that were resistant to cisPt [37,38]. This cytotoxicity concerned only an intracellular accumulation [37,38]. The reactivity, low with nucleobases and specific with sulfur ligands, suggests that the possible cellular target could be represented by aminoacid residues of proteins and enzymes involved in the pathway of apoptotic induction. In addition, mutagenic tests were performed on PtAcacDMS using cisPt as a positive control. Notably, whereas cisPt exhibits the renowned mutagenic activity, the new complex does not show revertant colonies. All these evidences together with intracellular signal transduction studies confirmed the biological activity of PtAcacDMS as the reaction with non-genomic biological targets [39], highlighting that DNA is not the main target of Pt(II) complex.

The new platinum compound [35,36] has been studied in MCF-7 cells [37,38,40], cells that are known to be resistant to many chemotherapeutics. It was confirmed that, compared with cisPt, the cytotoxicity of PtAcacDMS depends on its cell concentration in the tumour cells, not on its binding with DNA.

The presence of platinum in the developing brain tissue after PtAcacDMS administration [41] is in accordance with data obtained on HeLa and MCF-7 cells from *in vitro* studies [37,38]. Measurements of cellular accumulation of the novel cisPt analog is linearly correlated with its concentration, as it occurs in cisPt treated cells. PtAcacDMS concentration increases rapidly in the cells, and its cellular accumulation rate is calculated to be between 6 and 10 times higher than the cisPt one in HeLa and MCF-7 cells [37,38]. The cytostatic effect is closely related to the platinum accumulation in the cell. This issue could be an advantage for PtAcacDMS since it would permit the use of lower doses with consequent reduction of side effects and drug resistance risks.

In this article, the attention has been paid to the action of platinum compounds on intracellular calcium homeostasis [42]. To this aim we reported findings on the immunohistochemical changes of calcium protein markers in differentiating neurons which have a fundamental role for the neuroarchitecture and neural circuits' establishment during postnatal life development.

1.3. Immature CNS Areas in the Postnatal Life of Mammals

Development of CNS in mammals does not end at birth; in fact, it continues through the postnatal life. Various morphological and physiological changes occur also in the human brain during infancy and adolescence [27,43]. The rate of developmental changes are very high in the infancy, whereas adolescence—which is the transition stage between childhood and adulthood and represents one of the

most dynamic events of growth and development in the human—as a second surge of synaptogenesis still occurs. In these stages, developmental injuries and infections can result in several lasting CNS problems such as mental retardation, hydrocephalus and epilepsy. Neurotoxic agents including drugs and chemicals affect all steps of CNS development [25,28–30].

As models of postnatally developing CNS areas, the cerebellum [44,45] and hippocampal dentate gyrus (DG) [46–48] are brain regions particularly vulnerable in the developing animal as well as in newborn human because injury may alter physiology and cause neuropsychiatric disorders [49,50].

In the rat or mouse, both areas are later-developing brain regions with important neurodevelopmental changes [46,47,51–53], especially in the first three weeks of postnatal life when multiple interrelated processes occur in maturing neuroarchitecture. These range from cell proliferation, migration and differentiation to synaptogenesis and synaptic connectivity. Interestingly, the developing regions offer the opportunity to distinguish the events on which the platinum compounds act on DNA and non-DNA targets.

Considering the cerebellum, it is proved to be also a valuable model for studying naturally occurring cell death [54,55] *in vivo*. In the newborn, a germinative matrix—the external granular layer (EGL)—persists in the cerebellar cortex until the third week [52]. The matrix originates the granule cells [56] of only the internal granular layer (IGL), after their migration by Bergmann radial glia fibres. It is noteworthy that cerebellar defects were also found due to a failure of Bergmann radial glia, which is demonstrated to be a mechanical force of cerebellar foliation [57,58] in the maturation of the cerebellum architecture. The differentiation of the GABAergic Purkinje neurons even occurs postnatally, and it is regulated by the developing fiber systems in the cerebellum [52].

In the postnatally developing hippocampus, cell migration and differentiation continue to be very active. The critical steps in the histogenesis of rodent hippocampal formation have been described in detail [46,53,59]. While pyramidal cells and large interneurons arise during the prenatal life, DG granule cells originate at embryonic day E16 and continue to proliferate during postnatal development until they migrate to their final destination [51]. Therefore, cell migration and synaptogenesis are postnatal events of all cell types in the hippocampus [46,59].

Here, we focused the attention on cells that have a fundamental role in the neuroarchitecture and neural circuits' establishment in the cerebellum and hippocampus, *i.e.*, Purkinje cells and DG granule cells, respectively. The Purkinje neurons are key elements being the sole neurons projecting outside the cerebellar cortex on deep nuclei in the white matter [60]; these large neurons extend their branched dendrite in the molecular layer of cerebellar cortex, where they receive synaptic contacts by parallel and climbing fibres, and by basket and stellate axons. The DG granule cells are cells whose dendrites penetrate in the molecular layer; here, they receive afferents mainly from enthorynal cortex, while their axons project outside the DG on pyramidal layer of Cornus Ammonis (CA) [46].

2. Experimental Section

2.1. Animals and Schedule of the Experimental Plan

The cisPt (Teva Pharma, Italy) and the new compound PtAcacDMS were administered to 10-day-old (PD10) Wistar male rats as previously reported [41,61].

The rats were exposed to a 12:12 h light:dark artificial cycle and were given *ad libitum* access to food and tap water. Treated and untreated control animals were anesthetized at PD11 and PD17 with the 35% chloral hydrate intraperitoneal injection (100 μL/100 gbw, provided by Sigma, St. Louis, MO, USA). Then, brains were quickly removed and processed as reported in Cerri *et al.*, [41]. Paraplast-embedded brains were cut in sagittal sections of cerebellar vermis and in cross sections of hippocampus.

All experimental protocol was in line with the Italian Ministry of Health (DDL 116/92) guidelines. All efforts were made in order to minimize the number of rats used and their suffering.

2.2. Immunocytochemistry in Light Microscopy

The sections were incubated with an endogenous peroxidases blocking buffer and then with the normal serum as described in Cerri *et al.* [41]. The presence of Calbindin (CB) and Plasma Membrane Calcium ATPase 1 (PMCA1) was detected through the use of a rabbit polyclonal anti-CB 28kD (diluted 1:2000; provided by Sigma, St. Louis, MO, USA) or a rabbit polyclonal anti-PMCA1 (diluted 1:1000; provided by Abcam, Cambridge, UK) in PBS. The sections were incubated overnight in a dark moist chamber with these antibodies. Thereafter, the immunocytochemistry signal detection was carried out as reported by Cerri *et al.* [41]. Then, an Olympus BX51 microscope was used, and the images were acquired with the digital camera Olympus Camedia C-5050 and then stored on a PC. Using Paint Shop Pro-7 (Jasc Software Inc., Eden Prairie, MN, USA), the images were corrected and converted in grayscale. The control brain sections were incubated overnight with PBS instead of primary antibody and no immunoreactivity was detected.

2.3. Immunocytochemistry in Fluorescence Microscopy

Localization of CB was achieved by using a mouse monoclonal anti-CB 28kD (diluted 1:5000, provided by Swant, Bellinzona, Switzerland) in PBS. The sections were incubated overnight in a dark moist chamber. Thereafter, the immunocytochemistry signal detection was carried out using Alexa Fluor 488-conjugated anti-mouse (diluted 1:100; provided by Molecular Probes, Space, Milano, Italy) as reported by Cerri *et al.* [41]. Then, an Olympus BX51 supplied with a 100 W mercury lamp was used with the following conditions: (i) 450–480 nm excf; (ii) 500 nm dm; (iii) 515 nm bf. Images were acquired with the digital camera Olympus Camedia C-5050 and then stored on a PC. Paint Shop Pro-7 (Jasc Software Inc., Eden Prairie, MN, USA, 2000) was used to adjust and convert the images in greyscale. The control brain sections were incubated overnight with PBS instead of primary antibody and no immunoreactivity was detected.

2.4. Determination of Cell Immunoreactivity Intensity

The optical density (OD) of CB and PMCA1 immunoreactivity was measured in the cerebellar Purkinje cell layer and DG granule cell layer. The extent of the labelling was determined on digitized images of sections acquired with an exposure time adjusted to avoid pixel saturation effect. The signal intensity was quantified by the means of densitometric analysis using Image-J 1.46p (Software NIH, Bethesda, MA, USA). Moreover, the mask shape was adjusted according to the spatial distribution of the cells within the layers. All the measurements were done using the mean value of the intensity over the area.

The immunostaining intensity for CB and PMCA1 were measured in a total of 30 fields (10 fields per rats) for untreated and treated animals, at PD11 and PD17. Data were recorded and analysed by Microsoft Office Excel Software spreadsheets and were indicated as the Means ± SD (standard deviation). The student's *t*-test was performed to asses any statistical differences between control and cisPt or PtAcacDMS treated animals.

3. Results and Discussion

3.1. Platinum Compounds and Calcium Homeostasis

Despite the differences in the neurotoxic effects of the two platinum analogs, cisPt and PtAcacDMS, ascribable to a different mechanism of action, we can consider, as a common involved factor, the intracellular calcium concentration, that mediates the effectiveness and the toxicity of anticancer drugs. In fact, the modulation of intracellular calcium is a fundamental factor in the activation of cell death [42] or cell degeneration [62].

Overall, a central and critical role in neurogenetic events such as cellular proliferation, migration and differentiation, and synaptogenesis is plaid by calcium ions [63]. Disruption of function of calcium channels in signalling processes can lead to profound disturbances in brain cytoarchitecture and function. In particular, postnatal brain ontogenesis shows critical and vulnerable windows in which disturbances in calcium homeostasis should allow to dramatic consequences. In neurodegenerative mechanisms and neurological disorders, elevated levels of intracellular calcium are found [62]. On the other hand, elevated calcium transport controls the rate of cell migration, with spontaneous elevations in intracellular calcium levels [64].

Antitumor platinum compounds such as cisPt are often toxic through complex, not well understood mechanisms. CisPt may kill cells by various means such as apoptosis and necrosis. Perturbation of cellular calcium homeostasis [65] has been demonstrated in different *in vitro* models. Recently, Kawai *et al.* [66] showed in a non-tumour model, that relatively high concentrations of cisPt (250–750 μM) induce a rise in $[Ca^{2+}]_i$ while Liang and Huang [67] demonstrated in a cisPt-resistant cell line that $[Ca^{2+}]_i$ increases lesser and faster than in a cisPt-sensitive cell line. CisPt concentration-dependently increases $[Ca^{2+}]_i$ in HeLa-S3 (human cervix adenocarcinoma) and not in U2-OS (human osteosarcoma) cells [68]. One hypothesis regarding the interaction of cisPt and calcium homeostasis in HeLa-S3 cells is that cisPt might be actively transported into or out of the cell. When extracellular calcium enters the cytosol, an increase of $[Ca^{2+}]_i$ occurs and efflux transport mechanisms (Ca^{2+}-ATPases) is activated, resulting in a consequent net calcium increase in calcium stores. Moreover, when the amount of calcium entering the cell and the efflux mechanisms are balanced, there is no further increase of $[Ca^{2+}]_i$ and the cytosolic concentration is higher than in control conditions. Calcium-dependent calpain is activated by an elevated $[Ca^{2+}]_i$, triggering apoptosis just in HeLa-S3 and not in U2-OS cells [4,61].

In summary, the expected cisPt related mechanisms of calcium intracellular concentration variations are: (a) cisPt, in a concentration dependent manner, causes a reduction of calcium current through the activation of calcium channels; (b) cisPt opens a membrane associated pore allowing calcium entry in the cells from the extracellular space, with a consequent increase in $[Ca^{2+}]_i$.

It should be mentioned that also inositol phosphate-3 (IP3) receptors are involved in the calcium entry [61].

CisPt affects calcium homeostasis by binding to sulphydryl groups of proteins such as enzymes, channels and pumps [69]; as above mentioned the binding of cisPt to non-genomic targets may contribute to its biochemical mechanisms of action [32].

PtAcacDMS affects free $[Ca^{2+}]_i$ through protein kinase C (PKC)-α-mediated closure of a few channels and the PMCA activity inhibition; the increase in $[Ca^{2+}]_i$ is related to its ability of triggering rapid apoptosis in MCF-7 cells [40].

Since our aim is the *in situ* correlation between calcium intracellular changes and neuroarchitecture damages, we considered specific histochemical markers of proteins involved in the calcium homeostasis.

3.2. Histochemical Detection of Calcium Homeostasis and Differentiating Cells in the Immature Cerebellum and Hippocampus

Intracellular calcium is regulated by delicate balance between the calcium entry and the active mechanisms involved in the transport against its concentration gradient. Pumps or exchangers of the outer cellular membrane regulate the calcium concentration; there is also a possible re-entry (via Ca^{2+}-transport systems) to the calcium stores, mainly represented by mitochondria and endoplasmic reticulum. In the cell, calcium could also be bound to calcium-buffering proteins with consequent regulation of $[Ca^{2+}]_i$ [4]. Indeed, the association with various calcium binding proteins (CBPs) [70] can modulate intracellular calcium by a buffering action.

CBPs, including CB, parvalbumin (PV) and calretinin (CR), has been studied to identify different functional cell types in the brain neocortex, hippocampus, cerebellum and thalamus [71–73]. CBPs have been extensively studied as neuronal immunohistochemical markers of specific cell populations in the CNS [74–76] and have been implicated in neuroprotection in different pathological conditions since they function as buffers for calcium excess. Regarding the specific involvement, CB and PV sequester the excess calcium during development and synaptic plasticity. CBPs alter the duration of action potentials, and promote neuronal activity as protecting molecules against the damages derived from excessive calcium influx [74]. In the absence of CBPs, there is a high calcium accumulation inside the cytosol, causing hyperexcitability that often leads to neurodegeneration [71,72].

CBPs immunoreactivity has been detected in similar populations of neurons in mammals, such as humans, rodents and birds [77,78].

3.2.1. Calbindin

This article focused on two cellular phenotypes, cerebellar Purkinje neurons and DG granule cells, both expressing one of the CBPs, the CB D-28kDa.

CB is a member of the EF-hand family of CBPs and it has a low molecular weight. CB is able to bind Ca^{2+} with a fast association rate [79]. CB seems to be involved in the modulation of specific calcium-dependent activities of developing neurons, such as neurite elongation and spine formation. CB inside the neuronal cytosol might exert a protective role against the overfull calcium influx, which may cause degenerative processes [80].

Developmental studies have indicated that CB is expressed early in embryonic CNS, following the cessation of mitosis, when neurons are ready to migrate [81]. CB has been shown to be temporarily expressed during brain development in numerous nerve cell systems and animal species [82,83].

In the rodent cerebellum [71,72], CB, CR as well as PV are detected in the cytosol of one or more populations of neurons at relatively high concentrations. The fast buffer CB is exclusively present in Purkinje cells, in the soma dendrite branches and axons. Neurons rich in CB appeared relatively resistant to degeneration in several acute or chronic disorders [72]. In the developing cerebellum, CB is low until embryonic day 18 and reaches a peak at postnatal day 20. Thereafter, the CB levels remain high [72].

At the postnatal stages of PD11-PD17 of control (ctr) rats (Figure 1), in the Purkinje cell layer, the large neurons were immunopositive to CB in all compartments, *i.e.*, in the soma and dendrite tree, and axon. Dendrite tree of Purkinje cells were labelled in the fine branches and spines.

There is good evidence of the presence of CB in Purkinje cell dendritic spines that may change their morphology to partially compensate for changes in Ca^{2+} homeostasis due to the loss of CPBs [71]. The intensity of immunolabelling increased at PD17 *vs.* PD11 (Figure 1), and the dendrite branches grew in the molecular layer (ML). In the ML, parallel and climbing fibres regulate the branching of Purkinje cell dendrite by synapses on its spines [84,85].

In the hippocampus, CB is primarily demonstrated in DG granule cell layer; the somata of granule cells are intensely immunostained while their dendrites are moderately stained. CB is also expressed in a CA1 pyramidal cell subpopulation and in some interneurons [59,74,75,86]. In particular, CB is present in GABAergic neurons mainly innervating the distal dendrite of the principal cells, and controlling the efficacy of afferent inputs. Hippocampal CB positive interneurons appeared resistant to epileptic injury in rat models [87].

Researchers have studied the ontogeny of cells which express CB at early postnatal stages [88,89], and in fact they showed that CB is present in granule cells of DG during the very early postnatal stages. CB has been reported to reappear on PD2 in clusters of neurons in the *radiatum* and the *oriens* layers and in the granule cells of the mouse DG [90].

Progressive expression of CB appeared in an outside-in pattern in the DG granule cell layer as reported also by Abraham *et al.* [91] between PD11 and PD17 of control rat postnatal development (Figure 2).

Interneurons within the granular layer were also detectable as well as strongly CB labelled interneurons [48]. These latter were found at PD17 in the CA layers, where some groups of pyramidal cells were also stained. CB labelled fibers were also distributed in the ML and hilus of DG and beneath the CA3 pyramidal layer.

The intensity of labelling increased at PD17 *vs.* PD11. Changes in the immunolabelling to CB is indicative of changes in the level of the protein, since it has been shown that loss of CB after commissural kindling stimulation [92] is due to a decrease in the protein as shown by quantitative evaluations in granule cells of DG. The expression of CB is regulated by the functional state of the hippocampal circuit [79], since it is needed for normal short-term synaptic plasticity between the DG granule cells and CA3 neurons [93], and modulates the excitability of the CA1 pyramidal cells [94].

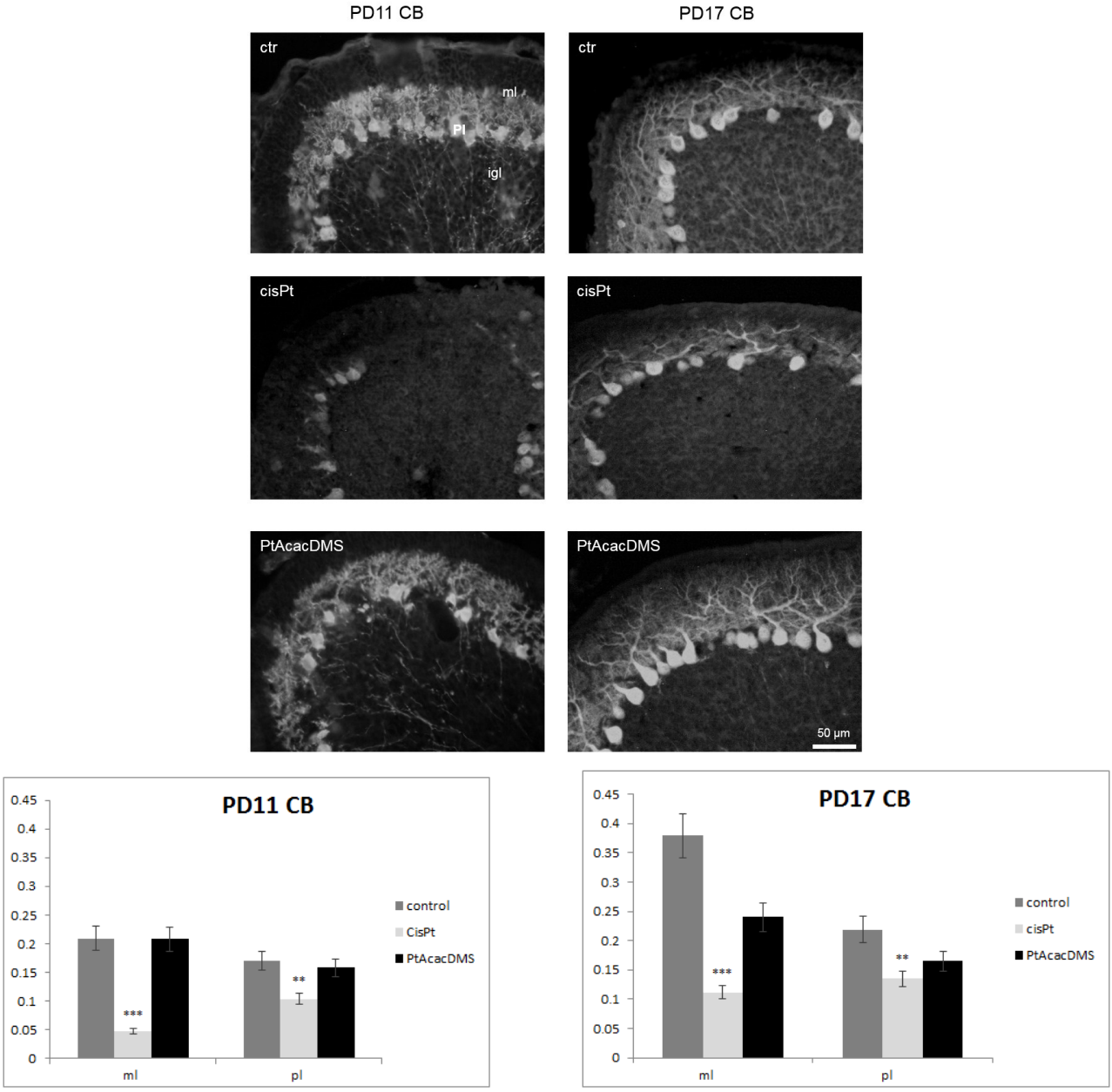

Figure 1. Calbindin immunocytochemistry in the Purkinje cell layer. At **PD11**, control rats (ctr) show intense labelling in the Purkinje cell cytoplasm; strong immunoreactivity is detected in the molecular layer, in the dendrite tree branches of Purkinje cells. After cisPt treatment, atrophy of Purkinje cell dendrite is observed as well as decreased intensity in the immunoreaction. After PtAcacDMS, Purkinje cells display the same intense labelling and dendrite morphology as in controls. At **PD17**, compared with controls, cisPt induces an evident decrease in the labelling of dendrite branches of Purkinje cells, while no changes are visible after PtAcacDMS. Histograms show the OD values and the significance of differences is reported (** $p < 0.01$; *** $p < 0.001$). ml: Molecular layer; igl: Internal granular layer; Pl: Purkinje cell layer. Scale bar: 50 µm.

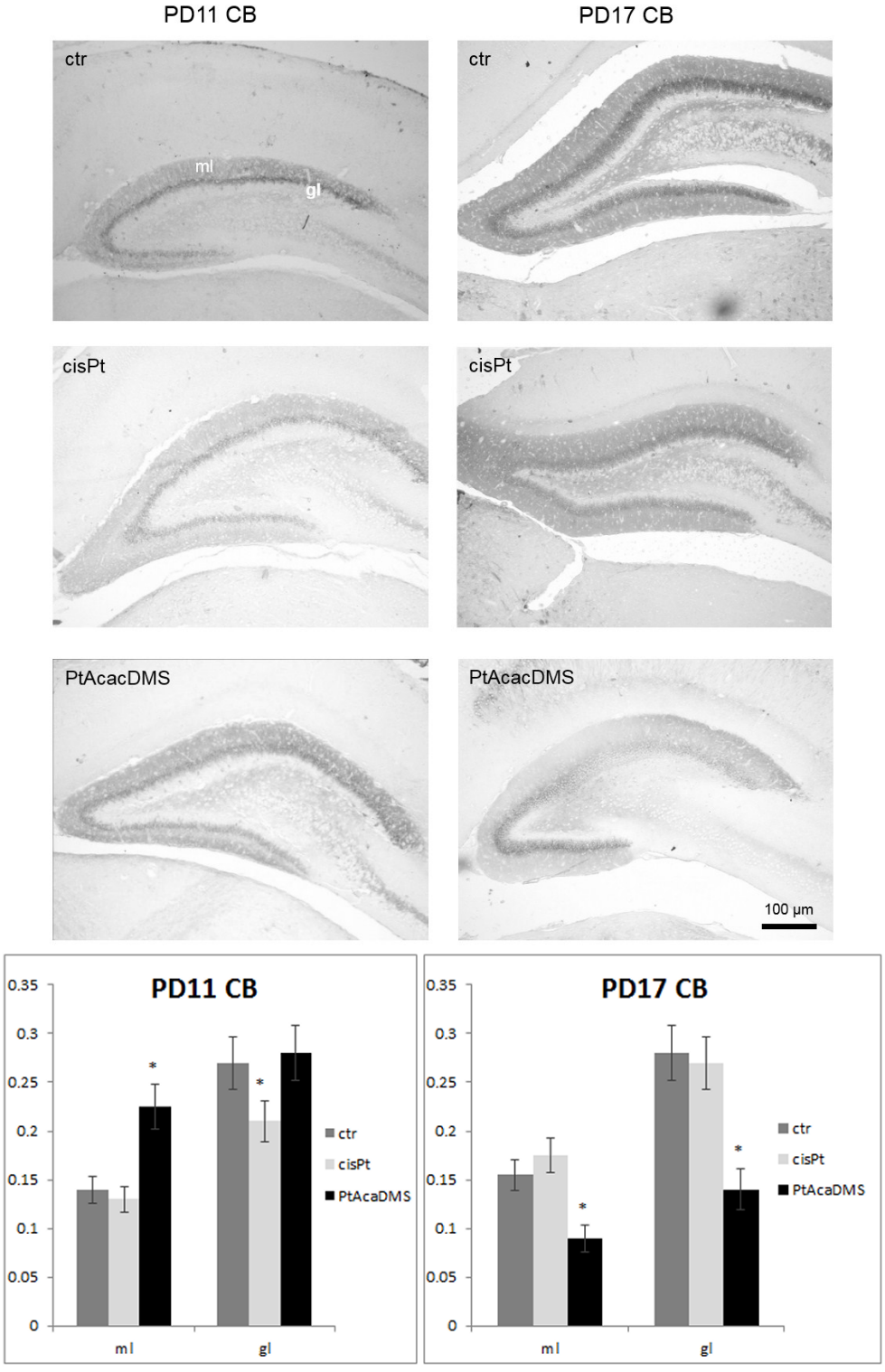

Figure 2. Calbindin immunocytochemistry in the DG granule cell layer. At **PD11**, the intensity of labelling in the DG granule cells decreases after cisPt and increases after PtAcacDMS. At **PD17**, decreased immunolabelling intensity is found after PtAcacDMS and not after cisPt. Histograms show the OD values and the significance of differences is reported (* $p < 0.05$). ml: Molecular layer; gl: Granule cell layer. Scale bar: 100 µm.

3.2.2. Plasma Membrane Calcium ATPase

PMCA is a family of P-type Ca^{2+}-ATPases found in the majority of eukaryotic cells [95]. PMCA is involved in maintaining a low cytosolic calcium concentration critical to neuronal function and survival; specifically, PMCA shows high affinity for calcium and acts by pumping this ion from the cytoplasm to the extracellular space [96].

In mammals, four PMCA isoforms (PMCA1-4) are expressed by four distinct genes, which generate over 20 variants by alternative splicing [95]. These isoforms show distinct activation kinetics and are distributed in a cell-specific manner [95,97]. All the PMCA isoforms are found in the adult brain, but not all of them are expressed at the same time, since they are related to specific cell types and to different maturation cell stages; this pattern of expression allows each neuron to control PMCA activity according to its calcium demands [98]. While little information is available on PMCA1, it is known that this isoform is expressed early in CNS development and is thus likely linked to synaptic maturation [99]. PMCA2 is induced on embryonic day E18 and attains high levels in the adult cerebellum [99,100]. The PMCA3 transcript appears during prenatal life and is generally upregulated in rodents during postnatal development [100]. An opposite profile is shown by PMCA4, *i.e.*, low expression throughout development and high levels in the adult nervous system [101].

PMCA activity is essential to avoid calcium overload that could be lethal to neurons [102], since calcium dysregulation is responsible for excitotoxicity, a process linked with neurodegeneration.

In the cerebellum [71], isoforms of Ca^{2+}-ATPases (SERCAs) with different biophysical properties are detected in endoplasmic reticulum cisterns of Purkinje cells and are involved in the re-uptake of Ca^{2+}, while Ca^{2+} is also extruded via plasma membrane Ca^{2+}-ATPases (PMCAs) [103,104], which are localized in the Purkinje cell plasma membrane [105].

The best isoform that is particularly abundant in cerebellar Purkinje cells is PMCA2 [106–108], which is found in cell bodies and dendrites. While PMCA2 is highly expressed in the whole Purkinje cells, PMCA1 and PMCA3 appear to be restricted to the soma and dendrite branches, respectively, and these distributions are evolving according to cell maturation [109]. Moreover, PMCA1 is ubiquitously expressed from the earliest developmental stages [110].

Since we focused on cerebellum and hippocampus neurons containing CB, and on developing CNS stages, we have chosen a marker expressed by both types of cells, PMCA 1, the isoform labelling the extrusion of calcium from the cell.

In the cerebellum (Figure 3), at PD11 control rats there was strong labelling for PMCA1 on plasma membrane of Purkinje cell soma, while weak positivity was shown inside the cytoplasm. The immunolabelling appeared to be present also on the growing dendrites. Instead, at PD17 there was a marked decrease in positivity in the Purkinje cell soma, whereas there was an increased labelling in the ML, likely due to synaptic contacts on dendrite branches. PMCA1 is one of the synaptic forms of the enzyme and, in fact, is being expressed as synaptic maturation progresses [111]. Our findings confirmed PMCA1 as a marker of immature Purkinje neurons and developing cerebellum [109].

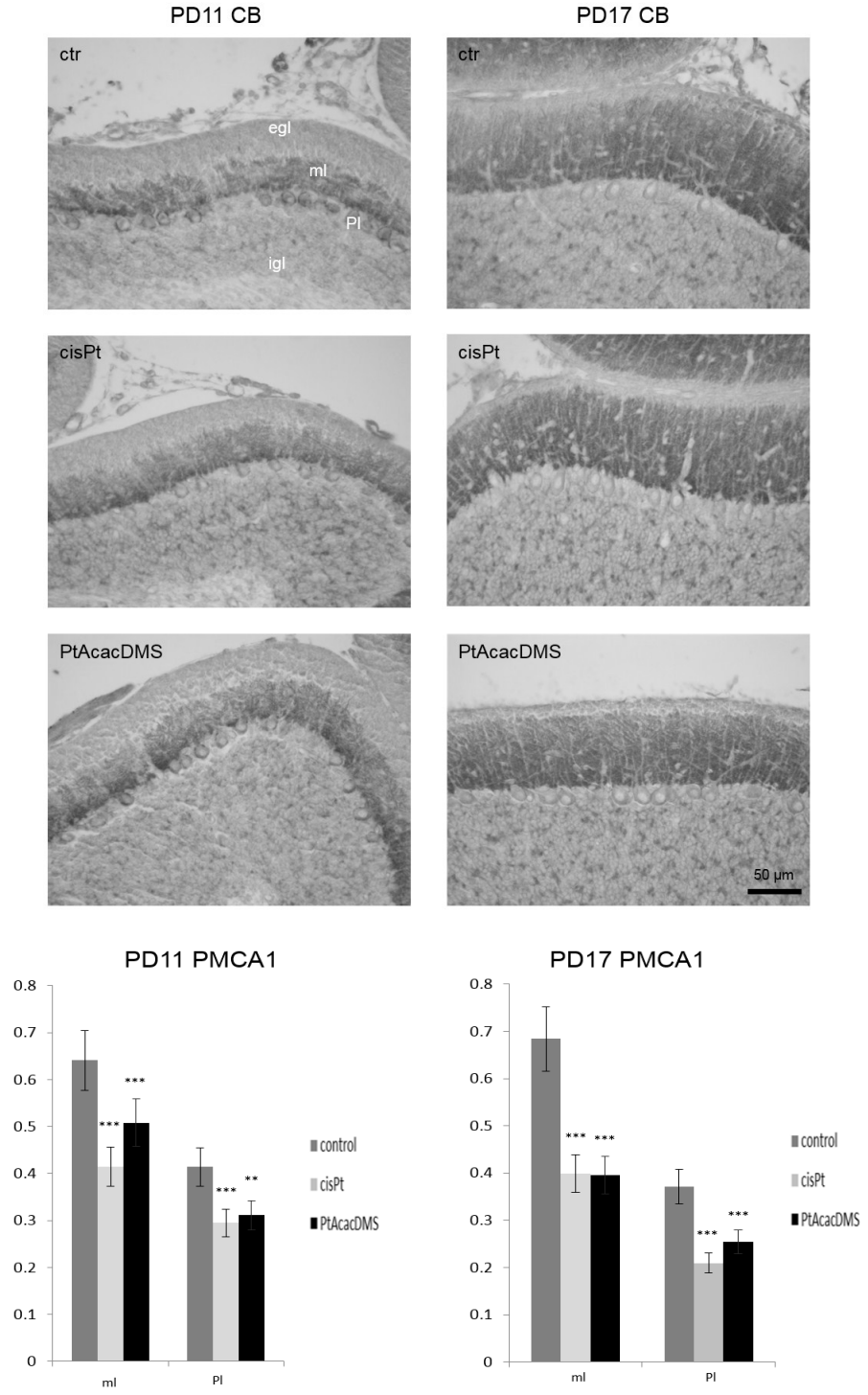

Figure 3. PMCA1 immunocytochemistry in the Purkinje neurons. At **PD11**, control rats (ctr) show intense labelling on the cell membrane of Purkinje cells; the cytoplasm is weakly positive while strong immunoreactivity is present in the molecular layer, in the Purkinje cell dendrite branches. After, cisPt and PtAcacDMS decreased labelling on the cell membrane and in the cytoplasm are observed, as well as in the molecular layer. At **PD17**, controls show a weak immunoreactivity *vs.* PD11; changes are observed after both platinum compounds treatment. Histograms show the OD values and the significance of differences is reported (** $p < 0.01$; *** $p < 0.001$). egl: External granular layer; ml: Molecular layer; igl: Internal granular layer; Pl: Purkinje cell layer. Scale bar: 50 µm

In the hippocampus labelling, PMCA1 was detected in granule and pyramidal cell layers, and reflected the low density typical of plasma membranes in these layers, while intense punctate staining was detected in the neuropil [98,100,112].

Data obtained here indicated the presence of PMCA1 immunolabelling in the DG granule cells and molecular layer (Figure 4), both at PD11 and PD17; no changes in intensity of immunoreactions were detectable in the DG granule cells.

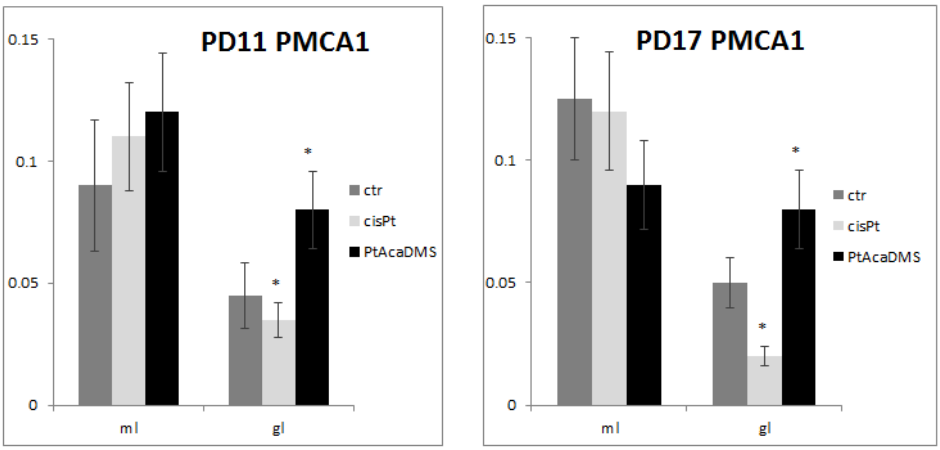

Figure 4. PMCA1 immunocytochemistry in the DG granule cell layer. Histograms show the OD values and the significance of differences is reported (* p<0.05). At **PD11**, the intensity of labelling decreases after cisPt and increases after PtAcacDMS. At **PD17**, decreased immunolabelling intensity is found after cisPt, while increased intensity is present after PtAcacDMS. ml: Molecular layer; gl: Granule layer.

3.3. Platinum Compounds and Calcium Homeostasis in the Immature Neuroarchitecture

Tables 1 and 2 summarize the trend of immunolabelling for CB and PMCA1 in the Purkinje and DG granule cell layers.

In the Purkinje cell layer, the treatment with cisPt caused at PD11 a strongly decreased CB immunoreactivity in the soma and dendrites, which appeared atrophic in several Purkinje neurons (Figure 1; Table 1). PMCA1 on the plasma membranes as well inside the cytoplasm markedly decreased (Figure 3). The decreased immunoreactivity of PMCA1 in the ML was localized in distinct puncta, likely due to synaptic contacts especially on Purkinje dendrite branches.

Table 1. Summary of the trends in the immunocytochemical indicators for CB and PMCA1 in the cerebellar Purkinje neurons with respect to controls following cisPt or PtAcacDMS treatment and the ensuing impact on $[Ca^{2+}]_i$.

Days of treatment	cisPt	PtAcacDMS
PD11	Decreased Ca^{2+} buffering: CB ↓ Decreased Ca^{2+} efflux: PMCA1 ↓	Steady Ca^{2+} buffering: CB = Decreased Ca^{2+} efflux: PMCA1 ↓
PD17	Decreased Ca^{2+} buffering: CB ↓ Decreased Ca^{2+} efflux: PMCA1 ↓	Steady Ca^{2+} buffering: CB = Decreased Ca^{2+} efflux: PMCA1 ↓

Table 2. Summary of the trends in the immunocytochemical indicators for CB and PMCA1 in the DG granule cells with respect to controls following cisPt or PtAcacDMS treatment and the ensuing impact on $[Ca^{2+}]_i$.

Days of treatment	cisPt	PtAcacDMS
PD11	Decreased Ca^{2+} buffering: CB ↓ Decreased Ca^{2+} efflux: PMCA1 ↓	Steady Ca^{2+} buffering: CB = Increased Ca^{2+} efflux: PMCA1 ↑
PD17	Steady Ca^{2+} buffering: CB = Decreased Ca^{2+} efflux: PMCA1 ↓	Decreased Ca^{2+} buffering: CB ↓ Increased Ca^{2+} efflux: PMCA1 ↑

Alteration of calcium homeostasis in the Purkinje neurons was described in mutants [71,72] and under experimental conditions in animal models as well as in human patients having neurological disorders. Notably, loss of CB (and PV) produces an alteration of the spine morphology which may be considered as compensatory mechanism. CB staining decreased in spinocerebellar ataxia and downregulation might cause alterations in the calcium homeostasis finally leading to Purkinje cell death. Moreover, the pivotal role of PMCA2 in the function of the cerebellum is shown by the phenotype of the PMCA2-null mouse and the deafwaddler 2 J, which is a mouse with a spontaneous mutation in the PMCA2 gene, and a consequent null pump activity. Both mice manifested cerebellar pathology consisting in motor deficit and ataxia [113]. In the cerebellum of PMCA2-null mouse, there was a reduction in the levels of mGlur1, which plays several essential roles in processes like motor coordination and associative learning. On the other hand, the dendrite branching of Purkinje cells as revealed by MAP2 immunocytochemistry was similar in wild type and knockout mouse; in addition, alterations in total and non-phosphorylated neurofilament-heavy (NF-H) immunoreactivity were shown [113]. These perturbations suggested altered formation of synaptic contacts, which might contribute to cerebellar dysfunction in absence of PMCA2.

On PD17, the strong loss of CB in the dendrite of Purkinje cells (Figure 1) was accompanied by a lower expression of PMCA1 in the soma (Figure 3). Thus, there was a down regulation of both calcium homeostasis systems.

After cisPt treatment, the early injury of both the systems regulating calcium homeostasis and their persistent imbalance in the most critical phase of Purkinje cell differentiation might alter deeply the growing of dendrite tree and synaptogenesis process. These alterations have been previously shown by the labelling for ionotropic and metabotropic glutamate receptors, and for the GABA enzyme GAD65 [84,85,114]. All these alterations are responsible for degeneration we observed several years ago in 20% of the Purkinje cell population [115].

In DG granule cell layer, the treatment with cisPt caused an early (one day after injection) decrease in CB immunoreactivity (Figure 2; Table 2). The loss of CB immunoreactivity was accompanied by decreased PMCA1 immunoreactivity (Figure 4). The loss and imbalance of calcium efflux and/or calcium buffering might be a possible or concomitant cause of cisPt neurotoxicity during DG postnatal maturation. Alteration of calcium homeostasis occurred in the superficial differentiating layers of DG and was accompanied by degeneration of mitotic granule cells that, on the contrary, are located in the deep granule cell layer [116]. Disturbance of the calcium ATPase pump in the DG persevered at PD17 (Figure 4), while CB immunoreactivity followed by recovery of calcium buffering (Figure 2).

The effects of PtAcacDMS on normal nerve cells differed from those of cisPt (Tables 1 and 2).

At an early stage, at PD11, the intense immunolabelling for CB (Figure 1) showed an almost normal dendrite branching of Purkinje cells. In particular, the reaction intensity was the same as in controls. The expression of PMCA1 (Figure 3) in the soma and on the growing dendrite changed *versus* control rats; the immunoreaction intensity decreased. Later, at PD17, the PMCA1 (Figure 3) immunoreactivity was significantly lowered as compared with control rats, while no significant change in the CB labelling was found (Figure 1).

Therefore, PtAcacDMS treatment did not alter early the efficiency of both calcium homeostasis systems. The presence of the CB calcium buffering protein alone might guarantee the correct differentiation of Purkinje neurons [41,117] and the formation on synaptic contacts on them [118].

At PD11, as in the Purkinje cells CB expression was unchanged in the DG granule cells (Figure 2), which experienced an increase in the PMCA1 immunoreactivity (Figure 4). This indicates efficient calcium efflux from cells. At PD17, the decreased CB concentration and subsequent decreased calcium buffering was balanced by an increase in calcium efflux. Unequivocally, the balance involves a mechanism of calcium homeostasis in the DG.

3.4. Platinum Compounds and Morphological and Molecular Damages in the Immature Cerebellum and Hippocampus

Multiple acute effects of a single injection of cisPt have been demonstrated during the postnatally developing cerebellum. CisPt induced morphological and molecular changes, including the early damage of proliferating and postmitotic differentiating neurons. Apoptotic cell death in the EGL with concomitant alteration of migratory process, atrophy of Purkinje cell dendrite branches and formation of altered synaptic contacts were detected [114]. Our studies on the effects of cisPt on neurotransmitter molecules connected with the brain maturation, showed that neurotransmitters such as GABA, glutamate, and monoamines affected the cisPt-induced changes of developing cerebellum architecture [84,85,115,119], and therefore in the formation of synaptic contacts.

The whole cerebellar cortex presented numerous hemorrhagic foci, mainly seven days after the treatment that was carried out at postnatal day 10. Findings demonstrate that cisPt alters the blood vessels endothelium and could pass the BBB [115].

A recent report [116] has shown that cisPt alters the differentiation and maturation of synaptic contacts of some types of cells and interneurons of the rat hippocampus formation. These evidences help to explain its neurotoxicity on the developing brain.

The investigations on the toxic effects of PtAcacDMS on normal tissues pointed to a reduced neurotoxicity of the new platinum complex. PtAcacDMS induces less serious changes than cisPt on fundamental events in cerebellum and hippocampus development, such as no significant apoptotic events and less injured neuroarchitecture. In particular, the balance between Bcl2/Bax proteins [117] favours the PtAcacDMS treated rats, ensuring normal features in the highly actively proliferating cells in the cerebellum without cell death and cell migration [41]. The Bcl2 family proteins, which play a key role in regulating apoptotic cell death of many cell types [120] showed that after both platinum compounds treatments, Bax (pro-apoptotic protein) expression in Purkinje cells was more intense in respect to the controls. Nevertheless, the labelling for Bcl2 (anti-apoptotic protein) in the same neurons was lowered after cisPt treatment but maintained the steady state after the PtAcacDMS administration

at lower dose and increased in the Purkinje cells at higher dose. Then, PtAcacDMS counterbalanced early the enhanced Bax immunoreactivity maintaining the Bcl2 control steady state, differently from cisPt. The balance might assure a limited cell death/cell degeneration in the Purkinje cell population [117].

The possible neuroprotective role of other specific cellular molecules, such as cellular prion (PrPc), has been studied [121]. After PtAcacDMS treatment, with respect to the controls, changes were detected in PrPc and apoptotic proteins. Instead, Bax immunopositive apoptotic bodies in the EGL were not detectable. The finding indicated that apoptotic cell death of proliferating granule cells is preserved. Co-localization of Bax and PrPc was clearly visible in the Purkinje cells; this may explain better the mechanisms through which PrPc and the apoptotic proteins cooperate. Based on the effects of both platinum compounds on Purkinje cell maturation, it should be emphasized that PrPc, supported by a synergistic action of the anti-apoptotic protein Bcl2, acts as a neuroprotective protein. Therefore, it counters the cytotoxicity in the postnatal critical phases of cerebellum development.

The mild cytotoxic effects of PtAcacDMS on the morphology of normal tissues may be due to the different subcellular targets of this compound. A greater efficiency of cell repair system, in the case of PtAcacDMS, to recognize the drug-target adducts and to repair them, may also be possible.

4. Conclusions

It is known that the favourable advantages and toxic effects of PtAcacDMS on endometrial cancer cells (HeLa) are due to a rapid and sustained apoptotic response characterized by (i) mitochondrial depolarization, (ii) cytosol accumulation of cytochrome c, (iii) translocation from cytosol to mitochondria of some proapototic proteins (the well-known Bax and the truncated form of Bid), (iv) activation of caspase 7 and 9, and v. chromatin condensation and DNA fragmentation [38]. In addition, data by Muscella *et al.* [40] on MCF-7 tumour cell lines showed that PtAcacDMS caused a decrease in the activity of PMCA (not SERCA or SPCA) and membrane permeability to calcium, resulting in the overall $[Ca^{2+}]_i$ increase. The effects of PtAcacDMS were also detectable when cells were stimulated with ATP; the decreased PMCA activity together with the closure of Ca^{2+} channels, opened by purinergic receptor, cause variations in Ca^{2+} level through the alteration of the purinergic system. Moreover, PtAcacDMS caused the activation of PKC-α and also the production of ROS that were involved in the calcium permeability changes and PMCA activity reduction. The overall effect of PtAcacDMS is to increase the $[Ca^{2+}]_i$, and may trigger rapid apoptosis in MCF-7 cells.

PtAcacDMS seemed to affect calcium homeostasis in the normal developing CNS differently than cisPt. Early, one day after treatment, although both platinum compounds affected PMCA activity, cisPt also actedon the CB buffering system. Instead, PtAcacDMS did not significantly affect the protein. Later, at seven days after treatment, the main difference between the two types of neurons is that, *in vivo*, the PMCA extruding calcium increased more in the DG granule cells in comparison with cisPt. Nevertheless, the Purkinje neurons conserve the capacity to cope with the calcium increase possibly induced by PtAcacDMS, although the calcium pump was lower in respect to controls. An intriguing hypothesis might be linked to multiple events having a role in the postnatal development of cerebellum and maturation of Purkinje neurons. All these events might be involved in the plasticity and recovery of cerebellar neuroarchitecture and function [84,85].

In conclusion, to cope with the excessive $[Ca^{2+}]_i$ which may injure neuron function and morphology, an efficient, rapidly-acting calcium buffering system or calcium pump shortly after treatment is essential.

Specifically, we have also demonstrated that the calcium pump may have an essential and a compensatory role when the buffering proteins are irrecoverable. At present, the evidence indicates the latter to be a possible mechanism to avoid calcium accumulation in nerve cells and thus prevent cell degeneration and death. The present study indeed emphasizes the need for further *in vivo* studies on the involvement of calcium homeostasis in the action of the platinum compounds. A deeper investigation on the different responses of cancer cells *versus* normal cells to platinum drugs is also required for a better understanding of their mechanisms of action.

Acknowledgments

These researches were supported by grants from "Fondi di Ateneo per la Ricerca" (FAR, University of Pavia), "Fondazione Banca del Monte di Lombardia" (Italy) and "Programmi di Ricerca di Rilevante Interesse Nazionale" (PRIN, 2009ZFPSPW).

Author Contributions

Graziella Bernocchi and Maria Grazia Bottone conceived and designed the experiments; Valeria M. Piccolini and Violetta Insolia performed the experiments; Violetta Insolia and Caterina Gasperini analyzed the data; Graziella Bernocchi, Maria Grazia Bottone, Francesco P. Fanizzi, Sandra A. De Pascali contributed reagents/materials/analysis tools; Graziella Bernocchi wrote the paper.

Conflicts of Interest

The authors declare no conflict of interest.

References

1. Screnci, D.; McKeage, M.J. Platinum neurotoxicity: Clinical profiles, experimental models and neuroprotective approaches. *J. Inorg. Biochem.* **1999**, *77*, 105–110.
2. Siddik, Z.H. Cisplatin: Mode of cytotoxic action and molecular basis of resistance. *Oncogene* **2003**, *22*, 7265–7279.
3. Rabik, C.A.; Dolan, M.E. Molecular mechanisms of resistance and toxicity associated with platinating agents. *Cancer Treat. Rev.* **2007**, *33*, 9–23.
4. Florea, A.M.; Büsselberg, D. Cisplatin as an anti-tumor drug: Cellular mechanisms of activity, drug resistance and induced side effects. *Cancers* **2011**, *3*, 1351–1371.
5. Sancho-Martinez, S.M.; Prieto-Garcia, L.; Prieto, M.; Lopez-Novoa, J.M.; Lopez Hernandez, F.J. Subcellular targets of cisplatin cytotoxicity: An integrated view. *Pharmacol. Ther*. **2012**, *136*, 35–55.
6. Jaggi, A.S.; Singh, N. Mechanisms in cancer-chemotherapeutic drugs-induced peripheral neuropathy. *Toxicology* **2012**, *291*, 1–9.
7. Chou, A.J.; Gorlick, R. Chemotherapy resistance in osteosarcoma: Current challenges and future directions. *Exp. Rev. Anticancer Ther.* **2006**, *6*, 1075–1085.
8. Gottesman, M.M. Mechanisms of cancer drug resistance. *Ann. Rev. Med.* **2002**, *53*, 615–627.

9. Ricci, G.; de Maria, F.; Antonini, G.; Turella, P.; Bullo, A.; Stella, L.; Filomeni, G.; Federici, G.; Caccuri, A.M. 7-nitro-2,1,3-benzoxadiazole derivatives, a new class of suicide inhibitors for glutathione S-transferases: Mechanism of action of potential anticancer drugs. *J. Biol. Chem.* **2005**, *280*, 26397–26405.
10. Pasetto, L.M.; D'Andrea, M.R.; Brandes, A.A.; Rossi, E.; Monfardini, S. The development of platinum compounds and their possible combination. *Crit. Rev. Oncol. Hematol.* **2006**, *60*, 59–75.
11. Cavaletti, G.; Mormiroli, P. Chemotherapy-induced peripheral neurotoxicity. *Nat. Rev*. **2010**, *6*, 657–665.
12. Argyriou, A.A.; Kyritsis, A.P.; Makatsoris, T.; Kalofonus, H.P. Chemotherapy-induced peripheral neuropathy in adults: A comprehensive update of the literature. *Cancer Manag. Res*. **2014**, *6*, 135–147.
13. Myers, J.S. Chemotherapy-related cognitive impairment: The breast cancer experience. *Oncol. Nurs. Forum* **2012**, *39*, E31–E40.
14. Hodgson, K.D.; Hutchinson, A.D.; Wilson, A.D.; Nettelbeck, T. A meta-analysis of the effects of chemotherapy on cognition in patients with cancer. *Cancer Treat. Rev.* **2013**, *39*, 297–304.
15. Seigers, R.; Fardell, J.E. Neurobiological basis of chemotherapy-induced cognitive impairment: A review of rodent research. *Neurosci. Biobehav. Rev.* **2011**, *35*, 729–741.
16. Sul, J.K.; de Angelis, L.M. Neurologic complications of cancer chemotherapy. *Semin. Oncol.* **2006**, *33*, 324–332.
17. Sterzing, F.; Grehn, F.; Dinkel, G.; Krempien, R.; Hartung, G.; Debus, J.; Harms, W. Severe reversible toxic encephalopathy induced by cisplatin in a patient with cervical carcinoma receiving combined radiochemotherapy. *Strahlenther. Onkol.* **2007**, *183*, 487–489.
18. Namikawa, K.; Asakura, M.; Minami, T.; Okazaki, Y.; Kadota, E.; Hashimoto, S. Toxicity of cisplatin to the central nervous system of male rabbits. *Biol. Trace Elem. Res.* **2000**, *74*, 223–225.
19. Abou-Elghait, A.; El-Gamal, D.A.; Abdel-Sameea, A.R.; Mohamed, A.A. Effect of cisplatin on the cerebellar cortex and spinal cord of adult male albino rat and the possible role of vitamin E: Light and electron microscopic study. *Egypt. J. Histol.* **2010**, *33*, 202–212.
20. Gong, X.; Schwartz, P.H.; Linskey, M.E.; Bota, D.A. Neural stem/progenitors and glioma stem-like cells have differential sensitivity to chemotherapy. *Neurology* **2011**, *76*, 1126–1134.
21. Andres, A.L.; Gong, X.; Di, K.; Bota, D.A. Low-doses of cisplatin injure hippocampal synapses: A mechanism for "chemo" brain. *Exp. Neurol.* **2014**, *255*, 137–144.
22. Prestayko, A.W.; D'Aoust, J.C.; Issell, B.F.; Crooke, S.T. Cisplatin (cis diamine-dichloroplatinum II). *Cancer Treat. Rev*. **1979**, *6*, 17–35.
23. Gilchrist, L.S.; Marais, L.; Tanner, L. Comparison of two chemotherapy-induced peripheral neuropathy measurement approaches in children. *Support Care Cancer* **2014**, *22*, 359–366.
24. Sioka, C.; Kyritsis, A. Central and peripheral nervous system toxicity of common chemotherapeutic agents. *Cancer Chemother. Pharmacol*. **2009**, *63*, 761–767.
25. Rodier, P.M. Chronology of neuron development: Animal studies and their clinical implications. *Dev. Med. Child Neurol.* **1980**, *22*, 525–545.
26. Rodier, P.M. Developing brain as a target of toxicity. *Environ. Health Perspect.* **1995**, *103*, 73–76.
27. Rodier, P.M. Environmental causes of Central Nervous System maldevelopment. *Pediatrics* **2004**, *113*, 1076–1083.

28. Ferguson, S.A. Neuroanatomical and functional alterations resulting from early postnatal cerebellar insults in rodents. *Pharmacol. Biochem. Behav.* **1996**, *55*, 663–671.
29. Fujii, T. Transgenerational effects of maternal exposure to chemicals on the functional development of the brain in the offspring. *Cancer Causes Control* **1997**, *8*, 524–528.
30. Fonnum, F.; Lock, E.A. Cerebellum as a target for toxic substances. *Toxicol. Lett.* **2000**, *112–113*, 9–16.
31. Roberts, J.J.; Pera, J.J., Jr. *Platinum, Gold, and other Metal Chemotherapeutic Agents*: *Chemistry and Biochemistry*; Lippard, S.J., Ed.; American Chemical Society: Washington, DC, USA, 1983; pp. 2–25.
32. Cepeda, V.; Fuertes, M.A.; Castilla, J.; Alonso, C.; Quevedo, C.; Pérez, J.M. Biochemical mechanisms of cisplatin cytotoxicity. *Anticancer Agents Med. Chem*. **2007**, *7*, 3–18.
33. Ormerod, M.G.; O'Neill, C.; Robertson, D.; Kelland, L.R.; Harrap, K.R. cisDiammine dichloroplatinum(II)-induced cell death through apoptosis in sensitive and resistant human ovarian carcinoma cell lines. *Cancer Chemother. Pharmacol.* **1996**, *37*, 463–471.
34. Henkels, K.M.; Turchi, J.J. Induction of apoptosis in cisplatin-sensitive and -resistant human ovarian cancer cell lines. *Cancer Res.* **1997**, *57*, 4488–4492.
35. De Pascali, S.A.; Papadia, P.; Ciccarese, A.; Pacifico, C.; Fanizzi, F.P. First examples of βdiketonate platinum II complexes with sulfoxide ligands. *Eur. J. Inorg. Chem.* **2005**, *5*, 788–796.
36. De Pascali, S.A.; Papadia, P.; Capoccia, S.; Marchiò, L.; Lanfranchi, M.; Ciccarese, A.; Fanizzi F.P. Hard/soft selectivity in ligand substitution reactions of β-diketonate platinum(II) complexes. *Dalton Trans.* **2009**, *37*, 7786–7795.
37. Muscella, A.; Calabriso, N.; de Pascali, S.A.; Urso, L.; Ciccarese, A.; Fanizzi, F.P.; Migoni, D.; Marsigliante, S. New platinum(II) complexes containing both an *O*,*O*′-chelated acetylacetonate ligand and a sulfur ligand in the platinum coordination sphere induce apoptosis in HeLa cervical carcinoma cells. *Biochem. Pharmacol.* **2007**, *74*, 28–40.
38. Muscella, A.; Calabriso, N.; Fanizzi, F.P.; de Pascali, S.A.; Urso, L.; Ciccarese, A.; Migoni, D.; Marsigliante, [Pt(*O*,*O*′-acac)(γ-acac)(DMS)], a new Pt compound exerting fast cytotoxicity in MCF-7 breast cancer cells via the mitochondrial apoptotic pathway. *Br. J. Pharmacol*. **2008**, *153*, 34–49.
39. De Pascali, S.A.; Lugoli, F.; de Donno, A.; Fanizzi, F.P. Mutagenic tests confirm that new acetylacetonate Pt(II) complexes induce apoptosis in cancer cells interacting with nongenomic biological targets. *Met. Based Drugs.* **2011**, *2011*, 763436.
40. Muscella, A.; Calabriso, N.; Vetrugno, C.; Fanizzi, F.P.; de Pascali, S.A.; Storelli, C.; Marsigliante, S. The platinum (II) complex [Pt(*O*,*O*′-acac)(gamma-acac)(DMS)] alters the intracellular calcium homeostasis in MCF-7 breast cancer cells. *Biochem. Pharmacol.* **2011**, *81*, 91–103.
41. Cerri, S.; Piccolini V.M.; Santin, G.; Bottone, M.G.; de Pascali, S.A.; Migoni, D.; Iadarola, P.; Fanizzi, F.P.; Bernocchi, G. The developmental neurotoxicity study of platinum compounds: Effects of cisplatin *versus* a novel Pt(II) complex on rat cerebellum. *Neurotoxicol. Teratol.* **2011**, *33*, 273–281.
42. Florea, A.M.; Büsselberg, D. Anti-cancer drugs interfere with intracellular calcium signaling. *Neurotoxicology* **2009**, *30*, 803–810.
43. Arain, M.; Haque, M.; Johal, L.; Mathur, P.; Nel, W.; Rais, A.; Sandhu, R.; Sharma, S. Maturation of the adolescent brain. *Neuropsychiatr. Dis. Treat.* **2013**, *9*, 449–461.

44. Altman, J.; Bayer, S.A. *Development of the Cerebellar System in Relation to its Evolution, Structure, and Functions*; CRC Press: Boca Raton, FL, USA, 1997.
45. Hashimoto, M.; Hibi, M. Development and evolution of cerebellar neural circuits. *Dev. Growth Differ.* **2012**, *54*, 373–389.
46. Danglot, L.; Triller, A.; Marty, S. The development of hippocampal interneurons in rodents. *Hippocampus* **2006**, *16*, 1032–1060.
47. Kempermann, G. *Adult Neurogenesis*; Oxford University Press: Oxford, UK, 2006.
48. Piccolini, V.M.; Bottone, M.G.; Bottiroli, G.; de Pascali, S.A.; Fanizzi, F.P.; Bernocchi, G. Platinum drugs and neurotoxicity: Effects on intracellular calcium homeostasis. *Cell Biol. Toxicol.* **2013**, *29*, 339–353.
49. Biran, V.; Verney, C.; Ferriero, D.M. Perinatal cerebellar injury in human and animal models. *Neurol. Res. Int.* **2012**, *2012*, 858929.
50. Villanueva, R. The cerebellum and neuropsychiatric disorders. *Psychiatry Res.* **2012**, *198*, 527–532.
51. Bayer, S.A. Development of the hippocampal region in the rat II. Morphogenesis during embryonic and early postnatal life. *J. Comp. Neurol.* **1980**, *190*, 115–134.
52. Altman, J. Morphological development of the rat cerebellum and some of its mechanisms. In *The Cerebellum-New Vistas*; Palay, S.L., Chan-Palay, V., Eds.; Springer: Berlin, Germany, 1982; pp. 8–49.
53. Altman, J.; Bayer, A.S. Migration and distribution of two populations of hippocampal granule cell precursors during the perinatal and postnatal periods. *J. Comp. Neurol.* **1990**, *301*, 365–381.
54. Lossi, L.; Cantile, C.; Tamagno, I.; Merighi, A. Apoptosis in the mammalian CNS: Lessons from animal models. *Vet. J.* **2005**, *170*, 52–66.
55. Lossi, L.; Castagna, C.; Merighi, A. Neuronal cell death: An overview of its different forms in central and peripheral neurons. *Methods Mol. Biol.* **2015**, *1254*, 1–18.
56. Zhang, L.; Goldman, J.E. Generation of cerebellar interneurons from dividing progenitors in white matter. *Neuron* **1996**, *16*, 47–54.
57. Sudarov, A.; Joyner, A.L. Cerebellum morphogenesis: The foliation pattern is orchestrated by multi-cellular anchoring centers. *Neural Dev.* **2007**, *2*, 26.
58. Cerri, S.; Piccolini, V.M.; Bernocchi, G. Postnatal development of the central nervous system: Anomalies in the formation of cerebellum fissures. *Anat. Rec.* **2010**, *293*, 492–501.
59. Freund, T.F.; Buszaki, G. Interneurons of the hippocampus. *Hippocampus* **1996**, *6*, 347–470.
60. Ito, M. Cerebellar circuitry as a neuronal machine. *Prog. Neurobiol.* **2006**, *78*, 272–303.
61. Dietrich, J.; Han, R.; Yang, Y.; Mayer-Pröschel, M.; Noble, M. CNS progenitor cells and oligodendrocytes are targets of chemotherapeutic agents *in vitro* and *in vivo*. *J. Biol.* **2006**, *5*, 22.
62. Mattson, M.P. Calcium and neurodegeneration. *Aging Cell* **2007**, *6*, 337–350.
63. Lohmann, C. Calcium signaling and the development of specific neuronal connections. *Prog. Brain Res.* **2009**, *75*, 443–452.
64. Komuro, H.; Kumada, T. Ca^{2+} transients control CNS neuronal migration. *Cell Calcium* **2005**, *37*, 387–393.
65. Gonzalez, V.M.; Fuertes, M.A.; Alonso, C.; Perez, J.M. Is cisplatin-induced cell death always produced by apoptosis? *Mol. Pharmacol.* **2001**, *59*, 657–663.

66. Kawai, Y.; Nakao, T.; Kunimura, N.; Kohda, Y.; Gemba, M. Relationship of intracellular calcium and oxygen radicals to cisplatin-related renal cell injury. *J. Pharmacol. Sci.* **2006**, *100*, 65–72.
67. Liang, X.; Huang, Y. Intracellular free calcium concentration and cisplatin resistance in human lung adenocarcinoma A549 cells. *Biosci. Rep.* **2000**, *20*, 129–138.
68. Splettstoesser, F.; Florea, A.M.; Büsselberg, D. IP(3) receptor antagonist, 2-APB, attenuates cisplatin induced Ca^{2+}-influx in HeLa-S3 cells and prevents activation of calpain and induction of apoptosis. *Br. J. Pharmacol.* **2007**, *151*, 1176–1186.
69. Florea, A.M.; Büsselberg, D. Occurrence, use and potential toxic effects of metals and metal compounds. *Biometals* **2006**, *19*, 419–427.
70. Persechini, A.; Moncrief, N.D.; Kretsinger, R.H. The EF-hand family of calcium-modulated proteins. *Trends Neurosci.* **1989**, *12*, 462–467.
71. Schwaller, B.; Meyer, M.; Schiffmann, S. "New" functions for "old" proteins: The role of the calcium binding proteins calbindin D-28k, calretinin and parvalbumin, in cerebellar physiology. Studies with knockout mice. *Cerebellum* **2002**, *1*, 241–258.
72. Bastianelli, E. Distribution of calcium-binding proteins in the cerebellum. *Cerebellum* **2003**, *2*, 242–262.
73. Jinno, S.; Kosaka, T. Cellular architecture of the mouse hippocampus: A quantitative aspect of chemically defined GABAergic neurons with stereology. *Neurosci. Res.* **2006**, *56*, 229–245.
74. Baimbridge, K.G.; Celio, M.R.; Rogers, J.H. Calcium-binding proteins in the nervous system. *Trends Neurosci.* **1992**, *15*, 303–308.
75. Celio. M.R. Calbindin D-28k and parvalbumin in the rat nervous system. *Neuroscience* **1990**, *35*, 375–475.
76. Celio, M.; Pauls, T.; Schwaller, B. (Eds.) *Guidebook to the Calcium Binding Proteins*; Oxford University Press: Oxford, UK, 1996.
77. Garcia-Segura, L.M.; Baetens, D.; Roth, J.; Norman, A.W.; Orci, L. Immunohistochemical mapping of calcium-binding protein immunoreactivity in the rat central nervous system. *Brain Res*. **1984**, *296*, 75–86.
78. Ulfig, N.; Chan, W.Y. Differential expression of calcium-binding proteins in the red nucleus of the developing and adult human brain. *Anat. Embryol.* **2001**, *203*, 95–108.
79. Nagerl, U.V.; Mody, I.; Jeub, M.; Lie, A.A.; Elger, C.E.; Beck, H. Surviving granule cells of the sclerotic human hippocampus have reduced Ca^{2+} influx because of a loss of calbindin-D(28k) in temporal lobe epilepsy. *J. Neurosci.* **2000**, *20*, 1831–1836.
80. Maskey, D.; Pradhan, J.; Aryal, B.; Lee, C.M.; Choi, I.Y.; Park, K.S.; Kim, S.B.; Kim, H.G.; Kim, M.J. Chronic 835-MHz radiofrequency exposure to mice hippocampus alters the distribution of calbindin and GFAP immunoreactivity. *Brain Res.* **2010**, *1346*, 237–246.
81. Enderlin, S.; Norman, A.W.; Celio, M.R. Ontogeny of the calcium binding protein calbindin D-28k in the rat nervous system. *Anat. Embryol.* **1987**, *177*, 15–28.
82. Hogan, D.; Berman, N.E. Transient expression of calbindin-D28k immunoreactivity in layer V pyramidal neurons during postnatal development of kitten cortical areas. *Brain Res. Dev. Brain Res*. **1993**, *74*, 177–192.
83. Friauf, E. Distribution of calcium-binding protein calbindin-D28k in the auditory system of adult and developing rats. *J. Comp. Neurol.* **1994**, *349*, 193–211.

84. Pisu, M.B.; Roda, E.; Avella, D.; Bernocchi, G. Developmental plasticity of rat cerebellar cortex after cisplatin injury: Inhibitory synapses and differentiating Purkinje neurons. *Neuroscience* **2004**, *129*, 655–664.
85. Avella, D.; Pisu, M.B.; Roda, E.; Gravati, M.; Bernocchi, G. Reorganization of the rat cerebellar cortex during postnatal development following cisplatin treatment. *Exp. Neurol.* **2006**, *201*, 131–143.
86. Keuker, J.I.; Rochford, C.D.; Witter, M.P.; Fuchs, E. A cytoarchitectonic study of the hippocampal formation of the tree shrew (*Tupaia belangeri*). *J. Chem. Neuroanat.* **2003**, *26*, 1–15.
87. Magloczky, Z.; Freund, T.F. Selective neuronal death in the contralateral hippocampus following unilateral kainate injections into the CA3 subfield. *Neuroscience* **1993**, *56*, 317–335.
88. Ciaroni, S.; Cecchini, T.; Ferri, P.; Cuppini, R.; Ambrogini, P.; Santi, S.; Benedetti, S.; del Grande, P.; Papa, S. Neural precursor proliferation and newborn cell survival in the adult rat dentate gyrus are affected by vitamin E deficiency. *Neurosci. Res.* **2002**, *44*, 369–377.
89. Brandt, M.D.; Jessberger, S.; Steiner, B.; Kronenberg, G.; Reuter, K.; Bick-Sander, A.; von der Behrens, W.; Kempermann, G. Transient calretinin expression defines early postmitotic step of neuronal differentiation in adult hippocampal neurogenesis of mice. *Mol. Cell. Neurosci.* **2003**, *24*, 603–613.
90. Soriano, E.; del Rio, J.A.; Martinez, A.; Super, H. Organization of the embryonic and early postnatal murine hippocampus. I. Immunocytochemical characterization of neuronal populations in the subplate and marginal zone. *J. Comp. Neurol.* **1994**, *342*, 571–595.
91. Abraham, H.; Veszpremi, B.; Kravjak, A.; Kovacs, K.; Gomori, E.; Seress, L. Ontogeny of calbindin immunoreactivity in the human hippocampal formation with a special emphasis on granule cells of the dentate gyrus. *Int. J. Dev. Neurosci.* **2009**, *27*, 115–127.
92. Braun, K. Calcium-binding proteins in avian and mammalian central nervous system: Localization, development and possible functions. *Prog. Histochem. Cytochem.* **1990**, *21*, 1–64.
93. Blatow, M.; Caputi, A.; Burnashev, N.; Monyer, H.; Rozov, A. Ca^{2+} buffer saturation underlies paired pulse facilitation in calbindin-D28k-containing terminals. *Neuron* **2003**, *38*, 79–88.
94. Arabadzisz, D.; Ylinen, A.; Emri, Z. Increased inter-spike intervals and fast after-hyperpolarization of action potentials in rat hippocampal pyramidal cells accompanied with altered calbindin immunoreactivity 10–12 months after global forebrain ischemia. *Neurosci. Lett.* **2002**, *331*, 103–106.
95. Strehler, E.E.; Zacharias, D.A. Role of alternative splicing in generating isoform diversity among plasma membrane calcium pumps. *Physiol. Rev.* **2001**, *81*, 21–50.
96. Carafoli, E.; Brini, M. Calcium pumps: Structural basis for and mechanism of calcium transmembrane transport. *Curr. Opin. Chem. Biol.* **2000**, *4*, 152–161.
97. Burette, A.; Rockwood, J.M.; Strehler, E.E.; Weinberg, R.J. Isoform-specific distribution of the plasma membrane Ca^{2+} ATPase in the rat brain. *J. Comp. Neurol.* **2003**, *467*, 464–476.
98. Kenyon, K.A.; Bushong, E.A.; Mauer, A.S.; Strehler, E.E.; Weinberg, R.J.; Burette, A.C. Cellular and subcellular localization of the neuron-specific plasma membrane calcium ATPase PMCA1a in the rat brain. *J. Comp. Neurol.* **2010**, *518*, 3169–3183.
99. Mata, A.M.; Sepulveda, M.R. Plasma membrane Ca-ATPases in the nervous system during development and ageing. *World J. Biol. Chem.* **2010**, *1*, 229–234.
100. Marcos, D.; Sepulveda, M.R.; Berrocal, M.; Mata, A.M. Ontogeny of ATP hydrolysis and isoform expression of the plasma membrane Ca^{2+}-ATPase in mouse brain. *BMC Neurosci.* **2009**, *10*, 112.

101. Zacharias, D.A.; DeMarco, S.J.; Strehler, E.E. mRNA expression of the four isoforms of the human plasma membrane Ca^{2+}-ATPase in the human hippocampus. *Brain Res. Mol. Brain Res.* **1997**, *45*, 173–176.
102. Berliocchi L.; Bano, D.; Nicotera, P. Ca^{2+} signals and death programmes in neurons. *Philos. Trans. R. Soc. Lond. B Biol. Sci.* **2005**, *360*, 2255–2258.
103. Garcia, M.L.; Strehler, E.E. Plasma membrane calcium ATPases as critical regulators of calcium homeostasis during neuronal cell function. *Front. Biosci.* **1999**, *4*, D869–D882.
104. Shull, G.E. Gene knockout studies of Ca^{2+}-transporting ATPases. *Eur. J. Biochem.* **2000**, *267*, 5284–5290.
105. De Talamoni, N.; Smith, C.A.; Wasserman, R.H.; Beltramino, C.; Fullmer, C.S.; Penniston, J.T. Immunocytochemical localization of the plasma membrane calcium pump, calbindin-D28k, and parvalbumin in Purkinje cells of avian and mammalian cerebellum. *Proc. Natl. Acad. Sci. USA* **1993**, *90*, 11949–11953.
106. Stahl, W.L.; Eakin, T.J.; Owens, J.W., Jr.; Breininger, J.F.; Filuk, P.E.; Anderson, W.R. Plasma membrane Ca(2+)-ATPase isoforms: Distribution of mRNAs in rat brain by *in situ* hydridization. *Brain Res. Mol. Brain Res.* **1992**, *16*, 223–231.
107. Stauffer, T.P.; Guerini, D.; Celio, M.R.; Carafoli, E. Immunolocalization of the plasma membrane Ca^{2+} pump isoforms in the rat brain. *Brain Res.* **1997**, *748*, 21–29.
108. Burette, A.; Weinberg, R.J. Perisynaptic organization of plasma membrane calcium pumps in cerebellar cortex. *J. Comp. Neurol.* **2007**, *500*, 1127–1135.
109. Sepulveda, M.R.; Hidalgo-Sanchez, M.; Marcos, D.; Mata, A.M. Developmental distribution of plasma membrane Ca^{2+}-ATPase isoforms in chick cerebellum. *Dev. Dyn.* **2007**, *236*, 1227–1236.
110. Zacharias, D.A.; Kappen, C. Developmental expression of the four plasma membrane calcium ATPase (Pmca) genes in the mouse. *Biochim. Biophys. Acta* **1999**, *1428*, 397–405.
111. Filoteo, A.G.; Elwess, N.L.; Enyedi, A.; Caride, A.; Aung, H.H.; Penniston, J.T. Plasma membrane Ca^{2+} pump in rat brain. Patterns of alternative splices seen by isoform-specific antibodies. *J. Biol. Chem.* **1997**, *272*, 23741–23747.
112. Kip, S.N.; Gray, N.W.; Burette, A.; Canbay, A.; Weinberg, R.J.; Strehler, E.E. Changes in the expression of plasma membrane calcium extrusion systems during maturation of hippocampal neurons. *Hippocampus* **2006**, *20*, 129–138.
113. Kurnellas, M.P.; Lee, A.K.; Li, H.; Deng, L.; Ehrlich, D.J.; Elkabes, S. Molecular alterations in the cerebellum of the plasma membrane calcium ATPase 2 (PMCA2)-null mouse indicate abnormalities in Purkinje neurons. *Mol. Cell. Neurosci.* **2007** *34*, 178–188.
114. Pisu, M.B.; Roda, E.; Guioli, S.; Avella, D.; Bottone, M.G.; Bernocchi, G. Proliferation and migration of granule cells in the developing rat cerebellum: Cisplatin effects. *Anat. Rec. A Discov. Mol. Cell. Evol. Biol.* **2005**, *287*, 1226–1235.
115. Scherini, E.; Bernocchi, G. CisDDP treatment and development of the rat cerebellum. *Prog. Neurobiol.* **1994**, *42*, 161–196.
116. Piccolini, V.M.; Cerri, S.; Romanelli, E.; Bernocchi, G. Interactions of neurotransmitter systems during postnatal development of the rat hippocampal formation: Effects of cisplatin. *Exp. Neurol.* **2012**, *234*, 239–252.

117. Bernocchi, G.; Bottone, M.G.; Piccolini, V.M.; Dal Bo, V.; Santin, G.; de Pascali, S.A.; Migoni, D.; Fanizzi, F.P. Developing central nervous system and vulnerability to platinum compounds. *Chemother. Res. Pract*. **2011**, *2011*, 315418.
118. Piccolini, V.M.; Esposito, A.; Dal Bo, V.; Insolia, V.; Bottone, M.G.; de Pascali, S.A.; Fanizzi, F.P.; Bernocchi, G. Cerebellum neurotransmission during postnatal development: [Pt(*O*,*O*′-acac)(γ-acac)(DMS)] *vs.* cisplatin and neurotoxicity. *Int. J. Dev. Neurosci.* **2015**, *40*, 24–34.
119. Roda, E.; Avella, D.; Pisu, M.B.; Bernocchi, G. Monoamine receptors and immature cerebellum cytoarchitecture after cisplatin injury. *J. Chem. Neuroanat.* **2007**, *33*, 42–52.
120. Vogel, M.W. Cell death, Bcl-2, Bax, and the cerebellum. *Cerebellum* **2002**, *1*, 277–287.
121. Bottone, M.G.; Dal Bo, V.; Piccolini V.M.; Bottiroli, G.; de Pascali, S.A.; Fanizzi, F.P.; Bernocchi, G. Developmental expression of cellular prion protein and apoptotic molecules in the rat cerebellum: Effects of platinum compounds. *J. Chem. Neuroanat.* **2012**, *46*, 19–29.

Int. J. Devl Neuroscience 40 (2015) 24–34

Contents lists available at ScienceDirect

International Journal of Developmental Neuroscience

journal homepage: www.elsevier.com/locate/ijdevneu

Cerebellum neurotransmission during postnatal development: [Pt(*O*,*O*′-acac)(γ-acac)(DMS)] vs cisplatin and neurotoxicity☆

Valeria Maria Piccolini[a,b], Alessandra Esposito[a], Veronica Dal Bo[a], Violetta Insolia[a], Maria Grazia Bottone[a,b], Sandra Angelica De Pascali[c], Francesco Paolo Fanizzi[c], Graziella Bernocchi[a,*]

[a] *Dipartimento di Biologia e Biotecnologie "L. Spallanzani" Università di Pavia, via Ferrata 9, 27100 Pavia, Italy*
[b] *Istituto di Genetica Molecolare del CNR, Sezione di Istochimica e Citometria, via Ferrata 9, 27100 Pavia, Italy*
[c] *Dipartimento di Scienze e Tecnologie Biologiche ed Ambientali, Università del Salento, 73100 Lecce, Italy*

ARTICLE INFO

Article history:
Received 31 July 2014
Received in revised form 20 October 2014
Accepted 20 October 2014
Available online 13 November 2014

Keywords:
Rat developing cerebellum
Glutamate
GABA
Platinum compounds

ABSTRACT

Several chemotherapeutic drugs are known to cause neurotoxicity. Platinum-based agents in use or in clinical trials display neurotoxic potential accompanied by neurological complications; recent studies have identified a large number of behavioural issues in paediatric oncology patients.

To understand the toxicity of platinum drugs at the molecular and cellular levels, this study compares the possible cytotoxic effects of an older platinum compound, cisplatin and a new platinum compound, [Pt(*O*,*O*′-acac)(γ-acac)(DMS)], on the CNS of postnatally developing rats, which is much more vulnerable to injury than the CNS of adult rats. Since several drugs interact with neurotransmitters during neuronal maturation, we performed immunostainings with antibodies raised against markers of glutamate and GABA, the major neurotransmitters in the cerebellum. After a single injection of cisplatin at postnatal day 10 (PD10), the labelling of Purkinje cells with the neurotransmitter markers evidenced alterations between PD11 and PD30, i.e. atrophy of the dendrite tree, changes in the distribution of synaptic contacts of parallel and climbing fibres, delay in the elimination of transient synapses on cell soma and severely impaired pinceau formation at the axon hillock. After treatment with [Pt(*O*,*O*′-acac)(γ-acac)(DMS)], the sole relevant change concerned the timing of climbing fibres elimination; the transient synapses disappearance on the Purkinje cell soma was delayed in some cells; instead, the growth of Purkinje cell dendrite tree was normal as was the formation of inhibitory synaptic contacts on these neurons.

These findings add new evidence not only on the lower neurotoxicity of [Pt(*O*,*O*′-acac)(γ-acac)(DMS)] vs cisplatin but also on the involvement of neurotransmitters and relative synaptic connections in the maturation of central nerve tissue.

1. Introduction

Several chemotherapeutic drugs are known to cause significant clinical neurotoxicity, which can result in the early cessation of treatment. Platinum compounds are widely used for child malignancies as an essential component of multidrug frontline therapy regimens for children (Prestayko et al., 1979) with CNS solid tumours (e.g., neuroblastoma) or with non-CNS malignancies (e.g. leukaemia) (Gilchrist et al., 2014). In this regard, it is interesting to note that recent studies have identified a large number of long-term behavioural issues (such as depression, anxiety, and antisocial behaviour) in paediatric oncology patients (Sugimoto et al., 1995). On the other hand, the immature CNS is much more vulnerable to injury from toxic agents than the adult CNS and prone to impairment (Rodier, 1995). In mammals, there are crucial phases

Abbreviations: CB, calbindin; cisPt, cisplatin; IGL, internal granular layer; ML, molecular layer; PD, postnatal day; PtAcacDMS, [Pt(*O*,*O*′-acac)(γ-acac)(DMS)]; VGluT1, vesicular glutamate transporter 1; VGluT2, vesicular glutamate transporter 2.

☆ This paper is dedicated to the memory of our friend Elda Scherini who passed away recently. Elda was among the first scientists to investigate, in the 1980s, the effect of cis-dichlorodiammineplatinum on the morphology of the developing rat cerebellum.

* Corresponding author. Tel.: +39 0382 986327; fax: +39 0382 986325.
E-mail addresses: valeria.piccolini@unipv.it (V.M. Piccolini), alessandra.esposito01@universitadipavia.it (A. Esposito), veronica.dalbo01@ateneopv.it (V. Dal Bo), violetta.isolia01@ateneopv.it (V. Insolia), mariagrazia.bottone@unipv.it (M.G. Bottone), sandra.depascali@unisalento.it (S.A. De Pascali), fp.fanizzi@unisalento.it (F.P. Fanizzi), graziella.bernocchi@unipv.it (G. Bernocchi).

http://dx.doi.org/10.1016/j.ijdevneu.2014.10.006
0736-5748/

of CNS maturation during which the brain regions may be differentially affected by various chemicals (Ferguson et al., 1996; Fujii, 1997).

More in general, eliminating the neurotoxicity of platinum drugs is a major goal in experimental and clinical research in addition to the focus on their biochemical mechanisms of action. To circumvent neurotoxicity and to study the cellular and molecular basis of toxicity, experimental approaches on animal models are made. The effects of cisplatin [cis-diamminedichloroplatinum(I)I] (cisPt), the most widely used drug in the chemotherapy of cancer (Brezden et al., 2000), in rodents is similar to that seen in patients. Several groups have studied the effects of cisPt on the peripheral nervous system of rats (De Koning et al., 1987; Holmes et al., 1998; Tomiwa et al., 1986) and mice (Carozzi et al., 2009). CisPt has been shown to be toxic to cell populations in culture (Bottone et al., 2008; Santin et al., 2011, 2013), to the developing CNS (Avella et al., 2006; Cerri et al., 2011; Piccolini et al., 2012; Pisu et al., 2004; review: Bernocchi et al., 2011). It is a current accepted paradigm that cisPt cytotoxicity is the result of its binding to nuclear DNA (Ahmad, 2010) and in this way initiates processes that may end in cell death (Baig et al., 2014; Bottone et al., 2008; Cepeda et al., 2007; Florea and Büsselberg, 2009; Kamal et al., 1996). There is, however, evidence that cisPt binds to non-DNA targets (Cepeda et al., 2007; Florea and Büsselberg, 2009) and activates a number of signal transduction pathways.

Another fundamental drawback of chemotherapeutic drugs is their chemoresistance. In fact, resistance to cisPt is generally considered to be a multifactorial phenomenon which is mainly due to reduced drug accumulation, increased repair of platinum–DNA adducts, failure of cell death pathways (Rabik and Dolan, 2007).

For these reasons, several strategies are underway to prevent or minimize the toxicities and conserve the effectiveness of the platinum chemotherapy drugs. One way may be to synthesize new platinum compounds with targets different from DNA and with low toxicity profile.

A novel platinum compound, [Pt(*O*,*O*′-acac)(γ-acac)(DMS)] (PtAcacDMS) has in fact been recently synthesized (De Pascali et al., 2005, 2009) and tested in MCF-7 cells (Muscella et al., 2007, 2008, 2010, 2011) which have proven resistance to many chemotherapeutic agents. These workers found that the cytotoxicity of PtAcacDMS, differently from cisPt, correlated with its concentration in the cell, not with DNA binding.

As model of developing CNS areas, the developing cerebellum offers the opportunity to distinguish the events on which the platinum compounds act on DNA and non-DNA targets. In fact, cerebellar development proceeds with such precision that any perturbations in CNS maturation can be readily identified. During postnatal life, neurogenesis and migration of granule cell precursors involve cell proliferation and apoptotic cell death (Bonfanti et al., 1997; Doetsch et al., 1999; Pisu et al., 2005), and the formation of synapses and neuronal circuits entails the differentiation of postmitotic neurons such as Purkinje cells (Lujan, 2007). The emergence of neuronal circuits through the formation and refinement of synaptic connections, in which Purkinje cells are key elements, focuses on some neurotransmitter systems. During cerebellar morphogenesis and cytodifferentiation, various types of neurons and fibres develop simultaneously and many neurotransmitters appear chronologically, also acting as morphogens (Buznikov et al., 1996; Huang et al., 2007; Kwong et al., 2000; Mattson, 1988; Takayama, 2005). Several drugs act with neurotransmitters during neuronal maturation (Fadda and Rossetti, 1998; Fonnum and Lock, 2000), including cisPt (Avella et al., 2006).

The aim of the present study was to compare the possible cytotoxic effects of cisPt and PtAcacDMS on neurotransmitter markers during cerebellar cortex development. Immunostaining with antibodies raised against markers of glutamate and GABA, the main neurotransmitters in the cerebellum (Manent and Represa, 2007; Marrs and Maynard, 2013; Mattson, 1988), was performed.

In this comparison, besides making an important contribution to knowledge on the neurotoxicity of platinum compounds that limit their clinical use, it emerges how essential are the genesis of neurons and the interactions between synaptic contacts and neurons for the correct development of CNS (Avella et al., 2006; Cerri et al., 2011).

2. Materials and methods

2.1. Animals and treatments

Ten-day-old Wistar rats were given a single subcutaneous injection of cisPt (0.5 mg/ml, Teva Pharma, Italy) or PtAcacDMS (De Pascali et al., 2005) at a dose of 5 μg/g body weight (corresponding to the therapeutic dose suggested by Bodenner et al., 1986; Dietrich et al., 2006). Twenty-four hours (postnatal day, PD11), 7 days (PD17) and 20 days (PD30) after drug administration, treated rats (3 per stage) and control (untreated) animals (3 per stage) of the same age were anaesthetized with an intraperitoneal injection of 35% chloral hydrate (100 μl/100 g bw; Sigma, St. Louis, MO, USA) and divided into two groups. Regarding the first group, the brains were quickly removed, fixed in Carnoy's solution (6 absolute ethanol/3 chloroform/1 acetic acid) for 48 h, then placed in absolute ethanol and in acetone, and embedded in Paraplast X-tra (Sigma). Sections (8 μm-thick) of the cerebellar vermis were cut in the sagittal plane and collected on silan-coated slides. The second group was perfused intracardially with saline followed by 4% paraformaldehyde in 0.1 M phosphate buffer, pH 7.3. The brains were immediately excised, postfixed in the same fixative medium at 4 °C for 1.5 h, kept in 30% sucrose in 0.1 M phosphate buffer at 4 °C for 48 h and frozen in liquid nitrogen. Twelve μm-thick cryostat sections of cerebellar vermis were cut on the sagittal plane and collected on silan-coated slides. The sections were then processed for immunocytochemical reactions as described below.

To avoid possible staining differences due to small changes in the procedure, the reactions were carried out simultaneously on slides from control and treated animals at all stages. All experiments were performed according with the guidelines for care and use of laboratory animals as published by the Italian Ministry of Health (DDL 116/92). All efforts were made to minimize the number of animals used and their suffering.

2.2. Immunoreactions at light microscopy

Paraplast-embedded sections of the cerebellar vermis were deparaffinized in xylene, rehydrated through a series of graded alcohol treatments and rinsed in phosphate-buffered saline (PBS, Sigma). Endogenous peroxidases were suppressed by incubation of the sections with 3% H_2O_2 in 10% methanol in PBS for 7 min. Subsequently, the sections were washed in PBS and incubated for 20 min in normal serum at room temperature in order to block nonspecific antigen binding sites. Localization of GAD67 was achieved by applying on the brain sections a rabbit monoclonal anti-GAD67 (1:200; Santa Cruz Biotechnology, Santa Cruz, CA) in PBS overnight in a dark, moist chamber. Thereafter, the sections were sequentially incubated with diluted biotinylated secondary antibody solution (1:200; Vector Laboratories, Burlingame, CA, USA) for 30 min. Sections were washed in PBS and incubated for 30 min at room temperature with Vectastain Elite ABC reagent (Vector Laboratories). Then, 0.05% 3,3′-diaminobenzidine tetrahydrochloride (DAB; Sigma) with 0.01% H_2O_2 in Tris–HCl buffer (0.05 M, pH 7.6) was used as a chromogen. After each reaction step, sections were washed thoroughly in PBS (two changes of 5 min each). Sections were dehydrated in ethanol, cleared in xylene, and mounted in Eukitt (Kindler, Freiburg, Germany). For control staining, some sections were incubated with PBS instead of the primary antibody. No immunoreactivity was present in this condition.

The slides were observed with an Olympus BX51 microscope, and the images were recorded with an Olympus Camedia C-5050 digital camera and stored on a PC. Corrections to brightness and contrast were made with Paint Shop Pro 7 (Jasc Software Inc.).

2.3. Immunoreactions at fluorescence microscopy

Localization of GluR2-3/CB (calbindin) was achieved by applying on the Paraplast-embedded sections a rabbit polyclonal anti-GluR2-3 (1:200; Chemicon, Teecula, CA) and a mouse monoclonal anti-CB (1:5000, Swant, Bellinzona, CH) in PBS. Sections were washed and incubated for 1 h with a mixture of secondary antibodies containing Alexa Fluor 488-conjugated anti-rabbit and Alexa Fluor 594-conjugated anti-mouse (1:100; Molecular Probes, Space, Milano, Italy).

Localization of VGluT1/CB and VGluT2/CB was achieved by applying on cerebellum cryostat sections, respectively:

- a guinea pig polyclonal antibody anti-VGluT1 (1:6000, Millipore, Temecula, CA) and a monoclonal antibody anti-CB (1:5000, Bellinzona, Switzerland),

- a guinea pig polyclonal antibody anti-VGluT2 (1:3000, Millipore, Temecula, CA) and a monoclonal antibody anti-CB (1:5000, Swant, Bellinzona, Switzerland).

in PBS overnight in a dark, moist chamber.

After washing, the sections were incubated for 1 h with a mixture of secondary antibodies containing Alexa Fluor 594-conjugated anti-guinea pig and Alexa Fluor 488-conjugated anti-mouse at a dilution of 1:100 (Molecular Probes, Space, Milan, Italy). After washing with PBS, coverslips were mounted in a drop of Mowiol (Calbiochem, San Diego, CA).

Both Paraplast-embedded sections and cryostat sections were viewed by fluorescence microscopy with an Olympus BX51 equipped with a 100 W mercury lamp used under the following conditions: 540 nm excf, 480 nm dm, and 620 nm bf for Alexa 594 and 450–480 nm excf, 500-nm dm, and 515 nm bf for Alexa 488. Images were recorded with an Olympus Camedia C-5050 digital camera and stored on a PC. Images were optimized for colour, brightness and contrast by using Paint Shop Pro 7 software (Jasc Software Inc.).

For control staining, some sections were incubated with PBS instead of the primary antibodies. No immunoreactivity was present in these sections.

2.4. Counts of nerve terminals

The number of VGluT2-immunopositive puncta surrounding Purkinje cell somata and dendrite branches was counted in micrographs obtained at 100× and 40× magnification, respectively.

At postnatal stages PD11, PD17 and PD30, Purkinje cell somata were examined; the VGluT2-positive puncta surrounding somata were counted in randomly chosen Purkinje cells in an investigator-blinded study. Counts ($n = 15$ in three sections per animal for a total of 45 evaluations per controls, 45 per cisPt-treated rats and 45 per PtAcacDMS-treated ones per each stage) were made at the apices of lobules VI–VIII. At PD30, the counts were made in a tract of the ML including about eight Purkinje cells ($n = 15$ counts in three sections per animal for a total of 45 measurements for controls, 45 for cisPt treated rats and 45 for PtAcacDMS-treated ones). Results were recorded on Microsoft Office Excel Software spreadsheets and are expressed as the mean ± SD (standard deviation). Statistical differences between control and treated animals were determined by Student's t test.

3. Results

The immunocytochemical expression of glutamate and GABA markers was studied in controls and age-matched treated rats. The observations were carried out in the apical part of the cerebellar vermis lobules VI–VIII in which proliferation and differentiation are more active than other lobules (Altman, 1972a,b, 1982) after cisPt or PtAcacDMS injection made at PD10. Rats were killed at PD11, PD17 and PD30, i.e. one, seven and 20 days after administration of the platinum compounds.

3.1. Glutamate markers

3.1.1. Double immunoreaction for GluR 2–3/CB

GluR 2–3, an ionotropic glutamate receptor, labels Purkinje neurons postsynaptically during postnatal development of the cerebellum (Hafidi and Hilman, 1997; Lòpez-Bendito et al., 2001; Pisu et al., 2003, 2004).

On PD11 (Fig. 1), controls showed GluR 2–3 labelling in the Purkinje cells; the immunoreactivity was intense in the cytoplasm and dendrites, especially in the dendritic cone. CB immunopositivity revealed the extension of dendrites at this stage of development. After cisPt injection, the soma of Purkinje cells were intensely immunopositive for GluR 2–3; the dendritic tree of most of Purkinje cells appeared atrophic with few branches and with less extension into the molecular layer, as better shown by CB immunostaining and merged. After PtAcacaDMS injection, Purkinje cells were intensely labelled for GluR 2–3; the dendritic branching was more closely similar to that of controls as shown by CB immunoreaction and merged.

On PD17 (Fig. 1), Purkinje cells of controls maintained GluR 2–3 labelling; some structural components of the internal granular layer (IGL), such as glomeruli and granule cells, were clearly identified. CisPt did not greatly change the immunoreactivity for GluR 2–3, but the dendrite extensions differed from postsynaptically control rats, and loss of dendritic branches occurred. After PtAcacDMS treatment, labelling for GluR 2–3 in the Purkinje cell cytoplasm was intense and the dendritic tree of these neurons was well branched.

On PD30, in comparison with controls, Purkinje cells of cisPt- and PtAcacDMS-treated rats showed GluR 2–3-fully immunofluorescent dendrites including the fine superficial branches (not shown).

Table 1
Number (mean ± SD) of VGluT2 immunopositive nerve terminals on the Purkinje cell soma and dendrite branches.

Stage	Control	cisPt	PtAcacDMS
PD11 (soma)	18 ± 4	19 ± 3	20 ± 3
PD17 (soma)	–	5 ± 4***	4 ± 4***
PD30 (soma)	–	–	–
PD30 (dendrite)	244 ± 30	170 ± 29***	202 ± 29***,°°

Comparison between control/cisPt and control/PtAcacDMS: *$P < 0.05$; **$P < 0.01$; ***$P < 0.001$.
Comparison between cisPt/PtAcacDMS: °$P < 0.05$;°°$P < 0.01$;°°°$P < 0.001$. n per stage: 15.

3.1.2. Double immunoreaction for VGluT1/CB

VGluT1, a vesicular glutamate transporter, labels the varicosities of the parallel fibres on Purkinje cells in the cerebellum (Avella et al., 2006; Fremeau et al., 2001, 2004; Hioki et al., 2003; Hisano et al., 2002; Ichikawa et al., 2002). It is also expressed in granule cells (Nunzi et al., 2003).

On PD11 (Fig. 2), controls showed immunoreactivity for VGluT1 in the area of the ML (molecular layer) occupied by the Purkinje cell dendritic tree. This zone of the ML was less extended after cisPt treatment in comparison with controls, as better shown by CB immunostaining and merged. Instead, after PtAcacDMS treatment, the branching and extension of Purkinje cell dendrites were the same as in controls.

On PD17 (Fig. 2) and PD30 (not shown), intense immunopositivity was still observed in the ML zone corresponding to the Purkinje cell dendrites of control rats; labelling was also observed in the glomeruli of the IGL. The cisPt and PtAcacDMS treatments did not show evident differences in comparison with controls, although there were damaged areas after cisPt due to the presence of haemorrhagic foci.

3.1.3. Double immunoreaction for VGluT2/CB

VGluT2, a vesicular glutamate transporter, selectively labels climbing-fibre terminals in the cerebellar cortex (Avella et al., 2006; Hioki et al., 2003; Hisano et al., 2002).

On PD11 (Fig. 3), the immunocytochemical expression of VGluT2 in controls showed labelling in the nerve terminals that form synapses on Purkinje cell soma and dendrite growth cones, as better seen by merged; intense immunopositivity was present in the synaptic contacts of IGL glomeruli. The cisPt and PtAcacDMS treatments did not induce changes in the number of the synaptic contacts on the Purkinje cell soma (see also Table 1), while, in parallel, a CB atrophic immunopositive dendritic tree was observed in cisPt-treated rats.

On PD17 (Fig. 3), rare nerve terminals on Purkinje cell soma were seen, but several VGluT2 synaptic contacts were present on the growing dendrites of control rats. Both after cisPt treatment and PtAcacDMS treatment, labelled nerve terminals were still observed on the Purkinje cell soma (see also Table 1). Dendritic branches maintained VGluT2 synaptic contacts after both treatments, although they appeared to be more concentrated on the stem dendrites in comparison with controls. Intense immunopositivity was present in the synaptic contacts of IGL glomeruli of control and treated rats.

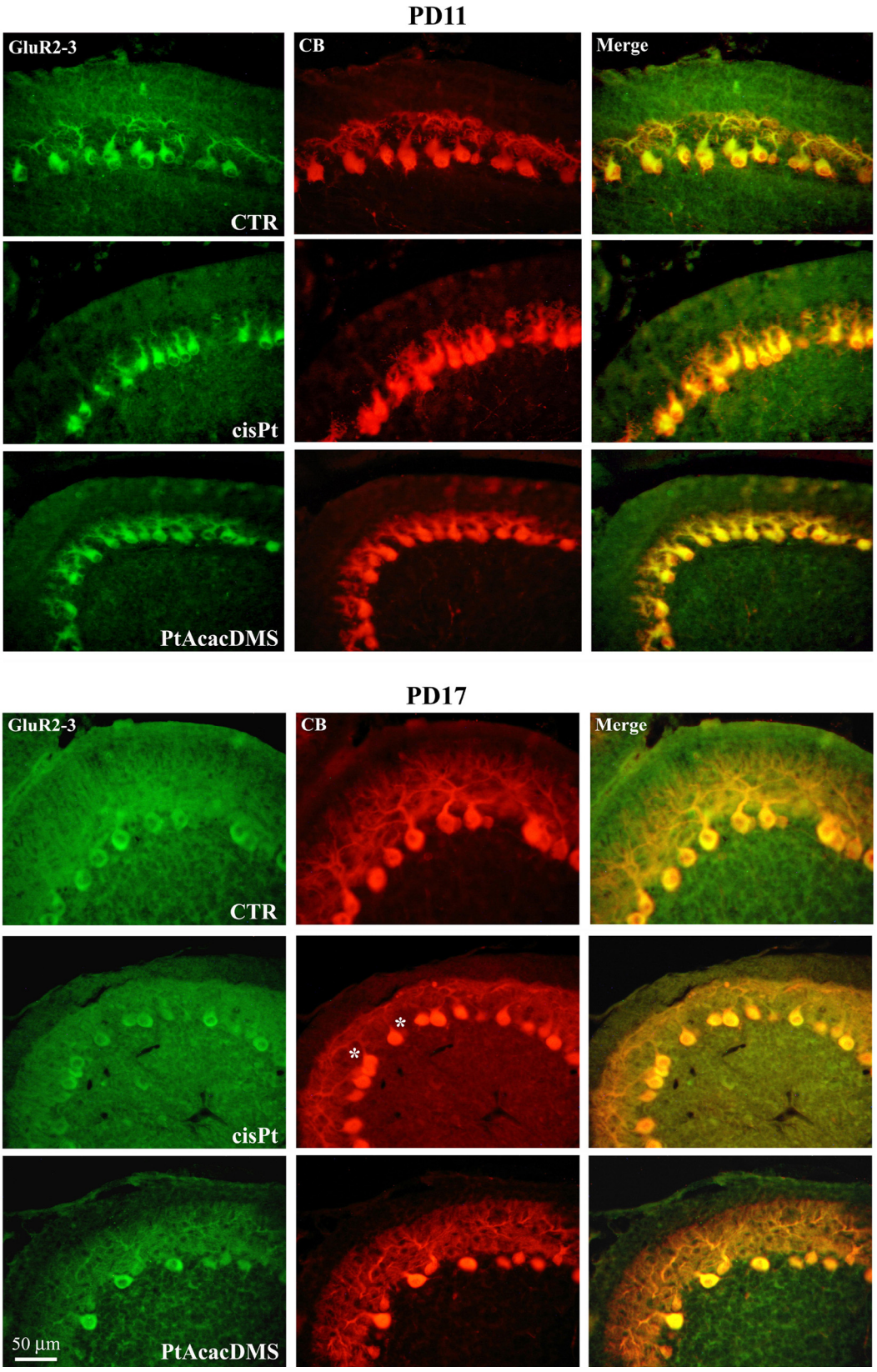

Fig. 1. GluR 2–3/CB immunofluorescence reaction at PD11 and PD17. On PD11, intense GluR 2–3 immunoreactivity is shown in the Purkinje cell cytoplasm and dendrites of control rats; CB labels the extension of dendrites. After cisPt injection, the soma of Purkinje cells is intensely immunopositive for GluR 2–3; the CB labelled dendritic tree of most of Purkinje cells appears atrophic, as better shown by merged. After PtAcacaDMS injection, GluR 2–3 labels Purkinje cells; the dendrite branching is similar to that of controls as shown by CB immunoreaction and merged. On PD17, Purkinje cells of controls are GluR 2–3 labelled; some structural components (glomeruli) of the internal granular layer (IGL) are immunopositive. After cisPt treatment the immunopositivity for GluR 2–3 is similar to that of controls; CB indicates loss of dendritic branches (asterisks), as better shown by merged. After PtAcacDMS treatment, GluR 2–3 labelling is intense in the Purkinje cell cytoplasm; the dendritic tree of these neurons is well branched, as shown also by CB and merged.

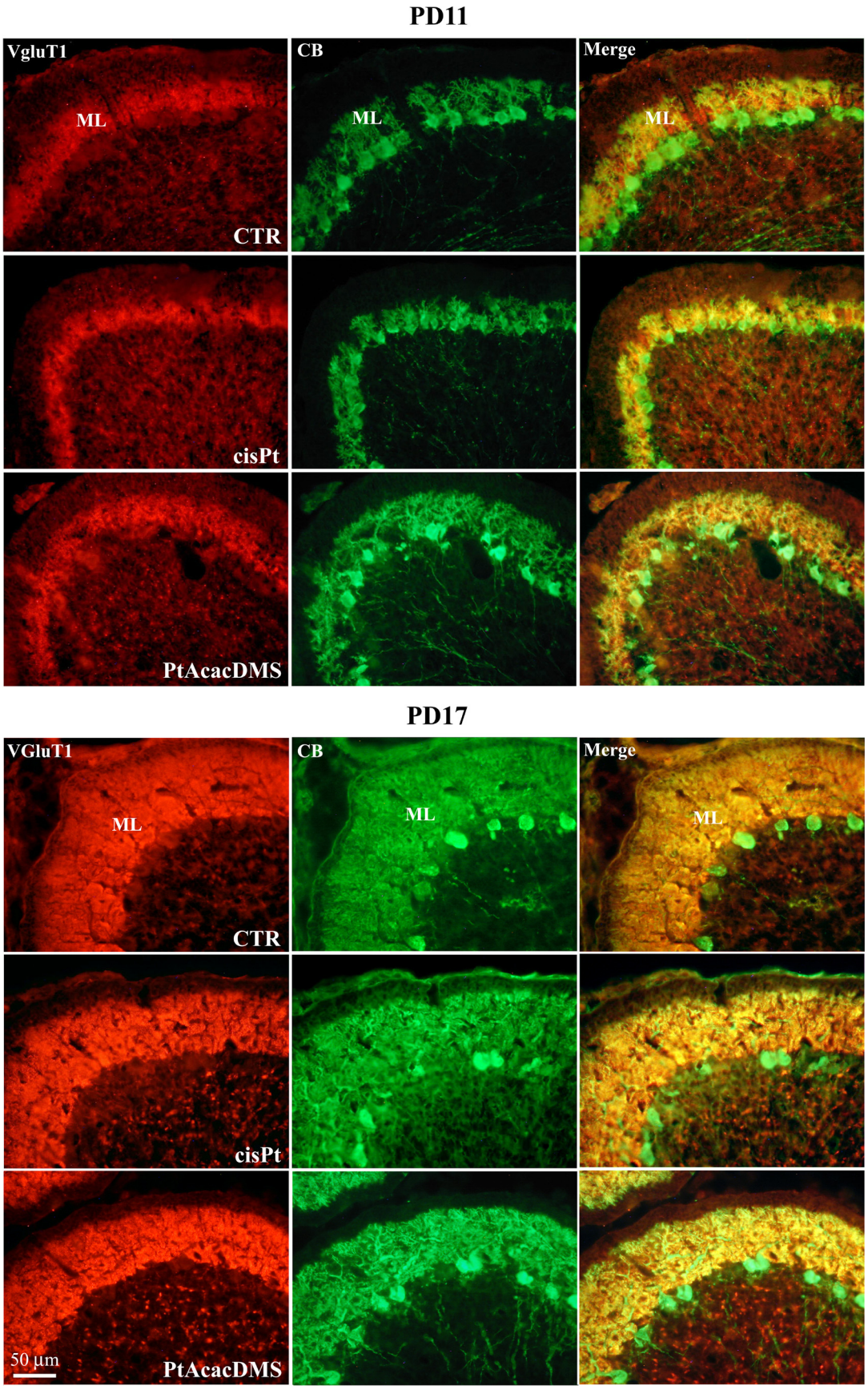

Fig. 2. VGluT1/CB immunofluorescence reaction at PD11 and PD17. On PD11, VGlut1 labels the area of the ML occupied by the Purkinje cell dendritic tree. After cisPt treatment, the zone appears less extended, as better shown by CB immunostaining and merged. After PtAcacDMS treatment, Purkinje cell dendrites show the same branching and extension as in controls. On PD17, intense immunopositivity is observed in the ML zone corresponding to the Purkinje cell dendrites of control rats; glomeruli of the IGL are also labelled. After the cisPt and PtAcacDMS treatments, no differences are visible in comparison with controls.

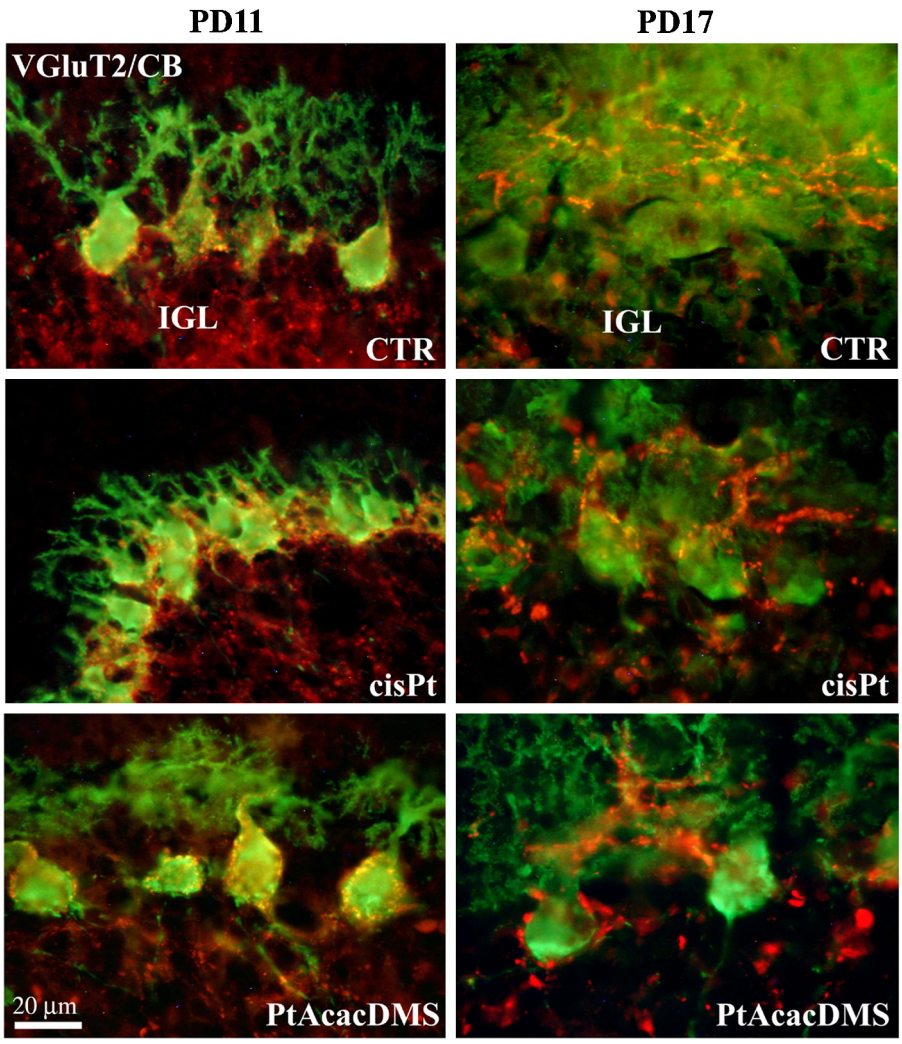

Fig. 3. VGluT2/CB immunofluorescence reaction at PD11 and PD17. On PD11, VGluT2 labelling is present in the labelled puncta (climbing fibre synaptic contacts) on Purkinje cell soma and dendrite growth cones, as better seen by merged; IGL glomeruli are intensely immunopositive. After cisPt treatment, the number of the synaptic contacts on the Purkinje cell soma does not change; a CB atrophic immunopositive dendritic tree is shown. After PtAcacDMS treatment, synaptic contacts are still present around Purkinje cell soma (see also Table 1); the CB immunopositive dendritic branches appear similar to controls. On PD17, rare nerve terminals on Purkinje cell soma of control rats are shown; several VGluT2 synaptic contacts are present on the CB labelled dendrites. After cisPt treatment, as well as after PtAcacDMS treatment, labelled puncta are still visible on the Purkinje cell soma. There are several VGluT2 synaptic contacts on dendrite branches after both treatments. Intense immunopositivity is present in the IGL glomeruli of control and treated rats.

On PD30 (not shown), absence of VGluT 2 nerve terminals on Purkinje cell soma was found in all conditions. Labelled puncta were located on the dendrites only. In comparison with controls, treatments caused a significant decrease in the number of nerve terminals, which appeared to be more concentrated at the stem dendrite; the loss was less severe after PtAcacDMS (see Table 1).

3.2. *GABA markers*

GAD67 is the synthesis enzyme of GABA. GAD67 is found in axonal regions as well as in Purkinje cell bodies (Bernocchi et al., 2011; Kang et al., 2001).

On PD11 (Fig. 4), in controls, Purkinje cell soma and stem dendrites and main branches were labelled by GAD67; baskets at the axon hillock were occasionally identifiable. Several labelled puncta were distributed in the ML and IGL. CisPt treatment produced Purkinje cell bodies with short labelled stem dendrites and a thinner ML containing labelled puncta. After PtAcacDMS treatment, the immunopositivity was similar to controls.

On PD17 (Fig. 4), the soma and main dendritic branches of Purkinje cells of control rats were immunopositive. There were several nerve puncta in the ML and baskets around Purkinje cell axon hillocks as well as glomerular components in the IGL. After cisPt treatment, a marked decrease in the density of nerve terminals in the ML was observed; moreover, the baskets at the axon hillock of Purkinje cells often appeared to be flattened. After PtAcacDMS treatment, the distribution of the immunopositive cells and components of the cerebellar cortex did not change in comparison with controls; in particular, baskets at the axon hillock of Purkinje cells were clearly identifiable.

On PD30 (not shown), as previously shown (Pisu et al., 2004), GAD67 terminals were located mostly in the lower half of the ML after cisPt injection and also formed contacts with the main branches of Purkinje cell dendrites. Few punctate terminals were found in both compartments of the ML. Flattened baskets at the Purkinje axon hillock were sometimes found. No changes with respect to control rats were noticed after PtAcacDMS.

4. Discussion

Neurotoxicity is a common side-effect of cancer treatment, since chemotherapeutic drugs may exert a direct noxious effect on the

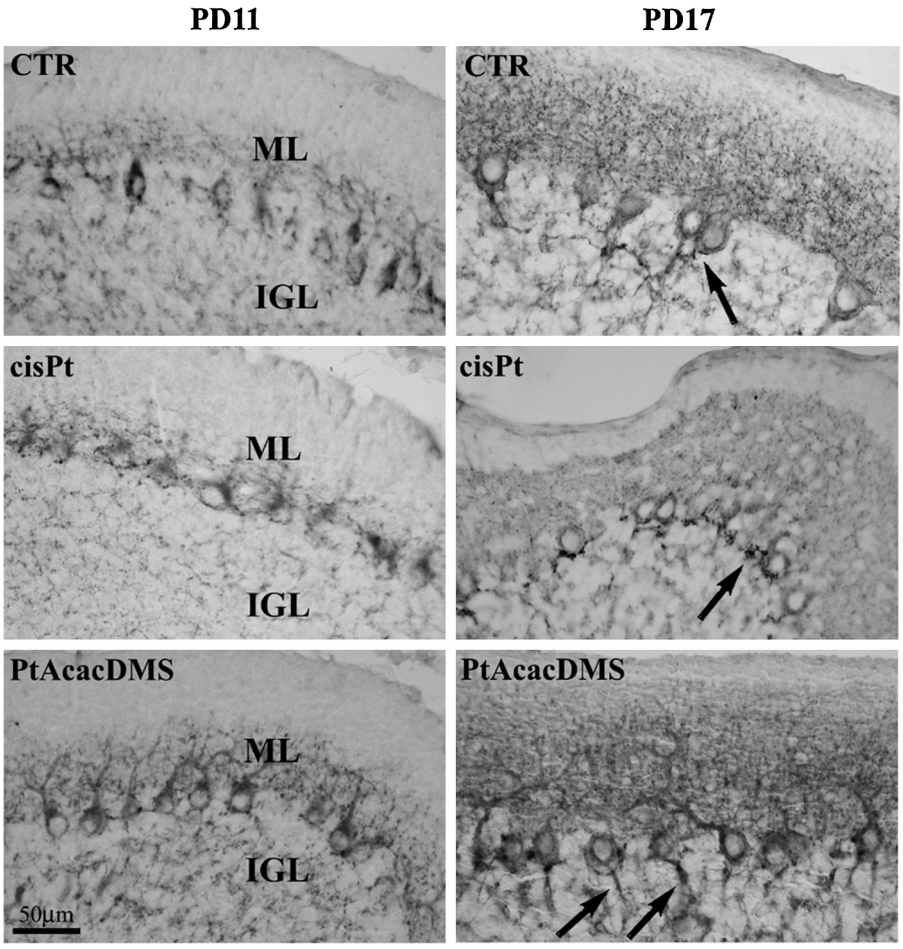

Fig. 4. GAD67 immunocytochemical reaction at PD11 and PD17. On PD11, controls show Purkinje cell soma and stem dendrites labelled by GAD67; at the axon hillock the basket is not identifiable. Several labelled puncta (inhibitory synaptic contacts) are distributed in the ML and IGL. After cisPt treatment, Purkinje cells have short, labelled stem dendrites; there are labelled puncta in a thinner ML. After PtAcacDMS treatment, the immunopositivity is similar to controls. On PD17, the soma and main dendritic branches of Purkinje cells of control rats are immunopositive. Several nerve terminal puncta in the ML and baskets around Purkinje cell axon hillocks (arrows) as well as glomerular components in the IGL are shown. After cisPt treatment, few nerve terminals in the ML are detectable; the baskets at the axon hillock of Purkinje cells are present, but often flattened (arrows). After PtAcacDMS treatment, the labelling is similar to that of controls; the baskets are clearly identifiable at the axon hillock of Purkinje cells, as in controls (arrows).

brain or peripheral nerves (review: Argyriou et al., 2014). Recently, measures of chemotherapy-induced peripheral neuropathy have been obtained in school-aged children (Gilchrist et al., 2014), and demonstrate greater sensory toxicity than motor toxicity.

In this study, attention was focused on brain development with the idea of promoting cancer therapy with less adverse effects on some pivotal events of maturing CNS morphology and physiology. Fundamental events of the postnatal development of the mammalian cerebellum, such as the differentiation of Purkinje neurons, the sole neuron representing the output from cerebellar cortex (Ito, 1984), and formation of inhibitory and excitatory synaptic contacts on them (Altman, 1972b) were examined in the lobules VI–VIII of the cerebellar vermis; these lobules being the last ones to be developed during postnatal histogenesis (Altman and Bayer, 1997).

The panel of immunocytochemical markers used here have confirmed some of the fundamental histogenetic changes that occur postnatally in control rats (Lujan, 2007):

i. in the second week of life, at PD11, the dendritic tree of Purkinje neurons (GluR 2–3 and CB immunopositive) develops concomitantly with inhibitory (GAD 67 immunopositive) and excitatory (VGluT1 and VGluT2 immunopositive) synaptic contacts; the presence of transient VGluT2-labelled synaptic contacts by climbing fibres on Purkinje cell soma merits particular attention (Crepel et al., 1981; Mariani and Changeu, 1981a,b; Hashimoto and Kano, 2003);
ii. in the third week of life, at PD17, until the end of cerebellar development at PD30, the main findings concern the extension of Purkinje cell dendrites and the formation of pinceau by basket cells at the axon hillock, as well as the increase in inhibitory and excitatory nerve terminals/synaptic contacts in the ML and IGL; the transient VGluT2 synaptic contacts by climbing fibres on Purkinje cell soma has disappeared.

After cisPt treatment at PD10, labelling with the neurotransmitter markers evidenced the following changes between PD11 and PD30:

i. the dendritic tree of Purkinje cells became atrophic;
ii. the distribution of synaptic contacts of parallel and climbing fibres had changed;
iii. the elimination of transient synapses on Purkinje cell soma was delayed;
iv. the formation of pinceau at the axon hillock of Purkinje cells was altered.

The above changes in Purkinje cell differentiation confirm previously reported data from this laboratory (Avella et al., 2006; Pisu

et al., 2004). The reduced or delayed growth of the Purkinje cell dendritic arbour may depend on the absence of the trophic effect of granule cells in the IGL (Altman and Bayer, 1982). In fact, the precursors of granule cells of the external granular layer coped with apoptotic cell death in cisPt-treated rats (Pisu et al., 2005); the ensuing possible reduction of granule cells affected the formation of parallel fibre synapses on Purkinje cell dendrites. Concurrent with the development of excitatory parallel fibres and Purkinje cell dendritogenesis, it must be emphasized that the formation of afferents on Purkinje cells is fundamental for the morphological basis of cerebellar function. A single parallel fibre can provide the same information to a large number of Purkinje cells, and a group of parallel fibres can carry a great deal of information to a single Purkinje cell (Huang and Huang, 1998). The synaptic inputs between parallel fibres and Purkinje cells are essential for the achievement of the espalier arrangement of the dendritic tree (Sotelo, 2004).

VGluT1 and VGluT2 are selectively expressed by the varicosities of the respective parallel and climbing fibres (Andjus et al., 2003; Fremeau et al., 2001, 2004; Hioki et al., 2003). These two fibre-specific markers were chosen because of the important role exerted by each type of excitatory fibre on Purkinje cell differentiation and dendritic tree growth.

CisPt did not affect the intensity of VGluT1 immunoreactivity, but the distribution of the parallel fibre terminals matched the growth and extension of Purkinje cell dendrites until one week after treatment. In fact, on PD11, the VGluT1-labelled area of the ML was not as wide in treated rats as in controls (Avella et al., 2006). Moreover, in treated rats, Purkinje cells showed shorter, less ramified dendritic trees (Pisu et al., 2003, 2004). These findings emphasize the close relationship between the developing parallel fibre system and the differentiating Purkinje cell dendrites (Altman and Bayer, 1997). At the end of histogenesis, after cisPt treatment, the VGluT1-positive ML area was as deep as the Purkinje cell dendritic extension and haemorrhage was visible (Avella et al., 2006). These findings indicate damage to the maturation of granule cells, an important trophic factor for Purkinje cell dendritic growth (Altman, 1982; Morrison and Mason, 1998; Petralia and Wenthold, 1992; Pisu et al., 2003).

However, one of the most important processes for the correct differentiation of Purkinje cells is the elimination of the supernumerary synapses of climbing fibres on the Purkinje cell somata that arise during the formation of the spiny branchlets and parallel fibre synapses, until only one climbing fibre branch contacts one Purkinje cell (on PD20) (Crepel et al., 1976). The regression, and perhaps the choice of the surviving climbing arbour, is under the dominant control of the parallel fibres (Scelfo and Strata, 2005). In the rat, Purkinje cells, which are contacted by several climbing fibres by the end of embryonic development (Chedotal and Sotelo, 1993; Morara et al., 2001), rapidly become innervated with an average of three to four fibres by PD5 (Carulli et al., 2004). A process of regression later occurs, leading to the adult pattern of monoinnervation during the second postnatal week (Crepel et al., 1981; Hashimoto and Kano, 2003; Mariani and Changeu, 1981a,b).

CisPt did not appear to have early effects (PD11) on the presence of VGluT2-positive fibre varicosities around Purkinje cell somata. However, at PD17, VGluT2-immunoreactive synaptic contacts on Purkinje cell soma were still present in the treated rats. This finding demonstrates, in accordance with our earlier findings (Avella et al., 2006), that cisPt is able to delay the process of climbing fibre regression. Regression of the multiple innervation of Purkinje cells made by climbing fibres has also been found to be incomplete in homozygous mGluR1 mutant mice and to be prevented by blockade of NMDA receptors in the cerebellar cortex of PD15 and PD17 mice (Kakizawa et al., 2000; Levenes et al., 1997; Rabacchi et al., 1992). Thus, these appear to be the molecular steps that precede the morphological changes resulting from the elimination of redundant climbing synapses (Sotelo, 2004). Upon completion of histogenesis, on PD30, the main branches of Purkinje cell dendrites projecting throughout the ML are innervated by VGluT2-positive fibre varicosities on a one-to-one basis (Sotelo, 2004). There was a significant decrease in climbing-fibre contacts after the administration of cisPt.

The net effect of cisPt in delaying the process of climbing fibre regression may be to curtail the function of postsynaptic glutamatergic GluR 2–3 receptors of the Purkinje cells, thus altering the growth of Purkinje cell dendrites in lobules VI–VII.

In fact, early, the Purkinje cell dendrites in lobules were atrophic as evidenced by the morphological features and GluR2-3 immunofluorescent intensity of the Purkinje cell dendrites. Moreover, loss of dendrite branches was evident at PD17. As mentioned above, the involvement of glutamate and its receptors in the growth of Purkinje cell dendrite appeared to emerge after cisPt treatment.

Furthermore, at a later stage (PD17), the appearance of flattened basket cells at the axon hillock, indicative of modified structure and possibly altered inhibitory activity, was likely the consequence of the impeded development of the Purkinje cells (Pisu et al., 2004; Scherini and Bernocchi, 1994). Axons of basket cells and stellate cells affect the growth of Purkinje cell dendrites (Altman, 1972a,b); the oriented perpendicular growth of a single dendrite depends on the presence of basket cell axons, and the outgrowth of smooth branches depends on the presence of stellate cell axons. The time period in which these inhibitory interneurons originate during postnatal cerebellar development provides further proof of the morphogenetic role of basket cells and stellate cells. The genesis of basket cells and stellate cells in the ML of rat cerebellum reaches a peak by PD 6–7 and PD 8–11, respectively (Altman, 1972a,b; Zhang and Goldman, 1996). We thus administered cisPt on PD10, thereby expecting to provoke changes in stellate cell number or distribution. We noticed changes in the distribution of GAD67 immunoreactive terminals (see above); these were present in the lower half of the ML, but were scarce in the upper portion; thereby showing two compartments in the distribution of synapses on the Purkinje cell dendrites in the ML in lobules VI–VIII. In treated rats, the density of GAD67 nerve terminals and interneurons was lower in both compartments of the ML with respect to controls (Avella et al., 2006), suggesting that cisPt destroyed inhibitory neurons of the ML.

After treatment with PtAcacDMS, the only relevant morphological changes found with the markers were:

i. the process of elimination of climbing fibre transient synapses on Purkinje cell soma was delayed in some cells;
ii. the growth of the Purkinje cell dendritic tree was normal as was the formation of inhibitory synaptic contacts on these neurons.

The limited changes after PtAcacDMS, especially as regards the normal growth of Purkinje cell arbour, is not in favour of a link between GluR 2–3 and climbing fibre elimination, as suggested after cisPt treatment. In fact, the normal development of the Purkinje cell dendritic tree requires the presence of granule cells providing trophic stimulus through parallel fibres; in accordance, the granule cell precursors of the EGL that migrate into the IGL could not cope with apoptotic cells death as they did after cisPt treatment (Cerri et al., 2011).

It is highlighted here that the different effects of cisPt and PtAcacDMS on proliferating normal cells can be ascribed to their different mechanisms of action. As opposed to cisPt, which acts intracellularly to form DNA adducts, PtAcacDMS acts specifically with sulfur ligands intracellularly, and at the same time shows poor reactivity with nucleobases. Nevertheless, PtAcacDMS is found to be more active than cisPt in tumour cells, producing a rapid, sustained apoptotic response characterized by (a) mitochondrial depolarization; (b) cytosol accumulation of cytochrome c; (c)

proapoptotic translocation of proteins (Bax and the truncated form of Bid) from cytosol to mitochondria; (d) activation of caspase 7 and 9; and (e) chromatin condensation and DNA fragmentation (Muscella et al., 2008). Moreover, PtAcacDMS affects free intracellular calcium concentration through PKC-α-mediated closure of some channels and the inhibition of PMCA (plasma membrane calcium ATPase) activity (Muscella et al., 2011). The mechanism of action linked to possible changes in calcium homeostasis can be invoked also in normal nerve tissue as recently found by Piccolini et al. (2013) after treatments with both cisPt and PtAcacDMS. Specific alterations of calcium homeostasis affect the processes of formation and maturation of synapses. Precisely, calcium plays a crucial role in different events of CNS development, including synaptogenesis (Lohmann, 2009; Wong and Ghosh, 2002), and on neurotransmission in general (Mattson, 1992).

5. Conclusions

Major neurological problems in modern oncology were found after cisPt treatment in both adult and paediatric patients. In particular, synaptic and dendritic damage might be responsible for cognitive impairment due to pathological changes of brain structure and function (Andres et al., 2014). Platinum compounds, as several other toxicants (Marrs and Maynard, 2013), may adversely affect neurotransmission, but the new platinum compound (PtAcacDMS) appears to be less toxic than cisPt to normal nerve tissue, e.g. changes in neuroarchitectural development are more modest, apoptotic events are not high, granule cell migration and Purkinje cell dendrite growth are less altered (Bernocchi et al., 2011; Cerri et al., 2011; Piccolini et al., 2013), and neurotransmission/synapse formation are less altered. PtAcacDMS may be a promising drug for reducing the central neurotoxic effects of chemotherapeutic drug treatment, without reducing their anti-tumour effectiveness.

The findings here obtained allow for some remarks on development. In the developing cerebellum, synapse elimination is considered to be the final step of neuronal circuit formation and connectivity maturation in which glutamate receptors and transporters are involved. In effect, during the elimination of synapses with climbing fibres, NMDA receptors, activated by an increased intracellular calcium concentration, play a fundamental role (Constantine-Paton et al., 1990; Kakizawa et al., 2000).

Although the elimination of transient synapses by climbing fibres on the soma takes place later for some Purkinje neurons, the treatment with PtAcacDMS, differently from cisPt (Avella et al., 2006; Pisu et al., 2005), does not alter the dendrite tree extension of Purkinje cells or the formation of inhibitory synapses that is likely ascribed to neurogenesis events of granule cells and ML interneurons (Altman, 1972a,b, 1982; Altman and Bayer, 1997). As we have previously demonstrated (Cerri et al., 2011), the genesis of granule cells coped with cell death after cisPt and not after PtAcacDMS treatment.

From a developmental point of view, it may be deduced that the rescue of proliferating cells from chemical insult may be the first fundamental cause for the synapse and connectivity formation that guarantees the normal architecture of the CNS and copes with neurotoxic effects. This possibility could overcome at least some of the CNS morphological and functional defects in paediatric patients that receive chemotherapeutic agents in the treatment for cancer.

However, we are aware that neurotoxic damage of transcription factors driving the developmental mature acquisition of Purkinje cells may occur; for example ROR alpha (the retinoic acid-related orphan receptor alpha, a member of the nuclear hormone-receptor superfamily), is necessary for the retraction of transient Purkinje cell dendrites. The loss of ROR alpha induces new climbing fibre multi-innervation, and the appearance of perisomatic spines, suggesting regressive changes with a reversal of developmental processes (Chen et al., 2013).

Acknowledgments

This research was supported by grants from the “Fondi di Ateneo per la Ricerca” (FAR, University of Pavia), “Fondazione Banca del Monte di Lombardia” (Italy) and “Programmi di ricerca di Rilevante Interesse Nazionale” (PRIN, 2009ZFPSPW).

References

Ahmad, S., 2010. Platinum–DNA interactions and subsequent cellular processes controlling sensitivity to anticancer platinum complexes. Chem. Biodivers. 7, 543–566.
Altman, J., 1972a. Postnatal development of the cerebellar cortex in the rat. I. The external granular layer and the transitional molecular layer. J. Comp. Neurol. 145, 353–398.
Altman, J., 1972b. Postnatal development of the cerebellar cortex in the rat. II. Phases in the maturation of Purkinje cells and of the molecular layer. J. Comp. Neurol. 145, 399–463.
Altman, J., 1982. Morphological development of the rat cerebellum and some of its mechanisms. In: The Cerebellum-New Vistas., pp. 8–49.
Altman, J., Bayer, S.A., 1982. Development of the cranial nerve ganglia and related nuclei in the rat. Adv. Anat. Embryol. Cell Biol. 74, 1–90.
Altman, J., Bayer, S.A., 1997. Development of the Cerebellar System in Relation to its Evolution, Structure, and Functions. CRC Press.
Andjus, P.R., Zhu, L., Cesa, R., Carulli, D., Strata, P., 2003. A change in the pattern of activity affects the developmental regression of the Purkinje cell polyinnervation by climbing fibers in the rat cerebellum. Neuroscience 121, 563–572.
Andres, A.L., Gong, X., Di, K., Bota, D.A., 2014. Low-doses of cisplatin injure hippocampal synapses: a mechanism for ‘chemo’ brain? Exp. Neurol. 255, 137–144.
Argyriou, A.A., Kyritsis, A.P., Makatsoris, T., Kalofonos, H.P., 2014. Chemotherapy-induced peripheral neuropathy in adults: a comprehensive update of the literature. Cancer Manag. Res. 6, 135–147.
Avella, D., Pisu, M.B., Roda, E., Gravati, M., Bernocchi, G., 2006. Reorganization of the rat cerebellar cortex during postnatal development following cisplatin treatment. Exp. Neurol. 201, 131–143.
Baig, M.H., Rizvi, S.M., Shakil, S., Kamal, M.A., Khan, S., 2014. A neuroinformatics study describing molecular interaction of cisplatin with acetylcholinesterase: a plausible cause for anticancer drug induced neurotoxicity. CNS Neurol. Disord. Drug Targets 13, 265–270.
Bernocchi, G., Bottone, M.G., Piccolini, V.M., Dal Bo, V., Santin, G., De Pascali, S.A., Migoni, D., Fanizzi, F.P., 2011. Developing central nervous system and vulnerability to platinum compounds. Chemother. Res. Pract. 2011, 315418.
Bodenner, D.L., Dedon, P.C., Keng, P.C., Katz, J.C., Borch, R.F., 1986. Selective protection against cis-diamminedichloroplatinum(II)-induced toxicity in kidney, gut, and bone marrow by diethyldithiocarbamate. Cancer Res. 46, 2751–2755.
Bonfanti, L., Peretto, P., Merighi, A., Fasolo, A., 1997. Newly-generated cells from the rostral migratory stream in the accessory olfactory bulb of the adult rat. Neuroscience 81, 489–502.
Bottone, M.G., Soldani, C., Veneroni, P., Avella, D., Pisu, M., Bernocchi, G., 2008. Cell proliferation, apoptosis and mitochondrial damage in rat B50 neuronal cells after cisplatin treatment. Cell Prolif. 41, 506–520.
Brezden, C.B., Phillips, K.A., Abdolell, M., Bunston, T., Tannock, I.F., 2000. Cognitive function in breast cancer patients receiving adjuvant chemotherapy. J. Clin. Oncol. 18, 2695–2701.
Buznikov, G.A., Shmukler, Y.B., Lauder, J.M., 1996. From oocyte to neuron: do neurotransmitters function in the same way throughout development? Cell Mol. Neurobiol. 16, 533–559.
Carozzi, V., Chiorazzi, A., Canta, A., Oggioni, N., Gilardini, A., Rodriguez-Menendez, V., Avezza, F., Crippa, L., Ceresa, C., Nicolini, G., Bossi, M., Cavaletti, G., 2009. Effect of the chronic combined administration of cisplatin and paclitaxel in a rat model of peripheral neurotoxicity. Eur. J. Cancer 45, 656–665.
Carulli, D., Buffo, A., Strata, P., 2004. Reparative mechanism in the cerebellar cortex. Prog. Neurobiol. 72, 373–398.
Cepeda, V., Fuertes, M.A., Castilla, J., Alonso, C., Quevedo, C., Pérez, J.M., 2007. Biochemical mechanisms of cisplatin cytotoxicity. Anticancer Agents Med. Chem. 7, 3–18.
Cerri, S., Piccolini, V.M., Santin, G., Bottone, M.G., De Pascali, S.A., Migoni, D., Iadarola, P., Fanizzi, F.P., Bernocchi, G., 2011. The developmental neurotoxicity study of platinum compounds. Effects of cisplatin versus a novel Pt(II) complex on rat cerebellum. Neurotoxicol. Teratol. 33, 273–281.
Chedotal, A., Sotelo, C., 1993. The creeper stage in cerebellar climbing fibre synaptogenesis precedes the pericellular nest-ultrastructural evidence with parvalbumin immunocytochemistry. Dev. Brain Res. 76, 207–220.
Chen, X.R., Heck, N., Lohof, A.M., Rochefort, C., Morel, M.P., Wehrlé, R., Doulazmi, M., Marty, S., Cannaya, V., Avci, H.X., Mariani, J., Rondi-Reig, L., Vodjdani, G., Sherrard, R.M., Sotelo, C., Dusart, I., 2013. Mature Purkinje cells require the retinoic acid-related orphan receptor-α (RORα) to maintain climbing fiber mono-innervation and other adult characteristics. J. Neurosci. 33, 9546–9562.

Constantine-Paton, M., Cline, H.T., Debski, E., 1990. Patterned activity, synaptic convergence, and the NMDA receptor in developing visual pathways. Annu. Rev. Neurosci. 13, 129–154.
Crepel, F., Mariani, J., Delhay-Bouchad, N., 1976. Evidence for a multiple innervation of Purkinje cells by climbing fibres in the immature rat cerebellum. J. Neurobiol. 7, 567–578.
Crepel, F., Delhaye-Bouchaud, N., Dupont, J.L., 1981. Fate of the multiple innervation of cerebellar Purkinje cells by climbing fibers in immature control, X-irradiated and hypothyroid rats. Brain Res. 227, 59–71.
De Koning, P., Neijt, J.P., Jennekens, F.G., Gispen, W.H., 1987. Evaluation of cis-diamminedichloroplatinum(II) (cisplatin) neurotoxicity in rats. Toxicol. Appl. Pharmacol. 89, 81–87.
De Pascali, S.A., Papadia, P., Ciccarese, A., Pacifico, C., Fanizzi, F.P., 2005. First examples of βdiketonate platinum II complexes with sulfoxide ligands. Eur. J. Inorg. Chem. 5, 788–796.
De Pascali, S.A., Papadia, P., Capoccia, S., Marchiò, L., Lanfranchi, M., Ciccarese, A., Fanizzi, F.P., 2009. Hard/soft selectivity in ligand substitution reactions of beta-diketonate platinum(II) complexes. Dalton Trans. 7, 7786–7795.
Dietrich, J., Han, R., Yang, Y., Mayer-Pröschel, M., 2006. Noble MCNS progenitor cells and oligodendrocytes are targets of chemotherapeutic agents in vitro and in vivo. J. Biol. 5, 22.
Doetsch, F., García-Verdugo, J.M., Alvarez-Buylla, A., 1999. Regeneration of a germinal layer in the adult mammalian brain. Proc. Natl. Acad. Sci. U.S.A. 96, 11619–11624.
Fadda, F., Rossetti, Z.L., 1998. Chronic ethanol consumption: from neuroadaptation to neurodegeneration. Prog. Neurobiol. 56, 385–431.
Florea, A.M., Büsselberg, D., 2009. Anti-cancer drugs interfere with intracellular calcium signaling. Neurotoxicology 30, 803–810.
Ferguson, S.A., Paule, M.G., Holson, R.R., 1996. Functional effects of methylazoxymethanol-induced cerebellar hypoplasia in rats. Neurotoxicol. Teratol. 18, 529–537.
Fonnum, F., Lock, E.A., 2000. Cerebellum as a target for toxic substances. Toxicol. Lett. 112–113, 9–16.
Fremeau Jr., R.T., Troyer, M.D., Pahner, I., Nygaard, G.O., Tran, C.H., Reimer, R.J., Bellocchio, E.E., Fortin, D., Storm-Mathisen, J., Edwards, R.H., 2001. The expression of vesicular glutamate transporters defines two classes of excitatory synapse. Neuron 31, 247–260.
Fremeau Jr., R.T., Voglmaier, S., Seal, R.P., Edwards, R.H., 2004. VGLUTs define subsets of excitatory neurons and suggest novel roles for glutamate. Trends Neurosci. 27, 98–103.
Fujii, T., 1997. Transgenerational effects of maternal exposure to chemicals on the functional development of the brain in the offspring. Cancer Causes Control 8, 524–528.
Gilchrist, L.S., Marais, L., Tanner, L., 2014. Comparison of two chemotherapy-induced peripheral neuropathy measurement approaches in children. Support. Care Cancer 22, 359–366.
Hafidi, A., Hilman, D.E., 1997. Distribution of glutamate receptors Glur 2/3 and NR1 in the developing rat cerebellum. Neuroscience 81, 427–436.
Hashimoto, K., Kano, M., 2003. Functional differentiation of multiple climbing fiber inputs during synapse elimination in the developing cerebellum. Neuron 38, 785–796.
Hioki, H., Fujiyama, F., Taki, K., Tomioka, R., Furuta, T., Tamamaki, N., Kaneko, T., 2003. Differential distribution of vesicular glutamate transporters in the rat cerebellar cortex. Neuroscience 117, 1–6.
Hisano, S., Sawada, K., Kawano, M., Kanemoto, M., Xiong, G., Mogi, K., Sakata-Haga, H., Takeda, J., Fukui, Y., Nogami, H., 2002. Expression of inorganic phosphate/vesicular glutamate transporters (BNPI/VGLUT1 and DNPI/VGLUT2) in the cerebellum and precerebellar nuclei of the rat. Brain Res. Mol. Brain. Res. 107, 23–31.
Holmes, J., Stanko, J., Varchenko, M., Ding, H., Madden, V.J., Bagnell, C.R., Wyrick, S.D., Chaney, S.G., 1998. Comparative neurotoxicity of oxaliplatin, cisplatin, and ormaplatin in a Wistar rat model. Toxicol. Sci. 46, 342–351.
Huang, C.M., Huang, R.H., 1998. Measuring parallel fiber length in the rat cerebellum. Brain Res. 801, 211–215.
Huang, Z.J., Di Cristo, G., Ango, F., 2007. Development of GABA innervation in the cerebral and cerebellar cortices. Nat. Rev. Neurosci. 8, 673–686.
Ichikawa, R., Miyazaki, T., Kano, M., Hashikawa, T., Tatsumi, H., Sakimura, K., Mishina, M., Inoue, Y., Watanabe, M., 2002. Distal extension of climbing fiber territory and multiple innervation caused by aberrant wiring to adjacent spiny branchlets in cerebellar Purkinje cells lacking glutamate receptor delta 2. J. Neurosci. 22, 8487–8503.
Ito, M., 1984. The Cerebellum and Neural Control. Raven Press, New York.
Kakizawa, S., Yamasaki, M., Watanabe, M., Kano, M., 2000. Critical period for activity-dependent synapse elimination in developing cerebellum. J. Neurosci. 20, 4954–4961.
Kamal, M.A., Nasim, F.H., Al-Jafari, A.A., 1996. Investigation of the effect of anti-neoplastic drugs, cyclophosphamide, cisplatin and methotrexate on the turnover kinetics of human erythrocyte acetylcholinesterase. Biochem. Mol. Biol. Int. 39, 293–302.
Kang, T.C., Kim, H.S., Seo, M.O., Choi, S.Y., Kwon, O.S., Baek, N.I., Lee, H.Y., Won, M.H., 2001. The temporal alteration of GAD67/GAD65 ratio in the gerbil hippocampal complex following seizure. Brain Res. 920, 159–169.
Kwong, W.H., Chan, W.Y., Lee, K.K., Fan, M., Yew, D.T., 2000. Neurotransmitters, neuropeptides and calcium binding proteins in developing human cerebellum: a review. Histochem. J. 32, 521–534.
Levenes, C., Daniel, H., Jaillard, D., Conquet, F., Crépel, F., 1997. Incomplete regression of multiple climbing fibre innervation of cerebellar Purkinje cells in mGluR1 mutant mice. NeuroReport 8, 571–574.
Lohmann, C., 2009. Calcium signalling and the development of specific neuronal connections. Prog. Brain Res. 175, 443–452.
Lòpez-Bendito, G., Shigemoto, R., Lujań, R., Juiz, J.M., 2001. Developmental changes in the localisation of the mGluR1a subtype of metabotropic glutamate receptors in Purkinje cells. Neuroscience 105, 413–429.
Lujan, R., 2007. Subcellular regulation of metabotropic GABA receptors in the developing cerebellum. Cerebellum 6, 123–129.
Manent, J.B., Represa, A., 2007. Neurotransmitters and brain maturation: early paracrine actions of GABA and glutamate modulate neuronal migration. Neuroscientist 13, 268–279.
Mariani, J., Changeu, J.P., 1981a. Ontogenesis of olivocerebellar relationships: I. Studies by intracellular recordings of the multiple innervation of Purkinje cells by climbing fibers in the developing rat cerebellum. J. Neurosci. 1, 696–702.
Mariani, J., Changeux, J.P., 1981b. Ontogenesis of olivocerebellar relationship: II. Spontaneous activity of inferior olivary neurons and climbing fibermediated activity of cerebellar Purkinje cells in developing rats. J. Neurosci. 1, 703–709.
Marrs, T.C., Maynard, R.L., 2013. Neurotransmission systems as targets for toxicants: a review. Cell. Biol. Toxicol. 29, 381–396.
Mattson, M.P., 1988. Neurotransmitters in the regulation of neuronal cytoarchitecture. Brain Res. 472, 179–212.
Mattson, M.P., 1992. Calcium as sculptor and destroyer of neural circuitry. Exp. Gerontol. 27, 29–49.
Morara, S., Van der Want, J.J.L., De Weerd, H., Provini, L., Rosina, A., 2001. Ultrastructural analysis of climbing fiber-Purkinje cell synaptogenesis in the rat cerebellum. Neuroscience 108, 655–671.
Morrison, M.E., Mason, C.A., 1998. Granule neuron regulation of Purkinje cell development: striking a balance between neurotrophin and glutamate signalling. J. Neurosci. 18, 3563–3573.
Muscella, A., Calabriso, N., De Pascali, S.A., Urso, L., Ciccarese, A., Fanizzi, F.P., Migoni, D., Marsigliante, S., 2007. New platinum(II) complexes containing both an O,O′-chelated acetylacetonate ligand and a sulfur ligand in the platinum coordination sphere induce apoptosis in HeLa cervical carcinoma cells. Biochem. Pharmacol. 74, 28–40.
Muscella, A., Calabriso, N., Fanizzi, F.P., De Pascali, S.A., Urso, L., Ciccarese, A., Migoni, D., Marsigliante, S., 2008. [Pt(O,O′-acac)(γ-acac)(DMS)], a new Pt compound exerting fast cytotoxicity in MCF-7 breast cancer cells via the mitochondrial apoptotic pathway. Br. J. Pharmacol. 153, 34–49.
Muscella, A., Calabriso, N., Vetrugno, C., Urso, L., Fanizzi, F.P., De Pascali, S.A., Marsigliante, S., 2010. Sublethal concentrations of the platinum(II) complex [Pt(O,O′-acac)(gammaacac)(DMS)] alter the motility and induce anoikis in MCF-7 cells. Br. J. Pharmacol. 160, 1362–1377.
Muscella, A., Calabriso, N., Vetrugno, C., Fanizzi, F.P., De Pascali, S.A., Storelli, C., Marsigliante, S., 2011. The platinum(II) complex [Pt(O,O′-acac)(gamma-acac)(DMS)] alters the intracellular calcium homeostasis in MCF-7 breast cancer cells. Biochem. Pharmacol. 81, 91–103.
Nunzi, M.G., Russo, M., Mugnaini, E., 2003. Vesicular glutamate transporters VGLUT1 and VGLUT2 define two subsets of unipolar brush cells in organotypic cultures of mouse vestibulocerebellum. Neuroscience 122, 359–371.
Petralia, R.S., Wenthold, R.J., 1992. Light and electron immunocytochemical localization of AMPA-selective glutamate receptors in the rat brain. J. Comp. Neurol. 318, 329–354.
Piccolini, V.M., Avella, D., Bottone, M.G., Bottiroli, G., Bernocchi, G., 2012. Cisplatin induces changes in the matrix metalloproteinases and their inhibitors in the developing rat cerebellum. Brain Res. 1484, 15–28.
Piccolini, V.M., Bottone, M.G., Bottiroli, G., De Pascali, S.A., Fanizzi, F.P., Bernocchi, G., 2013. Platinum drugs and neurotoxicity: effects on intracellular calcium homeostasis. Cell. Biol. Toxicol. 29, 339–353.
Pisu, M.B., Guioli, S., Conforti, E., Bernocchi, G., 2003. Signal molecules and receptors in the differential development of cerebellumlobules. Acute effects of cisplatin on nitric oxide and glutamate system in Purkinje cell population. Dev. Brain Res. 145, 229–240.
Pisu, M.B., Roda, E., Avella, D., Bernocchi, G., 2004. Developmental plasticity of rat cerebellar cortex after cisplatin injury: inhibitory synapses and differentiating Purkinje neurons. Neuroscience 129, 655–664.
Pisu, M.B., Roda, E., Guioli, S., Avella, D., Bottone, M.G., Bernocchi, G., 2005. Proliferation and migration of granule cells in the developing rat cerebellum: cisplatin effects. Anat. Rec. A Discov. Mol. Cell. Evol. Biol. 287, 1226–1235.
Prestayko, A.W., D'Aoust, J.C., Issell, B.F., Crooke, S.T., 1979. Cisplatin (cisdiamminedichloroplatinum II). Cancer Treat. Rev. 16, 17–39.
Rabacchi, S., Bailly, Y., Delhaye-Bechaud, N., Mariani, J., 1992. Involvement of the N-methyl-D-aspartate (NMDA) receptor in synapse elimination during cerebellar development. Science 256, 1823–1835.
Rabik, C.A., Dolan, M.E., 2007. Molecular mechanisms of resistance and toxicity associated with platinating agents. Cancer Treat. Rev. 33, 9–23.
Rodier, P.M., 1995. Developing brain as a target of toxicity. Environ. Health Perspect. 103, 73–76.
Santin, G., Piccolini, V.M., Veneroni, P., Barni, S., Bernocchi, G., Bottone, M.G., 2011. Different patterns of apoptosis in response to cisplatin in B50 neuroblastoma rat cells. Histol. Histopathol. 26, 831–842.
Santin, G., Piccolini, V.M., Barni, S., Veneroni, P., Giansanti, V., Dal Bo, V., Bernocchi, G., Bottone, M.G., 2013. Mitochondrial fusion: a mechanism of cisplatin-induced resistance in neuroblastoma cells? Neurotoxicology 34, 51–60.

Scelfo, B., Strata, P., 2005. Correlation between multiple climbing fibre regression and parallel fibre regression and parallel fibre response development in the postnatal mouse cerebellum. Eur. J. Neurosci. 21, 971–978.
Scherini, E., Bernocchi, G., 1994. CisDDP treatment and development of the rat cerebellum. Prog. Neurobiol. 2, 161–196.
Sotelo, C., 2004. Cellular and genetic regulation of the development of the cerebellar system. Prog. Neurobiol. 72, 295–339.
Sugimoto, S., Yamamoto, Y.L., Nagahiro, S., Diksic, M., 1995. Permeability change and brain tissue damage after intracarotid administration of cisplatin studied by double-tracer autoradiography in rats. J. Neurooncol. 24, 229–240.
Takayama, C., 2005. GABAergic signaling in the developing cerebellum. Int. Rev. Neurobiol. 71, 63–94.
Tomiwa, K., Nolan, C., Cavanagh, J.B., 1986. The effects of cisplatin on rat spinal ganglia: a study by light and electron microscopy and by morphometry. Acta Neuropathol. 69, 295–308.
Wong, R.O., Ghosh, A., 2002. Activity-dependent regulation of dendritic growth and patterning. Nat. Rev. Neurosci. 3, 803–812.
Zhang, L., Goldman, J.E., 1996. Generation of cerebellar interneurons from dividing progenitors in white matter. Neuron 16, 47–54.

Histochem Cell Biol (2016) 145:587–601
DOI 10.1007/s00418-015-1396-1

ORIGINAL PAPER

[Pt(*O*,*O′*-acac)(γ-acac)(DMS)] versus cisplatin: apoptotic effects in B50 neuroblastoma cells

Maddalena Grimaldi[1] · Giada Santin[1] · Violetta Insolia[1] · Veronica Dal Bo[1] · Valeria Maria Piccolini[1] · Paola Veneroni[1] · Sergio Barni[1] · Manuela Verri[1] · Sandra Angelica De Pascali[2] · Francesco Paolo Fanizzi[2] · Graziella Bernocchi[1] · Maria Grazia Bottone[1]

Accepted: 15 December 2015 / Published online: 9 January 2016

Abstract Cisplatin is one of the most active chemotherapeutic agents used in the treatment of childhood and adult malignancies. Cisplatin induces cell death through different pathways. Despite its effectiveness, the continued clinical use of cisplatin is limited by onset of severe side effects (nephrotoxicity, ototoxicity and neurotoxicity) and drug resistance. Therefore, one of the main experimental oncology purpose is related to the search for new platinum-based drugs to create different types of adducts or more specific and effective subcellular targets. Thus, [Pt(O,O′-acac)(γ-acac)(DMS)], which reacts preferentially with protein thiols or thioether, was synthesized. In our research, different approaches were used to compare cisplatin and [Pt(*O*,*O′*-acac)(γ-acac)(DMS)] effects in B50 rat neuroblastoma cells. Our results, using immunocytochemical, cytometric and morphological techniques, showed that these compounds exert a cytostatic action and activate apoptosis with different pathways. Long-term effects demonstrated that [Pt(*O*,*O′*-acac)(γ-acac)(DMS)] exerts cytotoxic effects in neuronal B50 cell line not inducing drug resistance. Analysis was performed both to compare the ability of these platinum compounds to induce cell death and to investigate the intracellular mechanisms at the basis of their cytotoxicity.

✉ Maria Grazia Bottone
bottone@unipv.it

[1] Department of Biology and Biotechnology "L. Spallanzani", University of Pavia, Via Ferrata 9, 27100 Pavia, Italy

[2] Department of Biological and Environmental Sciences and Technologies (DiSTeBA), University of Salento, Lecce, Italy

Keywords B50 neuroblastoma rat cells · Cisplatin · PtAcacDMS · Apoptosis · Cytoplasmic organelles

Abbreviations

cisPt	Cisplatin
PtAcacDMS	[Pt(*O*,*O′*-acac)(γ-acac)(DMS)]
JC-1	5,5V,6,6V-tetrachloro-1,1V,3,3V-tetraethylbenzimidazolcarbocyanine iodide
PI	Propidium iodide
TEM	Transmission electron microscopy

Introduction

Cisplatin (cisPt) belongs to the family of platinum-based cancer chemotherapeutic compounds. CisPt mechanism of action is represented by the formation of DNA adducts by means of intra- or interstrand, after an initial drug activation through hydrolysis. The adducts modify the structure of DNA molecule stopping basilar processes such as transcription and replication, leading the cell to the death (Sherman et al. 1985). CisPt action involves DNA damage response and mitochondrial apoptosis (Jamieson and Lippard 1999; Cohen and Lippard 2001; Bottone et al. 2008). Recently, Santin et al. (2011, 2012) have shown that cisPt can also induce cell death through cytoplasmic targets in B50 neuronal cells. This drug acts against several kind of malignancies; however, its major limitations are toxicity (nephrotoxicity, neurotoxicity, ototoxicity) and drug resistance (Bodenner et al. 1986; Beinert et al. 2000; Chaney and Sancar 1996; Bernocchi et al. 2011). Resistance mechanisms include high glutathione levels in the cytoplasm of the cell, the inability of cisPt to cross the plasma membrane or an efficient DNA repair activity (Rabik and Dolan 2007). Santin et al. (2012) confirmed that cisPt causes resistance phenomena also in B50 cells.

One of the main experimental oncology purposes is related to the search for new platinum-based drugs. The years ago, the team of Prof. Fanizzi (University of Salento, Lecce, Italy) synthesized a new platinum (II) complex containing acetylacetonate (acac) and a dimethylsulfide (DMS) in the coordination sphere of the metal: [Pt(*O*,*O*′-acac)(γ-acac)(DMS)] (PtAcacDMS) (De Pascali et al. 2005). The presence of a DMS indicates that protein thiols or thioethers are PtAcacDMS preferred targets (Muscella et al. 2007). This new platinum compound seems to (1) enter the cell quickly and with a higher cellular accumulation, and (2) have greater and more rapid cytotoxic effects than cisPt; moreover, like cisPt, it is able to activate the apoptotic pathway in human neuroblastoma cell line (Muscella et al. 2011). Compared with cisPt, PtAcacDMS induces less severe changes on fundamental events of neuroarchitecture development in rat cerebellum, such as no high apoptotic events, less altered granule cell migration and Purkinje cell dendrite growth, suggesting a low neurotoxicity of this new platinum complex for normal CNS (Bernocchi et al. 2011).

We investigated PtAcacDMS effects on B50 neuroblastoma rat cells, in comparison with cisPt by means of cytofluorimetric, immunocytochemical and western blotting analyses and through both transmission electronic and fluorescence microscopy. We tested different increasing concentrations of the compound to obtain the optimal one able to induce apoptotic cell death, and then, the acute and long-term effects at subcellular level were analyzed. In our experiments, as well as morphological features of organelles, we considered the different proteins involved in the apoptotic process, focusing on the intrinsic mitochondrial pathway: caspases 3 and 9, caspase 8, mtHSP70, AIF and Bax. Moreover, PARP-1, a nuclear enzyme involved in DNA repair (Veith and Mangerich 2015), was also analyzed to clarify the activation of apoptosis. Since Santin et al. (2012) have demonstrated the activation of cellular resistance against cisPt treatment in B50 cells, the expression of OPA1, a GTPase involved in the inner mitochondrial membrane fusion (Olichon et al. 2006), and Sirt1, a histone de-acetylase protein involved in the cell survival (Brunet et al. 2004; Yeung et al. 2004), was evaluated in B50 cells after treatment with PtAcacDMS to investigate whether this new platinum compound also induced drug resistance as long-term effect.

The aim of this work was to demonstrate the major apoptotic effects and effectiveness of PtAcacDMS compared with cisPt; PtAcacaDMS may be a tool to overcome the drug resistance mechanism which can invalidate cancer therapy.

Materials and methods

Cell culture

B50 neuroblastoma rat cells (ATCC, Rockville, MD, USA) were cultured in 75-cm^2 flasks in Dulbecco's minimal essential medium supplemented with 10 % fetal bovine serum, 1 % glutamine, 100 U penicillin and streptomycin (Celbio, Milan, Italy) in a 5 % CO_2-humidified atmosphere. Twenty-four hours before the experiments, cells were seeded on glass coverslips for fluorescence microscopy or grown in 75-cm^2 plastic flasks for flow cytometric, electron microscopy and western blotting analysis. Cells were submitted to:

1. Continued exposure to cisPt (Teva Pharma, Milan, Italy) or PtAcacDMS (De Pascali et al. 2005) at different concentrations (40, 20, 10 μM) for 48 h at 37 °C. These concentrations were chosen considering our in vivo experimental design (i.e., a single injection of 5 μg/g b. w.). This dose corresponds to the most commonly used chemotherapy (Bodenner et al. 1986; Dietrich et al. 2006). PtAcacDMS 10 μM was chosen on the base of our following experiments.

At a later stage, cells were submitted to:

1. Continued exposure to cisPt 40 μM or PtAcacDMS 10 μM for 48 h at 37 °C;
2. Continued exposure to cisPt 40 μM or PtAcacDMS 10 μM for 48 h and then recovery of 7 days in normal drug-free medium;
3. Continued exposure to cisPt 40 μM or PtAcacDMS 10 μM for 48 h and recovery of 7 days in normal drug-free medium, then cells were seeded and grown in normal medium for 96 h.

Analysis in flow cytometry

For cell cycle analysis, cells were detached by mild trypsinization (to obtain single-cell suspensions to be processed for flow cytometry), washed in phosphate-buffered saline (PBS) and, after permeabilization with ethanol 70 % for 10 min, treated with RNasi 100 U/ml and then stained for 10 min at room temperature with propidium iodide (PI) 50 μg/ml (Sigma-Aldrich, Milan, Italy) 1 h before flow cytometric analysis. DNA amount evaluations were taken by a Partec PAS III flow cytometer (Münster, Germany), equipped with argon laser excitation (power 200 mW) at 488 nm and 610-nm long-pass filter for PI red fluorescence detection. At least 20,000 cells/sample were measured, five independent experiments were carried out,

Table 1 Primary and secondary antibodies used for double immunofluorescence

Antigen	Primary antibody	Dilution (in PBS)	Secondary antibody (1:200 in PBS)
mtHSP70	Monoclonal antibody (alexis)	1:50	Alexa 488-conjugated anti-mouse (molecular probes)
Lysosomes	Human autoimmune serum recognizing lysosomal proteins	1:500	Alexa 594-conjugated antihuman (molecular probes)
Golgi apparatus	Human autoimmune serum recognizing proteins of Golgi apparatus*	1:250	Alexa 488-conjugated antihuman (molecular probes)
Microfilaments	α-Tubulin	1:200	Alexa 488-conjugated anti-mouse antibody (molecular probes)
Microfilaments	Alexa 488-conjugated phalloidin (molecular probes)	1:40	
AIF	Polyclonal anti-AIF antibody (cell signaling and technology)	1:100	Alexa 488-conjugated anti-rabbit antibody (molecular probes)
Bax	Polyclonal anti-BAX antibody (cell signaling and technology)	1:50	Alexa 488-conjugated anti-rabbit antibody (molecular probes)
PARP-1	Polyclonal anti-p89 antibody (cell signaling and technology)	1:200	Alexa 594-conjugated anti-rabbit antibody (molecular probes)

* Santin et al. (2011)

and the average of scores was used. Values are expressed as mean ± SD, and differences were compared using Student's *t* test (data and statistical analysis have n of at least 5/group).

Identification of apoptotic cells

For the identification of apoptotic cells through Annexin V/FITC versus PI, cells were detached by mild trypsinization as described above, incubated with FITC-conjugated Annexin V (3 μl/10^6 cells) (Bender MedSystem, Prodotti Gianni, Milan, Italy) and were counterstained with 2 μg/ml PI. After 10-min incubation, dual-parameter flow cytometric analysis was performed with the flow cytometer Partec PAS III, equipped with argon laser excitation (power 200 mW) at 488 nm, 510–540 nm interference filter for the detection of FITC green fluorescence and a 610-nm long-pass filter for PI red fluorescence detection. Five independent experiments were carried out, and the average of the scores was used. Values are expressed as the mean ± SD, and differences were compared using Student's *t* test (data and statistical analysis have n of at least 5/group).

Measurement of mitochondrial membrane potential with JC-1

Changes in mitochondrial membrane potential were monitored using JC-1 (5,5V,6,6V-tetrachloro-1,1V,3,3V-tetraethylbenzimidazolcarbocyanine iodide, Molecular Probes, Invitrogen, Italy). JC-1 emits either green or red fluorescence, depending on the mitochondrial membrane potential; the green signal indicates depolarized mitochondria, and the red signal indicates polarized mitochondria (Reers et al. 1995). Thus, the shift from red to green fluorescence is considered a reliable indication of a drop in mitochondrial membrane potential. Cells grown in flasks were harvested by mild trypsination with 0.25 % trypsin in PBS containing 0.05 % ethylenediaminetetraacetic acid and were incubated in culture medium with 2 μM JC-1 for 20 min at 37 °C in the dark. After two washes with PBS at 37 °C, cells in suspension were analyzed on flow cytometry using a Partec PAS III equipped with argon ion laser with 20 mW output power at 488 nm excitation and with 530/30 and 585/42 nm band-pass emission filters. Data were analyzed using FlowMax software from the same company. Values are expressed as the mean ± SD, and differences were compared using Student's *t* test (data and statistical analysis have n of at least 5/group).

Immunofluorescence reactions

For immunocytochemical analysis, after the treatments the samples grown on coverslips were fixed with 4 % formalin and post-fixed with 70 % ethanol for 30 min at −20 °C. Samples were rehydrated for 15 min in PBS and then immunolabeled with the antibodies listed in Table 1. All the incubations were performed at room temperature for 1 h. Cells were then counterstained for DNA with 0.1 μg/mL of Hoechst 33258 (Sigma-Aldrich, Milano, Italy) for 10 min, washed with PBS and mounted in a drop of Mowiol (Calbiochem, Inalco, Italy) for confocal microscopy.

Immunocytochemical staining for activated caspases

Cells on coverslips were fixed with acetone for 10 min, rehydrated with PBS and incubated with primary polyclonal antibodies recognizing the active form of different caspases listed in Table 2. All the incubations were performed at room temperature for 1 h. Cells were then counterstained for DNA with 0.1 μg/ml of PI (Sigma-Aldrich, Italy) for 10 min, washed with PBS and mounted in a drop of Mowiol (Calbiochem-Inalco, Italy) for confocal microscopy. The percentage of caspase-positive cells was obtained by counting the cells on coverslips. Values are expressed as the mean ± SD (data analysis have n of at least 3/group).

Transmission electron microscopy (TEM)

The cells were harvested by mild trypsinization (0.25 % trypsin in PBS containing 0.05 % EDTA), immediately fixed with 2 % glutaraldehyde in the culture medium (1 h at 4 °C) and post-fixed in 1 % OsO_4 in PBS for 1 h at room temperature. The cell pellets were embedded in 2 % agar, thoroughly rinsed with Sörensen buffer (pH 7.2) and dehydrated in ethanol. Finally, the pellets were embedded in Epon resin and polymerized at 60 °C for 24 h. Ultrathin sections were stained with uranyl acetate and lead citrate and observed under a Zeiss EM900 transmission electron microscope.

Confocal fluorescence microscopy

For confocal laser scanning microscopy, Leica TCS-SP system mounted on a Leica DMIRBE-inverted microscope was used. For fluorescence excitation, an Ar/UV laser at 364 nm was used for Hoechst 33258, an Ar/Vis laser at 488 nm was used for FITC, and an He/Ne laser at 543 nm was used for Alexa 594. Spaced (0.5 μm) optical sections were recorded using a 63 × oil immersion objective. Images were collected in the 1024 × 1024 pixel format, stored on a magnetic mass memory and processed by Leica confocal software. The "colocalization" analysis was done considering 30 cells for sample, and in at least 15 cells were considered three points of colocalization. The lines are drawn by a specialized operator using the software LAS AF combined with confocal microscopy system, the Leica TCS-SP, mounted on an inverted microscope Leica DMIRBE.

Fluorescence microscopy

An Olympus BX51 microscope equipped with a 100-W mercury lamp was used under the following conditions: 330–385 nm excitation filter (excf), 400 nm dichroic mirror (dm) and 420 nm barrier filter (bf) for Hoechst 33258; 450–480 nm excf, 500 nm dm and 515 nm bf for the fluorescence of Alexa 488; 540 nm excf, 580 nm dm and 620 nm bf for Alexa 594. Images were recorded with an

Table 2 Primary and secondary antibodies used for caspases immunocytochemical staining

Antigen	Primary antibody	Dilution (in PBS)	Secondary antibody (1:200 in PBS)
Caspase 3	Polyclonal anti-caspase 3 antibody (cell signaling and technology)	1:50	Alexa 488-conjugated anti-rabbit antibody (molecular probes)
Caspase 9	Polyclonal anti-caspase 9 antibody (cell signaling and technology)	1:50	Alexa 488-conjugated anti-rabbit antibody (molecular probes)
Caspase 8	Polyclonal anti-caspase 8 antibody (cell signaling and technology)	1:50	Alexa 488-conjugated anti-rabbit antibody (molecular probes)

Table 3 Primary and secondary antibodies used for western blotting analysis

Antigen	Primary antibody	Dilution (in PBS–Tween)	Secondary antibody (1:2000 in PBS–Tween)
Sirt1	Polyclonal anti Sirt1 antibody (cell signaling and technology)	1:1000	horseradish peroxidase conjugated anti-rabbit antibody (Dako)
Bax	Polyclonal anti-Bax antibody (cell signaling and technology)	1:1000	horseradish peroxidase conjugated anti-rabbit antibody (Dako)
OPA1	Polyclonal anti-OPA1 antibody (Abcam)	1:200	horseradish peroxidase conjugated anti-rabbit antibody (Dako)
PARP-1	Polyclonal anti-p89 antibody (cell signaling and technology)	1:1000	horseradish peroxidase conjugated anti-rabbit antibody (Dako)
α-Actin	Monoclonal anti-α-actin antibody (SIGMA)	1:10000	horseradish peroxidase conjugated anti-rabbit antibody (Dako)

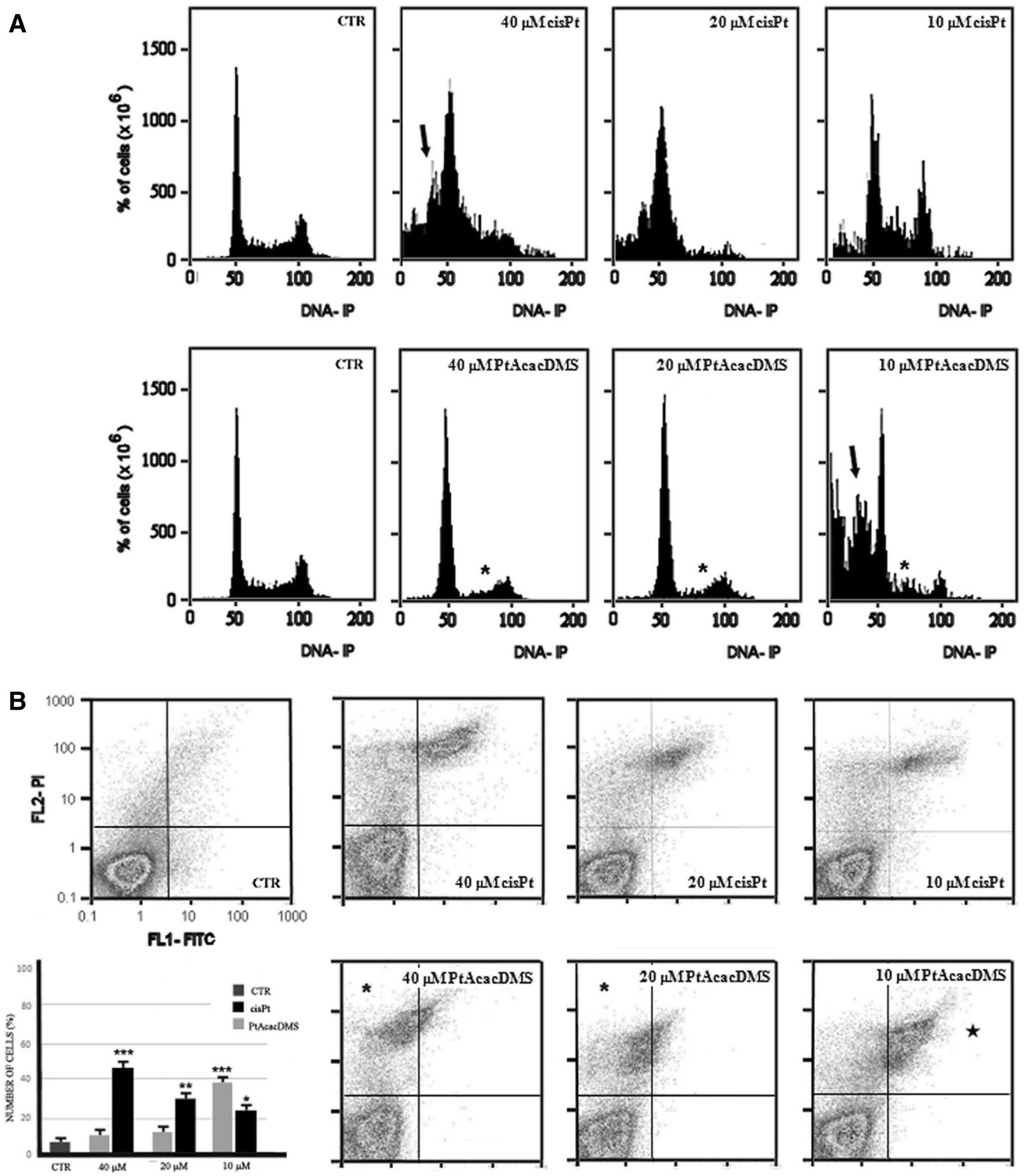

Fig. 1 **A** Cytofluorimetric histograms of DNA content after PI staining in control cells, 48-h cisPt- or 48-h PtAcacDMS-treated cells at different concentrations (10, 20 and 40 μM) *arrows*: sub-G1 apoptotic peak. Second *arrow* in 48-h PtAcacDMS 10 μM treated cells: presence of cell death in S phase. *Asterisks*: S and G2/M peaks. **B** Dual parameter cytograms of FITC-labelled Annexin V (FL1) versus PI staining (FL3). *Asterisks* indicate apoptotic cells after PtAcacDMS 10 μM and necrotic cells after 20 or 40 μM, respectively. *Bottom* on the *left*: graphic with percentage of Annexin V/PI positive cells. Statistical analysis: number of observations per control and treated samples: 5; significance of differences: $*p < 0.05$; $**p < 0.01$; $***p < 0.001$

Olympus MagniFire camera system and processed with the Olympus Cell F software.

Western blotting analysis

After treatments, cells were washed twice with PBS and lysed in RIPA buffer (Tris HCl 1 M pH 7.6, EDTA 0.5 M pH 8, NaCl 5 M, NP40 Nonidet 100 %, H_2O_d with the addition of proteases and phosphatases inhibitors) at 4 °C for 20 min. Bradford reagent (Sigma-Aldrich, Italy) was used for the count of protein amount. Samples were electrophoresed in a 7.5 or 12 % SDS-PAGE minigel and transferred onto a nitrocellulose membrane (BioRad, CA) by a semidry blotting for 1.45 h under a constant current of 70 mA. The membranes were saturated overnight with PBS containing 0.2 % Tween-20 and 5 % skim milk and incubated for 1 h with the different antibodies listed in Table 3. After several washes, the membranes were incubated for 30 min with the proper secondary antibodies. Visualization of immunoreactive bands was performed by an ECL system and Hyperfilm Photographic Film (Amersham Life Sciences, UK) using the manufacturer's instructions. Image J software was used to obtain the density bar chart of the protein bands which are normalized with the loading control. Statistical analysis of the results was performed using Student's *t* test (data and statistical analysis have n of at least 5/group).

Results

Cell cycle analysis and identification of apoptotic cells

First of all, cytofluorimetric experiments were planned to obtain the optimal concentration of PtAcacDMS (Fig. 1), comparing it with cisPt effects on B50 cell line.

The analysis of DNA amount (Fig. 1a) showed different decreasing concentrations of both cisPt and PtAcacDMS (from 40 to 10 μM): 10 μM PtAcacDMS was the most apoptogenic concentration as shown by sub-G1 peak (arrow). Moreover, the cells also went toward cell death in S phase of cell cycle (asterisk). PtAcacDMS's effect is

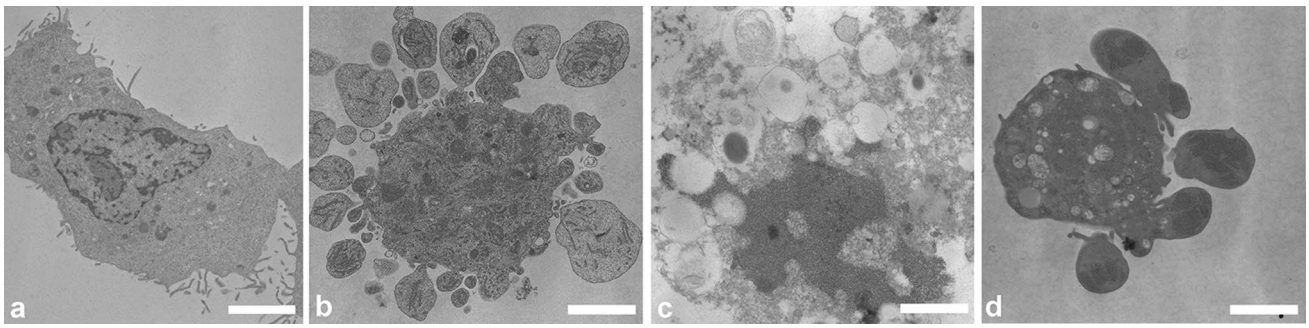

Fig. 2 Ultrastructural morphology of control cells (**a**), 48 h of cisPt 40 μM (**b**), 48 h of PtAcacDMS 40 μM (**c**) and 48 h of PtAcacDMS 10 μM treated cells (**d**). Magnifications: *bar* 1.5 μm

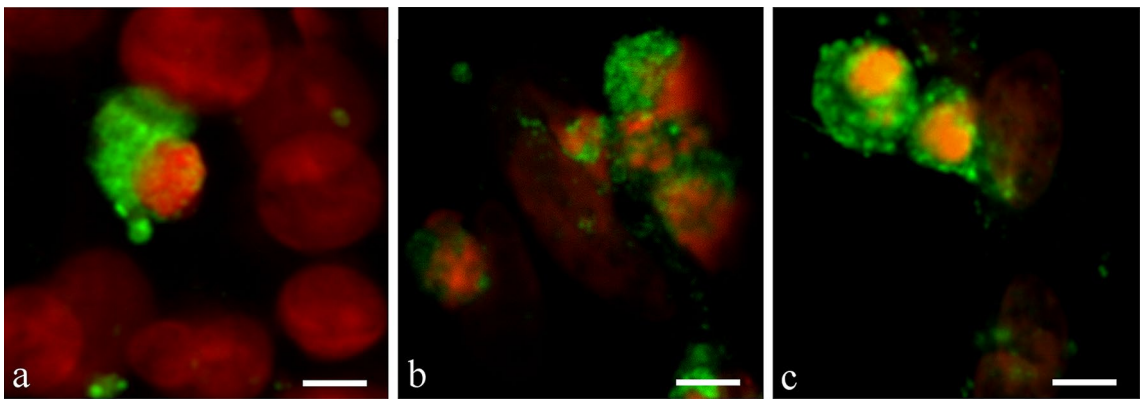

Fig. 3 Fluorescent microscopy: immunocytochemical detection of caspase 3 (**a**) caspase 9 (**b**) and caspase 8 (**c**) (*green fluorescence*) in 48-h 10 μM PtAcacDMS-treated cells. DNA was counterstained with PI. *Bar* 20 μm

comparable to 40 μM cisPt, revealing the presence of cells with fragmented DNA (sub-G1 peak, arrow). Comparing with cisPt, when PtAcacDMS is used at high concentrations (40 and 20 μM), no apoptotic cells fraction in favor of a decrease in both S and G2/M cell cycle phases (asterisks) was observed.

In Fig. 1b, the biparametric analysis with Annexin V-FITC versus PI confirmed the onset of apoptosis only after 10 μM PtAcacDMS (asterisk), while after 40 and 20 μM, necrotic cells were shown (asterisk). In particular, after treatment with 10 μM PtAcacDMS, there was an increase in apoptotic B50 cells as revealed by Annexin V positivity (Fig. 1b) of the late apoptotic fraction that is 54.3 % of cells in comparison with 48.6 % after cisPt 40 μM treatment. In Fig. 1b is also illustrated the histogram of these data giving the percentage of Annexin V/PI-positive cells in different conditions. The histogram clearly shows the increase in late apoptotic cells after PtAcacDMS 10 μM. These data were supported by electron microscopy: In fact, Fig. 2 shows a late apoptotic cell after cisPt 40 μM treatment (b) compared with control cell (a). Apoptotic bodies were detectable, with the presence of highlighted cells with typical apoptotic shape in 10 μM PtAcaDMS (d) and the activation of secondary necrosis in 40 μM PtAcaDMS (c).

Activation of intrinsic apoptotic pathway

To evaluate the activation of apoptotic pathway, immunocytochemical detection for the active caspase 3 and 9 was performed. The immunocytochemistry (Fig. 3a) confirmed the presence of apoptotic cell death after 10 μM PtAcacDMS, similar to 40 μM cisPt (Santin et al. 2011), through the activation of the effector caspase 3. After PtAcacDMS treatment for 48 h, the percentage of caspase 3-positive cells was 63 ± 1.3 %. Caspase 9 (Fig. 3b), the initial caspase involved in the intrinsic apoptotic pathway, was also activated, suggesting that the mitochondrial-mediated pathway was induced: After treatment with PtAcacDMS, the percentage of caspase 9-positive cells was 54 ± 0.9 %. As a matter of fact, mitochondria underwent damage after the treatment with PtAcacDMS as also occurred after cisPt treatment (Santin et al. 2012): Compared with control cells (Fig. 4a), the organellar fragmentation and the onset of dense perinuclear masses took place after treatment (Fig. 4b). Ultrasctructural analysis in Fig. 4a′, b′ showed mitochondria in control and PtAcacDMS-treated cells, respectively: In treated cells, mitochondria appeared with a round shape probably due to fragmentation, and more condensate than those in control cells.

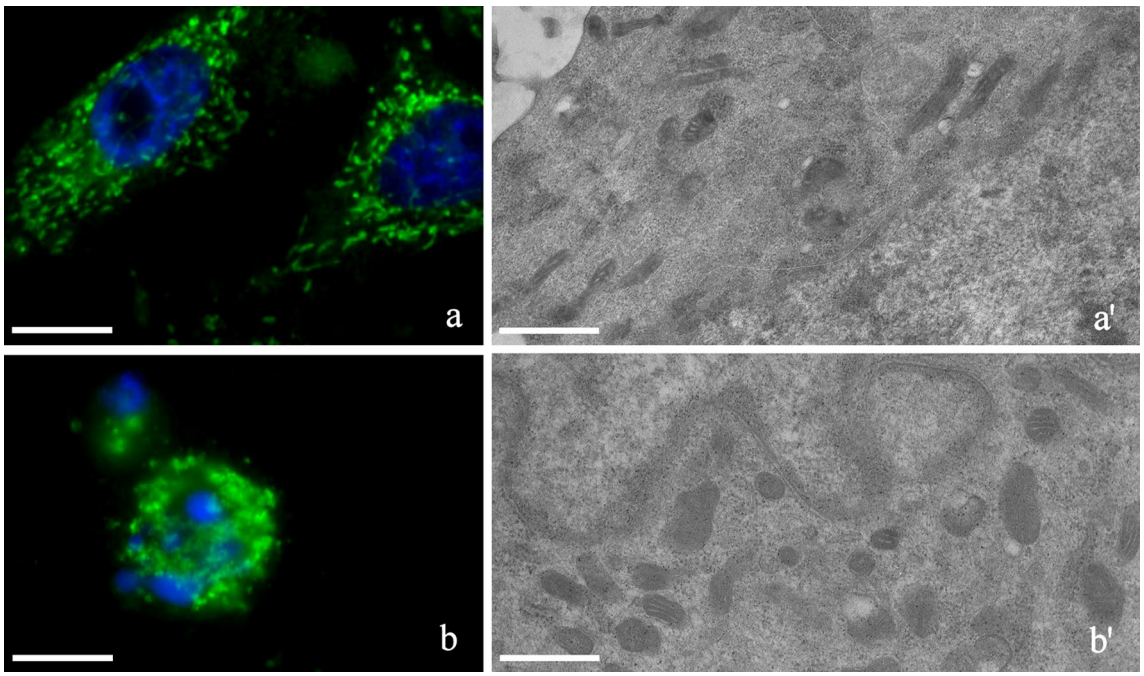

Fig. 4 On the *left*: immunocytochemical detection of mitochondria (*green fluorescence*) in control cells (**a**) and 10 μM 48-h PtAcacDMS-treated cells (**b**). DNA was counterstained with Hoechst 33258 (*blue fluorescence*). Magnifications: bar 20 μm. On the *right*: ultrastructural morphology of mitochondria in control cells (**a′**) and 10 μM 48-h PtAcacDMS-treated cells (**b′**). Magnifications: *bar* 0.6 μm

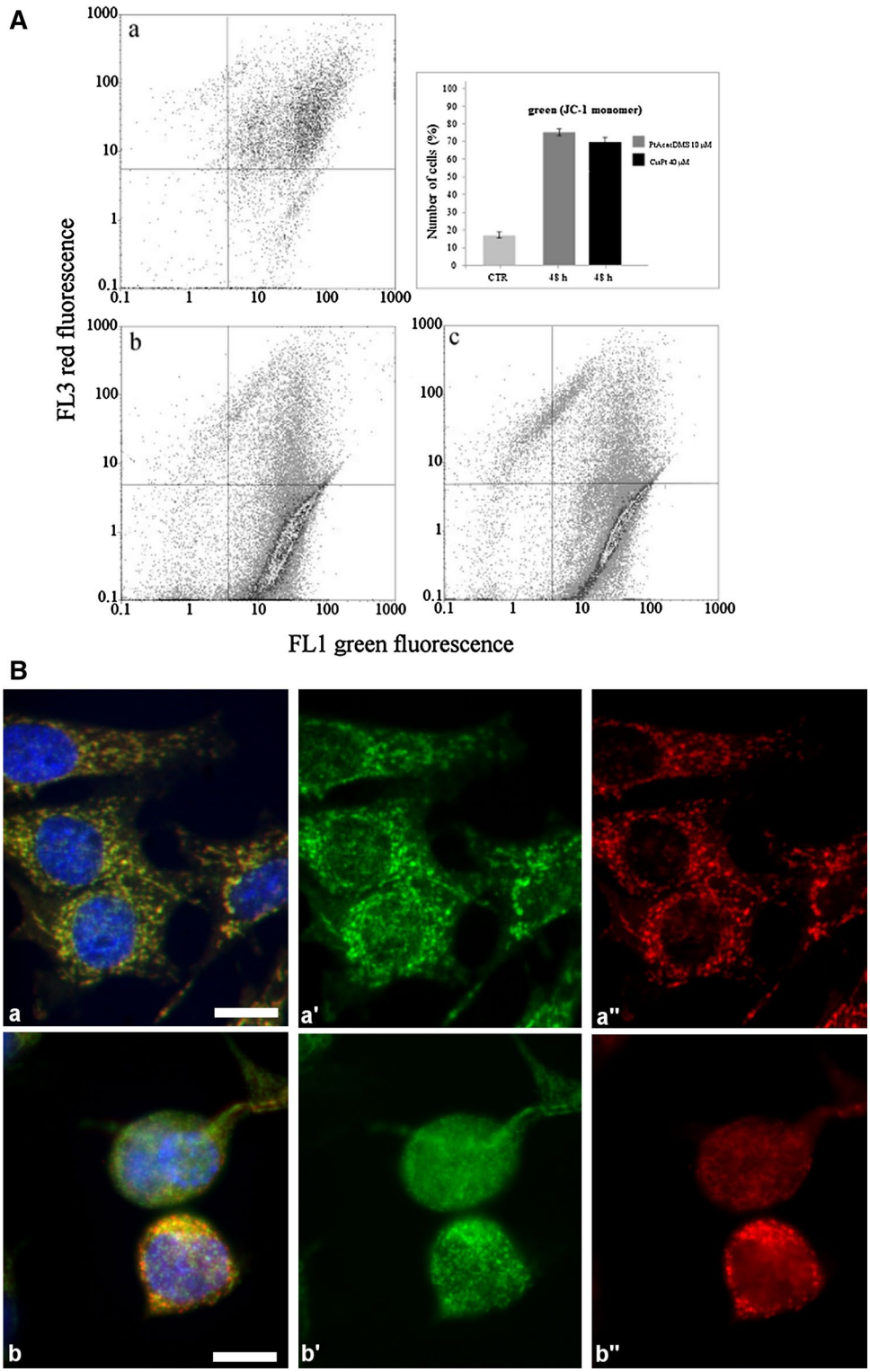

Fig. 5 Measurement of changes in mitochondrial membrane potential with JC-1, Bax, and HSP70 immunolabelling and HSP70 and AIF immunolabelling. **A** Cytometric analysis of *green fluorescence* of JC-1 showing effects of 10 μM PtAcacDMS treatment (**b**) or 40 μM cisPt (**c**). Compared to the control (**a**), there is an increase of the cell fraction with high *green fluorescence* (apoptotic cells). The *graphic* shows percentage of *green–red* JC-1 fluorescence positive cells *bar chart*. Statistical analysis: number of observations per control and treated samples: 5; significance of differences: $*p < 0.05$; $**p < 0.01$; $***p < 0.001$. **B** Confocal microscopy: double immuncytochemical detection of Bax (*green fluorescence*) and mitochondrial HSP70 (*red fluorescence*) in control cells (**a**), and 48-h PtAcacDMS 10 μM treated cells (**b**). In **a′**, **b′** immunolabelling for Bax, in **a″** and **b″**, immunolabelling for HSP70, respectively in control and treated cells. DNA was counterstained with Hoechst 33258 (*blue fluorescence*). Magnifications: Bar: 20 μm. **C** Confocal microscopy: double immunocytochemical detection of AIF (*green fluorescence*) and mitochondrial HSP70 (*red fluorescence*) in control cells (**a**, **b**) and 48-h PtAcacDMS 10 μM treated cells (**c**, early apoptotic cells; **d**, late apoptotic cells); DNA was counterstained with Hoechst 33258 (*blue fluorescence*). Magnifications: Bar: 20 μm. The emission spectra along the *white bars* in the insets demonstrate the colocalization of the *green* and *red fluorescence* (**b′**, **d′**), (**b″**, **d″**) of the *green* and *blue fluorescence* (**a′**, **c′**), (**a″**, **c″**), signals

Moreover, functional variations shown by JC-1 analysis (Fig. 5A) evidenced the changes of mitochondrial potential, which corresponded to morphological changes, after PtAcacDMS treatment (Fig. 5A, b) and an increase in mitochondria with membrane depolarization compared with cisPt-treated cells (Fig. 5A, c). B50 control cells (Fig. 5A, a) showed an equilibrium from red to green fluorescence. After treatment, the two-color cytofluorimetric analysis showed that the fluorescence switched from aggregated yellow-orange (JC-1 aggregates) to

Fig. 5 continued

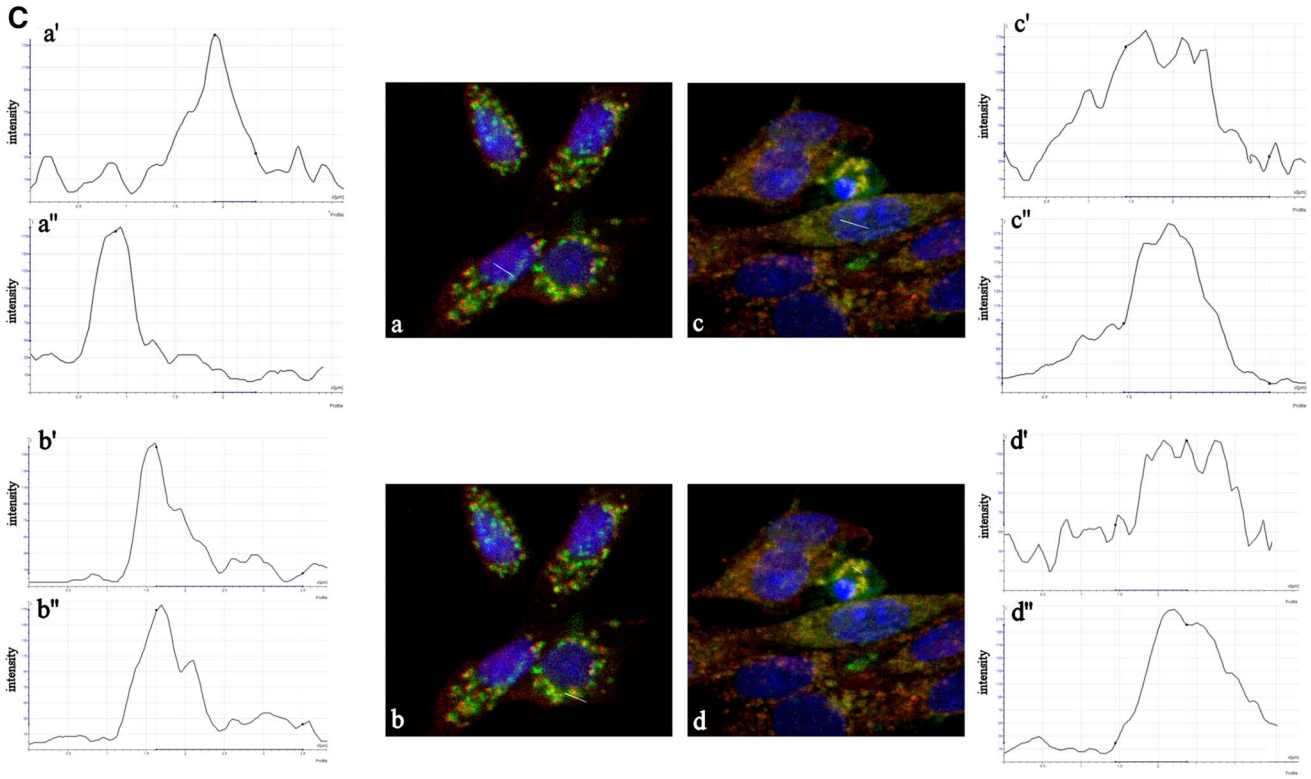

fluorescent green (JC-1 monomer), indicating significant mitochondrial membrane depolarization (Li et al. 1999). The graph showed referred the different percentage of cells with altered membrane potential after both treatments. The activation of the intrinsic apoptotic pathway was further confirmed by the involvement of mitochondrial proteins, Bax and AIF. Figure 5B shows a double immunostaining for Bax and mitochondrial HSP70: In control cells, pro-apoptotic protein Bax colocalized with mitochondria in the cytosol (Fig. 5B, a), whereas Bax translocated to mitochondria following an apoptotic stimulus both in cytosol and in the nucleus (Fig. 5B, b). In Fig. 5C, immunofluorescence confocal analysis revealed a colocalization between AIF and mitochondrial HSP70 in B50 control cells (Fig. 5C, b) and no colocalization with the nucleus (Fig. 5C, a). AIF, after treatment with PtAcacDMS for 48 h, translocated from mitochondria into nucleus in early apoptotic cells (Fig. 5C, c); in late apoptotic cells (Fig. 5C, d), AIF exited from the nucleus was localized in the cytoplasm.

Activation of extrinsic apoptotic pathway

Caspase 8 is synthesized as an inactive single polypeptide chain zymogen procaspase and is activated by proteolytic cleavage, through either autoactivation after recruitment into a multimeric complex or trans-cleavage by other caspases. The activation is induced by the death receptors Fas, tumor necrosis factor receptor 1 and death receptor 3. In Fig. 3c, after 48-h PtAcacDMS exposure of B50 cells, a high increase in caspase 8 cytoplasmic immunopositivity was observed. In fact, after this treatment, the percentage of caspase 8-positive cells was 48 ± 1.2 %.

Alteration of cytoplasmic organelles and cytoskeleton

Among cytoplasmic organelles damaged after PtAcacDMS treatment, there are also Golgi apparatus, lysosomes and cytoskeletal components (Fig. 6). Moreover, in comparison with the control (Fig. 6a–d, respectively), Golgi apparatus and cytoskeletal actin also underwent reorganization after 48 h of treatment: After the loss of the typical semilunar shape, Golgi apparatus went toward fragmentation and redistributed in the cytoplasm, sometimes forming dense aggregates (Fig. 6a′). The actin microfilaments, appeared strongly broke up, form bundles that became progressively thicker, especially at the cell periphery (Fig. 6b′). The microtubule cytoskeleton shows an extensive reorganization and morphological alterations resulting in large bundles all around the core (Fig. 6c′). Compared with control (Fig. 6d), lysosomes appeared more numerous and smaller after 48 h of PtAcacDMS exposure (Fig. 6d′).

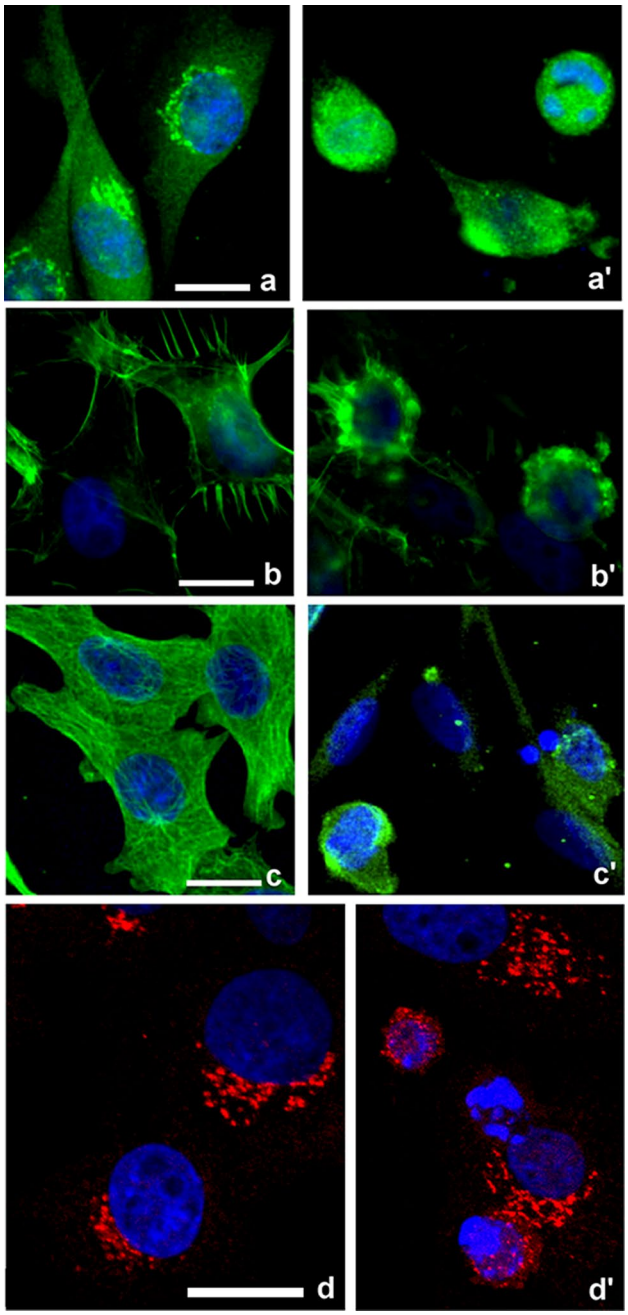

Fig. 6 Organelles and cytoskeleton immunolabeling. Fluorescent microscopy: immunocytochemical detection of Golgi apparatus (**a**, **a′**), actin (**b**, **b′**), and α-tubulin (**c**, **c′**) (*green fluorescence*) and lysosomes (*red fluorescence*) (**d**, **d′**) in control cells and 10 μM 48-h PtAcacDMS-treated cells. DNA was counterstained with Hoechst 33258 (*blue fluorescence*). Magnifications: bar 20 μm

Long-term effects of PtAcacDMS

Afterward, we investigated the effects of PtAcacDMS after long-term recoveries, as well as we did in previous experiments after cisPt treatment (Santin et al. 2013).

Fig. 7 Analysis of long-term effects of PtAcacDMS. **A** TEM: ultrastructural morphology of control cells (**a**), 10 μM 48-h PtAcacDMS-treated cells (**b**), recovered (**c**) and reseeded cells (**d**)). Both *arrow* in **b** and *asterisk* in **c** indicate apoptotic features. Magnifications: bar 1.5 mm. **B** Cytofluorimetric *histograms* of DNA content after propidium iodide (PI) staining in control cells, 10 μM 48-h PtAcac-treated cells, recovered and reseeded cells. *Bottom histogram* with percentage of cells in apoptosis. **C** Dual-parameter cytograms of FITC-labeled Annexin V (FL1) versus PI staining (FL3). On the *left*: *histogram* with percentage of Annexin V/PI-positive cells. Statistical analysis: number of observations per control and treated samples: 5; significance of differences: $*p < 0.05$; $**p < 0.01$; $***p < 0.001$

In Fig. 7A, the ultrastructural morphological features of PtAcacDMS-treated cells were presented: In comparison with the control (a), 48-h treated cells showed the typical apoptotic feature, with the nucleus condensation and the onset of the blebbing process (b). These alterations also persisted in recovered (c) and reseeded cells (d), besides accompanied by dilatation of the vesicular apparatus. The evaluation of DNA amount (Fig. 7B) and the analysis with Annexin V/FITC versus PI (Fig. 7C) confirmed the apoptotic process mainly in 48-h treated and both in recovered and reseeded cells, even if in a progressive decrease, supporting the ultrastructural TEM evidence.

Considering the observed effect of cisPt on mitochondria (Scovassi et al. 2009; Bottone et al. 2010), we investigated the 10 μM PtAcacDMS mechanism of action at the subcellular level. The JC-1 analysis (Fig. 8A) revealed a major mitochondrial membrane depolarization (green JC-1) after 48 h of PtAcacDMS treatment (b), where the onset of apoptosis was more evident. In recovered (c) and reseeded cells (d) was observed a progressive repolarization of mitochondrial membrane potential. The result was quantified by the bar chart. Furthermore, compared with control cells (Fig. 8B), mitochondria underwent morphological alterations with a fragmentation after 48 h of PtAcacDMS exposure (b), the elongation in recovered cells (c) and a return to spotted-like shape in reseeded cells (d). The histograms show the bar chart of the number of cells (%) with elongated mitochondria: The percentage was decreased after the reseeding period, even if the mitochondrial fusion process was restricted (ctr: 0.9 ± 0.095 %; 48-h 10 μM PtAcacDMS: 0.67 ± 0.1 %; recovered: 1.64 ± 0.3 %; reseeded: 0.85 ± 0.08 %). Moreover, in Fig. 8C, the western blotting analysis of GTPase OPA1 confirmed the presence of elongated mitochondria (Fig. 8B, e) mainly in recovered cells with a strong decrease of them in reseeded ones.

Furthermore, Fig. 9 shows the localization of PARP-1 in the nucleus in control B50 cells (a) by fluorescence microscopy. After 48 h of PtAcacDMS treatment (b), the cells underwent apoptosis: In early apoptosis, PARP-1 is still in the nucleus and the actin cytoskeleton collapsed. In late apoptosis, the nucleus is widely fragmented and PARP-1

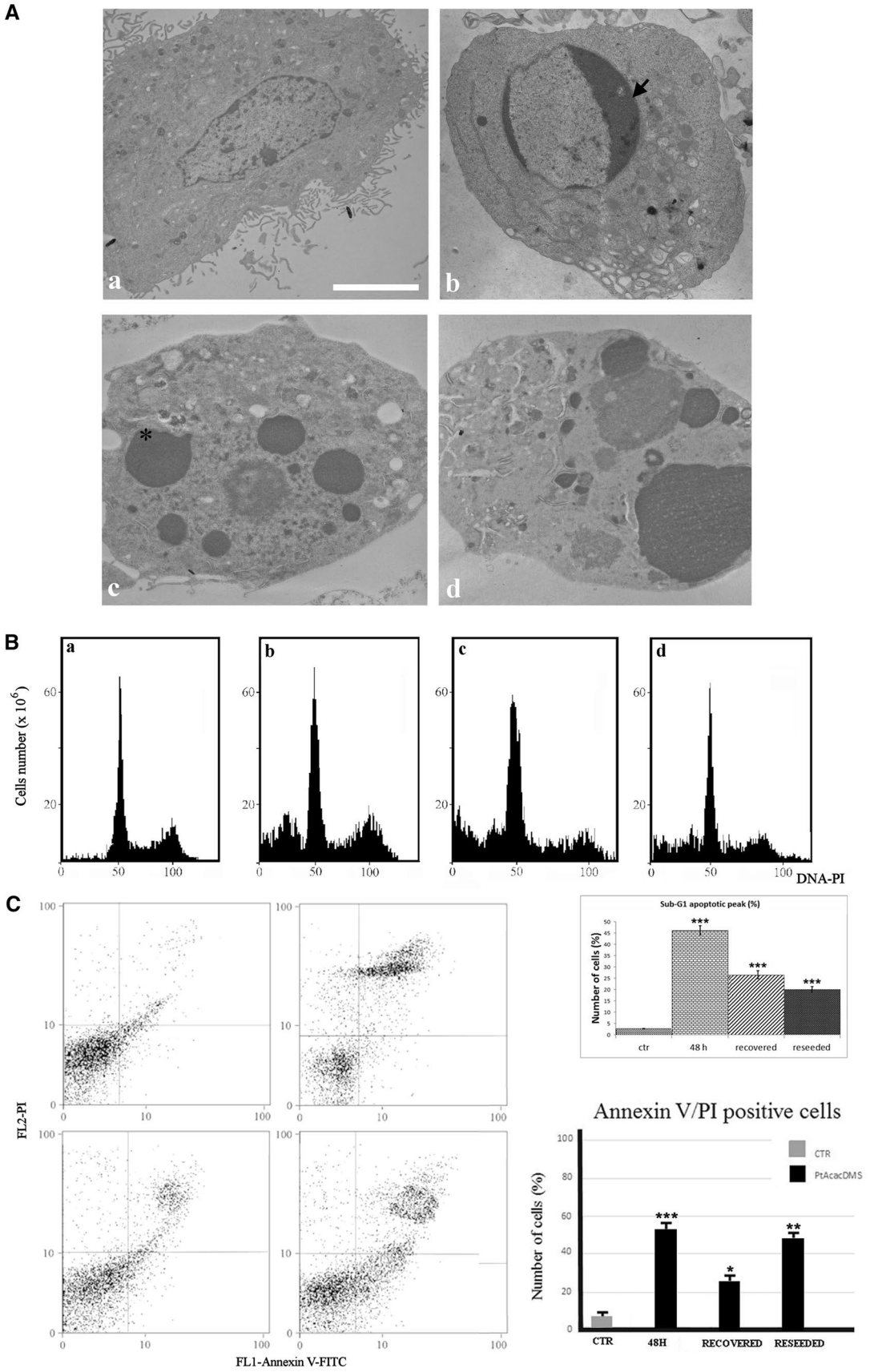
A
a
b
c
d
B
Cells number (x 10^6)
DNA-PI
C
FL2-PI
FL1-Annexin V-FITC
Sub-G1 apoptotic peak (%)
Number of cells (%)
ctr
48 h
recovered
reseeded
Annexin V/PI positive cells
CTR
PtAcacDMS
Number of cells (%)
CTR
48H
RECOVERED
RESEEDED

has migrated to the cytoplasm. PARP-1 was still in the nucleus after 7 days of cisPt-free medium recovery and reseeding period (c), whereas it migrated to the cytoplasm in both PtAcacDMS-recovered and reseeded cells (d) where it aggregated in heterogeneous clusters. Western blotting analysis (Fig. 9) showed that PARP-1 was cleaved after 48 h of PtAcacDMS treatment, generating the p89 fragment as also occurred after cisPt in our previous experiments (Santin et al. 2013). During recovery, PtAcacDMS-treated cells also showed a PARP-1 cleavage, suggesting that the cells activated apoptosis and failing their attempt to survive.

Furthermore, western blotting (Fig. 10) supplies a quantitative investigation on Sirt1 behavior. As shown by densitometric analysis, after PtAcacDMS treatment the amount of Sirt1 had a significant increase in recovered and reseeded cells compared with control, thus indicating that there might be a weak attempt for the cell to survive after the treatment with the new platinum compound. This result confirms that recovered and reseeded cells seemed to activate a mechanism of survival.

Discussion

CisPt is one of the best known drugs used in the treatment of different cancers. However, its clinical application is limited by severe toxicity and drug resistance. At present, data in the literature show that cisPt induces different patterns of apoptosis in neural cell lines (Bottone et al. 2008; Santin et al. 2012, 2013; Galluzzi et al. 2012; Su et al. 2013). In clinical settings, drug resistance or high cytotoxicity of cisPt has motivated the development of new compounds that show lower incidence of chemoresistance and toxicity (Cerri et al. 2011; Bernocchi et al. 2011). De Pascali et al. (2005) have synthesized a new compound PtAcacDMS based on platinum that seems to have a similar potential as cisPt, but less cytotoxic effects on epithelial tumor cell lines (Hela and MCF-7cells) (Muscella et al. 2007, 2008). The results obtained in this work demonstrated that PtAcacDMS acted at a concentration four times lower than cisPt (Muscella et al. 2007). This may be due to the fact that PtAcacDMS targets are cellular organelles and proteins, which could lead to the activation of different apoptotic patterns and consequently to an increase in cell death (Muscella et al. 2007, 2015; Cerri et al. 2010). Bottone et al. (2008) have shown that cisPt is able to induce cell death involving cytoplasmic organelles, such as mitochondria and both actin and tubulin cytoskeleton (Santin et al. 2012).

First of all, cytofluorimetric procedures were performed in order to obtain the optimal PtAcacDMS concentration for the treatment of B50 neuroblastoma rat cells. The results have shown that the maximum of apoptotic effect was detectable at 10 μM PtAcacDMS concentration, similar to 40 μM cisPt. On the other hand, the TEM analysis demonstrated that 40 and 20 μM 48-h PtAcacDMS-treated cells showed a necrotic morphology. The investigation of 48 h 10 μM PtAcacDMS effects at subcellular level highlighted damages at mitochondria and Golgi apparatus, and also at level of actin and tubulin cytoskeleton. Moreover, the lysosomes change in number and morphology, given that these organelles participate in apoptosis by permeabilization of lysosomal membrane, to allow the release of their proteases in the cytoplasm. The mitochondria morphological alterations, with a predominance of the fission (fragmentation) process accompanied by the activation of both caspases 3 and 9, draw attention to the intrinsic apoptotic pathway activation as the main mechanism of PtAcacDMS action, as it also occurs after cisPt (Santin et al. 2012). These data were supported by the immunocytochemical analysis of mitochondrial protein AIF, which moved from mitochondria into the nucleus where, according to its apoptotic role, it activates the DNA fragmentation in cooperation with endonuclease G, leading to cell death.

Similarly to what was previously performed with cisPt, we also investigated PtAcacDMS effects after recovery in drug-free medium and reseeding after 48 h of drug treatment: We detected a progressive decrease in the apoptotic events by both TEM and cytofluorimetric analysis of DNA amount, Annexin V versus PI and JC-1, suggesting the implementation of survival mechanisms. On the other hand, the western blotting analysis of Opa1 revealed a presence of mitochondrial fusion events as a drug resistance mechanism in recovered cells. This result was further confirmed by the double immunodetection of mitochondria and AIF, which showed a colocalization of them in recovered cells, as well as in the control cells, but not in reseeded ones. Analysis of PARP-1 revealed a different localization in untreated cells and in 48-h treated cells. After an apoptotic stimulus,

Fig. 8 Analysis of long-term effects of PtAcacDMS at the subcellular level. Panel **A** Measurement of mitochondrial membrane potential with JC-1. Cytometric analysis of green versus red fluorescence of JC-1 showing effects of 48-h PtAcacDMS 10 μM treatment (**b**), recovered (**c**) and reseeded cells (**d**). Compared to the control (**a**), there is an increase in the cell fraction with mitochondrial membrane depolarization and high *green fluorescence* (*arrow*) after 48 h of PtAcacDMS treatment and a progressive repolarization of mitochondrial membrane in recovered and reseeded cells (**c**, **d**). The *graphic* shows percentage of *green–red* JC-1 fluorescence-positive cells *bar chart*. Statistical analysis: number of observations per control and treated samples: 5; significance of differences: $*p < 0.05$; $**p < 0.01$; $***p < 0.001$. Panel **B** Confocal microscopy: immunocytochemical detection of mitochondria (green fluorescence) in control cells (**a**), 10 μM 48-h PtAcacDMS-treated cells (**b**), recovered (**c**) and reseeded cells (**d**). DNA was counterstained with Hoechst 33258 (*blue fluorescence*). *Bar chart* indicates the number of cells (%) with elongated mitochondria. Bar. 20 μm Panel **C** western blotting of OPA1 (100 kDa) and α-actin (47 kDa) in control cells, 48-h PtAcacDMS 10 μM

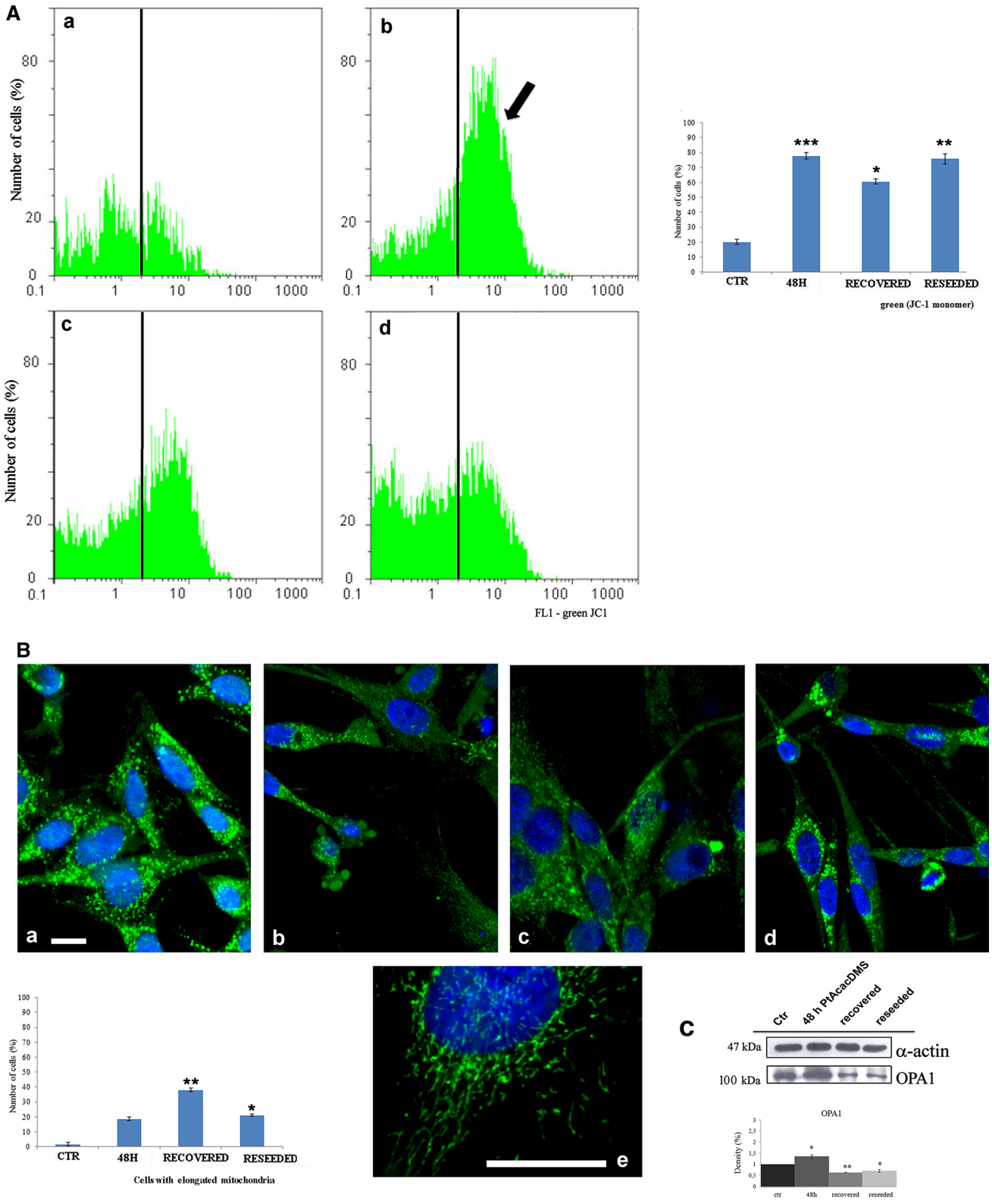

PARP-1 is cleaved by caspase 3, generating p89 and p24 fragments (Soldani et al. 2001). The presence of PARP-1 cleavage in western blot further confirmed the ability of PtAcacDMS to induce apoptosis in B50 neuroblastoma cells. After 7 days of recovery, apoptotic cells were still observed after PtAcacDMS, as confirmed by activation of caspase 3 and 9. During the recovery period, the cells also activated the apoptotic cascade and there was a relocalization of PARP-1.

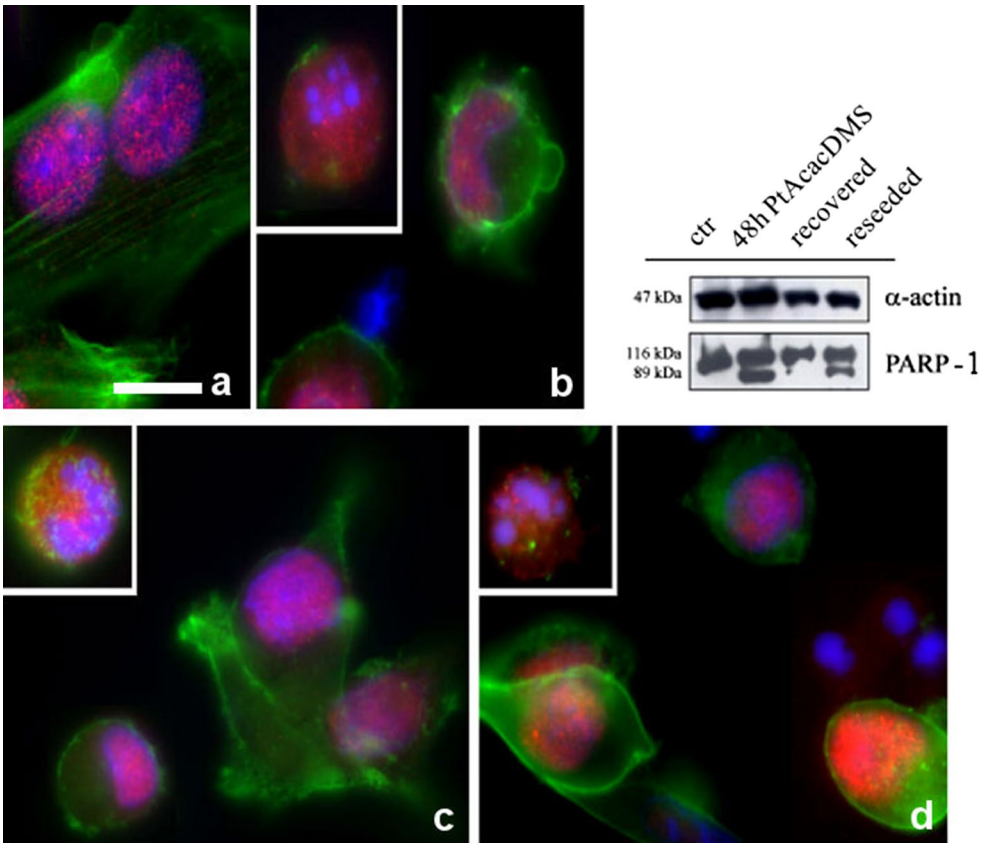

Fig. 9 Immunolabeling and western blotting of PARP-1. Fluorescent microscopy: immunocytochemical detection of PARP-1 (*red fluorescence*) and actin cytoskeleton (*green fluorescence*) in control cells (**a**), 10 μM 48-h PtAcacDMS-treated cells (**b**), recovered (**c**) and reseeded cells (**d**). DNA was counterstained with Hoechst 33258 (*blue fluorescence*). *Squares*: apoptotic cells (**b**, **c**, **d**). Bar 20 μm. Western blotting of PARP-1 (full-length: 116 kDa; cleaved: 89 kDa) and α-actin (47 kDa) in control cells, 48-h 10 μM PtAcacDMS-treated cells, recovered and reseeded cells

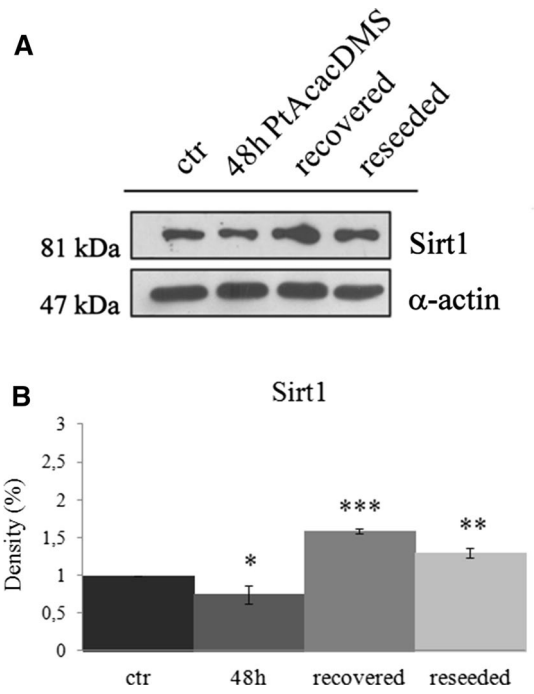

Fig. 10 Western blotting analysis. **a** Western blotting of Sirt1 (81 kDa) and <-actin (47 kDa). **b** *Bar charts*: bands density of Sirt1. Statistical analysis: number of observations per control and treated samples: 5; significance of differences: $*p < 0.05$; $**p < 0.01$; $***p < 0.001$

At last, western blotting analysis also evidences the activation of the effector caspase 3 both after 48-h PtAcacDMS treatment and reseeding period, whereas the initial caspase 9 was cleaved mainly in 48-h PtAcacDMS-treated cells, suggesting that cells may undergo apoptosis in both conditions, but with a different mechanism. Mitochondrial protein Bax expression increased only in 48-h PtAcacDMS-treated cells. Moreover, western blotting analysis of Sirt1 revealed an increase in the protein expression in recovered cells, suggesting the activation of drug resistance mechanisms.

In conclusion, these data support the hypothesis that the new compound PtAcacDMS used at a concentration four times lower than cisPt is able to induce, similarly to cisPt itself, apoptotic cell death in B50 neuroblastoma rat cells. Apoptosis is initially triggered by activating both caspase-independent and intrinsic apoptotic pathways, demonstrating that there may be an interface and reciprocal modulation between the different apoptotic pathways (Dawson and Dawson 2004), based on the interaction with the organelles (Ferri and Kroemer 2001). The mechanism of resistance activated put in place by cells after drug treatment could be a mitochondrion-mediated mechanism as it occurs after cisPt treatment (Santin et al. 2012). Moreover, autophagy could contribute to resistance of cancer cells against chemotherapy (Platini et al. 2010). The less drug resistance and

toxicity of PtAcacDMS put this new platinum compound in a preferential position in comparison with cisPt in cancer therapy, but it needs further investigations about the mechanism by which it induces apoptosis at longer time.

Acknowledgments Confocal fluorescence images were taken at the Centro Grandi Strumenti of the University of Pavia. The research was supported by the following Italian Institutions: Fondazione Banca del Monte di Lombardia 2011 and the University of Pavia (FAR—Fondi di Ateneo per la Ricerca, 2013).

Compliance with ethical standards

Conflict of interest The authors declare that they have no conflict of interest.

References

Beinert T, Masuhr F, Mwela E, Schweigert M, Flath B, Harder H et al (2000) Neuropathy under chemotherapy. Eur J Med Res 5:415–423

Bernocchi G, Bottone MG, Piccolini VM, Dal Bo V, Santin G, De Pascali SA et al (2011) Developing central nervous system and vulnerability to platinum compounds. Chemother Res Pract. doi:10.1155/2011/315418

Bodenner DL, Dedon PC, Keng PC, Katz JC, Borch RF (1986) Selective protection against cis-diamminedichloroplatinum (II)-induced toxicity in kidney, gut, and bone marrow by diethyldithiocarbamate. Cancer Res 46:2751–2755

Bottone MG, Soldani C, Veneroni P, Avella D, Pisu M, Bernocchi G (2008) Cell proliferation, apoptosis and mitochondrial damage in rat B50 neuronal cells after cisplatin treatment. Cell Prolif 41:506–520

Bottone MG, Giansanti V, Veneroni P, Scovassi AI, Bernocchi G, Pellicciari C (2010) The apoptosis-inducing factor (AIF) moves from mitochondria to the nucleus and back to the cytoplasm, during apoptosis. In: Svensson OL (ed) Mitochondria: structure, functions and dysfunctions. Nova Science Publishers, Hauppauge NY, pp 1–34

Brunet A, Sweeney LB, Sturgill JF, Chua KF, Greer PL, Lin Y et al (2004) Stress-dependent regulation of FOXO transcription factors by the SIRT1 deacetylase. Science 303:2011–2015

Cerri S, Piccolini VM, Bernocchi G (2010) Postnatal development of the central nervous system: anomalies in the formation of cerebellum fissures. Anat Rec 293:492–501

Cerri S, Piccolini VM, Santin G, Bottone MG, De Pascali SA, Migoni D et al (2011) The developmental neurotoxicity study of platinum compounds. Effects of cisplatin versus a novel Pt(II) complex on rat cerebellum. Neurotoxicol Teratol 33:273–281

Chaney SG, Sancar A (1996) DNA repair: enzymatic mechanisms and relevance to drug response. J Natl Cancer Inst 88:1346–1360

Cohen SM, Lippard SJ (2001) Cisplatin: from DNA damage to cancer chemotherapy. Prog Nucleic Acid Res Mol Biol 67:93–130

Dawson VL, Dawson TM (2004) Deadly conversations: nuclear-mitochondrial cross-talk. J Bioenerg Biomembr 36:287–294

De Pascali SA, Papadia P, Ciccarese A, Pacifico C, Fanizzi FP (2005) First examples of βdiketonate platinum II complexes with sulfoxide ligands. Eur J Inorg Chem 5:788–796

Dietrich J, Han R, Yang Y, Mayer-Pröschel M, Noble M (2006) CNS progenitor cells and oligodendrocytes are target of chemotherapeutic agents in vitro and in vivo. J Biol 5:22–34

Ferri KF, Kroemer G (2001) Organelle-specific initiation of cell death pathways. Nat Cell Bio 3:255–263

Galluzzi L, Senovilla L, Vitale I, Michels J, Martins I, Kepp O et al (2012) Molecular mechanisms of cisplatin resistance. Oncogene 31:1869–1883

Jamieson ER, Lippard SJ (1999) Structure, recognition, and processing of cisplatin-DNA adducts. Chem Rev 99:2467–2498

Li E, Bedner X, Gorczyca W, Melamed MR, Darzynkiewicz Z (1999) Analysis of apoptosis by laser scanning cytometry. Cytometry 35:181–195

Muscella A, Calabriso N, De Pascali SA, Urso L, Ciccarese A, Fanizzi FP et al (2007) New platinum(II) complexes containing both an *O*, *O*′-chelated acetylacetonate ligand and a sulfur ligand in the platinum coordination sphere induce apoptosis in HeLa cervical carcinoma cells. Biochem Pharmacol 74:28–40

Muscella A, Calabriso N, Fanizzi FP, De Pascali SA, Urso L, Ciccarese A et al (2008) Pt(*O*, *O*'-acac)(γ-acac)(DMS)], a new Pt compound exerting fast cytotoxicity in MCF-7 breast cancer cells via the mitochondrial apoptotic pathway. Br J Pharmacol 153:34–49

Muscella A, Calabriso N, Vetrugno C, Fanizzi FP, De Pascali SA, Storelli C et al (2011) The platinum (II) complex [Pt(*O*, *O*′-acac)(γ-acac)(DMS)] alters the intracellular calcium homeostasis in MCF-7 breast cancer cells. Biochem Pharmacol 81:91–103

Muscella A, Vetrugno C, Calabriso N, Cossa LG, De Pascali SA, Fanizzi FP et al (2015) [Pt(*O*, *O*′-acac)(γ-acac)(DMS)] alters SH-SY5Y cell migration and invasion by the inhibition of Na +/H + exchanger isoform 1 occurring through a PKC-ε/ERK/mTOR pathway. PLoS ONE 10(3):e0118490

Olichon A, Guillou E, Delettre C, Landes T, Arnauné-Pelloquin L, Emorine LJ et al (2006) Mitochondrial dynamics and disease, OPA1. Biochim Biophys Acta 1763:500–509

Platini F, Pérez-Tomás R, Ambrosio S, Tessitore L (2010) Understanding autophagy in cell death control. Curr Pharm Des 16:101–113

Rabik CA, Dolan ME (2007) Molecular mechanisms of resistance and toxicity associated with platinating agents. Cancer Treat Rev 33:9–23

Reers M, Smiley ST, Mottola-Hartshorn C, Chen A, Lin M, Chen LB (1995) Mitochondrial membrane potential monitored by JC-1 dye. Methods Enzymol 260:406–417

Santin G, Piccolini VM, Veneroni P, Barni S, Bernocchi G, Bottone MG (2011) Different patterns of apoptosis in response to cisplatin in B50 neuroblastoma rat cells. Histol Histopathol 26:831–842

Santin G, Scietti L, Veneroni P, Barni S, Bernocchi G, Bottone MG (2012) Effects of Cisplatin in neuroblastoma rat cells: damage to cellular organelles. Int J Biol Cell. doi:10.1155/2012/424072

Santin G, Piccolini VM, Barni S, Veneroni P, Giansanti V, Bo Dal et al (2013) Mitochondrial fusion: a mechanism of cisplatin-induced resistance in neuroblastoma cells? NeuroToxicol 34:51–60

Scovassi AI, Soldani C, Veneroni P, Bottone MG, Pellicciari C (2009) Changes of mitochondria and relocation of the apoptosis-inducing factor during apoptosis. Ann NY Acad Sci 1171:12–17

Sherman SE, Gibson D, Wang AH, Lippard SJ (1985) X-ray structure of the major adduct of the anticancer drug cisplatin with DNA: cis-[Pt(NH3)2(d(pGpG))]. Science 230:412–417

Soldani C, Bottone MG, Pellicciari C, Scovassi AI (2001) Two-color fluorescence detection of Poly (ADP-Ribose) polymerase-1 (PARP-1) cleavage and DNA strand breaks in etoposide-induced apoptotic cells. Eur J Histochem 45:389–392

Su J, Xu Y, Zhou L, Yu HM, Kang JS, Liu N et al (2013) Suppression of chloride channel 3 expression facilitates sensitivity of human glioma U251 cells to cisplatin through concomitant inhibition of Akt and autophagy. Anat Rec 296:595–603

Veith S, Mangerich A (2015) RecQ helicases and PARP1 team up in maintaining genome integrity. Ageing Res Rev 23:12–28

Yeung F, Hoberg JE, Ramsey CS, Keller MD, Jones DR, Frye RA et al (2004) Modulation of NF-kappaB-dependent transcription and cell survival by the SIRT1 deacetylase. EMBO J 23:2369–2380